

27753

NATIONAL LIBRARY  
OTTAWA



BIBLIOTHÈQUE NATIONALE  
OTTAWA

NAME OF AUTHOR....SHARON E. VOSSENGH!

TITLE OF THESIS....VISCOELASTIC FINGERING

...IN IMMISCIBLE

DISPLACEMENT

UNIVERSITY....U. of A.

DEGREE FOR WHICH THESIS WAS PRESENTED....P.h.D.

YEAR THIS DEGREE GRANTED....1976

Permission is hereby granted to THE NATIONAL LIBRARY  
OF CANADA to microfilm this thesis and to lend or sell copies  
of the film.

The author reserves other publication rights, and  
neither the thesis nor extensive extracts from it may be  
printed or otherwise reproduced without the author's  
written permission.

(Signed)....*J. Vossengh*

PERMANENT ADDRESS:

C/o....Dept. of Chem. Eng.  
The U. of A.  
Edmonton, Alta.

DATED....Feb 11.....1976

NL-91 (10-68)

INFORMATION TO USERS

THIS DISSERTATION HAS BEEN  
MICROFILMED EXACTLY AS RECEIVED

This copy was produced from a microfiche copy of the original document. The quality of the copy is heavily dependent upon the quality of the original thesis submitted for microfilming. Every effort has been made to ensure the highest quality of reproduction possible.

PLEASE NOTE: Some pages may have indistinct print. Filmed as received.

Canadian Theses Division  
Cataloguing Branch  
National Library of Canada  
Ottawa, Canada K1A 0N4

AVIS AUX USAGERS

LA THESE A ETE MICROFILMEE  
TELLE QUE NOUS L'AVONS RECUE

Cette copie a été faite à partir d'une microfiche du document original. La qualité de la copie dépend grandement de la qualité de la thèse soumise pour le microfilmage. Nous avons tout fait pour assurer une qualité supérieure de reproduction.

NOTA BENE: La qualité d'impression de certaines pages peut laisser à désirer. Microfilmée telle que nous l'avons reçue.

Division des thèses canadiennes  
Direction du catalogage  
Bibliothèque nationale du Canada  
Ottawa, Canada K1A 0N4

THE UNIVERSITY OF ALBERTA

VISCOUS FINGERING IN IMMISCIBLE DISPLACEMENT

by

SHAPOUR VOSSOUGHI

(C)

A THESIS

SUBMITTED TO THE FACULTY OF GRADUATE STUDIES AND RESEARCH IN

PARTIAL FULFILMENT OF THE REQUIREMENTS FOR THE DEGREE OF

DOCTOR OF PHILOSOPHY

in

CHEMICAL ENGINEERING

DEPARTMENT OF CHEMICAL ENGINEERING

EDMONTON, ALBERTA

SPRING, 1976

UNIVERSITY OF ALBERTA

FACULTY OF GRADUATE STUDIES AND RESEARCH

The undersigned certify that they have read, and recommend to the Faculty of Graduate Studies and Research for acceptance a thesis entitled "Viscous Fingering in Immiscible Displacement", submitted by Shapour Vossoughi in partial fulfilment of the requirements for the degree of Doctor of Philosophy in Chemical Engineering.

H.....  
Supervisor

W. Cale

James Bentzen

Ali A. Nadir

J. M. Melrose

External Examiner

Date

4/6/76

To my beloved wife

Siba

and lovely daughter

Anshita

## ABSTRACT

An experimental study was conducted to investigate the occurrence and growth of macroscopic instabilities in immiscible displacement of oils from porous media. A second objective was to investigate any effects polymer additives might have on the instabilities.

Viscous fingering was photographically studied in a 43.2-cm wide x 53.5-cm long x 1.3-cm thick transparent bed packed with beads of either 0.47 cm or 0.15 cm in diameter. Dow Corning 200 Fluids with viscosities of 100, 1000, or 12500 cs were used as the oil phase. Water, various concentrations of glycerol, and polymer solutions were used as the displacing phase. Breakthrough recovery and saturation profiles were obtained for flow rates ranging between 0.6 to 15.9  $\text{cm}^3/\text{sec}$ .

A new analytical approach, which eliminates use of relative permeabilities was developed to describe the displacement behavior. In this approach a saturation dependent viscosity is used in Darcy's law to describe flow in the flooded zone. Assuming that the power-law model adequately describes viscous properties of the polymer solution, the present approach was generalized for polymer floods.

It was determined that the advance rate of the zero water saturation plane, which corresponded to the tip of the longest finger, was linear with time or pore volume injected. Also, the pressure gradient of the mixed zone was found to be constant and independent of the position of the interface until breakthrough occurred. Good agreement was obtained between predicted breakthrough recovery and the available experimental data.

The predicted saturation distributions were very close to the experimental profiles for cases in which severe fingering prevailed. However,

disagreement occurred when displacement was more or less uniform. The functional form of the average viscosity defined for a mixture of two immiscible fluids could be responsible for this disagreement.

The expression for the breakthrough recovery of a polymer flood reflected ~~in~~ the power-law exponent, n. In particular, lower values of n, which corresponded to the more non-Newtonian behavior of the polymer solution, resulted in lower recovery efficiency. The compatibility of the present analysis and the experimental results leads to the conclusion that the displacement behavior of a polymer flood could be adequately described by a power-law model.

## ACKNOWLEDGMENTS

Appreciation is expressed to the Petroleum Aid to Education fund and the National Research Council who provided partial support for the project.

The author wishes to express his sincere gratitude and appreciation to Dr. F. A. Seyer, research supervisor, for his generous help, enthusiasm, and constructive criticism.

Appreciation is also extended to:

The Imperial Embassy of Iran in Canada for their financial support during part of the study.

The staff of the workshop and the Instrument shop for their assistance in building the equipment.

Mr David Sands who helped in setting up the camera and optical equipment.

Dr. F. H. Vitovec, Chairman of the Department of Mineral Engineering, who made it possible to use the scanning instrument and Mr. Tom Forman who gave instructions for using the equipment.

The Dow Chemical Company who donated the polymer used in this research.

Daphne Cornelius who typed the manuscript.

## TABLE OF CONTENTS

Chapter		Page No.
I. INTRODUCTION		
I.1	General .....	1
I.2	Viscous Fingering .....	2
	I.2.1 Instability Theory .....	3
	I.2.2 Buckley-Leverett Approach .....	6
I.3	Purpose and Scope .....	12
II. THEORY		
II.1	Method of Characteristics .....	14
II.2	Derivation of Buckley-Leverett Equation .....	16
II.3	Volumetric Average Saturation .....	19
II.4	Fractional Flow Function .....	21
II.5	Dynamic Relative Permeability .....	25
II.6	Saturation Distribution .....	26
II.7	Volumetric Recovery Efficiency at Breakthrough .....	27
II.8	Modification of the Theory for the Power-Law Model Fluid .....	28
II.9	Discussion and Application of the Theory .....	31
III. SCALING LAWS		
III.1	General Scaling Laws .....	41
III.2	Scaling Laws for Unstable Immiscible Displacement .....	44
III.3	Application of the Scaling Laws .....	46
IV. EXPERIMENTAL EQUIPMENT AND PROCEDURE		
IV.1	Model Porous Media .....	48
	IV.1.1 Multi-cylinder Matrices .....	48
	IV.1.2 Packed Glass Beads Model .....	52

Chapter		Page No.
IV.	IV.2 Experimental Fluids .....	56
	IV.3 Pumping .....	56
	IV.4 Motion Picture Photography .....	57
	IV.5 Film Scanning .....	57
	IV.6 Pressure Drop Measurement .....	59
	IV.7 Procedure for Displacement Tests .....	59
V.	RESULTS	
	V.1 Pressure Drop .....	64
	V.2 Frontal Plane Advance .....	64
	V.3 Volumetric Recovery Efficiency at Breakthrough .....	69
	V.4 Saturation Profile .....	69
VI.	DISCUSSION OF THE RESULTS	
	VI.1 Pressure Drop .....	107
	VI.2 Frontal Plane Advance .....	111
	VI.3 Volumetric Recovery Efficiency at Breakthrough .....	115
	VI.4 Saturation Profile .....	117
	VI.5 Effect of Polymer Solution Elasticity on Displacement Process .....	118
VII.	CONCLUSIONS AND RECOMMENDATIONS	
	VII.1 Conclusions .....	122
	VII.2 Recommendations .....	124
	BIBLIOGRAPHY .....	126
	APPENDIX A      Rheological Properties of the Experimental Solutions .....	131

Chapter		Page No.
APPENDIX B	Modified Friction Factor and Reynolds Number .....	142
APPENDIX C	Deborah Number .....	148
APPENDIX D	Breakthrough Recovery with Connate Water and/or Residual Oil Saturation .....	150
APPENDIX E	Pressure Transducer Calibration .....	152
APPENDIX F	Experimental Data Points .....	157
	F.1 Specification of the Experimental Runs .....	157
	F.2 Frontal Plane Advance .....	162
	F.3 Pressure Drop Measurement of Single Phase Flow .....	173
	F.4 Pressure Drop Measurement of the Displacement Tests .....	180
	F.5 Breakthrough Recovery .....	200
	F.6 Saturation Profiles .....	209
APPENDIX G	Error Analysis .....	223
	G.1 Pressure Drop Data .....	223
	G.2 Frontal Plane Advance and Breakthrough Recovery .....	224
	G.3 Saturation Profile .....	225
APPENDIX H	Effective Viscosity of the Mixed Zone .....	228

LIST OF TABLES

Table		Page
VI-1	Comparison of the Separan and Pusher Displacement Recoveries .....	121
A-1	Viscometric Measurement of Glycerol Solutions .....	139
A-2	Viscometric Measurements of Separan AP-273 Solutions .....	140
A-3	Comparison of the Viscometric behaviour of 0.2% Pusher 500 and 0.1% Separan AP-273 .....	141
E-1	Pressure Transducer Calibration Data .....	155
F-1	Specification of the Experimental Runs .....	157
F-2	Position of the Zero Saturation Plane .....	163
F-3	Pressure Drop Measurement of Single Phase Newtonian Fluid Flow, Large Beads .....	174
F-4	Pressure Drop Measurement of Single Phase Newtonian Fluid Flow, Small Beads .....	176
F-5	Pressure Drop Measurement of Single Phase Non-Newtonian Fluid Flow, Large Beads .....	177
F-6	Pressure Drop Measurement of Single Phase Non-Newtonian Fluid Flow, Small Beads .....	178
F-7	Pressure Gradient of the Flooded Zone .....	182
F-8	Friction Factor and Reynolds Number of the Flooded Zone .....	198
F-9	Breakthrough Recovery Efficiency .....	201
F-10	Breakthrough Recovery vs. Viscosity Ratio Obtained from Table II of Everett, et al. (69) .....	204

LIST OF TABLES (Continued)

Table		Page
F-11	Breakthrough Recovery vs. Viscosity Ratio Obtained from Figure 5 of Engelberts, et al. (2) .....	205
F-12	Breakthrough Recovery Efficiency Obtained from Table III of Jones-Parra, et al. (70) .....	206
F-13	Breakthrough Recovery vs. Viscosity Ratio Obtained from Figure 2 of Crogs, et al. (51) .....	208
F-14	Water Saturation Distribution from Film Scanning - Effect of Vertical Bar Insignificant .....	211
F-15	Water Saturation Distribution from Film Scanning - Effect of Vertical Bar Significant .....	218
H-1	Apparent Viscosity of the Polymer Solutions Based on the Wall Shear Rate .....	235

LIST OF FIGURES

Figure		Page
II-1	Schematic Representation of the Characteristic Lines for the Case of Stable Displacement .....	32
II-2	Schematic Representation of the Characteristic Lines for the Case of Unstable Displacement ...	33
II-3	Schematic Representation of Shock Formation .....	34
IV-1	Triangular-Pitch Unit Cell .....	49
IV-2	Multi-Cylinder Matrix - Bed No. 1 with an Artificial Large Opening at the Center .....	49
IV-3	Schematic of Bed No. 2 .....	51
IV-4	Packed Beads Model .....	53
IV-5	Flow Distributor No. 1 .....	54
IV-6	Flow Distributor and Screen Holder .....	54
IV-7	Fingering in a Linear Waterflood, Flow Rate: $1.59 \text{ cm}^3/\text{sec}$ (Roll No. 11, Run No. 3) .....	61
IV-8	Fingering in a Linear Waterflood, Flow Rate: $6.35 \text{ cm}^3/\text{sec}$ (Roll No. 11, Run No. 2) .....	62
V-1	Friction Factor vs. Reynolds Number for Single Phase Flow .....	66
V-2	Friction Factor vs. Reynolds Number for Displacement Tests .....	68
V-3	Water Displacing 100 cs Dow Corning, Large Beads ..	70

Figure		Page
V-4	Water Displacing 100 cs Dow Corning, Small Beads ..	71
V-5	Water Displacing 100 cs Dow Corning, $q = 1.5885 \text{ cm}^3/\text{sec.}$ .....	72
V-6	Glycerol Solutions Displacing 100 cs Dow Corning, Small Beads .....	73
V-7	25 cp Glycerol Solution Displacing 100 cs Dow Corning, Small Beads .....	74
V-8	17 cp Glycerol Solution Displacing 100 cs Dow Corning, $q = 3.177 \text{ cm}^3/\text{sec.}$ .....	75
V-9	0.05% Separan AP-273 Displacing 100 cs Dow Corning ..	76
V-10	0.05% Separan AP-273 Displacing 100 cs Dow Corning, $q = 6.354 \text{ cm}^3/\text{sec.}$ .....	77
V-11	0.1% Separan AP-273 Displacing 100 cs Dow Corning ..	78
V-12	0.2% Separan AP-273 Displacing 100 cs Dow Corning, Large Beads .....	79
V-13	0.2% Separan AP-273 Displacing 100 cs Dow Corning, $q = 3.177 \text{ cm}^3/\text{sec.}$ .....	80
V-14	0.2% Separan AP-273 Displacing 12500 cs Dow Corning, Large Beads .....	81
V-15	Separan AP-273 Solutions Displacing 100 cs Dow Corning, $q = 6.354 \text{ cm}^3/\text{sec.}$ .....	82
V-16	Separan AP-273 Solutions Displacing 100 cs Dow Corning, $q = 3.177 \text{ cm}^3/\text{sec.}$ .....	83
V-17	100 cs Dow Corning Displacing Water, $q = 3.4 \text{ cm}^3/\text{sec.}$ , Large Beads .....	84

Figure		Page
V-18	Polymer Solutions Displacing 1000 cs Dow Corning, Small Beads .....	85
V-19	Waterflood Breakthrough Recovery vs. Viscosity Ratio .....	87
V-20	Polymer Flood Breakthrough Recovery vs. Viscosity Ratio .....	89
V-21	Breakthrough Saturation Profile of Run No. 1, Roll No. 8 (Waterflood) .....	90
V-22	Breakthrough Saturation Profile of Run No. 5, Roll No. 8 (Waterflood) .....	91
V-23	Breakthrough Saturation Profile of Run No. 5, Roll No. 8 (Waterflood) .....	92
V-24	Breakthrough Saturation Profile of Run No. 7, Roll No. 10 (Waterflood) .....	93
V-25	Breakthrough Saturation Profile of Run No. 1, Roll No. 11 (Waterflood) .....	94
V-26	Breakthrough Saturation Profile of Run No. 2, Roll No. 11 (Waterflood) .....	95
V-27	Breakthrough Saturation Profile of Run No. 3, Roll No. 11 (Waterflood) .....	96
V-28	Breakthrough Saturation Profile of Run No. 5, Roll No. 9 (Polymerflood) .....	97
V-29	Breakthrough Saturation Profile of Run No. 6, Roll No. 9 (Polymerflood) .....	98
V-30	Breakthrough Saturation Profile of Run No. 2 and 4, Roll No. 13 (Polymerflood) .....	99

Figure		Page
V-31	Breakthrough Saturation Profile of Run No. 5, Roll No. 12 (Glycerol Solution Flood) .....	100
V-32	Breakthrough Saturation Profile of Run No. 6, Roll No. 12 (Glycerol Solution Flood) .....	101
V-33	Breakthrough Saturation Profile of Run No. 7, Roll No. 12 (Glycerol Solution Flood) .....	102
V-34	Breakthrough Saturation Profile of Run No. 1, Roll No. 10. (Polymerflood) .....	103
V-35	Breakthrough Saturation Profile of Run No. 5, Roll No. 10 (Polymerflood) .....	104
V-36	Breakthrough Saturation Profile of Run No. 4, Roll No. 11 (Polymerflood) .....	105
V-37	Breakthrough Saturation Profile of Run No. 7, Roll No. 11 (Polymerflood) .....	106
VI-1	Pressure Drop Data for Absolute Permeability Measurement .....	108
VI-2	Dependence of Elasticity Effect upon Deborah Number, for Different Concentration of Separan AP-273 ...	110
VI-3	Effect of Flow Rate on Recovery .....	113
A-1	Viscometric Behaviour of Glycerol Solutions .....	134
A-2	Shear Stress vs. Angular Velocity for Separan AP-273 Solutions .....	135
A-3	Shear Stress-Shear Rate Behaviour of Separan AP-273 Solutions .....	136

Figures		Page
A-4	Shear Stress vs. Angular Velocity for Polymer Solutions .....	137
A-5	Shear Stress-Shear Rate Behaviour of Polymer Solutions .....	138
B-1	Flow in Cylindrical Tube .....	142
E-1	Schematic of Pressure Transducer Calibration .....	154
E-2	Pressure Transducer Calibration .....	156
H-1	Schematic Representation of the Mixed Zone .....	228

## NOMENCLATURE

A	cross sectional area, $\text{cm}^2$
a	an arbitrary function of x, y, z
a'	an arbitrary constant
$a_1$	radius of the cup, $\text{cm}$
$A_r$	portion of the cross sectional area occupied by connate water and/or residual oil saturation, $\text{cm}^2$
b	an arbitrary function of x, y, z
b'	an arbitrary constant
$b_1$	radius of the cylinder, $\text{cm}$
C	solute concentration, $\text{g cm}^{-3}$
c	an arbitrary function of x, y, z
$C_N$	net number of counts obtained from scanning
$C_t$	tortuosity factor or geometric constant, dimensionless
$C_v$	solvent volume concentration, $\text{cm}^3 \text{ of solute/cm}^3 \text{ of solvent}$
d	greatest lateral dimension of the bed, $\text{cm}$
$d_1, d_2$	minimum and maximum pore opening, respectively, $\text{cm}$
$d_r$	dynamic relative permeability, dimensionless
$D_p$	mean particle diameter, $\text{cm}$
E	effective viscosity ratio, dimensionless
$E_R$	volumetric recovery efficiency at breakthrough, dimensionless
$E_V$	friction loss, erg/sec
F	fractional flow rate in terms of relative permeabilities, dimensionless
f	fractional flow rate, dimensionless
$f_k$	friction factor defined by Eq'n. (B-25), dimensionless
g	gravity acceleration, $\text{cm sec}^{-2}$
H	viscosity level parameter, defined by Eq'n. (B-24) $\text{g cm}^{-n} \text{ sec}^{n-2}$

$h$	height of the cylinder, cm
$H_t$	heterogeneity effects parameter
$K$	absolute permeability, $\text{cm}^2$
$k$	effective permeability, $\text{cm}^2$
$k_1$	apparatus constant, $\text{cm}^3$
$k_C$	conversion factor defined by Eq'n. (F-1)
$k_r$	relative permeability, dimensionless
$k_t$	torsion bar constant, dyne cm per micron movement of the transducer
$L$	length of the bed, cm
$\ln$	natural logarithm
$M$	viscosity ratio defined by Eq'n. (II-43), dimensionless
$m$	power-law parameter, $\text{g cm}^{-1} \text{ sec}^{n-2}$
$M_1$	solute molecular weight, g-mole
$M_p$	viscosity ratio defined by Eq'n. (II-64), dimensionless
$M_R$	mobility ratio, dimensionless
$M_S$	shock mobility ratio, dimensionless
$n$	power-law parameter, dimensionless
$N_{\text{Deb}}$	Deborah number defined by Eq'n. (C-2), dimensionless
$N_{\text{Re}}$	Reynolds number defined by Eq'ns. (B-27,28), dimensionless
$P$	first partial derivative of $z$ w.r.t. $x$
$p$	pressure, dyne $\text{cm}^{-2}$
$\Delta P$	pressure drop, dyne $\text{cm}^{-2}$
$Q$	first partial derivative of $z$ w.r.t. $y$
$q$	total volumetric flow rate, $\text{cm}^3 \text{ sec}^{-1}$
$R$	radius of the tube, cm

$r$	radial distance, cm
$R_g$	gas constant, g $\text{cm}^2 \text{ sec}^{-2} \text{ g-mole}^{-1} \text{ K}^{-1}$
$R_H$	hydraulic radius, cm
$r_m$	mean radius, cm
$R_p$	cumulative oil production at breakthrough, % of oil in place
$S$	saturation, dimensionless
$S_1$	torque transducer sensitivity, micron volt $^{-1}$
$\bar{S}_w$	volumetric average water saturation defined by Eq. n. (II-29)
	dimensionless
$T$	temperature, °C
$t$	time, sec
$T_a$	absolute temperature, °K
$T_o$	torque, ergs
$\Delta t$	movement of torsion head transducer, volts
$U$	superficial velocity, $\text{cm sec}^{-1}$
$u$	average interstitial velocity, $\text{cm sec}^{-1}$
$u_m$	average velocity, $\text{cm sec}^{-1}$
$u_z$	velocity in the z-direction, $\text{cm sec}^{-1}$
$V$	total volume of the box, $\text{cm}^3$
$V_v$	void volume, $\text{cm}^3$
$X$	dimensionless x, i.e. $x/L$
$x$	position in the bed, cm

#### Greek Symbols

- $\alpha$  contact angle of the system oil-water-solid material  
 $B$  empirical constant, dimensionless

$\Gamma$	average nominal shear rate, sec <sup>-1</sup>
$\dot{\gamma}$	shear rate, sec <sup>-1</sup>
$\dot{\gamma}_w$	wall shear rate, sec <sup>-1</sup>
$\eta$	apparent viscosity of the polymer solution defined by Eq'n (II-59), poise
$\eta_w$	apparent viscosity of the polymer solution based on the wall shear rate, poise
$\theta$	relaxation time, sec
$\theta_{pr}$	duration of a process, sec
$\lambda$	wavelength, cm
$\mu$	viscosity, poise
$\pi$	3.14159 ...
$\rho$	density, g cm <sup>-3</sup>
$\Delta\rho$	density difference between water and oil, g cm <sup>-3</sup>
$\Sigma$	summation
$\sigma$	water-oil interfacial tension, dyne cm <sup>-1</sup>
$\sigma^*$	effective or pseudo-interfacial tension, dyne cm <sup>-1</sup>
$\tau$	shear stress, dyne cm <sup>-2</sup>
$\tau_R$	wall shear stress, dyne cm <sup>-2</sup>
$\phi$	porosity, dimensionless
$\Omega$	angular velocity, rad sec <sup>-1</sup>
$\omega$	defined by Eq'n (B-17)

#### Subscripts

a	average
b <sub>t</sub>	breakthrough
c	critical

CW	connate water
e	effective
f	fluid
l	limiting value
m	maximum
o	oil or non-wetting phase
p	Pusher 500
ro	residual oil
s	Separan AP-273
So	solvent
T	total
w	water or wetting phase
W	wall

#### Abbreviations

cm	centimeter
cp	centipoise
cs	centistoke
d	darcy
D.C.	Dow Corning 200 fluid
g	gram
in	inch
md	milidarcy
min	minute
No.	number
psi	pound per square inch
Rdg.	reading

Spec. sec. onal  
rep. remain. App.  
Trans. transducer  
vol. volume



## CHAPTER I

1

### INTRODUCTION

#### I.1 General

The paper presented by J. G. Debanné (1) reveals a clear picture of the vital role of the oil and petroleum in the new world political and wealth order. No matter what politics dictate, the proper recovery and use of the petroleum is in the interest of everyone. The period of cheap oil is gone and it is widely recognized that global petroleum reserves are limited. More effort and research should be conducted to find better and more efficient ways of oil recovery.

The need for more efficient production and higher prices have recently caused some considerable improvements in the Secondary Oil Recovery techniques. Enhanced recovery schemes are being looked upon more seriously.

The problems and difficulties involved in different schemes are common. How is it possible to obtain better volumetric sweep efficiency which requires improvement in areal and microscopic sweep efficiencies? What factors are responsible for such a low oil recovery efficiency, which in the case of heavy oil could be even lower than 20 percent? Presently the problems are known but the answer to how-to-deal-with in the desired direction is scarce. For example, it has been known for quite a long time that development of a stable oil bank ahead of the water zone in the case of water flooding is responsible for high recovery efficiency. However, in almost every field operation water encroachment into the oil zone has been inferred. This phenomenon is called Fingering. The mechanism of this phenomenon is not fully understood. Therefore, a well-paved path to eliminate the inception or growth of the

fingers cannot be established. No general prediction method of the oil recovery at or after breakthrough is presently available. Even the effect of very basic parameters such as viscosities of the displacing and displaced fluid are not fully understood. Theoretical approaches and experimental evidence have always been subject to considerable ambiguity and contradiction. The term "due to the complexity of the geometry" is often encountered in the literature. Is it possible to resolve this complexity and obtain a clear vision of the process? This question remains to be answered in the future.

### I.2 Viscous Fingering

The ideal piston-like displacement seldom occurs when an oil is displaced by a less viscous fluid. In 1950 Engelbert and Klinkenberg (2) visually observed the intrusion of the water phase into the oil phase in a finger shaped manner and coined the term "Viscous Fingering". Thereafter many investigators (3-32) focused on this phenomenon from different points of view. It is well documented (33) that in a homogeneous and uniform porous medium viscous fingering occurs whenever the mobility ratio of invading to original fluid exceeds the value of unity.

Viscous fingering can be studied from two different approaches. The first approach is to look at the finger as an individual entity of the system. This might also be termed a microscopic approach. In this approach one expects to obtain information about the inception, growth and the number of the fingers. Mathematically speaking this can be studied by applying perturbation theory to the flood front (3-12).

In the second approach one overlooks the fingers and attention is focused on the average properties of the bed, say saturation. A continuous distribution of saturation is being considered from one end

of the bed to the other. A stable or no-finger process corresponds to the piston-like displacement. More precisely saturation is discontinuous from one phase to another and is constant in each phase. The second approach which was mentioned above originates from Buckley-Leverett theory (13) therefore, it will be called Buckley-Leverett approach.

#### I.2.1 Instability Theory

It is claimed that a critical velocity exists at which the displacement tends to be unstable. It seems from the literature that Hill (14) was the first who calculated the critical velocity at which the transition zone in the vertical displacement of immiscible liquids became unstable. The experimental results of Blackwell, et al. (15) confirmed the existence of the critical velocity. A thorough discussion of the critical velocity is given by Hawthorne (16).

Instability and fingering can be demonstrated mathematically by perturbation theory. In general, any disturbance can be represented as a Fourier Series, of which only the least stable terms need be considered. This is applicable only to the very beginning of the occurrence of the instabilities where the displacement equations can be linearized. Chuoke, et al. (3) applied the above approach to the immiscible displacement and showed how the prevailing flow potentials affect the various spectral components of a displacement front. Their analysis was based upon a parallel plate model in which a moving interface separated two regions of constant, unequal mobilities. However, they generalized the results to the porous media by assuming an effective or pseudo-interfacial tension  $\sigma^*$ . They concluded that instability would occur for all rates greater than a

critical rate defined by  $U_c$ , such that,

$$\left( \frac{u_2}{k_2} - \frac{u_1}{k_1} \right) U_c + \left( \rho_2 - \rho_1 \right) g \cos (zz') = 0 \quad (I-1)$$

and provided the perturbation contains wave lengths greater than a critical wave length given by  $\lambda_c$ ,

$$\lambda_c = 2 \sqrt{\left[ \frac{\sigma^*}{\left( \frac{u_2}{k_2} - \frac{u_1}{k_1} \right) \left( U - U_c \right)} \right]}^{1/2} \quad (I-2)$$

In (I-2)  $U$  is average volumetric velocity, or injected volume of liquid per unit time per unit of total area normal to  $Z$ . It is sometimes referred to as superficial velocity. And  $Z$  is the axis directed from fluid 1 to fluid 2, perpendicular to the macroscopic interface;  $zz'$ , the angle between the  $Z$ -axis and the  $z$ -axis which is directed vertically upward. The variable  $\sigma^*$  is an effective interfacial tension, which in the case of displacement between parallel plates, equals the ordinary bulk interfacial tension.

Equation (I-2) indicates that wave lengths in a perturbation which are longer than  $\lambda_c$  will grow. Linear theory also predicts that there exists a wave length of maximum instability given by,

$$\lambda_m = \sqrt{3} \lambda_c \quad (I-3)$$

This maximum instability wave length is expected to be the peak-to-peak separation of viscous fingers for the two-dimensional perturbations. A similar attempt applicable only to miscible fluids has been undertaken by Perrine (4, 5).

As Scheidegger (6) points out, the weakness of the Chuoke treatment (3) is inherent in the fact that in the absence of capillary pressure the theory predicts the faster rate of growth for smaller wavelengths. Or in the extreme limit the rate of the growth becomes infinite for the wave length approaching zero which is unrealistic. Scheidegger (6, 7) included a random heterogeneity spectra for the porous medium which he believed was responsible in starting the fingers. He assumed that the phenomenon of fingering was not solely governed by the prevailing flow potentials, but also by the spectrum of heterogeneities in the porous medium. This enabled him to overcome the difficulty encountered by Chuoke, et al. (3). Scheidegger (7) revealed that the generation of fingers is independent of the displacement velocity. He concluded that since the growth of the finger after its inception was entirely controlled by the macroscopic flow potentials, therefore, the whole process of fingering should also be independent of the displacement velocity.

Rachford (8) included a transition zone behind the flood front and eliminated the need for introducing pseudo-interfacial tension as in the case of Chuoke. Predictions of Rachford's analysis did not correlate with the parallel plate model. His results seem to be very sensitive to the shape of the chosen relative permeability and capillary pressure curves. From his analysis, Rachford concluded that the effect of flow velocity on the onset of instabilities was small and although the recovery efficiency decreased the instabilities did not necessarily become more severe with increasing viscosity ratio. In fact the viscosity ratio appeared to have a damping effect on instability which was in contrast with the parallel plate model.

Outmans (9, 10) generalized the analyses further and included non-linear terms in the equations describing conditions at the interface of the liquids. His initiative was based on the fact that the non-linear terms in hydrodynamics problems cannot always be neglected and are sometimes quite important (72). Inclusion of the non-linear terms makes the mathematical treatment much more rigorous and difficult to handle. By solving a fourth order approximation, he showed that no particular sinusoidal disturbance existed which along its entire length would grow more rapidly than any other. This means that the wave length with maximum instability,  $\lambda_m$  in equation (I-3), predicted by linear theory is at least questionable.

Perturbation theory and its predictions, if valid, is only applicable to the very beginning of the occurrence of the instabilities. The drastic simplification involved in the theoretical treatment obviously makes the predictions questionable.

### I. 2.2 Buckley-Leverett Approach

The Buckley-Leverett theory (13) is the first systematic approach in this field. The theory did not predict the growth, size or shape of fingers and even could not predict that fingering would occur at all. However, it had the advantage of being easily adapted to obtain the important results such as oil recovery and water - oil ratio as a function of pore volumes injected. According to the Buckley-Leverett theory the rate of advance of each saturation plane  $S_w$  in a linear flood is given by,

$$\left( \frac{dx}{dt} \right)_{S_w} = \frac{q}{\phi A} \cdot \frac{df_w(S_w)}{d S_w} \quad (I-4)$$

where  $f_w$ , the fractional flow rate of wetting phase, is defined by,

$$f_w = \frac{q_w}{q} \quad (I-5)$$

It is clear that a similar equation can be written for the non-wetting phase. Equation (I-4) is sometimes referred as the frontal advance equation.

In applying the above theory to the qualitative determination of the course of a displacement they fell into the difficulty of the triple-valued saturation problem. In their application they considered the case where gravity and capillary effects were negligible. To resolve the difficulty of the multiple-valued saturation they stated that the real saturation profile was discontinuous and the point of discontinuity was determined from a material balance.

In 1951 Holmgren, et al. (17) and Terwilliger, et al. (18) made use of the frontal advance equation to describe gas-oil gravity drainage performance. In their paper, Terwilliger et al. (18) developed the concept of the stabilized and non-stabilized zones. The stabilized zone which should not be confused with stabilized flood was defined to be the lower region where all the saturation planes moved downstream at the same velocity, while in the non-stabilized zone the saturation planes continued to move further apart. The stabilized zone is characterized by having a higher saturation gradient than the non-stabilized region. They showed that by drawing a tangent to the fractional flow curve the saturation at the upstream end of the stabilized zone could be defined. Later Welge (19) showed that construction of the tangent to the fractional flow curve was indeed equivalent to the material balance applied by Buckley and Leverett (13) to find the point of the discontinuity. The theoretical and experimental work of Rapoport, et al. (20) indicated that the non-stabilized zone was responsible for the rate dependency of the laboratory water

flooding recovery. They concluded that it is the stabilized zone where the Buckley-Leverett theory is applicable.

Most of the investigators, including Buckley and Leverett, have contended that the multiple-valued saturation would not have arisen had they been able to take capillarity effects into account. The results of numerical studies published in papers by Fayers, et al. (21) and Havanessian, et al. (22) confirms this original belief. However, the ambiguity of the non-capillary displacement remains to be resolved.

Sheldon, et al. (23) studied the discontinuity of the saturation profile from the standpoint of shock formation using the method of characteristics and the concept of shocks. Their treatment is indeed equivalent to the Buckley-Leverett approach but more logical. Buckley and Leverett introduced a discontinuity in the saturation profile to resolve the difficulty of the physically impossible multiple-valued saturation while Sheldon, et al. considered the multiple-valued saturation as a point where the characteristic lines intersect and form a shock wave. This shock wave proceeds along the bed with a definite speed called the shock velocity. The physical picture of their approach is a thin, moving region of high saturation gradient in which the exact flow behaviour is unknown. But does this layer exist at all?

Generally all attempts have been to rationalize the prediction of multi-valued saturation encountered during the course of application of the Buckley-Leverett theory. This situation arises mainly due to the use of S-shaped fractional flow curves which may be due to neglect of capillary forces. It is evident that the experimental relative permeability curves may not be a proper choice for the unsteady state displacement process. Cardwell (24) seems to be one of the few

investigators in the literature who brings up this point. However, he does proceed with the same justification as Sheldon, et al. (23).

Van Meurs, et al. (25) questions the validity of the laboratory measured relative permeability curves based on the fact that the same distribution of the water and oil present in practice could hardly be reproduced in the laboratory during the course of relative permeability measurement. They proposed an idealized flow mechanism initiated from their visual observation (26). They pictured the flow pattern as water fingers with immobile protrusions and oil pockets, assuming that the fraction of both immobile oil and water in a cross section of the formation is independent of time and position. Their ultimate results for the fractional flow function could be achieved by assuming a linear dependency of relative permeabilities with saturation which was later derived by Scheidegger, et al. (27).

In 1963, Koval (28) introduced the K-factor method for miscible displacement which was analogous to the Buckley-Leverett method. He viewed the fingering to be brought on by viscosity differences and also by channeling and longitudinal dispersion. The effects of the factors such as channeling and longitudinal dispersion were included via a single parameter,  $H_t$ , called heterogeneity effects. The transition or mixing zone developed due to the solvent fingers was looked upon as an effective displacing agent. The ratio of the viscosity of the oil to that of the assumed effective displacing solvent, was defined as the effective viscosity ratio, E. The product of  $H_t$  by E was termed the K-factor. In his analysis, the assumption of a single valued viscosity characterizing the mixed zone is inherent. This average viscosity was calculated from a correlation based on the fourth-root mixing rule,

$$\frac{1}{(\mu_{B+C})^{\frac{1}{4}}} = \frac{\text{Vol. Fraction B}}{(\mu_B)^{\frac{1}{4}}} + \frac{\text{Vol. Fraction C}}{(\mu_C)^{\frac{1}{4}}}$$

They also assumed linear dependency of relative permeability with saturation. Their reason justifying the linear dependency was that they assumed no interaction between solvent and oil, that is even if they mix, they would retain their individual identities. The linearly dependent relative permeabilities with saturation was also used by Verma (29) who studied fingering behavior from a statistical point of view in an heterogeneous porous medium with capillary pressure.

Dougherty (30) introduced three more parameters in addition to the heterogeneity factor, to account for the effect of dispersive mixing. He, too, assumed the relative permeability of each phase to be proportional to its volume fraction. Peaceman (31) applied numerical calculations to multidimensional miscible displacement taking into account the influence of gravity, permeability distribution, diffusion, and fluid viscosities and densities. In their numerical calculations they introduced an averaged viscosity for the mixed zone given by,

$$\ln \mu = X \ln \mu_{so} + (1 - X) \ln \mu_o \quad (I-7)$$

where,

$$X = \frac{C_v}{C_v + \beta (1 - C_v)} \quad (I-8)$$

and  $C_v$  is the solvent volume concentration. The subscripts "o" and "so" refer to the oil and solvent respectively, and  $\beta$  is an empirical constant.

In a recent paper, Hagoort (32) modified the Buckley-Leverett displacement model by assuming a shock front in the saturation profile followed by a zone of gradually changing saturation. Further, he

assumed the saturation gradient to be negligible behind the shock front so that he could choose a single valued saturation for this zone called the shock saturation. Consequently the Buckley-Leverett displacement model can be formulated in terms of the Muskat segregated flow model (33) with the difference that the displacing phase is a mixture of oil and water at the shock saturation. Hagoort introduced a new term called the shock mobility ratio,  $M_s$ . The shock mobility ratio was defined as the mobility ratio of the fluids behind and ahead of the shock front. He revealed that the displacement was unstable if the shock mobility ratio was greater than unity provided the wave-length of the instabilities was smaller than the width of the experimental model. He also studied the effect of the capillary forces on the instabilities via an energy approach. He reasoned that in an unstable displacement the instabilities would give rise to an extra production of capillary energy and an extra energy dissipation caused by viscous forces. Both terms in general depend on the wave-length,  $\lambda$ . Only those wave-lengths can occur for which the net energy dissipation (viscous dissipation minus the capillary energy production) is positive. He concluded that the predominant wave-length is proportional to the capillary number. It also appeared to be a function of the shape of the capillary pressure curve and displacement characteristics such as relative permeabilities and viscosity ratio. Finally he investigated the validity of the assumption that there existed a relatively small frontal transition zone by requiring  $\lambda_m/L_{TR}$  such that,

$$M_R < 57$$

(I-9)

### I.3 Purpose and Scope

In the former work (34) flow distribution of Newtonian and non-Newtonian fluids in a non-uniform porous bed was studied in hopes of defining conditions leading to formation of fingers. It was found that the microscopic non-homogeneity of the porous bed affected the flow distribution significantly. Thus it was possible to postulate that the inception of fingers might be due to the microscopic non-homogeneity of the porous bed. The effect of polymer solution was to suppress variations in the velocity with pore opening to levels below those for Newtonian fluids. Therefore, in the light of these findings, a displacement experiment was performed in a similar bed having an artificial large opening or heterogeneity. This opening was more than ten times larger than the openings of average pores. In spite of the presence of such a large opening the fingering pattern did not seem to change significantly. The prominent fingers which had already formed before the front reached the large opening continued on their path. And although a new finger could be created at this large opening, it did not seem to be the prominent one and was often suppressed after a few rows. These visual observations suggested that displacement characteristics such as the mobility ratio, viscous, capillary, and gravity forces could be more important than the local heterogeneities in governing the fingering pattern. This conclusion does not weaken the fact that the local heterogeneities have a significant role in the inception of the fingers.

After this preliminary study, attention was focused on the displacement characteristics. The experiments were designed so that capillary and gravity forces could be kept negligible and thus attention could be focused on the effect of viscosity for the Newtonian and non-

Newtonian fluids.

Modification of the Buckley-Leverett solution based on the power law model and consideration of the irreversibility of the displacement of polymer flood is also a part of the scope of the present study. It is hoped that the effect of the polymer solution粘彈性 will be demonstrated by comparing the experimental results with predicted behavior of polymer flood from the modified Buckley-Leverett model.

## CHAPTER II

## THEORY

II.1 Method of Characteristics

The method of characteristics is a powerful tool to deal with a system of linear partial differential equations. These are commonly encountered in the propagation of the plane waves. Roughly speaking, a characteristic is a propagation path along which a physical disturbance or entity is propagated. In spite of its long historical background in Gas Dynamics, the method of characteristics has been only recently introduced into the displacement analysis (23, 33). In 1959, Sheldon, et al. (23) applied this method to solve the so called Buckley-Leverett partial differential equation. He made use of the definition of characteristic paths and obtained a differential equation which was identical to the Buckley-Leverett equation (I-4).

In the present text the general treatment of the linear differential equations given by Abbott (35) will be followed. Consider a linear first order partial differential equation given by,

$$aP + bQ - c = 0 \quad (II-1)$$

where  $a$ ,  $b$  and  $c$  are functions of  $x$ ,  $y$  and  $z$  and,

$$P = \frac{\partial z}{\partial x} \quad (II-2)$$

$$Q = \frac{\partial z}{\partial y} \quad (II-3)$$

The total derivative of  $z$  is given by,

$$dz = Pdx + Qdy$$

Equations (II-1,4) can be combined into the following system:

$$\begin{bmatrix} a & b \\ dx & dy \end{bmatrix} \begin{bmatrix} P \\ Q \end{bmatrix} = \begin{bmatrix} c \\ dz \end{bmatrix}$$

It can be proven (35) that along the characteristics the following determinant, constructed from the above system must be simultaneously identical to zero.

$$\begin{vmatrix} a & b \\ dx & dy \end{vmatrix} = 0 \quad (II-6)$$

$$\begin{vmatrix} a & c \\ dx & dz \end{vmatrix} = 0 \quad (II-7)$$

$$\begin{vmatrix} c & b \\ dz & dy \end{vmatrix} = 0 \quad (II-8)$$

It follows that,

$$\frac{dx}{a} = \frac{dy}{b} = \frac{dz}{c}$$

This is the equation of the line called the characteristic line, or more precisely, the characteristic of zero order.

## II. 2 Derivation of Buckley-Leverett Equation

Let us consider two-phase incompressible flow along the  $x$ -axis in a porous medium. It is assumed that no flow is occurring transverse to  $x$ . The positive direction of the  $x$ -axis is taken from inlet toward outlet of the bed with  $S$  defined as volume fraction of the respective phases, the continuity equation for this system is given by,

$$\frac{\partial q_w}{\partial x} = - \phi A \frac{\partial S_w}{\partial t} \quad (\text{II-10})$$

$$\frac{\partial q_o}{\partial x} = - \phi A \frac{\partial S_o}{\partial t} \quad (\text{II-11})$$

where subscripts  $w$  and  $o$  stand generally for the displacing and displaced phases or simply water and oil respectively. Also we have,

$$S_w + S_o = 1 \quad (\text{II-12})$$

Therefore,

$$\frac{\partial}{\partial x} (q_w + q_o) \equiv 0 \quad (\text{II-13})$$

That is for a constant injection rate  $q$ ,

$$q_w + q_o = q = \text{Const.} \quad (\text{II-14})$$

We can make the following definitions for the fractional flow rates,

$$f_w = \frac{q_w}{q} \quad (\text{II-15})$$

$$f_o = \frac{q_o}{q} \quad (\text{II-16})$$

Neglecting capillary and gravity forces the fractional flow equation in terms of relative permeability by Darcy's law, comes out to be,

$$F_w = \frac{1}{1 + \frac{k_{r,w}}{k_{r,o}} \frac{\mu_w}{\mu_o}} \quad (II-17)$$

where  $k_r$ 's are conventional relative permeabilities.

With the definitions (II-15, 16) Equations (II-10) or (II-11) can be transformed into,

$$\frac{\partial S}{\partial t} + \frac{q}{\phi A} f'(S) \frac{\partial S}{\partial x} = 0 \quad (II-18)$$

where,

$$f'(S) = \frac{df}{dS} \quad (II-19)$$

The subscript has been omitted because similar equations are produced for wetting and non-wetting phases. From Equation (II-10 and 11) it is understood that  $q_w$  and  $q_o$ , consequently  $f_w$  and  $f_o$  are functions of  $x$  and  $t$ . Therefore, in arriving at Equation (II-18) the following transformation is implicit,

$$f(x, t) \rightarrow f(S, t) \quad (II-19a)$$

or,

$$\frac{\partial f}{\partial x} = \frac{\partial f}{\partial S} \frac{\partial S}{\partial x} \quad (II-19b)$$

Further assumption that  $f$  is a function of  $S$  only will be justified later when the fractional flow function is derived for the non-capillary displacement.

On the other hand,

$$S = S(x, t) \quad (II-20)$$

The total derivative of  $S$  is given by,

$$dS = \frac{\partial S}{\partial x} dx + \frac{\partial S}{\partial t} dt \quad (II-21)$$

Equations (II-18, 21) are combined into the following matrix form,

$$\begin{bmatrix} 1 & \frac{q}{\phi A} f'(S) \\ dt & dx \end{bmatrix} \begin{bmatrix} \frac{\partial S}{\partial t} \\ \frac{\partial S}{\partial x} \end{bmatrix} = \begin{bmatrix} 0 \\ dS \end{bmatrix} \quad (II-22)$$

Along the characteristics,

$$\begin{vmatrix} 1 & \frac{q}{\phi A} f'(S) \\ dt & dx \end{vmatrix} = 0 \quad (II-23)$$

$$\begin{bmatrix} 1 & 0 \\ dt & ds \end{bmatrix} = 0 \quad (II-24)$$

$$\begin{bmatrix} 0 & \frac{q}{\phi A} f'(S) \\ ds & dx \end{bmatrix} = 0 \quad (II-25)$$

From (II-23),

$$\frac{dx}{dt} = \frac{q}{\phi A} f'(S) \quad (\text{II-26})$$

and from (II-24),

$$dS = 0. \quad (\text{II-27})$$

That is,

$$S = \text{Const.} \quad (\text{II-28})$$

which also satisfies equation (II-25). Therefore  $S$  is constant along the characteristic line, the equation of which is given by (II-26).

Equation (II-26) is identical to the Buckley-Leverett theory given by equation (I-4). In derivation of equation (II-26) no assumption was made concerning rheological properties of the fluids involved. Therefore equation (II-26) would be applicable to the Newtonian as well as non-Newtonian fluids. That is by proper choice of a fractional flow function, the Buckley-Leverett theory holds for polymerflood as well as waterflood.

### II.3 Volumetric Average Saturation

The volumetric average saturation,  $\bar{S}_w$ , at or before breakthrough is defined as the total volume of fluid injected divided by the total volume of the porous bed invaded by the displacing phase, such that

$$\bar{S}_w = \frac{qt}{\phi Ax_0} \quad (\text{II-29})$$

in which  $x_0$  is taken as the position of the zero saturation plane.

It was noticed from the experimental data given in Appendix (F.4) Table (F-7) that the volumetric average saturation remained constant till breakthrough occurred. It is understood that since the interface is quite flat before flooding is started, no mixed zone or saturation distribution exists at the very beginning of the displacement. Therefore  $\bar{S}_w$  at  $t = 0$  is undefined. However, when displacement starts fingers are created so that mixed zone is developed and  $\bar{S}_w$  achieves its fixed value. As it is observed in Figures (V-3) to (V-18), the data points lie on the eye-fit line from the very beginning of the displacement; therefore, it is safe to claim that the transition time for  $\bar{S}_w$  to achieve its final fixed value is very short and insignificant.

From equation (II-29) for the constant  $\bar{S}_w$ ,

$$\frac{dx_o}{dt} = \frac{q}{\phi A} \frac{1}{\bar{S}_w} \quad (II-30)$$

By comparison of the equations (II-26, 30) it is concluded that,

$$\bar{S}_w = \frac{1}{f'_w(S_w)} \quad (II-31)$$

$S_w = 0$

That is the volumetric average saturation is equal to the inverse of the derivative of the fractional flow function with respect to  $S_w$  evaluated at  $S_w = 0$ . Also, it is inherent in the definition of the average volumetric saturation that  $\bar{S}_w$  is indeed numerically equal to the volumetric sweep efficiency,  $E_R$ , at or before breakthrough,

Therefore,

$$E_R = \frac{1}{f_w(S_w)} \quad |_{S_w = 0} \quad (\text{II-32})$$

#### II.4 Fractional Flow Function

From the foregoing analysis it is understood that a properly defined fractional flow function with respect to saturation is required. First it was decided to proceed with the more common method of obtaining the functional dependency of  $f_w$  with  $S_w$ . That is to measure the steady state relative permeability curves and calculate the fractional flow function from equation (II-17). In this work as in others experiment was carried on by simultaneous flow of water and oil measurement of the pressure drop at a steady state condition. It can be shown that the relative saturation in the bed is not simply the relative flow rates except when  $\mu_o/\mu_w = 1$  and linear effective permeabilities with saturation pertain. During the course of the experiment it was visually noticed that the flow pattern was significantly different from that of the displacement process. In the case of simultaneous flow each fluid tended to have its own path and channeling was quite evident. In other words the flow of the two fluids tended to be completely segregated on a scale much larger than the bead diameters. It was observed that the portion of the total area of the bed covered by one phase was not equal to the relative flow rate of that phase. For example in the case of flowing 50 percent water and 50 percent oil, the portion of the total area of the bed occupied by the water was much less than 50 percent. Therefore, the saturation is not simply the ratio of the flow rates of the two phases. This phenomenon has been noticed and reported in the

literature. For example, the experimental data reported by Richardson et al, (36) all indicate severe channeling. In all the cases the oil saturation far from the outlet was much larger than the relative flow rates of the two phases. They measured the oil saturation distribution by weighing the different segments of the core after each test. For the oil and gas relative flow rates of  $q_o/q_g = 0.002, 0.008$  and  $0.004$  the measured oil saturations were reported to be approximately 60, 64, and 63 percent respectively.

Jennings (37) used a radioactive tracer technique to determine the saturation. In this technique a radioactive component is added to the oil phase so that the oil saturation in the core could be monitored with a scintillation counter. This technique eliminates the error in the saturation determination due to the unknown hold up but does not correct for any effect that channeling might have on pressure drop.

The phenomenon of the channeling is quite different from end effect. End effects are due to the capillary pressure - saturation relationship. End effects can be avoided by measuring the pressure far from the ends while the independent flow or channeling of the phases occurs throughout the experimental bed.

In the case of displacement the oil is driven by the displacing phase and no independent force exists in the oil phase. Also the distribution of the displacing phase across any plane perpendicular to the flow direction seems to be in a random fashion.

The observed dissimilarity of flow patterns forced the author to discontinue this approach and to proceed with an alternative method to obtain the function dependency of  $f_w$  with  $S_w$ . Attention was focused

on the pressure drop measurements. It was noticed that the overall pressure gradient of the mixed zone was almost constant and independent of the position of the interface. The overall pressure gradient of the mixed zone is defined as the total pressure drop of the mixed zone divided by the length of the mixed zone. This pressure gradient was of course quite different from that of a single phase. The constant value of the overall pressure gradient in the mixed zone suggests that the flow regime of the mixed zone is controlled by a single-valued viscosity which is neither the viscosity of the displacing nor displaced phase. This brings up the possibility that a properly defined average viscosity could be sufficient to characterize the flow regime of the displacement process when the capillary and gravity forces are negligible. The criterion to consider the effect of the capillary forces being negligible was the absence of the residual oil saturation.

The experimental pressure gradient of the mixed zone was introduced into Darcy's law to calculate the effective viscosity of the mixed zone. This calculated effective viscosity from the experimental pressure gradient was reasonably close to the arithmetic average of the displacing and displaced fluid viscosities,

$$\mu_e = \frac{\mu_w + \mu_o}{2} \quad (II-33)$$

where subscript "e" stands for "effective". In Appendix H, it is shown that equation (II-33) can be directly derived from the integration of the local behavior of the bed. The local behavior of the bed is assumed to be characterized by an average viscosity defined for a mixture of two immiscible fluids. An Arrhenius type correlation (39), in which the exponent is taken as saturation of the two phases is applied,

$$\mu_a = \mu_w^{s_w} \mu_o^{s_o} \quad (II-34)$$

where subscript "a" stands for "average". Further the mixed zone is considered to be constructed of a continuous distribution of saturation planes, the viscosity of which are given by Equation (II-34). That is every plane of saturation has a single-valued viscosity characterizing its flow regime. A similar correlation of (II-34) was used by Peaceman, et al. (31) in their numerical calculation which was given by Equation (I-7). Ignoring capillary effects, Darcy's law is written in the following form,

$$q_w = - \frac{KA_w}{\mu_w} \frac{dP}{dx} \quad (II-35)$$

$$q_o = - \frac{KA_o}{\mu_o} \frac{dP}{dx} \quad (II-36)$$

$$q = - \frac{KA}{\mu_a} \frac{dP}{dx} \quad (II-37)$$

and as before,

$$q = q_w + q_o \quad (II-38)$$

where  $K$  is the absolute permeability  $A_w$  and  $A_o$  are the insitu cross-sectional areas available for flow of the water and oil-respectively. It is noticed that the steady state relative permeability term usually used in applying Darcy's law to unsteady state displacement process has been avoided. Instead the relative cross sectional areas of the wetting and non-wetting phases have been introduced. In connection with the conventional terminology, the group  $KA_w/\mu_w$  will be called "dynamic mobility" and the corresponding relative permeability, which will be derived later, is termed "dynamic relative permeability". From equation (II-35) to (II-38) one obtains,

$$\frac{A_w}{\mu_w} + \frac{A_o}{\mu_o} = \frac{A}{\mu_a} \quad (\text{II-39})$$

In the absence of connate water and residual oil saturation, the total cross sectional area of the porous bed, A, is equal to the sum of the areas available for the flow of water and oil phases, so that,

$$A = A_w + A_o \quad (\text{II-40})$$

The pertinent analysis for the case with connate water and/or residual oil saturation is given in Appendix (D). Solving for  $A_w$  and  $A_o$  from equations (II-39, 40) and applying (II-34) yields,

$$A_w = \frac{S_w - 1}{M - 1} A \quad (\text{II-41})$$

$$A_o = \frac{M - M_w}{M - 1} A \quad (\text{II-42})$$

where, M is the viscosity ratio of the oil to the water,

$$M = \frac{\mu_o}{\mu_w} \quad (\text{II-43})$$

From the definition of  $f_w$  given by equation (II-15), it is easily derived that,

$$f_w = \frac{M - M_w}{M - 1}^{1-S_w} \quad (\text{II-44})$$

This justifies the formerly made assumption that with fixed fluids or M,  $f_w$  is a function of  $S_w$  only.

### II.5 Dynamic Relative Permeability

To obtain the dynamic relative permeability function with respect to saturation that corresponds to the preceding analysis one needs to write Darcy's law for each phase with dynamic relative permeability

term as

$$q_w = \frac{Kd_{r,w}A}{\mu_w} \frac{dp}{dx} \quad (II-45)$$

$$q_o = \frac{Kd_{r,o}A}{\mu_o} \frac{dp}{dx} \quad (II-46)$$

where  $d_r$ 's are called dynamic relative permeability to avoid confusion with conventional steady state relative permeability. Comparing Equations (II-45, 46) with Equations (II-35, 36) respectively and introducing the results of Equations (II-41, 42) the expressions for dynamic relative permeabilities are,

$$d_{r,w} = \frac{M_w - 1}{M - 1} \quad (II-47)$$

$$d_{r,o} = \frac{M - M_w}{M - 1} \quad (II-48)$$

which are just the same as the ratio of areas given by Equations (II-41, 42). In contrast to the conventional relative permeabilities, the sum of the wetting and non-wetting dynamic relative permeabilities is equal to unity. Or in general, when connate water and/or residual oil saturation exist, this sum is equal to a constant less than unity.

## II.6 Saturation Distribution

Differentiating  $f_w$  from Equation (II-44) with respect to  $S_w$  and substituting in Equation (II-26) yields,

$$\frac{dx}{dt} = \frac{q}{\phi A} \frac{M_w}{M - 1} \frac{1 - S_w}{S_w \ln M} \quad (II-49)$$

upon integration with initial condition of  $x|_{t=0} = 0$ ,

$$x = \frac{qt}{\phi A} \frac{\frac{1-S_w}{M} \ln M}{M-1} \quad (II-50)$$

Hence the saturation distribution is obtained by solving  $S_w$  from Equation (II-50),

$$S_w = 1 - \frac{1}{\ln M} \left[ \ln \frac{x(M-1)\phi A}{qt \ln M} \right] \quad (II-51)$$

In plotting  $S_w$  vs  $x$  one should consider the fact that physically  $S_w$  can not accept values larger than 1. Therefore Equation (II-51) should be modified as following,

$$S_w = 1 \quad \text{for all } x < x \quad |_{S_w = 1}$$

$$S_w = 1 - \frac{1}{\ln M} \left[ \ln \frac{x(M-1)\phi A}{qt \ln M} \right] \quad (II-51a)$$

$$\text{for all } x \geq x \quad |_{S_w = 1}$$

## II.7 Volumetric Recovery Efficiency at Breakthrough

Volumetric recovery efficiency at breakthrough,  $E_R$ , is obtained either from Equation (II-32), or directly from the saturation distribution. By substituting the derivative of  $f_w$  evaluated at  $S_w = 0$  into Equation (II-32),  $E_R$  is given by,

~~$$E_R = \frac{M-1}{M \ln M} \quad (II-52)$$~~

It is understood from Equation (II-52) that the limit of  $E_R$  is unity when  $M \rightarrow 1$ . However, similar to the case of saturation profile, there exists a physical restriction which is not reflected in Equation (II-52). This is simply the fact that  $E_R$  cannot accept values greater

than unity from the physical point of view. This physical constraint is imposed on the theoretical prediction of Equation (II-52) as following,

$$E_R = 1 \text{ for all } M < 1 \quad (\text{II-52a})$$

$$E_R = \frac{M - 1}{M \ln M} \text{ for all } M \geq 1$$

Also from a simple material balance one obtains,

$$L \bar{S}_{w,bt} = x_1 + \int_{x_1}^L S_w dx \quad (\text{II-53})$$

where,

$$x_1 = x_{S_w=1} = \frac{qt \ln M}{(M-1)\phi A} \quad (\text{II-54})$$

and L is the total length of the bed,  $x_1$ , the length of the bed which has been swept completely and  $\bar{S}_{w,bt}$  is water saturation at breakthrough.

Substituting  $S_w$  from Equation (II-51) and performing integration the expression for the water saturation at breakthrough is obtained as,

$$\bar{S}_{w,bt} = \frac{M - 1}{M \ln M} \quad (\text{II-55})$$

which is identical to Equation (II-52).

### II.8 Modification of the Theory for the Power-law Model Fluid

Equation (II-36) remains unchanged while  $\mu_w$  in Equations (II-34, 35) must be replaced by apparent viscosity,  $\eta$ , and these become;

$$\mu_a = \eta \frac{S_w}{\mu_o} \frac{S_o}{\mu_o} \quad (\text{II-56})$$

$$q_w = - \frac{KA_w}{\eta} \frac{dp}{dx} \quad (\text{II-57})$$

Therefore, the expression for  $f_w$  would be,

$$f_w = \frac{\mu_o - \mu_a}{\mu_o - n} \quad (\text{II-58})$$

where  $\mu_a$  and  $n$  both are functions of  $S_w$ . Assuming the power-law model to approximate the polymer solution behaviour,  $n$  is given by,

$$n = H \left( \frac{q_w}{A_w} \right)^{n-1} \quad (\text{II-59})$$

where,  $H$  is the viscosity level parameter given by Equation (B-24). The viscosity level parameter does not have the units of viscosity and is a factor which accounts for the additional dependency of the superficial velocity,  $U$ , on  $K$  and  $\phi$  due to non-Newtonian behaviour of the fluid. As it is shown in Appendix B, the viscosity level parameter appears in the modified form of Darcy's law obtained from solving the generalized flow equation for a power-law model.

From Equations (II-37, 57, 59) the expression for  $n$  becomes,

$$n = H^{1/n} U^{\frac{n-1}{n}} \mu_a^{\frac{n-1}{n}} \quad (\text{II-60})$$

Solving Equations (II-56) and (II-60) for  $n$  and  $\mu_a$ , their final expressions in terms of  $S_w$  are obtained,

$$n = (H U^{n-1}) \frac{1}{n(1-S_w) + S_w} \mu_o^{\frac{(1-S_w)(n-1)}{n(1-S_w) + S_w}} \quad (\text{II-61})$$

and,

$$\mu_a = (H U^{n-1}) \frac{\frac{S_w}{n(1-S_w) + S_w}}{\mu_0} \frac{n(1-S_w)}{n(1-S_w) + S_w} \quad (II-62)$$

Consequently, breakthrough recovery efficiency,  $E_R$ , can be easily calculated from Equation (II-32),

$$E_R = \frac{n \left[ M_p^{1/n} - 1 \right]}{M_p^{1/n} \ln M_p} \quad (II-63)$$

where  $M_p$  is analogous to the viscosity ratio,  $M$ , in the case of Newtonian fluid and is given by,

$$M_p = \frac{\mu_0}{H U^{n-1}} \quad (II-64)$$

It is evident that for Newtonian fluids or for which  $n = 1$ , Equation (II-63) becomes identical to the Equation (II-52).

To obtain saturation profiles one needs to know the derivative of  $f_w$  with respect to  $S_w$ . From Equation (II-58), considering the fact that  $\mu_a$  and  $\eta$  both are functions of  $S_w$ , it is derived,

$$\frac{df_w}{dS_w} = \frac{\left[ n\mu_a\mu_0 + n(\mu_0 - n\mu_0 - \mu_a) \right] \ln M_p}{\left[ n(1 - S_w) + S_w \right]^2 (\mu_0 - n)^2} \quad (II-65)$$

Integration of Equation (II-26) with initial condition  $x|_{t=0} = 0$  gives,

$$x = \frac{qt}{\phi A} \frac{df_w}{dS_w} \quad (II-66)$$

where  $\frac{df_w}{dS_w}$  is substituted from Equation (II-65).

It is obvious from (II-66) that in this case it is not possible to obtain an explicit relation for  $S_w$  in terms of  $x$ . However, the saturation profile can be easily established by assuming values between 0 and 1 for  $S_w$  and calculating  $x$  from Equations (II-65, 66). This procedure has been used to obtain the saturation profiles presented in Figures (V-28 to 30) and (V-34 to 37).

### II.9 Discussion and Application of the Theory

Since the first derivative of the fractional flow function is only a function of  $S_w$ , Equation (II-26) indicates that the characteristic curve of each saturation plane is a straight line. The assumption of the homogeneity of the bed is, of course, inherent in the foregoing statement. Therefore, a plot of  $\frac{qt}{\phi A}$ , the position of each saturation plane, v.s.  $qt/\phi A$  must yield a set of straight lines the slope of which is equal to the first derivative of the fractional flow function evaluated at that specific saturation. Depending on the functional form of  $f(S)$  three different situations can be distinguished;

- a) The slopes of the lines are the same which means that  $f'(S)$  is a constant or say,

$$f'(S) = a' \quad (II-67)$$

Therefore,

$$f(S) = a' S + b' \quad (II-68)$$

where  $a'$  and  $b'$  are constants.

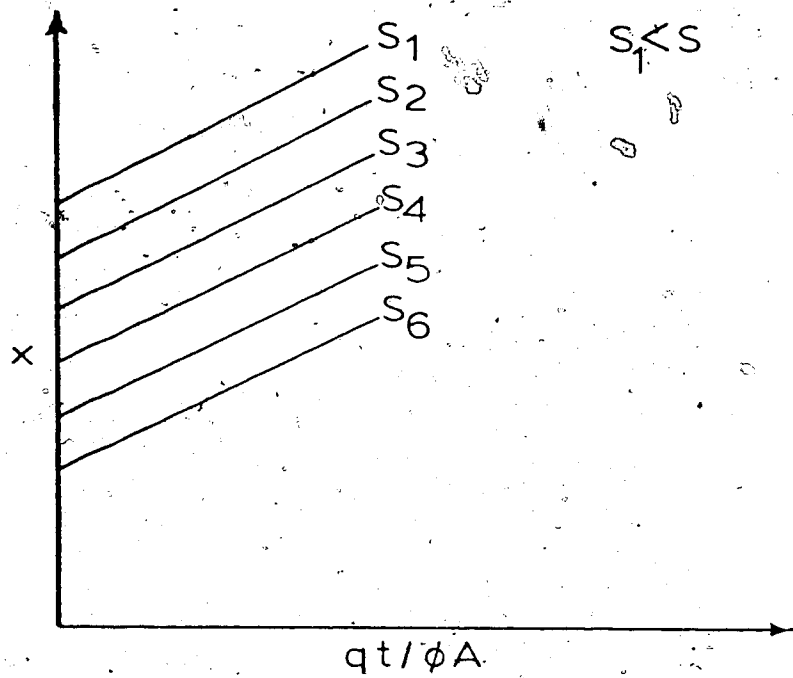


FIGURE II-I SCHEMATIC REPRESENTATION OF THE CHARACTERISTIC LINES FOR THE CASE OF STABLE DISPLACEMENT.

The physical meaning of this case is that all the planes of different saturation move with the same speed. That is the initial saturation distribution profile does not change with time. This corresponds with a completely stable displacement.

- b) The slope of the lines increases with decreasing  $S$ , which means that the second derivative of "f" is negative for all values of  $S$ ,

$$\frac{d^2 f(S)}{dS^2} < 0 \quad (II-69)$$

From the mathematical point of view, condition (II-69) corresponds with a curve of "f" v.s. "S" being concave downward.

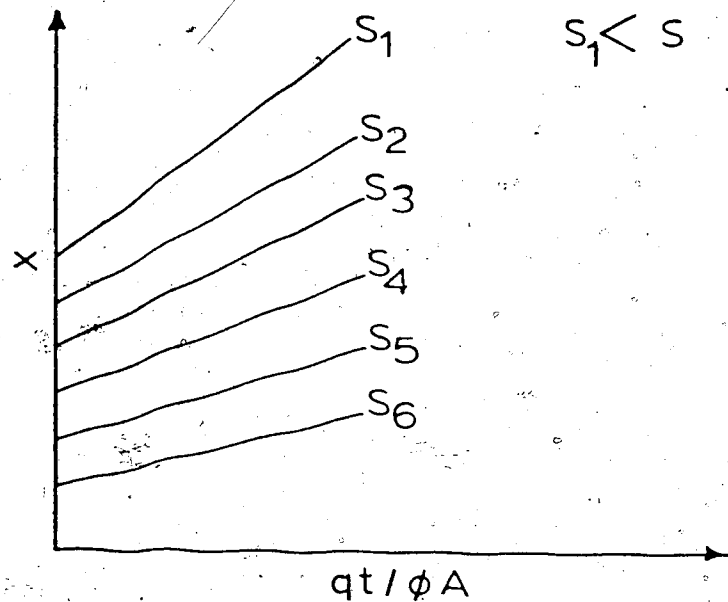


FIGURE II-2 SCHEMATIC REPRESENTATION OF THE CHARACTERISTIC LINES FOR THE CASE OF UNSTABLE DISPLACEMENT.

The physical meaning of this case is that planes of low saturation move faster than planes of higher saturation. That is the length of the mixed zone is increasing. This corresponds with an unstable displacement. The degree of the instability or the severeness of the fingering can be studied from the relative departure of the planes from each other.

- (c) The slope of the lines increases with  $S$ , that is the second derivative of  $f$  is positive for all values of  $S$  or

$$\frac{d^2 f}{d S^2} > 0$$

(II-70)

This is a sufficient and necessary condition for the fractional flow curve to be concave upward.

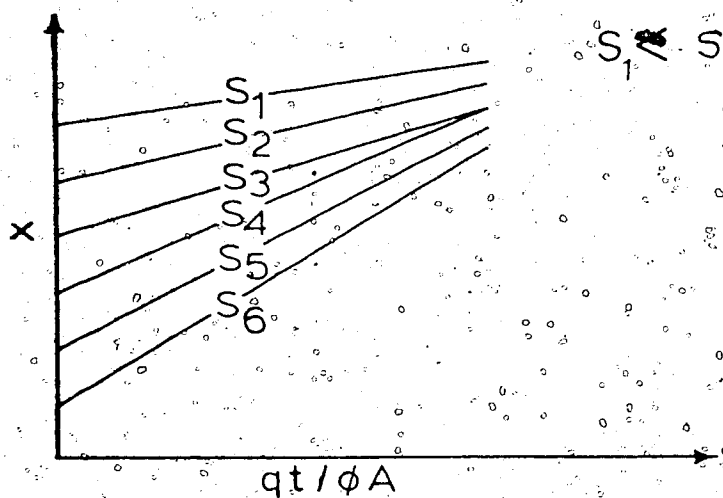


FIGURE II-3. SCHEMATIC REPRESENTATION OF SHOCK FORMATION.

In this case, contrary to the former one the planes of higher saturation move faster than the planes of lower saturation. At a certain time they will intersect each other causing the physically impossible multiple saturation case. This is equivalent to the moment when certain of the characteristics intersect and a shock or discontinuity in the saturation profile is formed.

The lower portion of the experimental S-type fractional flow curves is concave upward which causes the difficulty of shock formation. The experimental S-shaped curves are based on steady state relative permeability measurements. As thoroughly discussed in section I.2.2. the validity of these measurements in representing the real situation in displacement processes is at best questionable. This subject will be later referred to in this section.

The plane which can be easily studied experimentally is the plane of zero saturation. This plane corresponds with the tip of the longest finger. From Equation (11-26) and the foregoing discussion, it is important that a plot of the position of this plane,  $x_0$ , v.s.  $y_0$  (PA) must be a straight line. The slope of this line is,

$$\text{slope} = \frac{d x_0(S_w)}{d y_0(S_w)} = \frac{d x_0(S_w)}{d S_w} = \frac{d x_0}{d S_w} \Big|_{S_w = 0}$$

This would hold for water flood, polymer flood, as well as miscible floods.

The experimental work published by Bertram, et al. (58) verified the above

linearity prediction for a miscible displacement. They studied the effect

of distance displaced upon viscous finger length or frontal distortion, for

both open and packed models. They took three or four frames from the

16-mm movie film for each run which showed the front for three or four

different average positions in the model. By tracing the outline of the

front, they determined the mean frontal position from the integrated area

of the displacing fluid. Indeed, they converted the traced front to a

rectangular shape corresponding to the planar frontal shape. Next, they

divided the model width into 20 equal-width slices, or elements, and found

the mean frontal position for each element in the same way as before. The

distance between the mean frontal position of each element and the mean frontal

position of the whole width was taken as frontal distortion. The absolute

values of the frontal distortion in each of the 20 elements were arranged

from maximum to minimum and a number was assigned to each value of frontal

distortion. This number gave the percentage in the total front having

distortions equal to or less than the value of that frontal distortion.

A plot of frontal distortion as a function of mean frontal position revealed a linear behaviour. Therefore, a linear dependence of frontal distortion D, upon the mean frontal position or distance displaced was concluded. The line of "99.99% of front having distortion less than D corresponds to the plane of zero saturation in the present study.

The experimental data indicating the linear progress of the zero saturation plane will be presented in Chapter V. As will be observed in Figures (V-3) to (V-18) the linearity holds for Newtonian as well as non-Newtonian displacing fluids.

The advancing rate of other saturation planes cannot be determined as easily as the zero saturation plane. Therefore some theoretical analysis, based on the assumption that the local behaviour of the bed could be characterized by an average viscosity for a mixture of two immiscible fluids, was undertaken. This made it possible to derive the advancing rate of any saturation plane. The advancing rate of the different saturation planes was ultimately linked to the breakthrough recovery which can be easily checked by the experimental data.

The dynamic relative permeability functions derived from the present analytical treatment are given by Equations (I-47, 48). It should be noticed that the viscosity ratio dependence of the dynamic relative permeability functions, is stronger than the dependence shown by published experimental relative permeabilities. In the present analysis dynamic relative permeability is nothing more than the relative flow areas occupied by each of the phases. It has already been mentioned in section (II-4) that in the usual experiment for determinations of relative permeability by simultaneous, steady-state flow of the two fluids, strong channeling was observed when the viscosity ratio was

significantly different from unity. Noting that when the flow area of the wetting phase decreases because of channeling it is possible that the compensating effects of area change in the non-wetting phase may mask the dependence of relative permeability on viscosity ratio. A further consequence would be that the usual relative permeability is not very sensitive to the details of the flow pattern. This can be demonstrated by the following example. Consider a porous bed in which we are conducting the usual experiment to measure relative permeability by measuring pressure drop at steady state for simultaneous flow of oil and water. Suppose that the flow ratio is unity and half of the bed is occupied by the water, so that there is no channeling. The total dissipation loss in the bed,  $E_v$ , is the sum of losses in the oil and water phases and is given by,

$$E_v = E_{v,w} + E_{v,o} \quad (\text{II-72})$$

If for example, the viscosity of oil is ten times larger than water,

$$E_{v,o} = 10 E_{v,w} \quad (\text{II-73})$$

or,

$$E_v = 11 E_{v,w} \quad (\text{II-74})$$

Now, supposing that instead of the ideal case, there is significant channeling so the water saturation is not equal to its fractional flow rate but less than that. For example, assume that water occupies half of the former area. In this case,

$$E'_v = E'_{v,w} + E'_{v,o} \quad (\text{II-75})$$

where prime indicates the new situation.

However by proportion of areas and viscosities

$$E_{v,w} = 2 E_{v,w} \quad (\text{II-76})$$

$$E_{v,o} = \frac{2}{3} E_{v,o} = \frac{20}{3} E_{v,w} \quad (\text{II-77})$$

From Equations (II-75 to 77),

$$E_v = \frac{26}{3} E_v \quad (\text{II-78})$$

or,

$$\frac{E_v}{E_v} = \frac{33}{26} \quad (\text{II-79})$$

Since total friction dissipation is proportional to measured pressure drop of the bed,

$$\frac{\Delta P_T}{\Delta P'_T} = \frac{33}{26} \quad (\text{II-79a})$$

which is also just the ratio in relative permeability that would be calculated. This is, although the water saturation has decreased by half, the change in relative permeability would be approximately twenty percent. It is a straight forward algebraic exercise to show that this observation holds to the limit of severe channeling or zero flow area of the water. This simple calculation reveals that the experimental relative permeabilities which are based on pressure drop measurement are expected to be somewhat insensitive toward the relative area occupied by the channeling fluid. Since the severity of channeling is in turn related to the viscosity ratio the example suggests a similarly weak dependence on viscosity ratio. Thus the qualitative difference cited above between the dynamic and conventional relative permeabilities may be a consequence not only of definition but also because of difference in

the experiments which are performed in their determination.

For polymer flood additional uncertainty arises due to the fact that the same pair of relative permeability curves as in the case of water flood have been applied (42-45, 56). Based on the conclusion derived from the present analysis, both displacing and displaced phase dynamic relative permeabilities change if either phase is changed. Therefore, by substituting the polymer solution for water as the displacing phase the former dynamic relative permeability curves do not represent the new situation.

The advantage of the present analysis lies in the fact that the analysis can be easily modified to the polymer flood assuming that the power-law model describes the behaviour of the fluid. Due to the shear dependency of the polymer solution its apparent viscosity changes with saturation. The apparent viscosity at each plane of saturation is given by Equation (II-61) which clearly shows the error involved in assuming a single apparent viscosity applicable all over the bed. This is particularly important in the case that saturation distribution covers a significant portion of the bed. The latter situation is encountered when viscous fingering is severe.

Breakthrough recovery for a linear polymer flood is given by Equation (II-63). It is understood from Equation (II-63) that the recovery efficiency depends not only on the viscosity level of the polymer solution but also upon the power-law parameter  $n$ . Larger  $n$  produces larger recovery. Therefore, a Newtonian fluid,  $n = 1$ , at an equivalent viscosity ratio defined by Equation (II-64), is expected to yield higher recovery than a polymer solution. It is well known that the polymer with higher molecular weight produces smaller  $n$  and larger elasticity effect. Therefore, by

choosing two different molecular weights of polymers and adjusting their concentration to obtain the same approximate viscosity level, one could check the effect of the polymer solution elasticity on the displacement recovery. If the elastic behaviour of the polymer solution has any significant effect on the displacement process, the experimental recovery efficiency of the higher molecular weight polymer solution would deviate from the prediction of Equation (II-63) which is based on purely viscous behaviour of the polymer solution.

## CHAPTER III

### SCALING LAWS

#### III.1 General Scaling Laws

Scaling laws can be obtained either from dimensional analysis or from a more mathematical approach called inspectional analysis. Dimensional analysis and physical similarity have been used in other fields for a long time and the pertinent theory is adequately given in the literature (46 - 49). In 1941, Leverett, et al. (50) applied dimensional analysis to the two phase flow displacement and studied the similarity criteria for radial and also linear displacement. Following Leverett's work, Engelberts et al. (2) studied the scaling laws of linear flow systems in more detail. They believed in five important scaling factors, two of which were considered to guarantee the geometrical similarity such as length and inclination of the bed and the rest which are given below were considered to preserve the physical similarity,

$$\frac{\mu_o}{\mu_w}, \quad \frac{\Delta \rho g K}{U \mu_w}, \quad \frac{\Delta \rho g L \sqrt{K}}{\sigma \cos \alpha}$$

In these groups,  $\Delta \rho$  is the density difference between water and oil and  $\alpha$ , the contact angle of the oil-water-solid system. Their experimental studies showed that breakthrough recoveries depended on most of the factors except  $\Delta \rho g L \sqrt{K} / \sigma \cos \alpha$ . They concluded that capillary forces were not expected to have substantial effects on water drive processes under field conditions.

A continuation and extension of Engelberts et al.'s experimental work was later undertaken by Croes, et al (51). Rapoport and Leas (20)

reported the results of scaled experiments on waterflooding and brought up a discussion of the stabilized zone which was mentioned in section (I-2.2). They revealed that a linear flood can be characterized by means of the scaling factor  $U L u_w$ . Later, Rapoport (52) obtained a more general form of scaling coefficient by including the water-oil interfacial tension,  $\sigma$ , and the contact angle,  $\alpha$ . His treatment was based on the more theoretical inspectional analysis. He summarized the conditions required for proper modelling of water-oil flow processes as:

1. Geometrical similarity such as boundaries, well distribution, well penetration, etc.
2. Initial distribution as well as the succession and distribution of operations (water injections and all oil withdrawals) must be the same for model and prototype.
3. Relative permeability functions and the oil-water viscosity ratio must be the same for model and prototype.
4. Capillary pressure functions applying to model and prototype must be related to each other either by direct proportionality or by a general linear transformation.
5. The ratio of gravitational gradient to capillary pressure gradient must be the same for model and prototype.
6. The ratio of capillary pressure gradient to flowing pressure gradient must be the same for model and prototype.

In 1956, Geertsma, et al. (53) combined the two methods of dimensional and inspectional analysis and applied the scaling criteria to three types of displacement namely cold water drive, hot water drive and

solvent injection. Their mobility groups to be considered for a solution drive were reported to be:

$$\frac{D_w}{D_o} = \frac{k_{o,w}}{k_{w,o}} \cdot \frac{\mu_{o,w}}{\mu_{w,o}} \cdot \frac{C_{o,w}}{C_{w,o}} \cdot \frac{\rho_{w,o}}{\rho_{o,w}}$$

In view of the practically negligible influence of mineral heterogeneity on the significant, therefore, the mobility group can be left out of account. The latter scaling factors were applied by Van Meeteren to develop a transparent three-dimensional model for studying the mechanism of solution processes in oil reservoirs.

So far the relative permeability and capillary pressure relations have been considered to be the same functions of saturation in the model of the prototype. Perkins, et al., (34) related the relative permeability and saturation in a way to permit the model to have different relative permeability and capillary pressure relations. Their new equations for saturation and relative permeability terms were:

$$S_{w,r} = S_{w,ro} + S_{w,ro}^2 / (1 - S_{w,ro}) \cdot S_{w,ro}^{1/2}$$

$$k_{r,w} = \frac{k_w}{k_{w,ro}}$$

$$k_{r,o} = \frac{k_o}{k_{o,ro}}$$

where,  $S_{w,ro}$  is the residual oil saturation,  $S_{w,cw}$ , the connate water saturation,  $k_{w,ro}$ , the specific permeability to water at the residual oil saturation and  $k_{o,cw}$  is the specific permeability to oil at the connate-water saturation.

The dimensionless parameters produced from the equation of continuity combined with Darcy's law are given below,

$$\frac{L_2}{L_1}, \frac{L_3}{L_1}, \frac{K_w, ro \mu_o}{K_o, cw \mu_w}, \frac{\sigma K_w, ro}{U \mu_w L_1} (\frac{\phi}{K})^{1/2} \text{ and}$$

$$\frac{K_w, ro g \Delta \rho L_3}{U \mu_w L_1}$$

where  $L_1$ ,  $L_2$  and  $L_3$  are some characteristic lengths along the three rectangular Cartesian coordinates.

The principal difference between the scaling criteria outlined by Perkins, et al. (54) and those formerly mentioned lies in the modified definitions of dimensionless saturations and relative permeabilities. It is understood that in this treatment mobility ratio appears to be a scaling criterion instead of viscosity ratio.

Nielsen, et al. (55) numerically studied the performance of a hypothetical gas reservoir subject to water drive and its scaled model to find the effect of unscalable variables such as exact boundary conditions or capillary and relative permeability curves. They revealed that the performance of the reservoir and model was very sensitive to the shape of the relative permeability and capillary curves. However, the situation did not appear to be that serious for the boundary conditions.

### III.2 Scaling Laws for Unstable Immiscible Displacement

In the case of studying the fingering phenomenon, some other scaling factors seem to be inevitable. During their theoretical and experimental investigation of unstable immiscible displacement, Chuoke, et al. (3) revealed that a properly scaled model for the study of the viscous

fingering phenomenon not only should satisfy the conventional similarity groups but also its greatest lateral dimension  $d$ , must be greater than a critical wave length,  $\lambda_c$ . They argued that if  $\lambda_c$  exceeds the greatest lateral dimension,  $d$ , of the model the displacement would be stable and lead to higher recoveries than in the reservoir. Therefore, they included the following additional scaling criteria,

$$\left(\frac{\lambda_m}{d}\right)^2 \text{ or } \left[\left(\frac{\mu_o}{k_o} - \frac{\mu_w}{k_w}\right) \left(U - U_c\right)\right] \frac{\sigma}{d^2}$$

This in general, need not be exactly the same in both model and prototype. If  $\lambda_c/d$  is either large or small compared to unity in both model and prototype, either no fingers or a large number of fingers will appear in both and the relative effects on behaviour will be the same. Thus only if  $\lambda_c/d$  is approximately unity would exact scaling be required. The new scaling criterion proposed by Chuoke, et al. has been recently supported by Hagoort (32) via an energy approach in studying instability of water drives in water-wet reservoirs.

Chuoke, et al's analysis was based on a parallel plate model and was challenged by Rachford (8) on the basis that the performance of such floods might not properly represent waterfloods in strongly water-wet porous systems. Rachford introduced a transition zone behind the flood and carried on a first order analysis of the perturbed displacement equations numerically. He contradicts the scaling requirement of Chuoke, et al. (3) and stated that no additional scaling requirements appeared necessary to insure proper treatment of the instability. He believed that

since in any rigorously scaled model the same dimensionless differential equation describing the prototype, is applicable, the analysis should give identical stability predictions for model and prototype.

From the higher order approximation of the instability theory undertaken by Outmans (10) some different criteria for similarity were deduced. He distinguished two different cases depending on whether the gravity and interfacial tension were negligible. In the case of the gravity and interfacial tension being negligible, the model and prototype not only must be kinematically similar but also the initial disturbance should be identical. This criterion cannot be met unless the permeability fluctuations starting the fingers have been scaled down. He, therefore, concluded that this type of model study was not a reliable method for evaluating sweep efficiency in the reservoir. However, in the case when the gravity and interfacial tension were significant a complete similarity required equality of a dimensionless group somewhat similar to the Weber number in hydrodynamics (72).

### III.3 Application of the Scaling Laws

For the purpose of the present study, in which gravity and capillary effects are assumed to be negligible, it is concluded that the only criterion to be considered from the general scaling laws is that the flow regime must be in laminar region. That is, Darcy's law must describe the flow rate-pressure drop behavior. The scaling laws for fingering phenomenon, contrary to the kinematic similarity, have not been well established. However, the fact that the critical wave length must be smaller than the width of the bed seems to be easy and safe to consider. It is emphasized that this scaling criterion has been predicted from the linear theory (3) as well as an energy approach (32). Therefore, a

stronger ground is furnished to believe its validity.

The width of the packed bed employed in the present investigation was one foot. A multiple number of fingers even at low flow rates were observed in most cases. Therefore, it is safe to claim that the ratio of the bed width to the critical wave length was large enough to ensure instabilities were not influenced by an inadequate bed width.

## CHAPTER IV

## EXPERIMENTAL EQUIPMENT AND PROCEDURE

IV.1 Model Porous Media

Four different beds were used during the present investigation. The first two were composed of regularly spaced matrices of 6 mm diameter glass rods in a triangular arrangement. Figure (IV-1) illustrates a unit cell of triangular pitch. The last two beds were packed with different sized beads. The multi-cylinder matrices produced two-dimensional flow while the packed beads provided three dimensional flow at the microscopic level.

Displacement tests were performed in the second multi-cylinder matrix (Figure IV-3) and the motion pictures obtained were used to show the existence of a linear advance rate of the frontal plane or plane of zero water saturation. Results were identical to those presented in Figures (V-3) to (V-18). However, no pressure drop measurements were performed on this kind of geometry.

Since the packed beads are presumably a better simulation of flow in real porous media except for qualitative description and completeness, only the data points of the packed beads will be analysed and presented here.

IV.1.1 Multi-cylinder Matrices

The first multi-cylinder matrix was exactly the same one that was used in a former study (34). The cylinders were contained in a rectangular channel of inside cross section 5.2 cm x 6.5 cm - Figure (IV-2). The model contained 40 rows of cylinders with each row alternatively 9 or 10 cylinders in width. This arrangement left a large space near the wall in

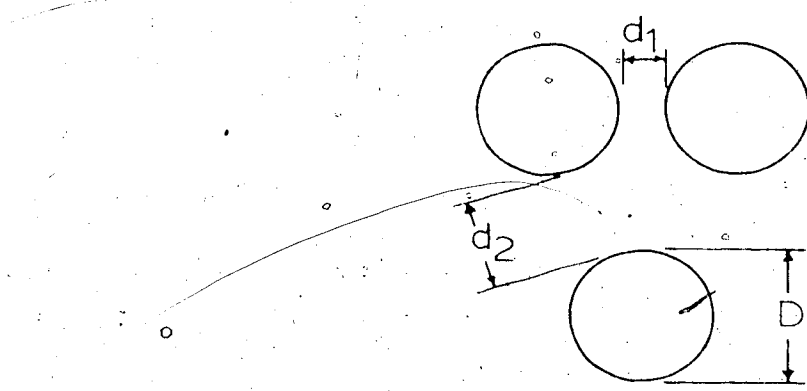


FIGURE IV-1 TRIANGULAR-PITCH UNIT  
CELL

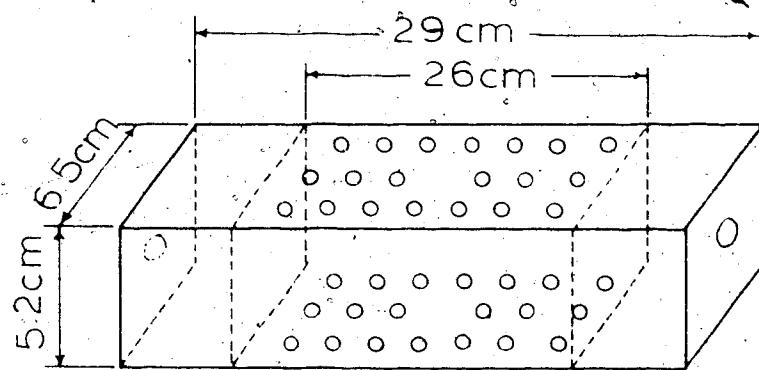
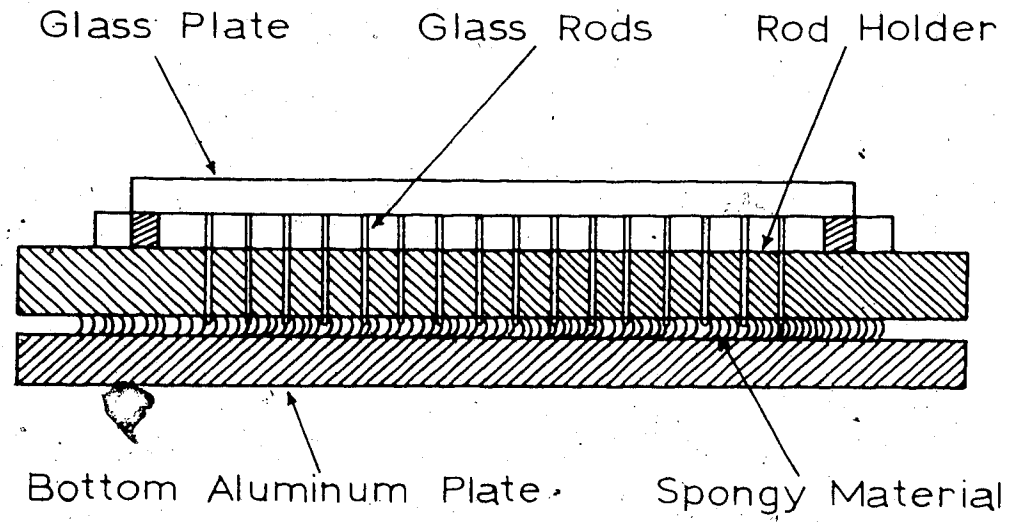


FIGURE IV-2 MULTI-CYLINDER MATRIX--  
BED NO.1 WITH AN  
ARTIFICIAL LARGE OPENING  
AT THE CENTER

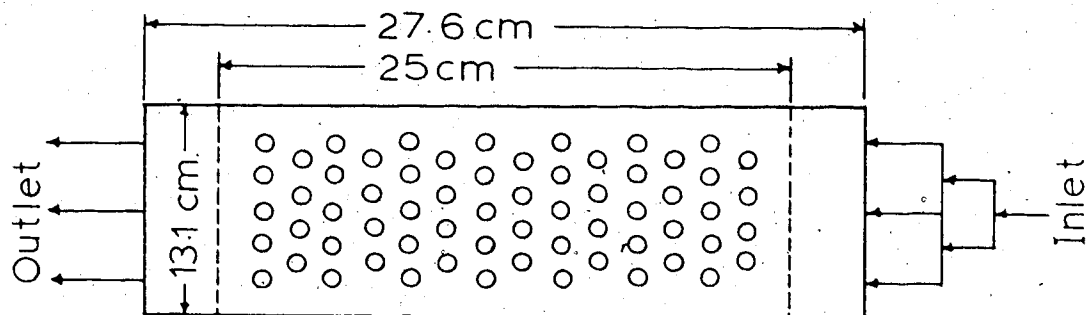
each row with nine cylinders. To eliminate by-pass flow at the walls and to effect uniform resistance of each row, the 3 mm diameter cylinders were placed next to the wall in each of these rows. The minimum and maximum pore openings, shown as  $d_1$  and  $d_2$  in Figure (IV-1), were approximately 0.3 and 1 mm, respectively. The volumetric porosity of the bed was 0.30. In this work the middle rod of row No. 16 was removed to create an artificial large opening at the center. This large opening was produced to study the effect of a large heterogeneity on incipient fingers.

The second multi-cylinder matrix was based on the same design as the first one but of different dimensions. In this case the cylinders were contained in a rectangular channel of inside cross section 1.4 cm x 15.1 cm x 3.8 cm, as shown in Figure (IV-3). The shorter depth was chosen to eliminate fingering at different depths of the bed. The top and the side wall facing the light source were made of 1/2" clear glass plate. To insure that the tops of the rods were touching the top glass plate, a 1/2 cm sheet of spongy material was placed beneath the glass rods. The bottom plate was made of 1/4" Aluminipor plate. A one-inch thick aluminium plate with necessary holes was placed on the top of the spongy material and served to hold the cylinders in place.

To minimize inlet and outlet disturbances, two flow distributors 2.5 cm apart were placed before and after the rows of cylinders. The first flow distributor was located 1.3 cm above the inlet and the same distance was kept between the second distributor and the outlet. The model contained 41 rows of cylinders, each row alternatively having 19 or 20 cylinders across. The minimum and maximum pore openings were as before, 0.3 and 1 mm respectively. The volumetric porosity,  $\phi$ , of the bed was 0.30. As mentioned before, to eliminate the by-pass channels, smaller cylinders of 3 mm diameter



SIDE VIEW



TOP VIEW

FIGURE IV-3 SCHEMATIC OF BED NO. 2

were inserted at the large openings next to the walls.

#### IV.1.2 Packed Glass Beads Model

As shown by Figure (IV-4) the model was made up of two transparent plates of 3/4 in thick UPVC (Unplasticized Polyvinyl Chloride) with dimensions 18 inches wide by 24 inches long. The plates were spaced 1/2 inch apart. The internal dimensions of the packed region were 43.2 - cm wide x 53.5 - cm long x 1.3 - cm thick. To obtain a uniform injection front, the injection head was composed of three inlets. In addition a flow distributor was placed 1 inch downstream of the injection head. This distributor was made up of 1/16 - in thick brass plate with holes distributed as shown in Figure (IV-5). A second distributor consisting of two brass plates (IV-6) holding a 30 - mesh stainless steel screen was placed 1 $\frac{1}{2}$  inches downstream from the first. The beads were resting on this screen. To eliminate fluidization and to maintain uniform flow distribution to the end of the bed a similar rectangular 30 - mesh screen was placed at the top of the packed bed just before the outlet head. The outlet head was composed of three outlets to further assist in maintaining uniform flow. The distance between the outlets and the screen was 1/2 inch.

To eliminate bulging due to pressure within the bed the back and front plates were supported by six 2 - inch wide steel bars. These bars, positioned laterally pressed two vertical bars against the surface of the back and front UPVC plates - refer to Figure (IV-4).

Oil was pumped into the bed through five inlets located on the surface of the front UPVC plate and between the first and the second distributor.

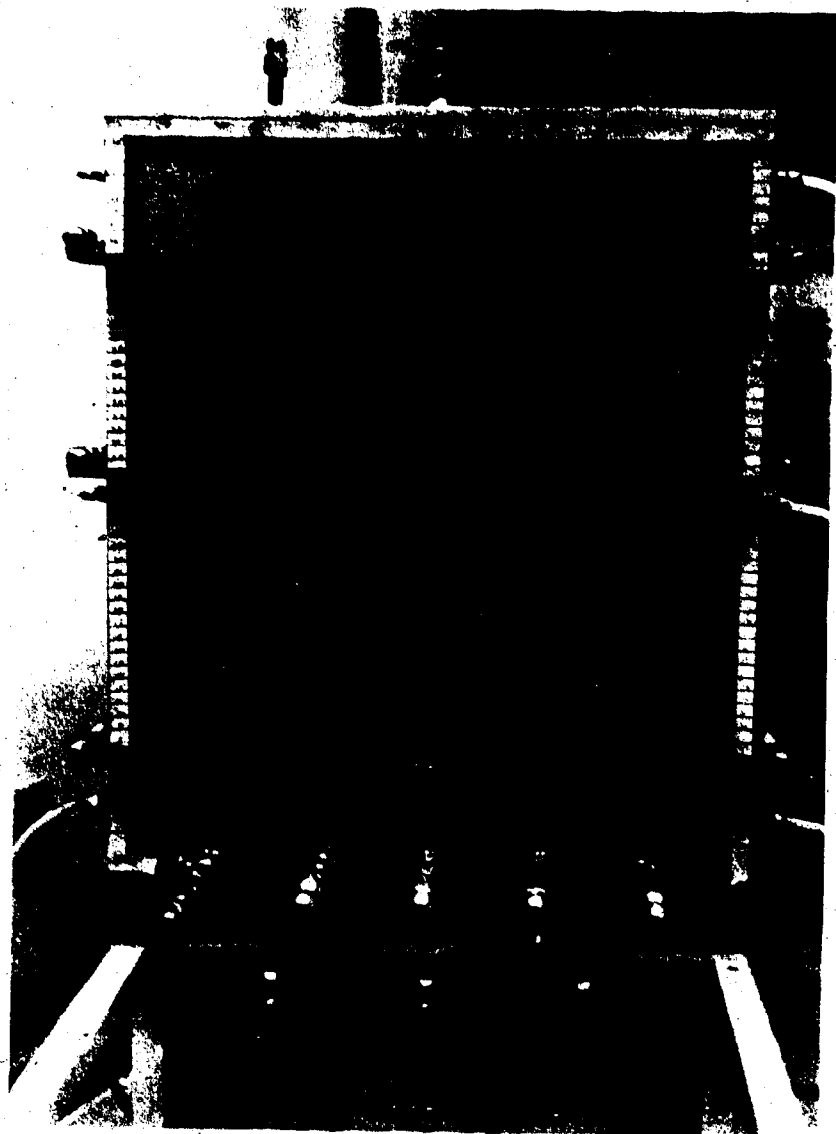


FIGURE IV-4 PACKED BEADS MODEL

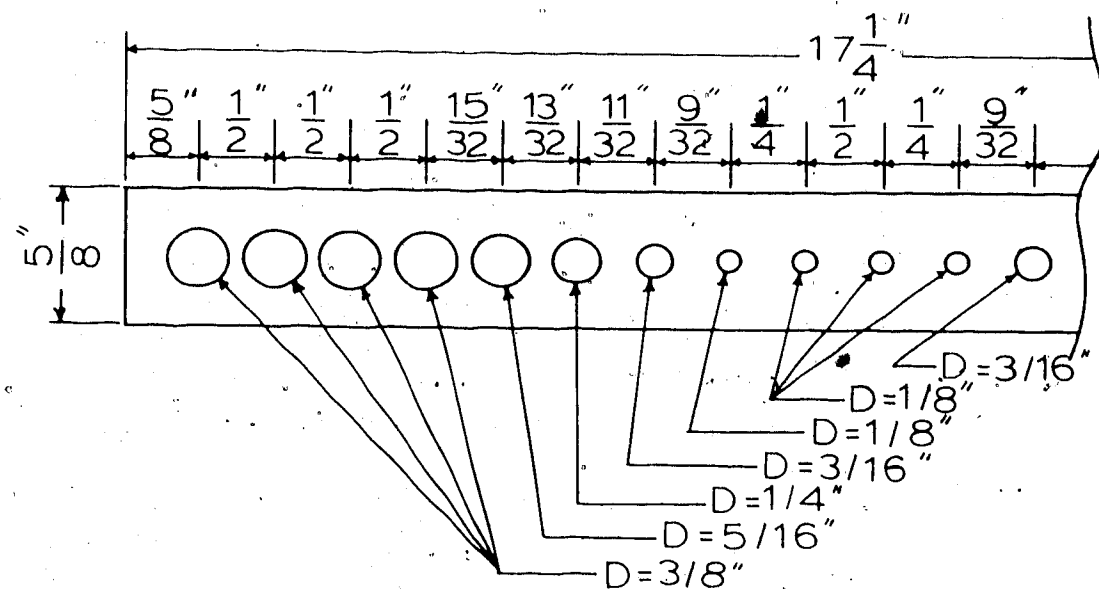


FIGURE IV-5 FLOW DISTRIBUTOR NO.1

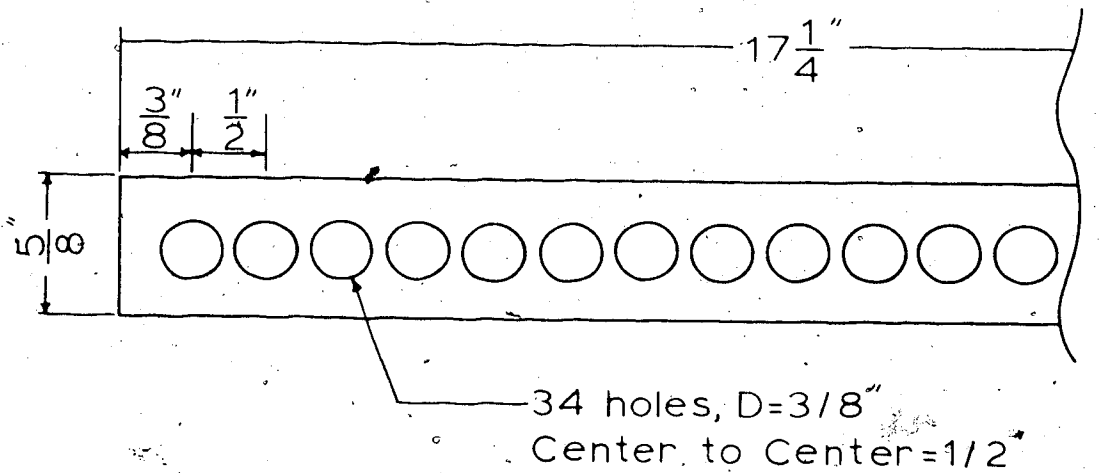


FIGURE IV-6 FLOW DISTRIBUTOR AND SCREEN HOLDER

To ensure uniform packing of the beads the following procedure was used to fill the bed. The bed was positioned vertically with the outlet head unattached. Three vibrators were connected to the body of the bed. Then beads were poured from the top while the vibrators were on. Approximately after every inch of beads had been added a T-shaped bar was used to tap the beads from the top. After the bed was filled, the outlet head was attached and high flow rate water from the domestic tap was run from the top of the bed for 24 hours while the vibrators were on. The outlet head was then opened and additional beads were added to completely fill the bed.

As mentioned earlier two sizes of beads were studied. The larger bead size was  $0.47 \pm 0.05$  cm diameter and the smaller was  $0.15 \pm 0.04$  cm diameter. The smaller size beads were screened through 14 and 9 mesh sieves. The volumetric porosities,  $\phi$ , of the beds were obtained by direct measurement of the amount of fluid necessary to fill the void volumes. To do this the Instron was set at a constant low flow rate,  $q$ , then the time  $t$ , required to fill the packed region of the bed was measured by a stopwatch. Therefore,

$$\phi = \frac{qt}{V}$$

where,  $V$  is the total internal volume of the box. The measurement was performed several times and at different flow rates. The average volumetric porosity obtained for the beds were calculated to be 0.42 and 0.39 for the large and small beads respectively with reproducibility  $\pm 0.02$ .

#### IV.2 Experimental Fluids

Dow Corning 200 Fluid was used as the oil phase for all of the experiments. Dow Corning 200 Fluid is the trade mark of a clear silicone liquid available in viscosities from 1 to 100,000 centistokes. Only three ranges of viscosity were used for the present study namely, 100, 1000, and 12,500 cs. Their specific gravities were 0.96, 0.971 and 0.975 respectively. Oil was usually separated from the water phase by decantation and recycled.

Water, different concentrations of glycerol, and polymer solutions were used as the displacing phase. The displacing fluids were coloured with a small amount of red food colouring to visualize the fingering pattern and enable photographs to be obtained. The displaced fluid was colourless.

The polymer used was a partially hydrolyzed polyacrylamide product of Dow Chemical Co., trade name Separan AP-273. Its solution in water shows effects of elasticity. Domestic tap water was used for preparation of polymer solutions and care was taken to avoid mechanical degradation of the polymer molecules by stirring the solution very gently.

To compare with Separan AP-273 several additional runs were made using a less elastic Pusher 500 solution. Pusher 500 is also a partially hydrolyzed polyacrylamide with smaller molecular weight than Separan AP-273. Rheological properties of the experimental fluids are reported in Appendix A.

#### IV.3 Pumping

A constant-rate Zenith Gear pump driven by a variable speed transmission was used for initially filling the bed with oil phase. Filling rate was very slow, at a rate of  $0.7 \text{ cm}^3 \text{ sec}^{-1}$  to eliminate the

possibility of trapping air bubbles in the porous bed. The oil phase was introduced into the bed from the five taps installed in the transparent plate just below the packed region and above the injection head. The displacing phase was introduced into the bed from the injection head by using a single-acting, 6 - inch I.D. X 20 - inch hydraulic cylinder powered by an Instron model TTEM tester. In displacement tests this allowed flows from  $0.159 \text{ cm}^3 \text{ sec}^{-1}$  to  $15.9 \text{ cm}^3 \text{ sec}^{-1}$ .

The hydraulic cylinder was evacuated each time before filling with the experimental fluid. This eliminated the air pocket in the cylinder so that an instantaneous steady state flow from the Instron could be obtained.

#### IV.4 Motion Picture Photography

A slow motion Beaulieu movie camera with 25 mm focal length lens was used to record the progress of each displacement run on 16 - mm coloured movie film. Usually the minimum speed of the camera which was 2.1 frames/sec was used. In the case of low flow rates the camera was stopped periodically for a known length of time as measured by a stop watch. The camera was placed at a distance approximately 2 meters from the vertically positioned bed.

A light source was located behind the bed. The light source was composed of three 18 - inch 32 watts fluorescent lamps type BL 118. The lamps were positioned in a 66 - cm x 48 - cm box made up of 22 gauge galvanized sheets. To obtain as much light as possible a 46 - cm x 61 - cm mirror was placed behind the lamps.

#### IV.5 Film Scanning

A Wooster Automatic Recording Microdensitometer, Mark II, was used for scanning the films to obtain saturation profiles. This

instrument was coupled to a Hewlett-Packard Strip Chart Recorder with an Integrator which allowed a continuous measurement of the light intensity. The Microdensitometer allows determination of concentration of the coloured material by measuring the intensity of light transmitted to a photocell.

The necessary optical adjustments were performed according to the instruction pamphlet supplied with the equipment. These included the adjustment of the microscopes and prisms so that the light beam passing through the slit plates fell onto the same region of the sensitive surface of the photocell. The glass film-carrying plate was set parallel to the instrument rails and the desired wedge having suitable gradient was chosen and inserted into the wedge carriage. The proper choice of a wedge is the wedge which has a minimum density just less than the minimum density of the film under test and a maximum density just greater than that of the film.

To increase the amount of light falling on the film and wedge, lenses of 50 mm focal length were inserted under the film and wedge. The lens holders had a pinhole stop to reduce the effects of double scatter or to increase resolution.

To allow scanning in any direction, the glass film - carrying plate was supported on two carriages which provided two perpendicular movements of the film. The position of the carriages could be read from a millimeter scale.

The present experimental work was not originally performed for the purpose of the scanning. Consequently, one of the major difficulties was the fact that the density of the colour of different batch solutions was not the same. Therefore, measurement of the diffused light or saturation had to be performed on a comparison basis.

Two frames of each displacement run were chosen: one before flooding or when the bed was full of clean oil, and the other at breakthrough. The desired frames were converted into 35 mm negative black-and-white slides for the purpose of scanning. The positions of the bars on the frame were used to locate positions within the bed. Scanning along several lines perpendicular to the flow direction was performed at the same position on each frame. The amount of coloured material encountered along a line was registered as a number of counts by the recorder. The number of counts after flooding were subtracted from the counts before flooding to obtain the net number of counts due to flooding. The necessary calculations to obtain the saturation profile are given in Appendix E.6.

The speed of scanning was 9.6 mm/min and the strip chart was run at a speed of 1 in/min.

#### IV.6° Pressure Drop Measurement

Three pressure taps were located on each side wall of the bed. The pressure taps were 24.5 cm apart. Pressure drop measurement was performed by using Validyne DP 15 differential pressure transducers, manufactured by Validyne Engineering Corporation of Northridge, California. Diaphragm plates rated at 1, 5, and 20 psi were used depending upon the range of pressure drop encountered in the bed. A Model 7100 B Hewlett-Packard Strip Chart Recorder with two channels was used to continuously record the pressure signal of the transducers. The transducers were always positioned below the lowest pressure tap so that a constant static head was applied to both sides of the transducers.

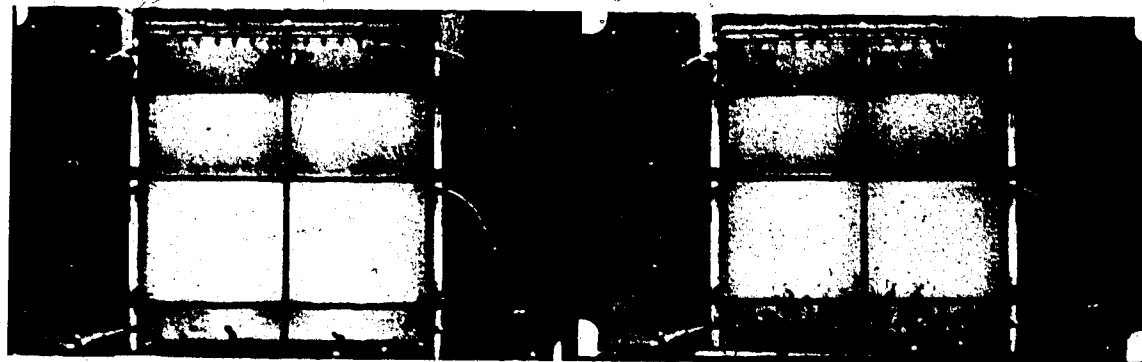
The calibration of transducers and the pertinent data points are presented in Appendix E.

#### IV.7 Procedure for Displacement Tests

The experimental bed was positioned vertically in all cases. Prior to a displacement test the bed was always cleaned and dried as described later. Therefore, all the displacement runs were at zero connate water saturation. The displacing phase was first injected from the injection head to a level just below the oil taps. Then the oil taps were opened and the oil was pumped in at a very small rate to eliminate trapping of air in the bed. In the case of the more viscous oil the filling period was as long as three or four hours. After the bed was filled the pressure taps were opened and the transducers zeroed. The Instron was set at a very small flow rate such as  $0.16 \text{ cm}^3 \text{ sec}^{-1}$  of displacing fluid to bring the displacing fluid-oil interface to a level just below the screen. The Instron was stopped and reset at the desired flow rate. Camera and lighting system were set and the experiment was then started.

The displacement test was usually stopped a few minutes after breakthrough. The recovered oil was collected in a cylinder and was allowed to separate from the water phase over night. The recovered oil was reused in subsequent experiments. After each run the bed was washed with water, varsol, alcohol, and again with varsol. After washing was completed, air was blown through the bed for several hours until the beads were dry.

To show the quality of the pictures taken, and also to illustrate the fingering configuration, two series of four frames are presented in Figures (IV-7) and (IV-8). The flow rate of Figure (IV-7) is  $1.59 \text{ cm}^3 \text{ sec}^{-1}$  and that of Figure (IV-8) is  $6.35 \text{ cm}^3 \text{ sec}^{-1}$ . These pictures are for water displacing 100 cs Dow Coming. Therefore, the oil-water viscosity ratio was 96.



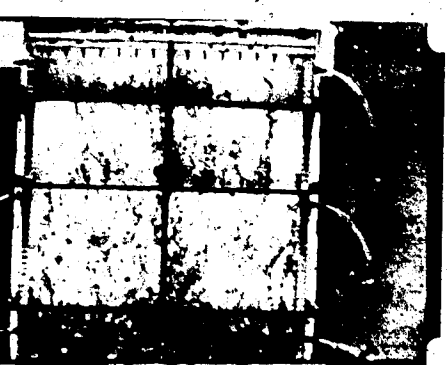
Photograph A  
 $t = 0$



Photograph B  
 $qt/\phi AL = 0.03$

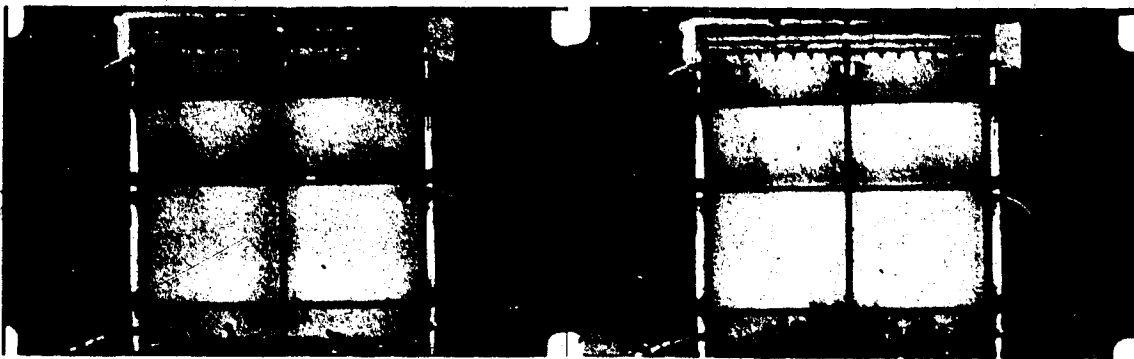


Photograph C  
 $qt/\phi AL = 0.11$



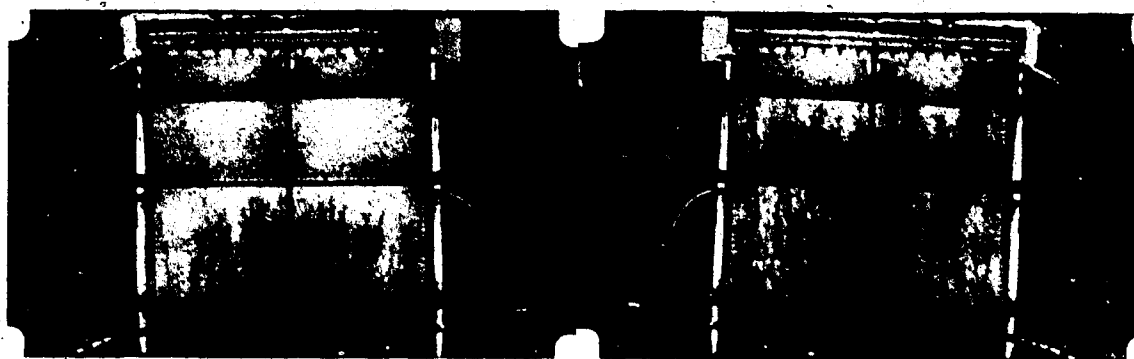
Photograph D  
Breakthrough

FIGURE IV-7 FINGERING IN A LINEAR  
WATERFLOOD, FLOW RATE  
 $1.59 \text{ cm}^3/\text{sec}$  (Roll No.11, Run No.3)



Photograph A  
 $t = 0$

Photograph B  
 $qt/\phi AL = 0.03$



Photograph C  
 $qt/\phi AL = 0.11$

Photograph D  
Breakthrough

FIGURE IV-8 FINGERING IN A LINEAR  
WATERFLOOD, FLOW RATE  
 $6.35 \text{ cm}^3/\text{sec}$  (Roll No.11; Run No.2)

Photograph A of each Figure was taken at  $t = 0$  in which the interface between oil and displacing fluid is completely flat. Photograph B which was taken at 0.03 pore volume injected reveals that the fingering pattern has already become established. Photograph C is included to present the growth of the fingers and show the advance rate of zero saturation plane which is discussed in sections VI.2. Finally Photgraph D was taken at breakthrough.

It can be seen from comparing Figures (IV-7) and (IV-8) that the width of fingers is reduced at the higher flow rate while the number of fingers is increased significantly which helps to achieve higher recovery. This point will be considered again in section VI.2

## CHAPTER V

## RESULTS

V.1 Pressure Drop

The measured pressure drop of a single phase Newtonian fluid of known viscosity was used to determine the absolute permeabilities of the beds. The data points of these pressure drop measurements are reported in Appendix F.3. The arithmetic average of the different runs in Table (F-3) and (F-4) has been chosen to approximate the permeabilities of the beds which were:

$$K = 1.97 \times 10^{-4} \text{ cm}^2 \text{ for the large beads}$$

$$K = 2.42 \times 10^{-5} \text{ cm}^2 \text{ for the small beads}$$

Figure (V-1) shows the friction factor vs. Reynolds number for Newtonian and non-Newtonian solutions. The equations used in this plot are equations (B-25, 27, 28). The Separan data points of this plot are recorded in Tables (F-5,6) and those of the Newtonian fluids in Tables (F-3,4).

The pressure drop of the mixed zone was determined by subtracting the calculated pressure drop of the unflooded portion from the total pressure drop measurement. The procedure and the pertinent data points are given in Appendix F.4; Table (F-7). Friction factor - Reynolds number behaviour for the mixed zone is shown in Figure (V-2) and the corresponding data points are given in Table (F-8). Reynolds numbers of the mixed zone are based on the effective viscosity defined by Equation (II-33). The equations of the friction factor and Reynolds number used in Figure (V-2) are the same as those of single phase flow with modification of the viscosity.

V.2 Frontal Plane Advance

The position of the zero saturation plane defined in section II-9 is

Legend For Figure V-1

Large Beads

- Tap Water
- △ 100 cs Dow Corning
- 12500 cs Dow Corning
- ▼ 0.05% Separan AP-273
- ★ 0.1% Separan AP-273

Small Beads

- Tap Water
- ▲ 100 cs Dow Corning
- 0.05% Separan AP-273
- ▼ 0.1% Separan AP-273
- ★ 0.2% Separan AP-273

— Equation (B-26)

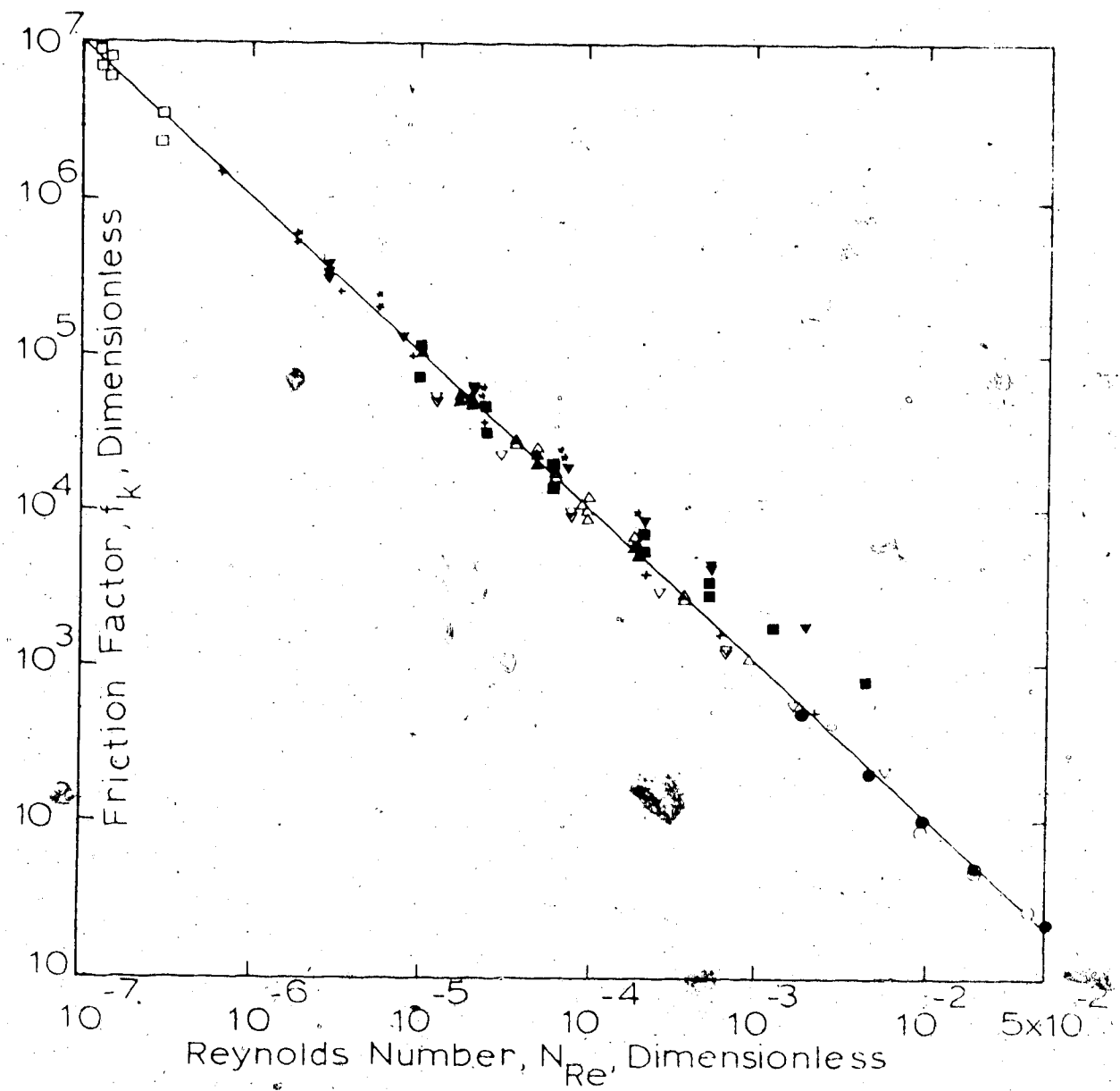


FIGURE V-1 FRICTION FACTOR VS. REYNOLDS NUMBER FOR SINGLE PHASE FLOW

Legend For Figure V-2

Large Beads

- Water Displacing 100 cs Dow Corning
- 0.05% Sep. Displacing 100 cs Dow Corning
- △ 0.1% Sep. Displacing 100 cs Dow Corning
- ▽ 0.2% Sep. Displacing 100 cs Dow Corning
- ◊ 0.2% Sep. Displacing 12500 cs Dow Corning

Small Beads

- Water Displacing 100 cs Dow Corning
- ★ Glycerol Solutions Displacing 100 cs Dow Corning
- 0.05% Sep. Displacing 100 cs Dow Corning
- ▲ 0.1% Sep. Displacing 100 cs Dow Corning
- † 0.2% Sep. Displacing 100 cs Dow Corning
- ▼ 0.1% Sep. Displacing 1000 cs Dow Corning
- ◆ 0.2% Pusher Displacing 1000 cs Dow Corning

— Equation (B-26)

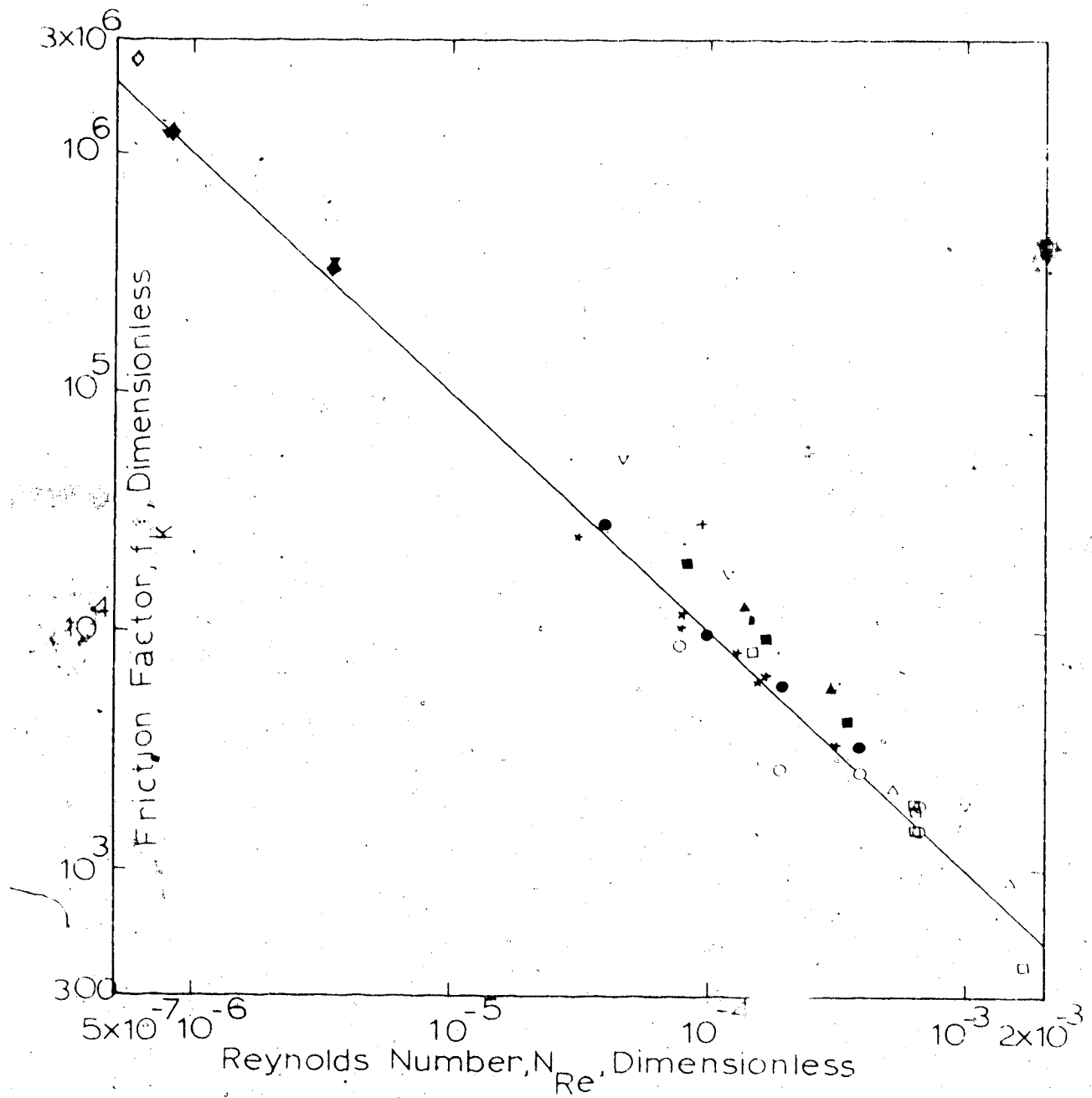


FIGURE V-2 FRICTION FACTOR VS. REYNOLDS  
NUMBER FOR DISPLACEMENT  
TESTS

plotted vs.  $qt/\Delta\phi$  in Figures (V-3) to (V-18). The pertinent data points and the specification of each run are given in Appendices F.1, 2.

### V.3 Volumetric Recovery Efficiency at Breakthrough

Volumetric recovery efficiency at breakthrough is plotted vs. viscosity ratio for the Newtonian flood in Figure (V-19). The theoretical curve predicted by Equation (II-52) and some experimental data points available in the literature are also included in the Figure.

Figure (V-20) presents the volumetric recovery efficiency at breakthrough for the polymer floods. Also, in the same Figure, the theoretical curves predicted by Equation (II-63) for  $n = 0.45, 0.58, 0.67$  and  $1.0$  are given. The theoretical curve of  $n = 1.0$ , which corresponds to the Newtonian flood is identical to that of Figure (V-19). Power law parameters  $n = 0.45, 0.58$ , and  $0.67$  correspond to  $0.2, 0.1$  and  $0.05$  percent Separan AP-273 solutions respectively. The pertinent data for Figures (V-19, 20) are presented in Tables (F-9 to 13).

### V.4 Saturation Profile

Figures (V-21) to (V-37) are plots of water saturation vs. position,  $x$ , in the bed. The pertinent data are presented in Tables (F-14, 15). The procedure to obtain the saturation profile from the data points of the film scanning is discussed in Appendix F.6. Figures (V-21) to (V-27) are for waterflood, (V-31) to (V-33) for glycerol solution flood and the remainder are for polymerfloods.

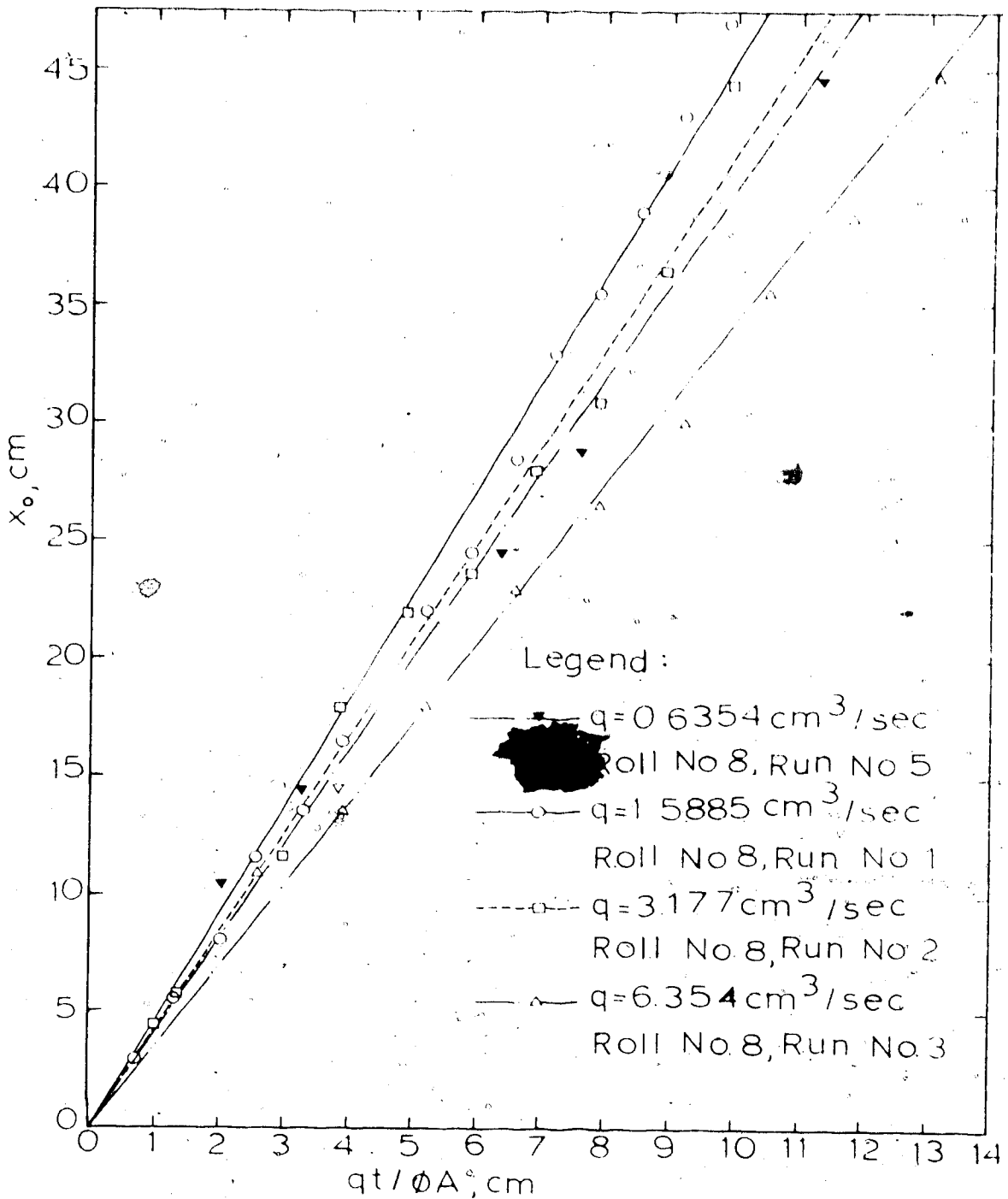


FIGURE V-3 WATER DISPLACING 100cs DOW  
CORNING, Large Beads

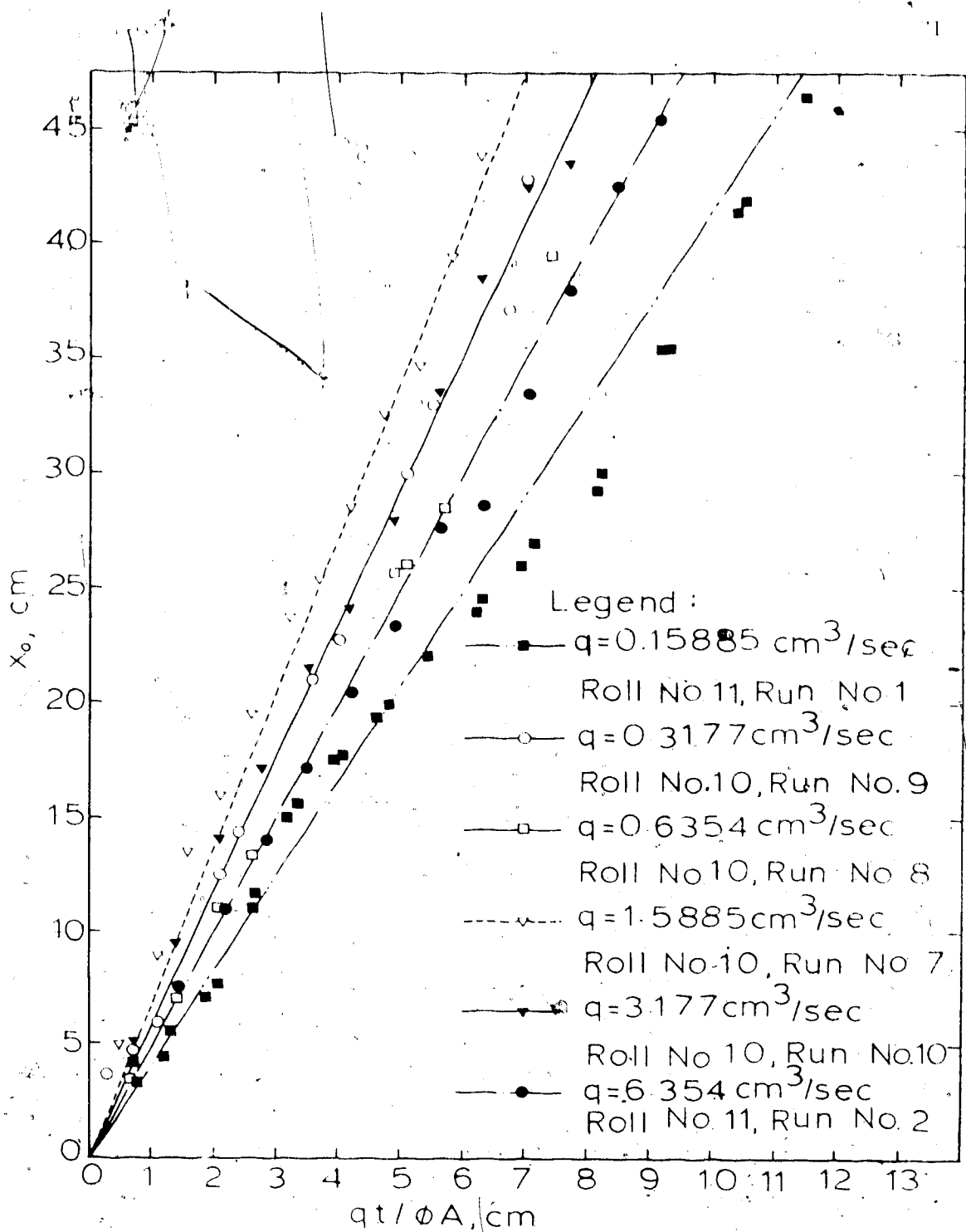


FIGURE V-4 WATER DISPLACING 100 cs DOW CORNING, Small Beads

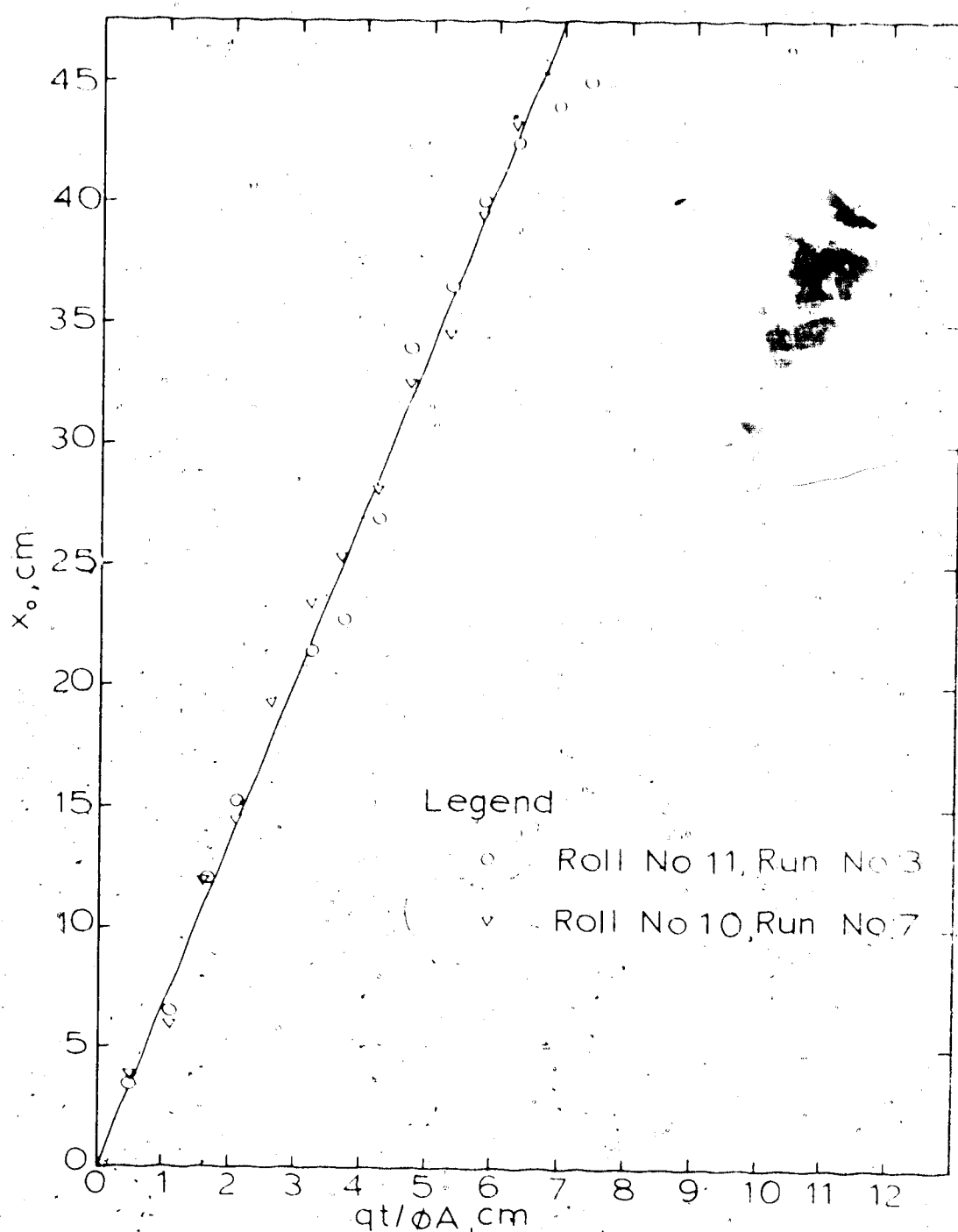


FIGURE V-5 WATER DISPLACING 100cs DOW CORNING,  $q = 1.5885 \text{ cm}^3/\text{sec}$

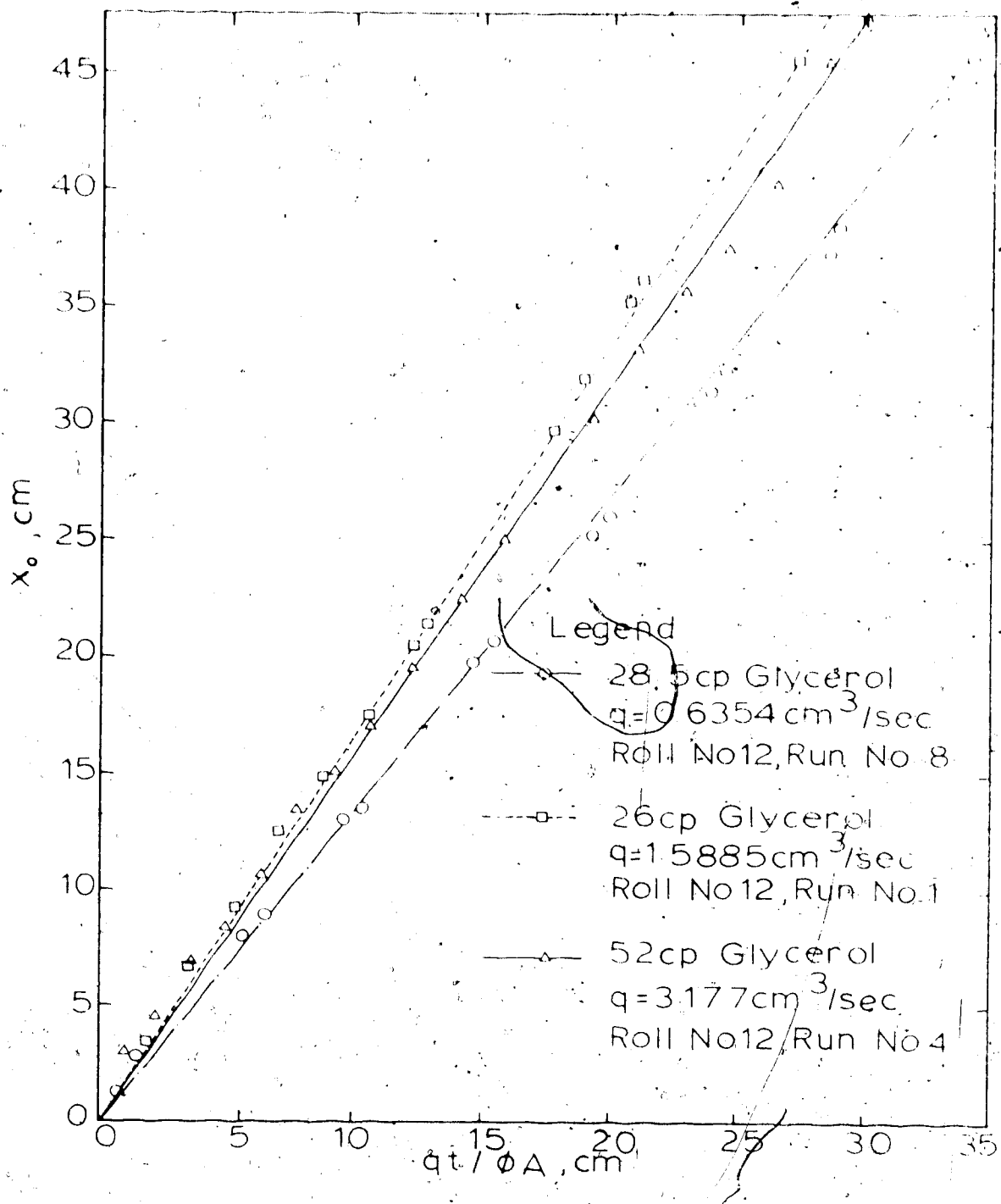


FIGURE V-6 GLYCEROL SOLUTIONS DISPLACING  
 100cs DOW CORNING, Small Beads.

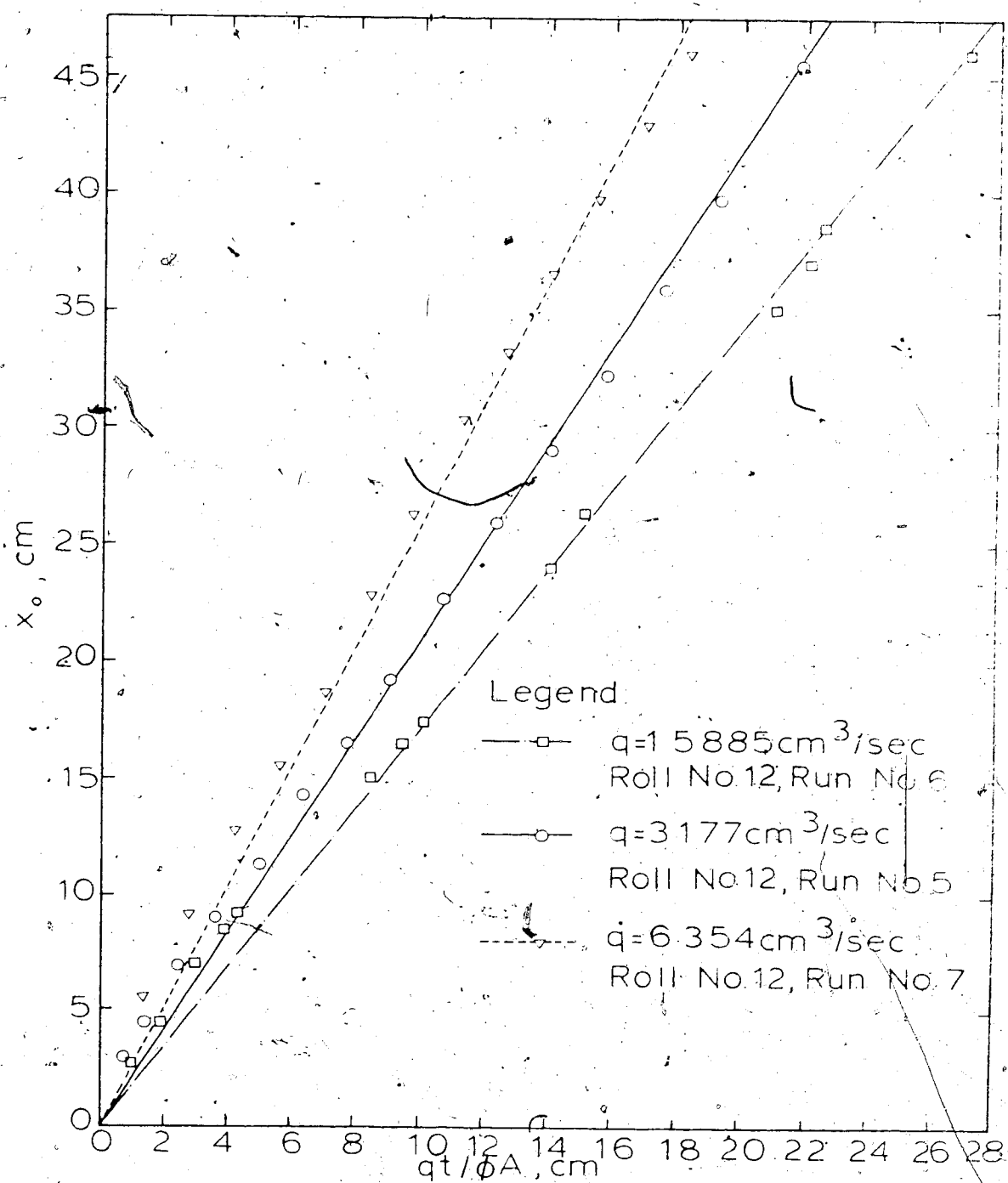


FIGURE V-7 25cp GLYCEROL SOLUTION  
DISPLACING 100cs DOW CORNING,  
Small Beads.

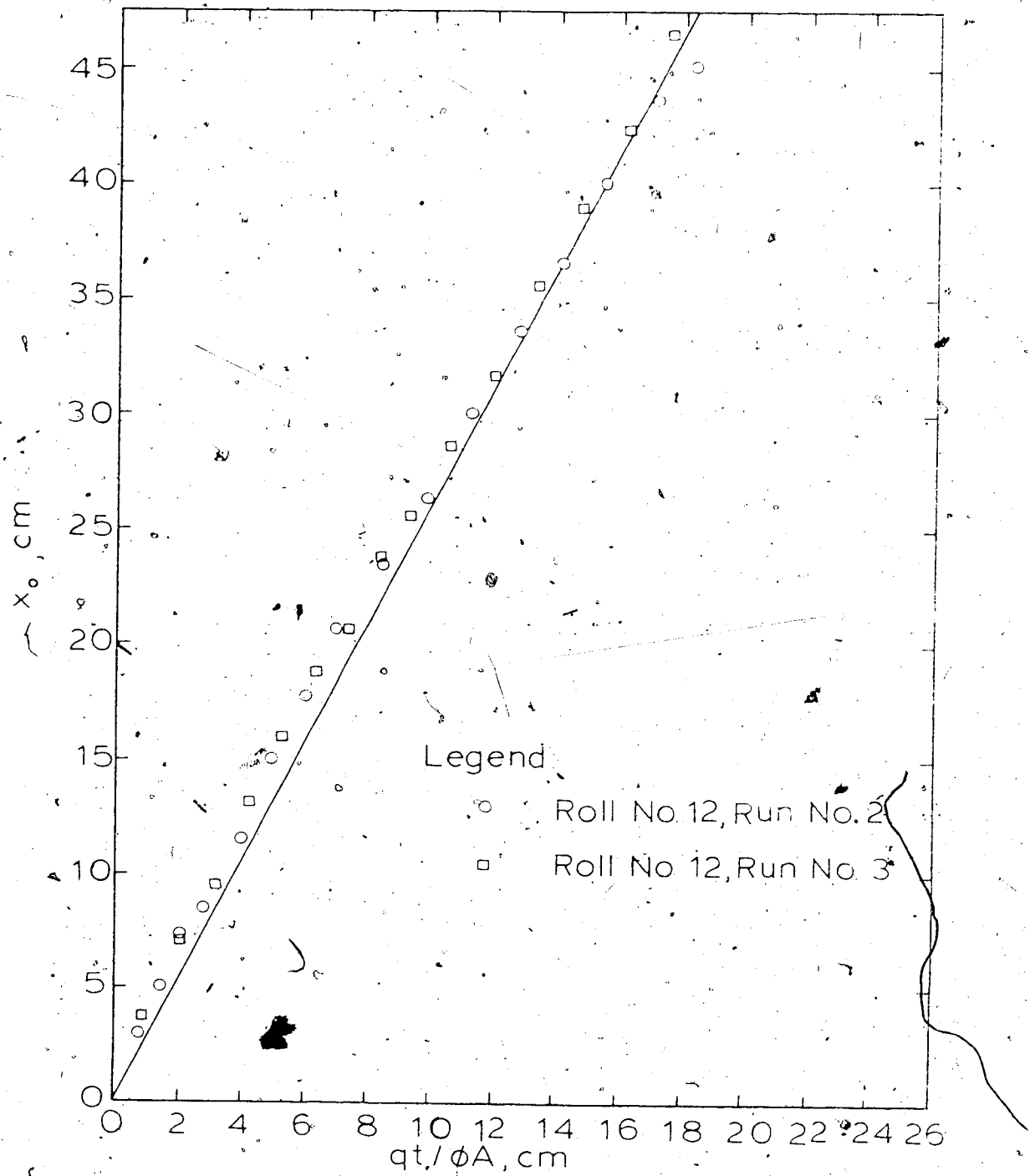


FIGURE V-8 17cp GLYCEROL SOLUTION  
DISPLACING 100cs DOW CORNING,  
 $q = 3.177 \text{ cm}^3/\text{sec}$

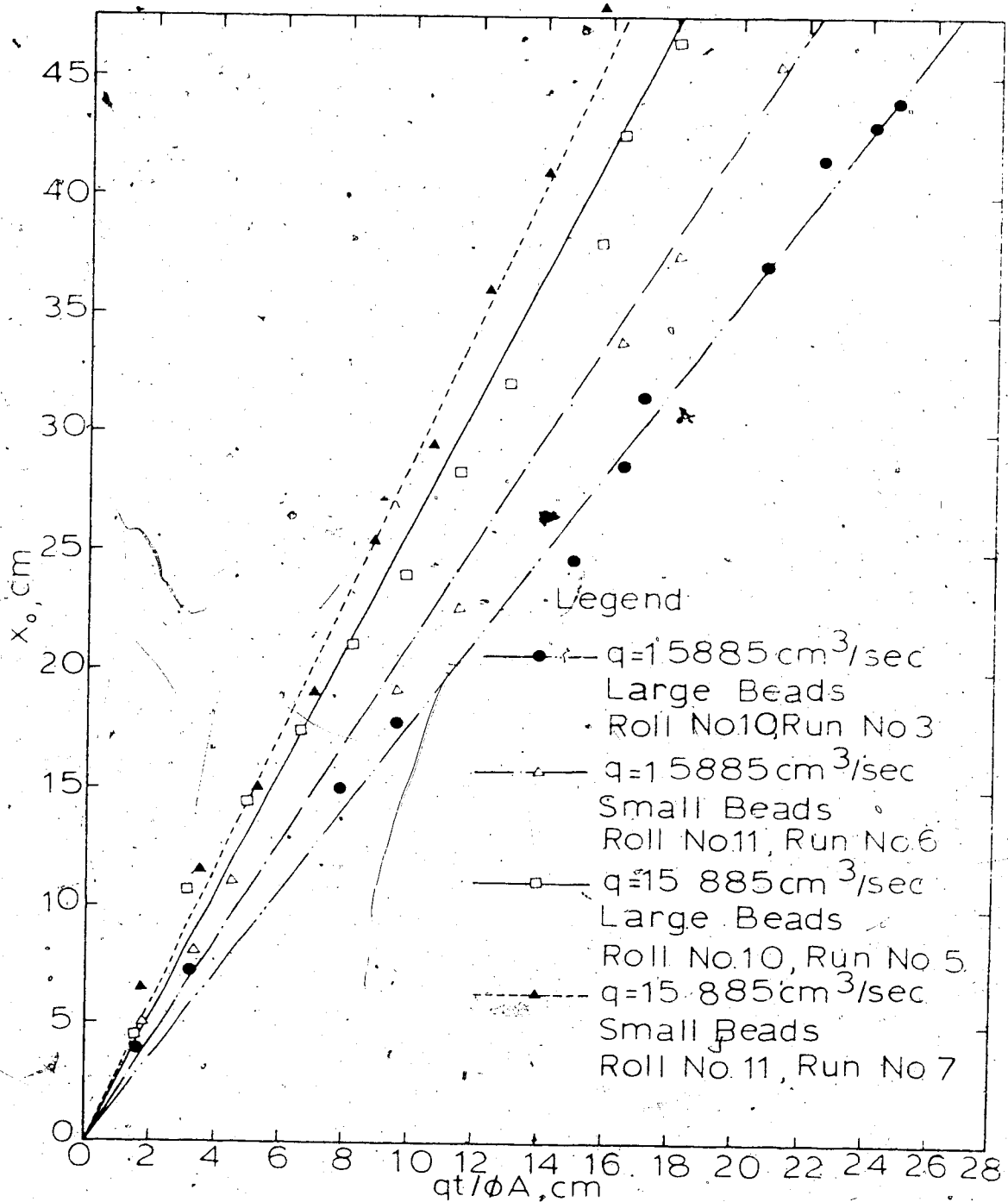


FIGURE V-9 0.05% SEPARAN AP-273  
DISPLACING 100cs DOW CORNING

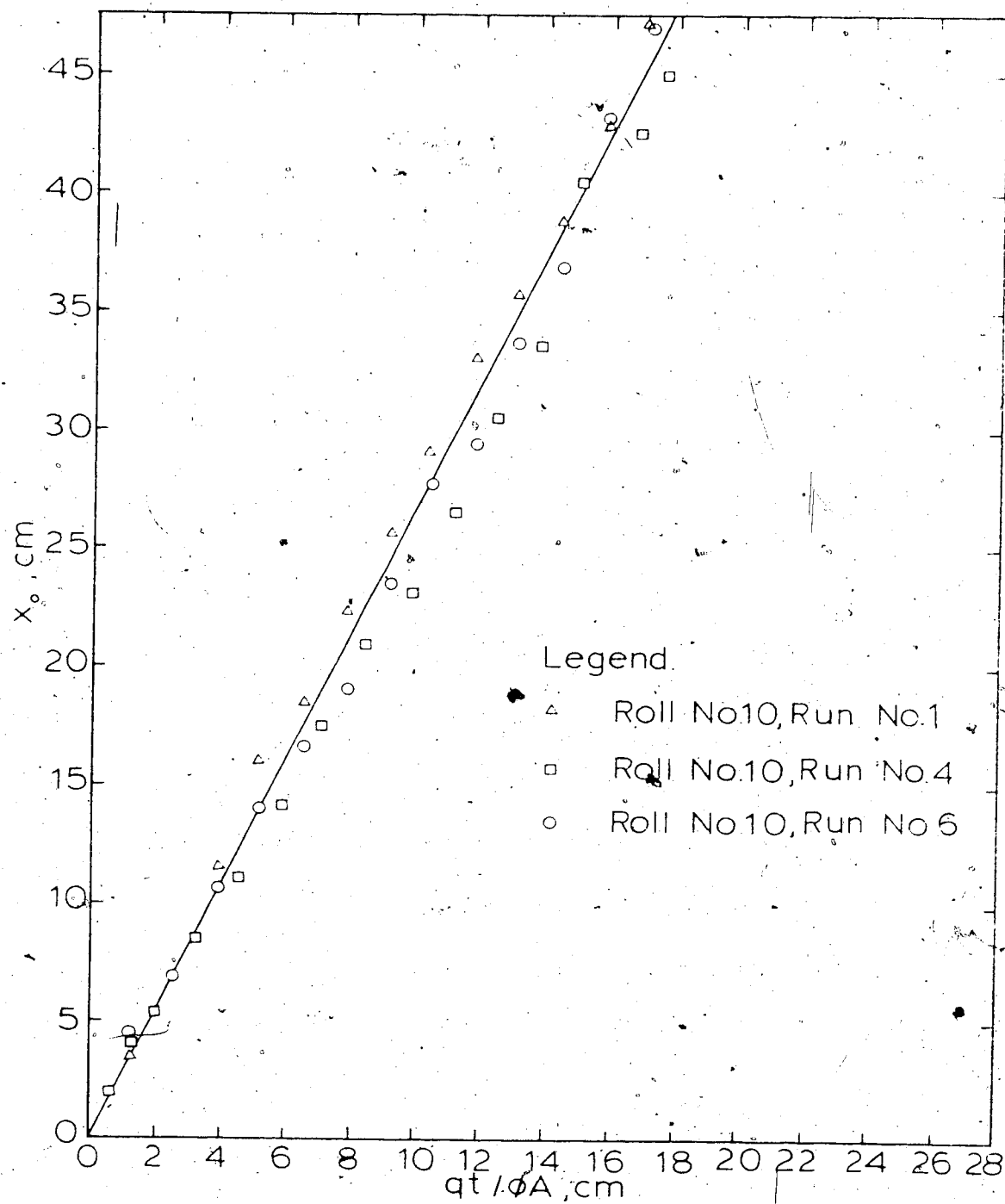


FIGURE V-10 0.05% SEPARAN AP-273  
DISPLACING 100cs DOW CORNING,  
 $q = 6.354 \text{ cm}^3/\text{sec}$

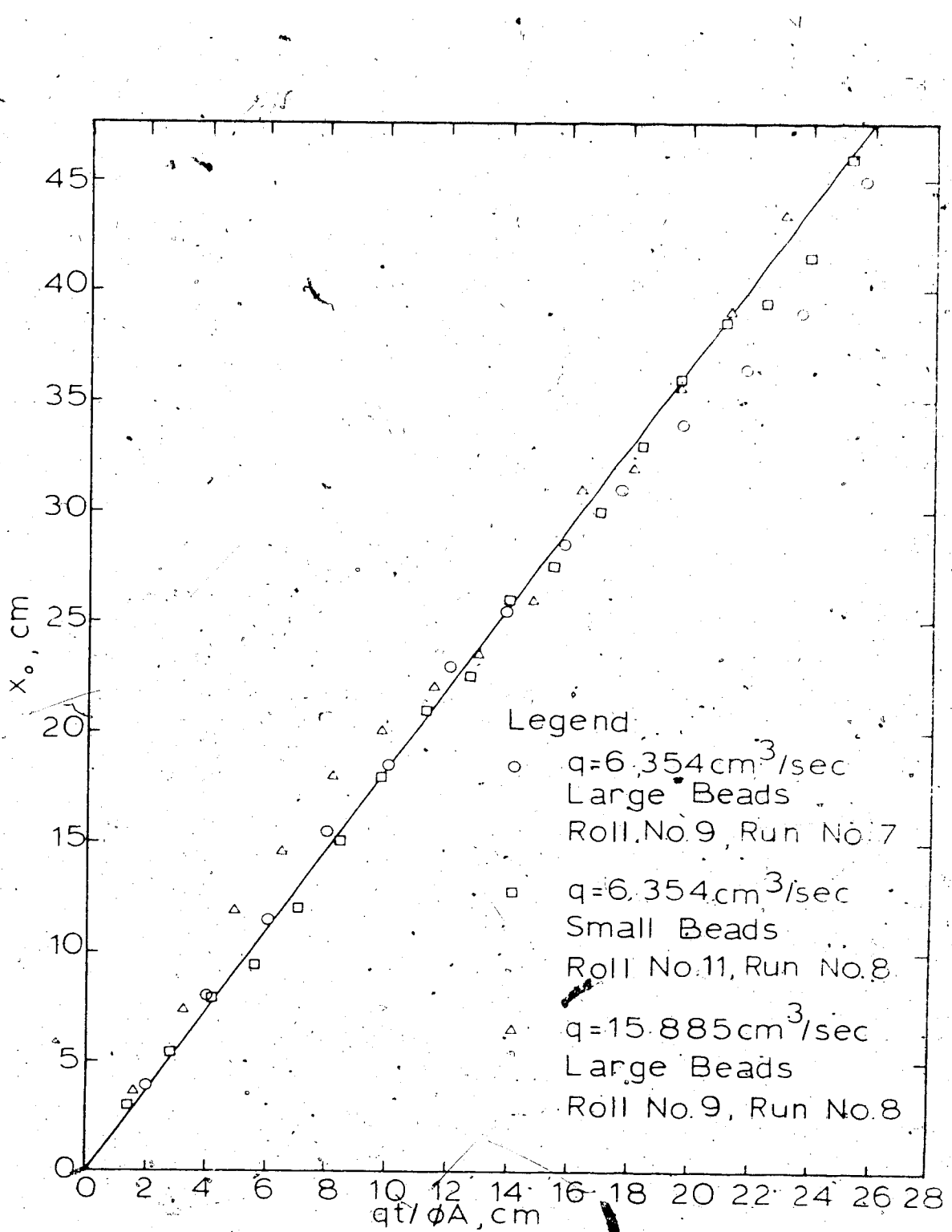
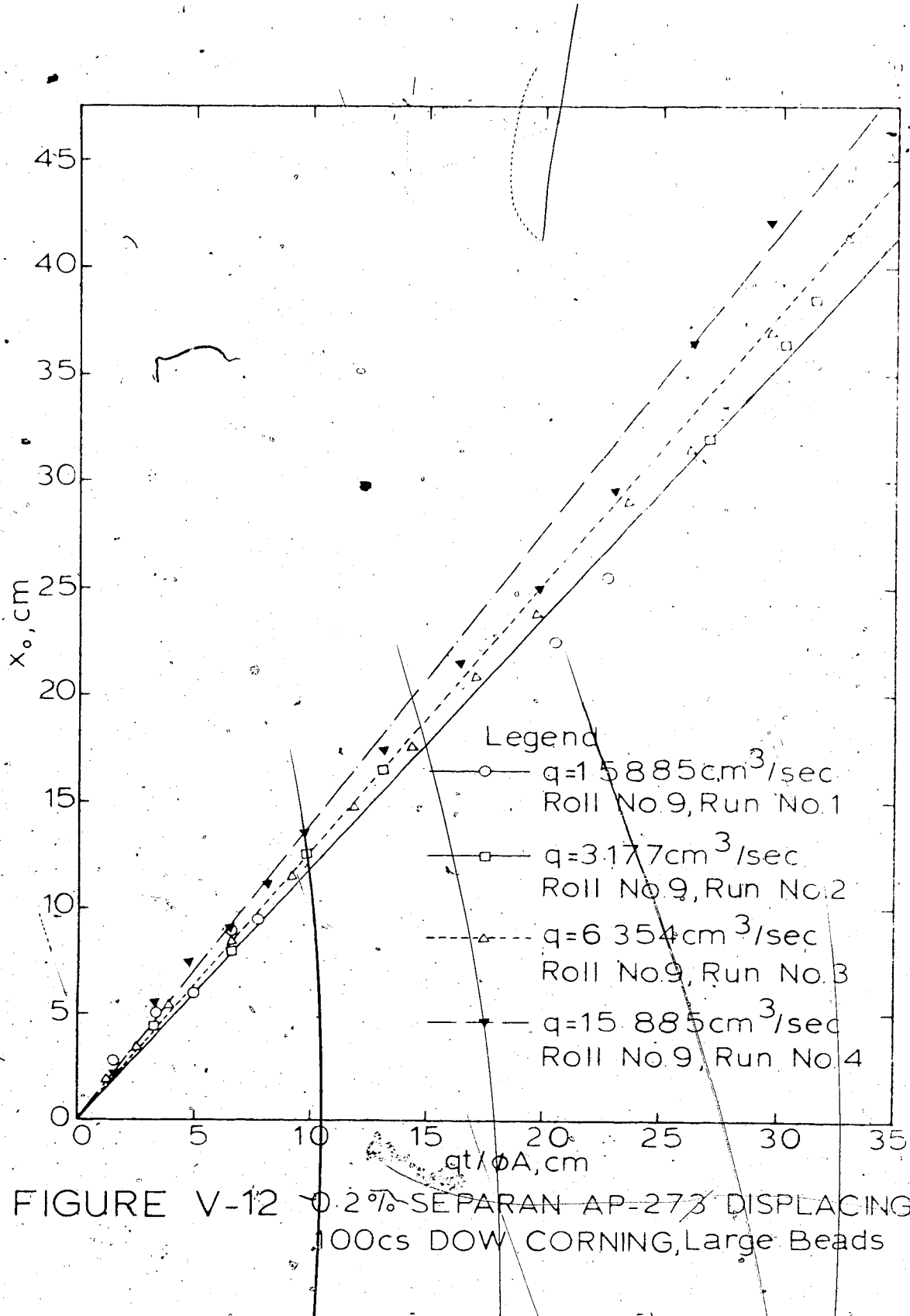


FIGURE V-11 0.1% SEPARAN AP-273 DISPLACING  
100cs DOW CORNING



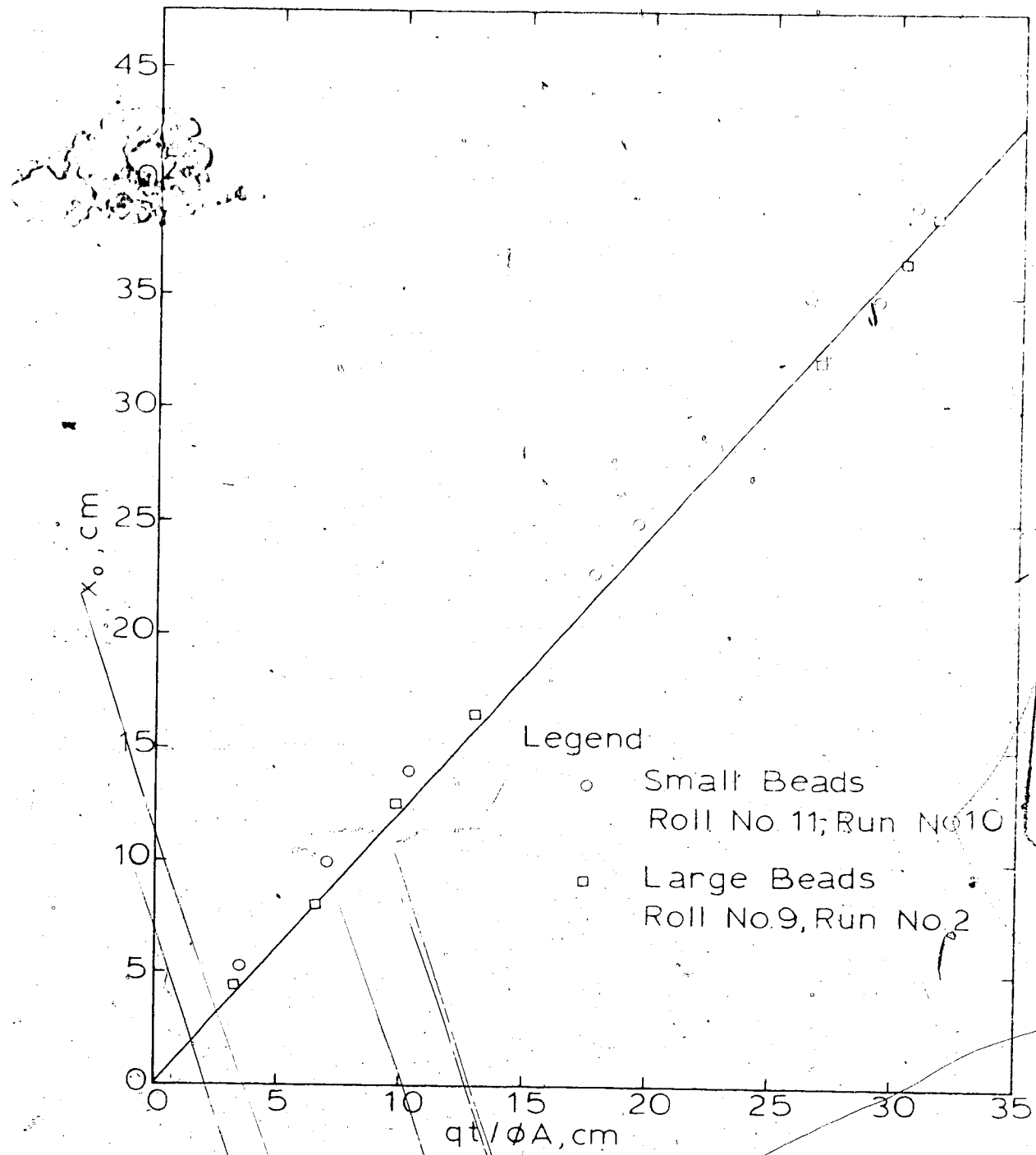


FIGURE V-13 0.2% SEPARAN AP-273 DISPLACING  
100cs DOW CORNING,  $q=3177 \text{ cm}^3/\text{sec}$

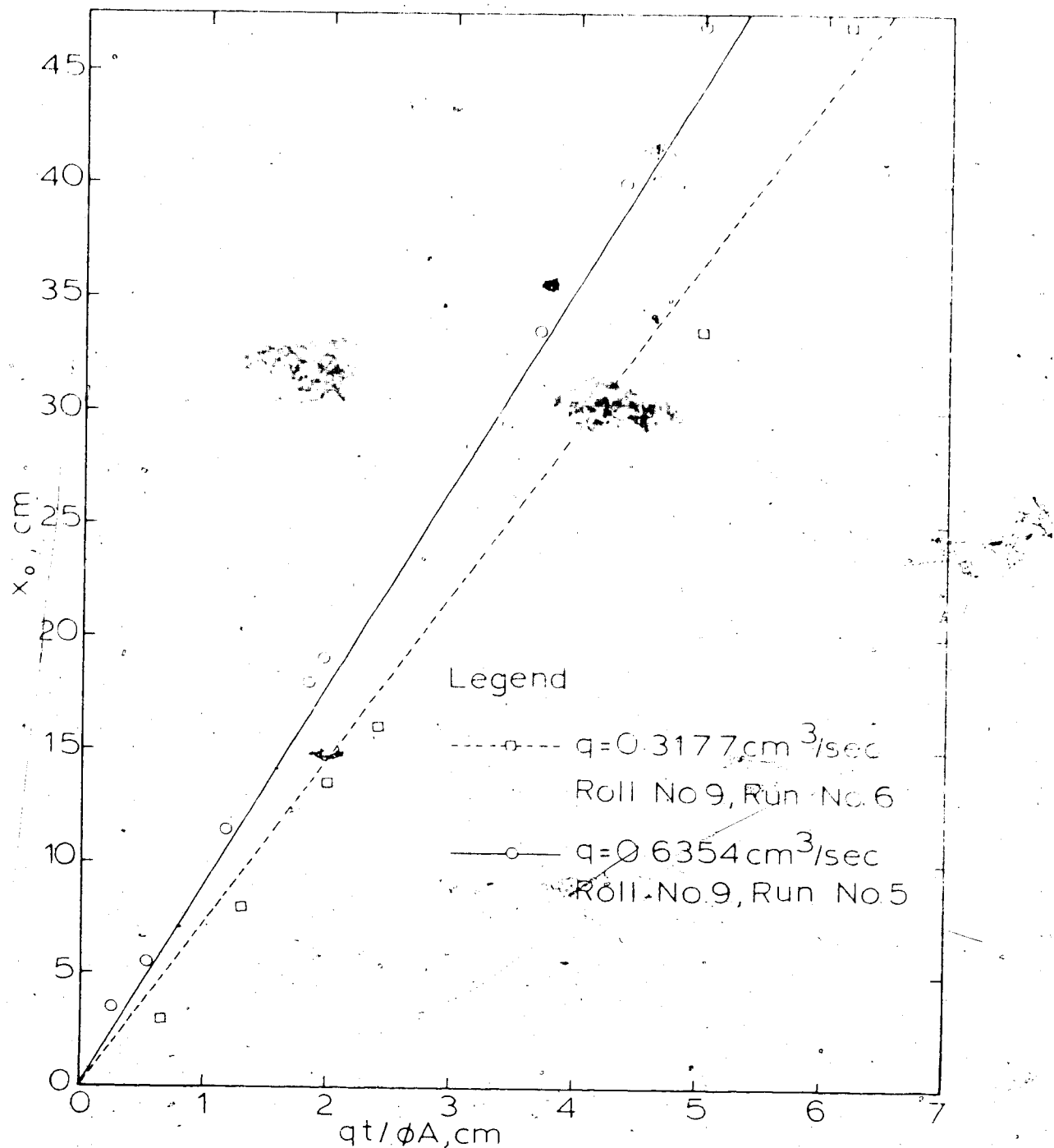


FIGURE V-14 0.2% SEPARAN AP-273 DISPLACING  
1250Qcs DOW CORNING, Large Beads

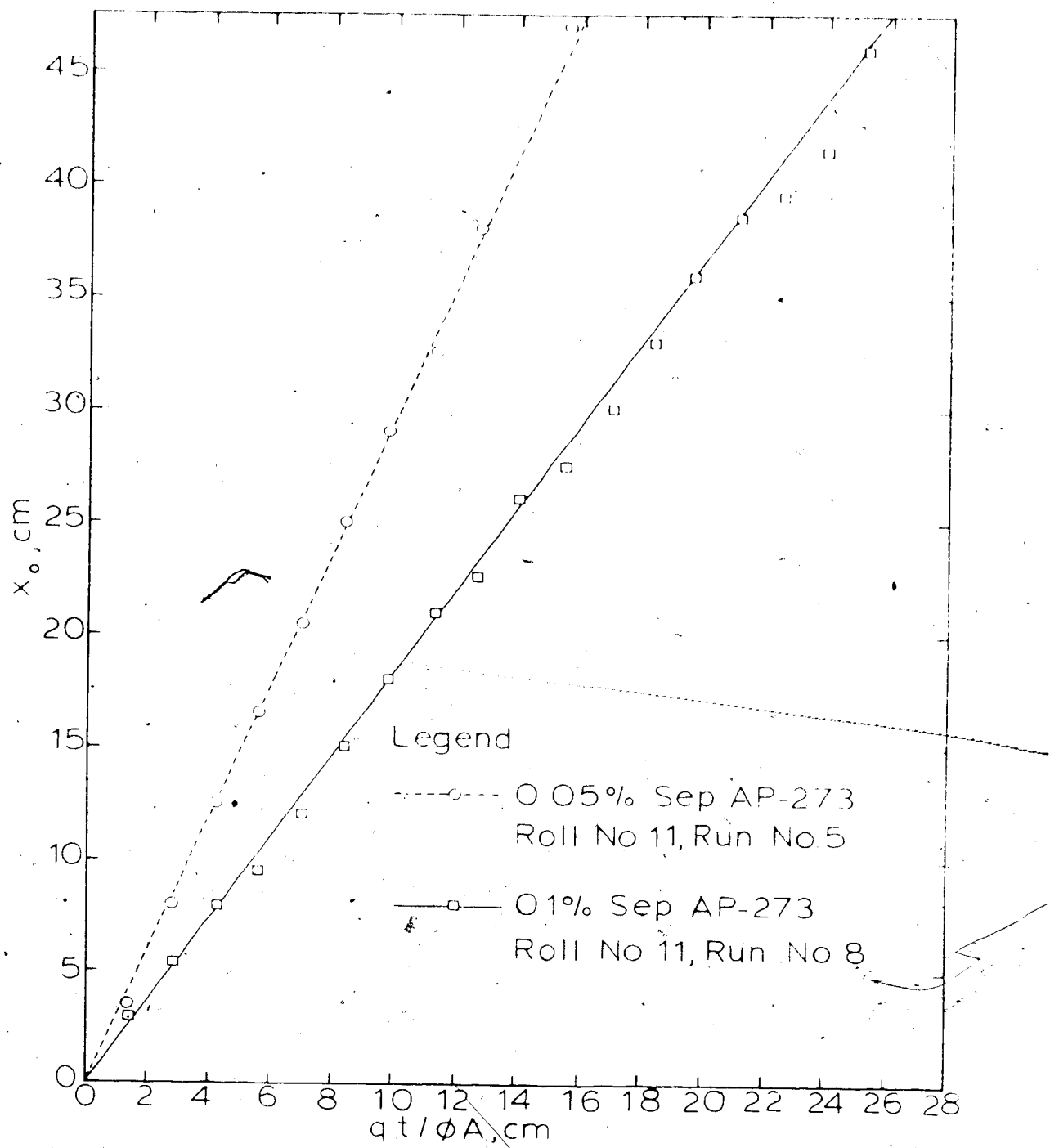


FIGURE V-15 SEPARAN AP-273 SOLUTIONS  
DISPLACING 100cs DOW CORNING  
 $q = 6.354 \text{ cm}^3/\text{sec}$

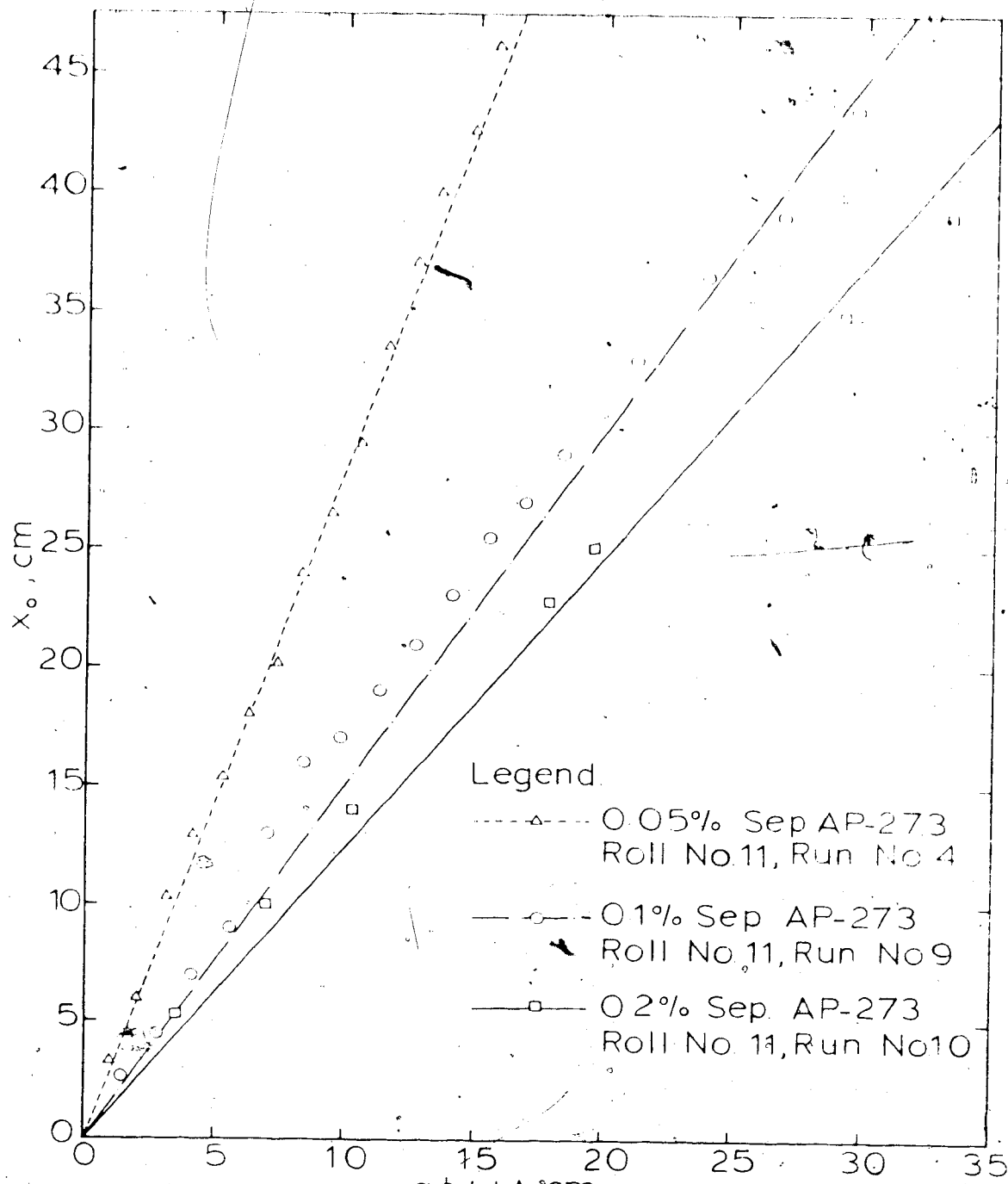


FIGURE V-16 SEPARAN AP-273 SOLUTIONS  
DISPLACING 100cs DOW CORNING  
 $q=3.177 \text{ cm}^3/\text{sec}$

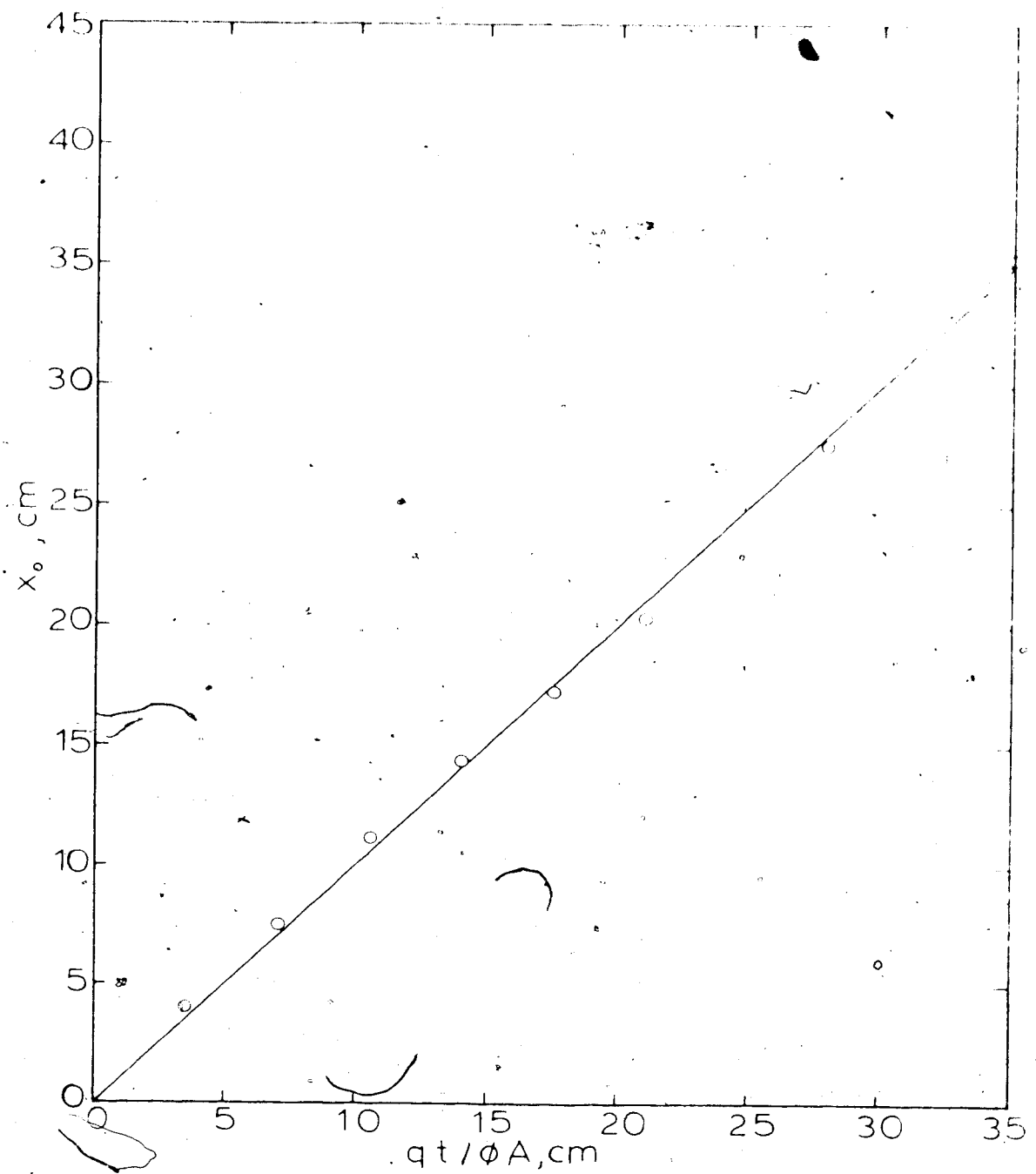


FIGURE V-17 100cs DOW CORNING DISPLACING  
WATER,  $q=3.4 \text{ cm}^3/\text{sec}$ , Large Beads

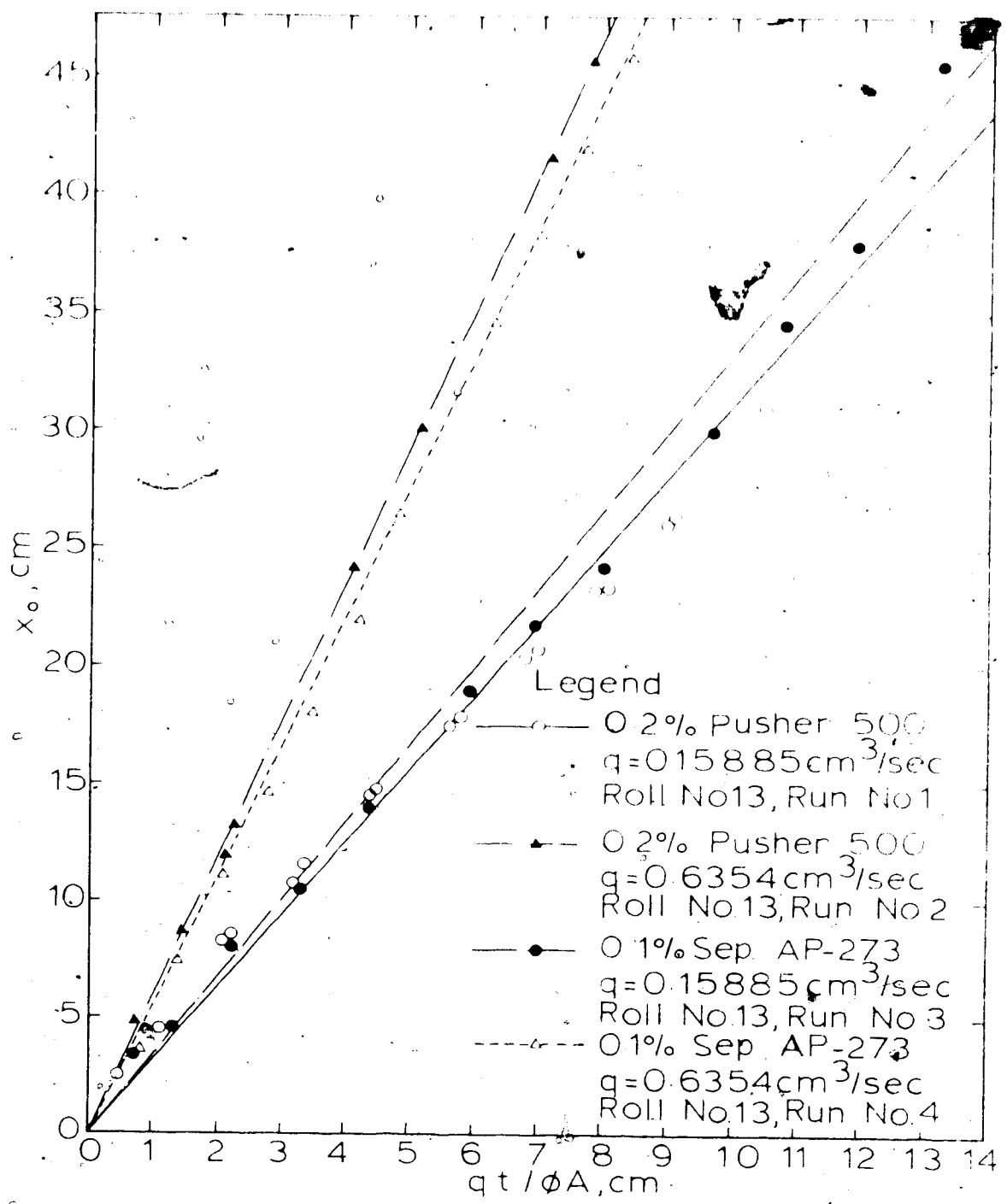


FIGURE V-18 POLYMER SOLUTIONS DISPLACING  
1000cs DOW CORNING, Small Beads

Legend For Figure V-19

- Data Points from Everett, et al., (Table I-10)
- △ Data Points from Engelberts, et al., (Table I-11)
- Data Points from Jones-Parr, et al., (Table I-12)
- Data Points from Cloes, et al., (Table I-13)
- ▲ Present Work: Water Displacing 100% Dow Corning
- Present Work: Glycerol Solutions Displacing  
100% Dow Corning
- Equation II-S2a

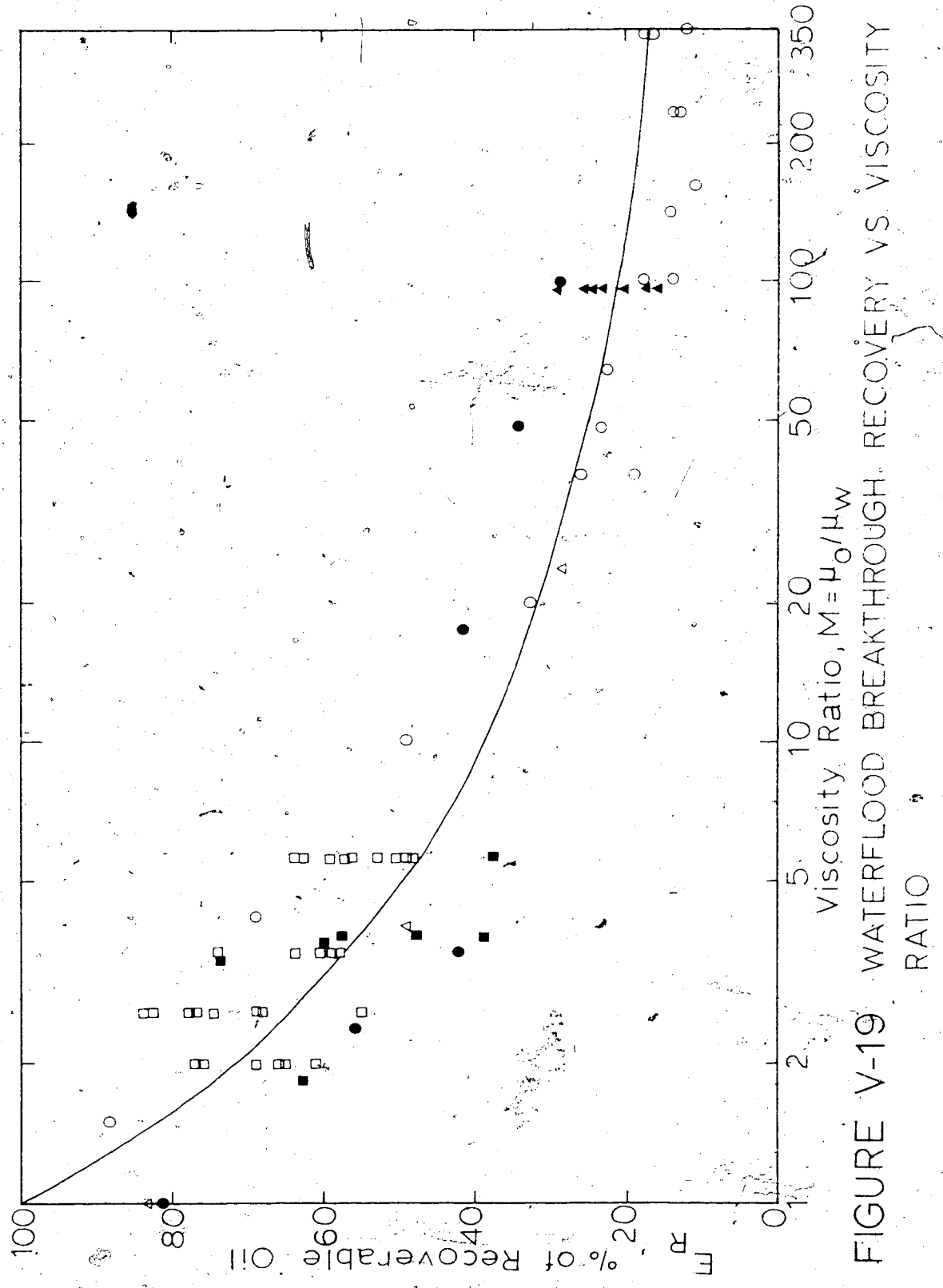


FIGURE V-19 WATERFLOOD BREAKTHROUGH RECOVERY VS. VISCOSITY RATIO

Legend For Figure V-20

Large Beads

- △ 0.05% Sep. Displacing 100 cs Dow Corning
- 0.1% Sep. Displacing 100 cs Dow Corning
- 0.2% Sep. Displacing 100 cs Dow Corning
- ▽ 0.2% Sep. Displacing 12500 cs Dow Corning

Small Beads

- 0.05% Sep. Displacing 100 cs Dow Corning
- ▼ 0.1% Sep. Displacing 100 cs Dow Corning
- ▲ 0.1% Sep. Displacing 1000 cs Dow Corning
- 0.2% Sep. Displacing 100 cs Dow Corning
- \* 0.2% Pusher Displacing 1000 cs Dow Corning

Equation 11-63

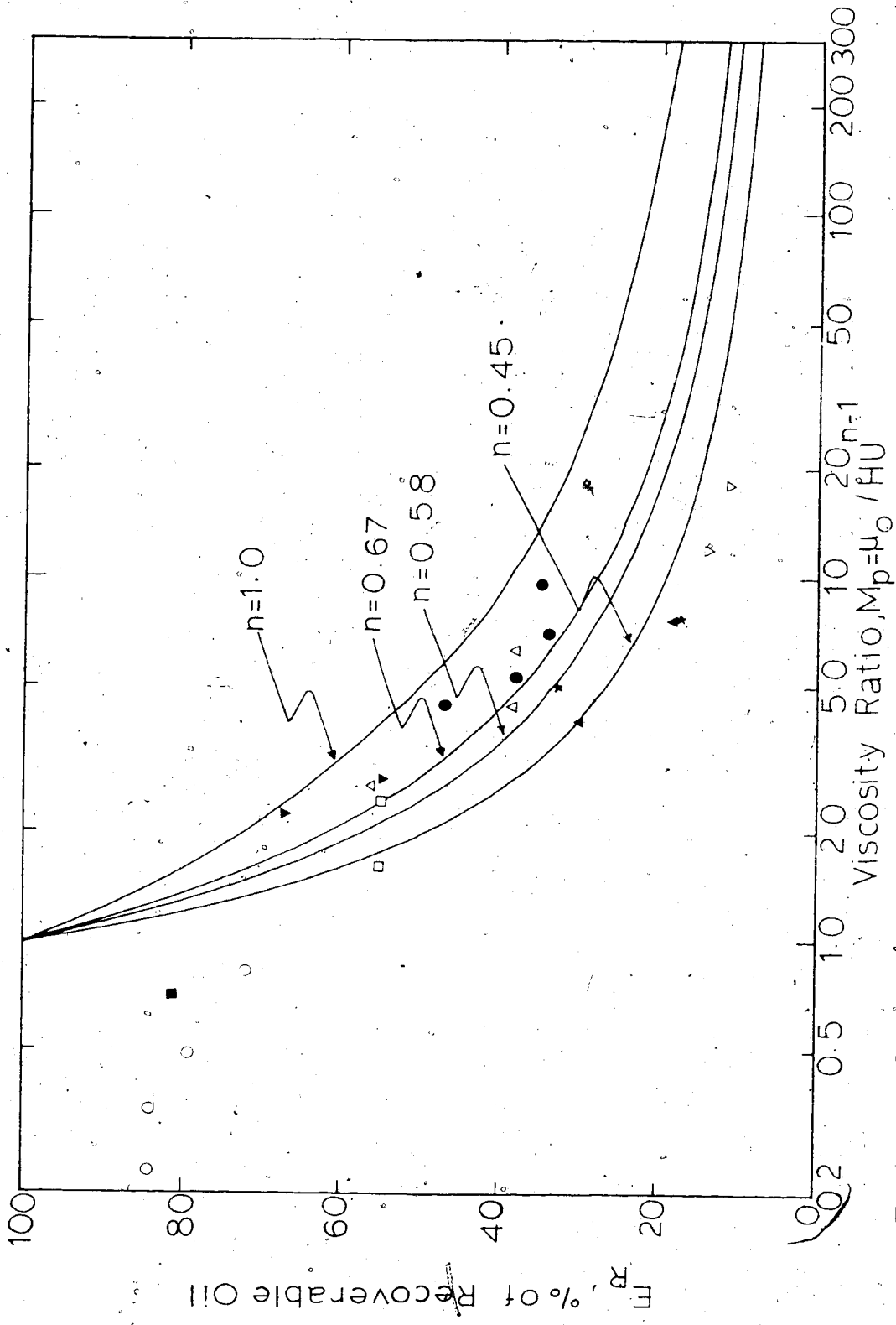


FIGURE V-20 POLYMERFLOOD BREAKTHROUGH RECOVERY VS. VISCOSITY RATIO

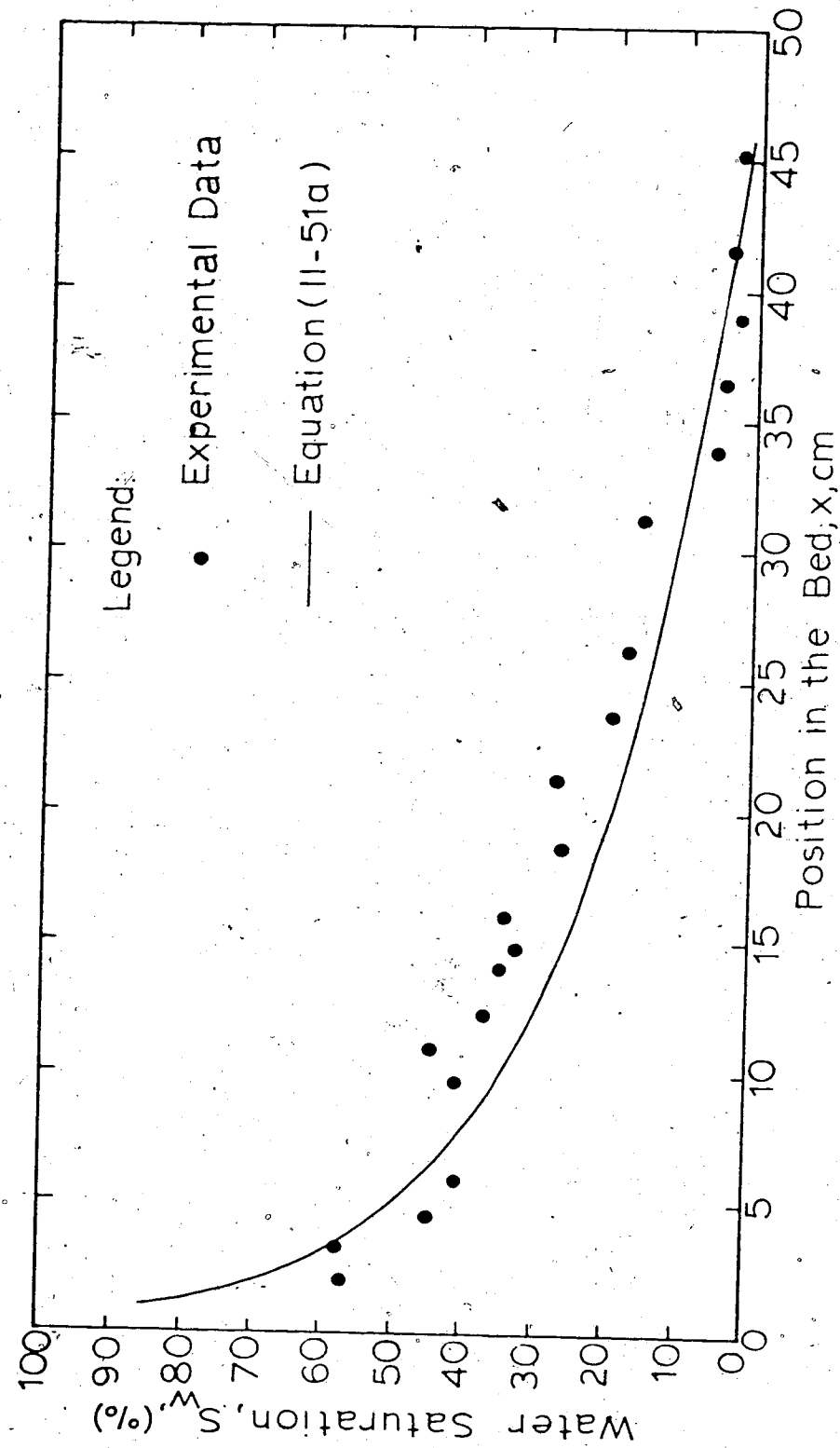


FIGURE V-21 BREAKTHROUGH SATURATION PROFILE OF RUN  
NO.1, ROLL NO.8, (WATERFLOOD)

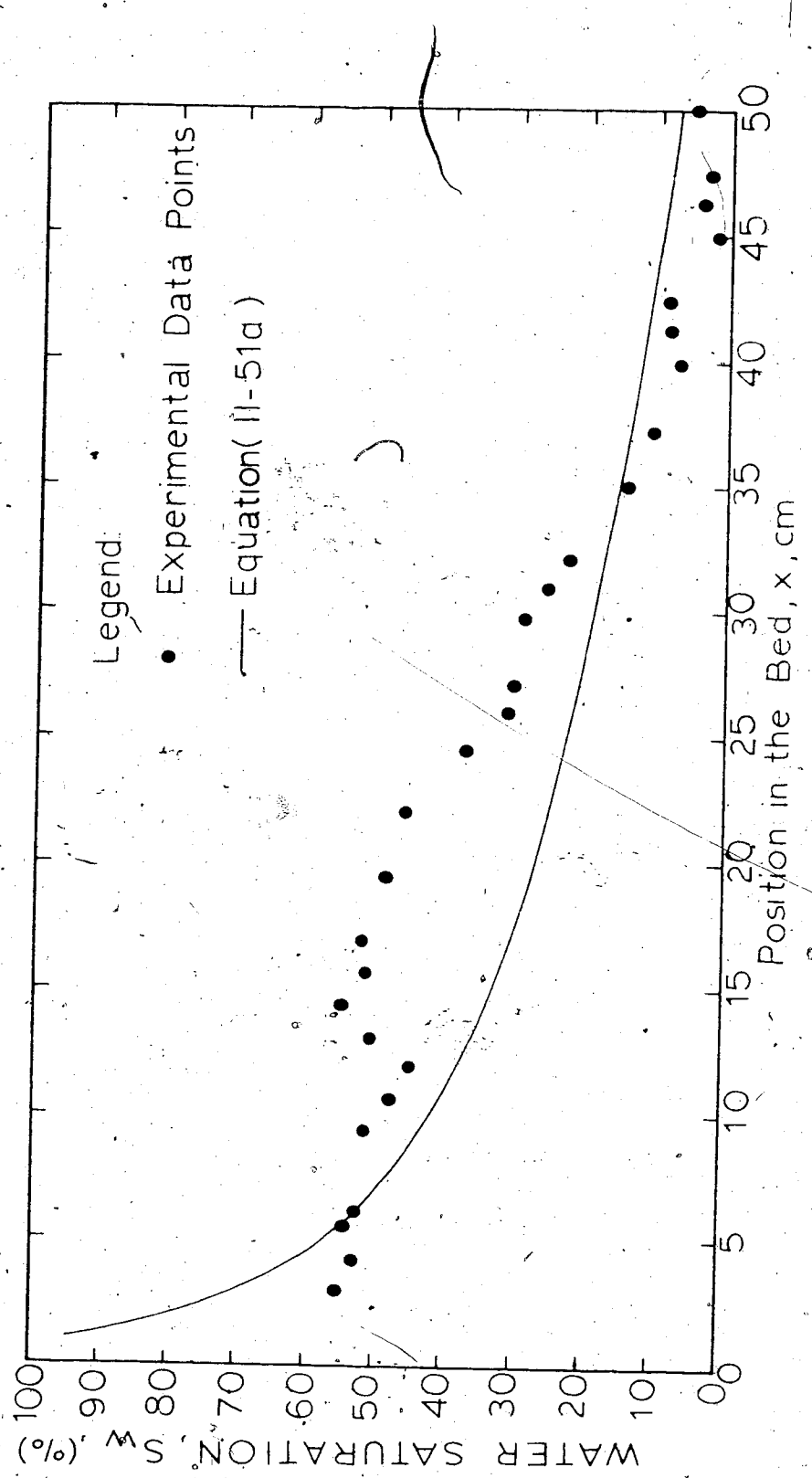


FIGURE V-22 BREAKTHROUGH SATURATION PROFILE OF RUN NO. 3, ROLL NO. 8 (WATER FLOOD)

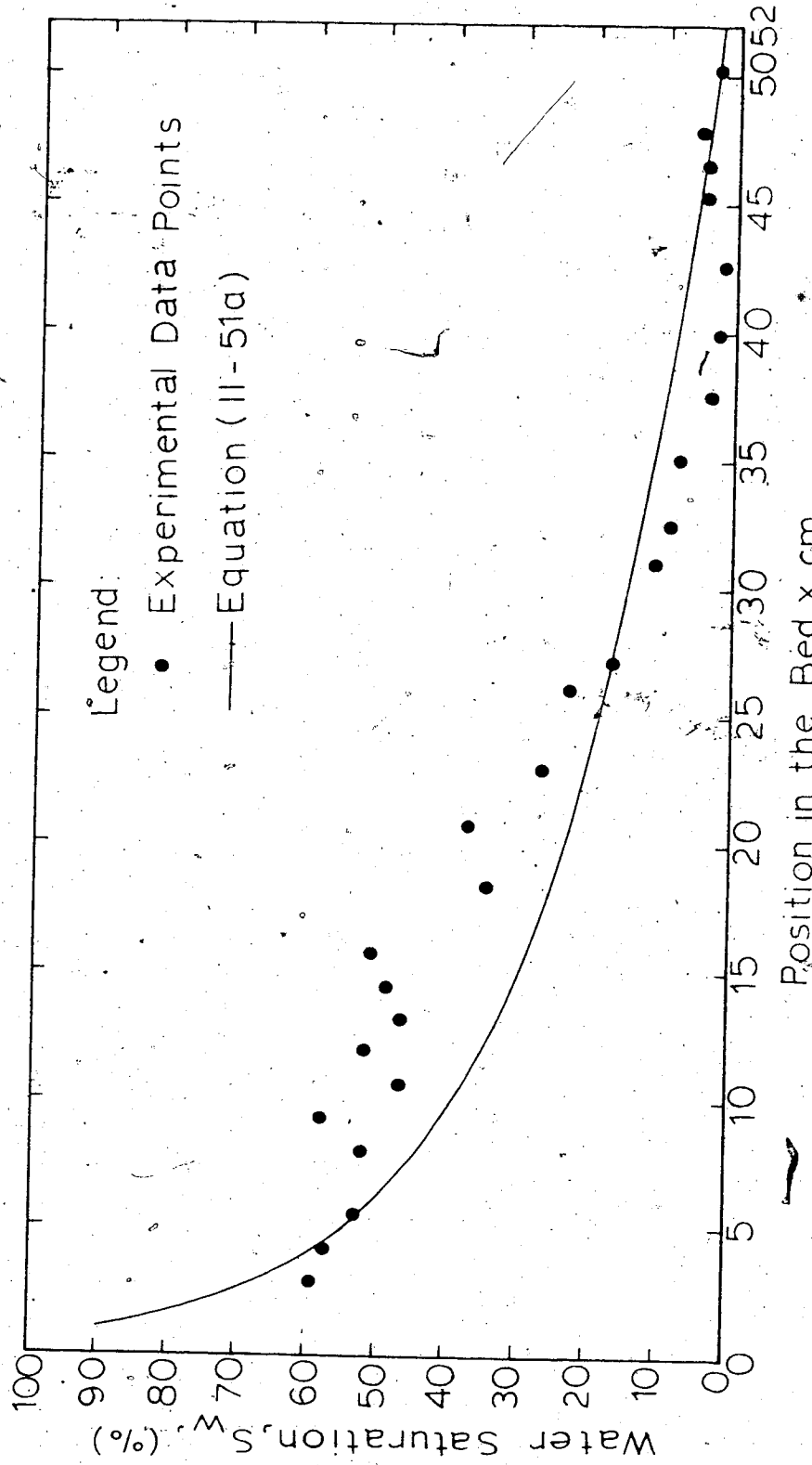


FIGURE V-23 BREAKTHROUGH SATURATION PROFILE OF RUN  
NO. 5, ROLL NO. 8 (WATERFLOOD)

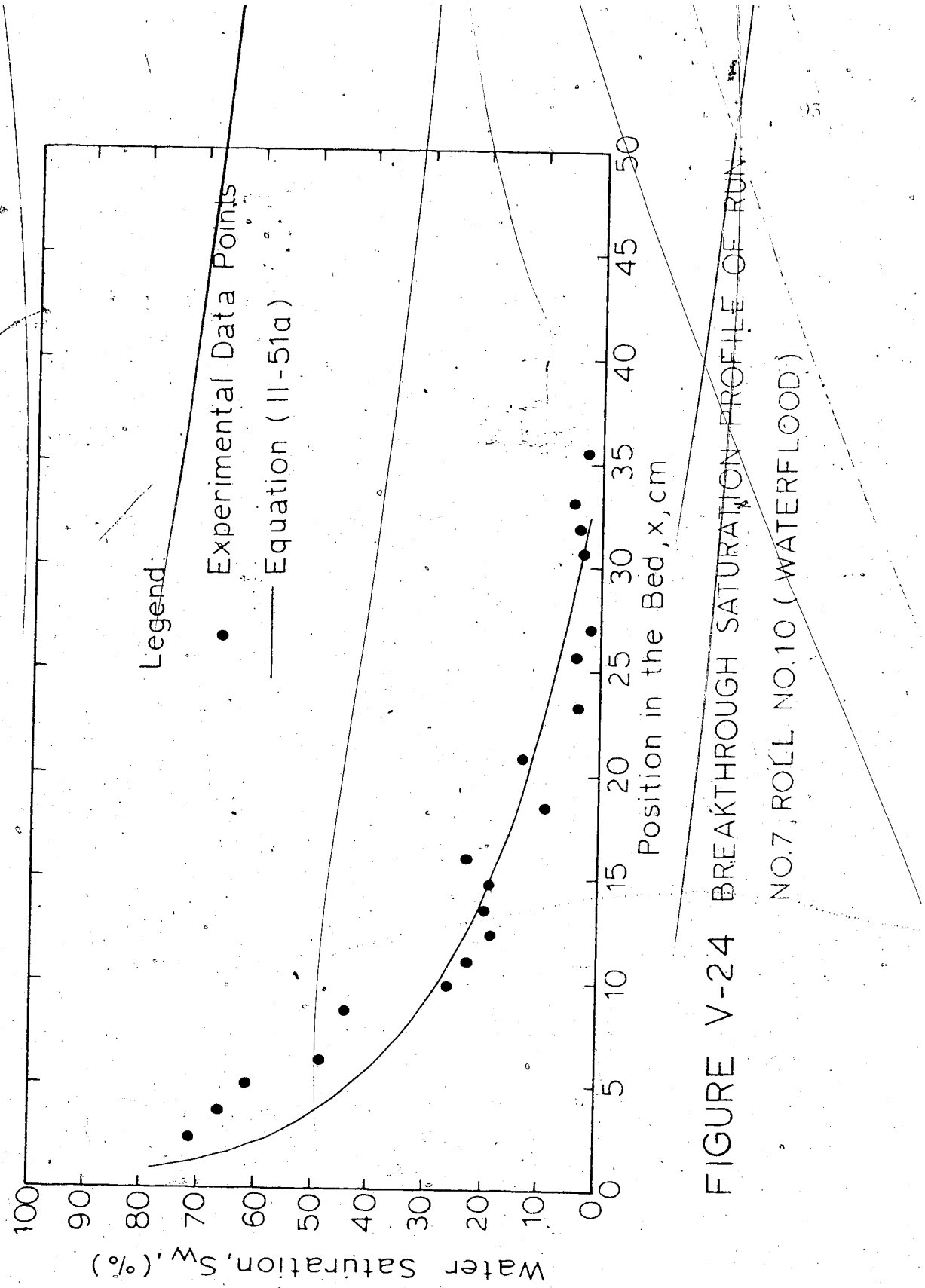


FIGURE V-24 BREAKTHROUGH SATURATION PROFILE OF RUN  
NO.7, ROLL NO.10 (WATERFLOOD)

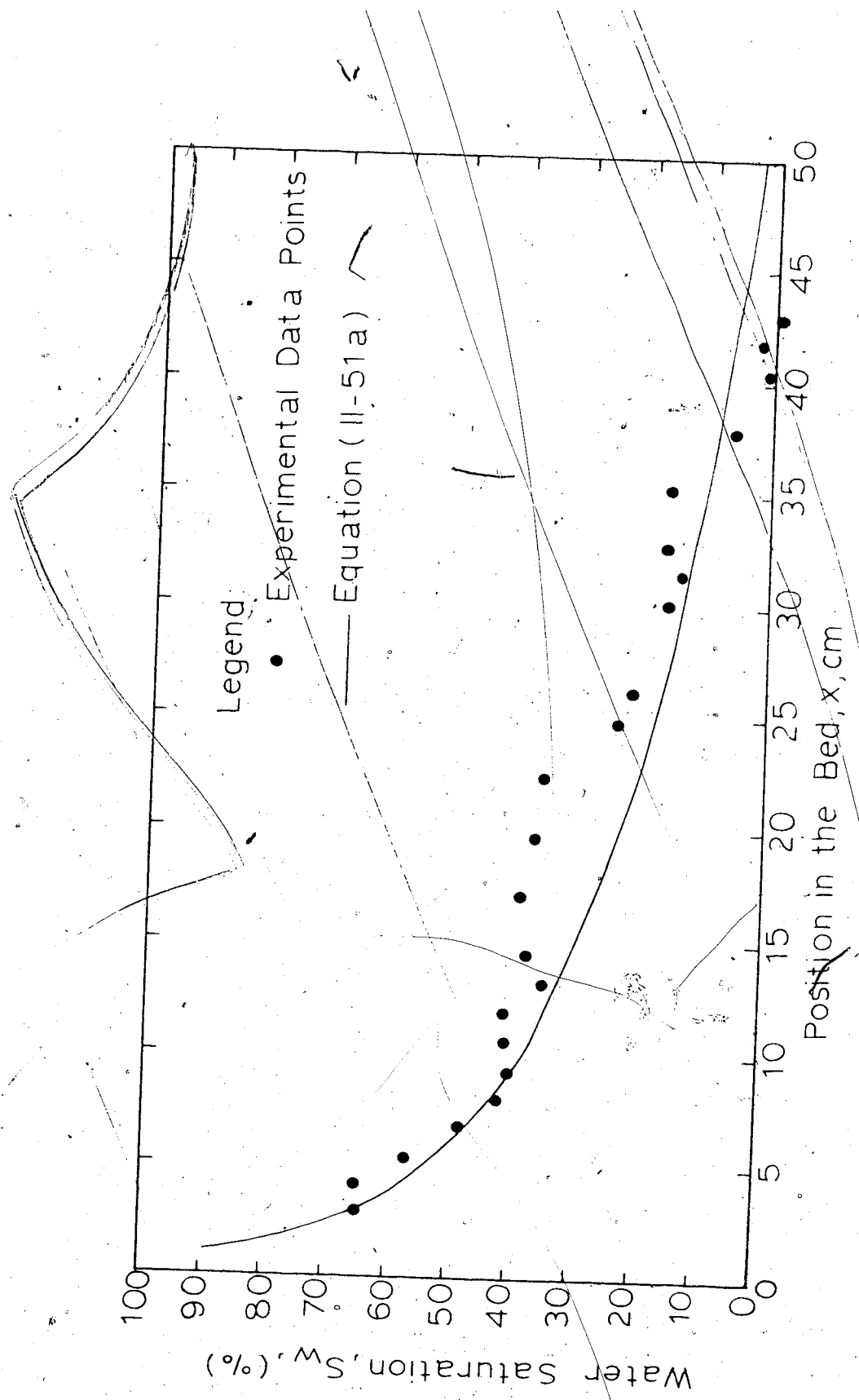


FIGURE V-25 BREAKTHROUGH SATURATION PROFILE OF RUN  
NO.1, ROLL NO.11 (WATERFLOOD)

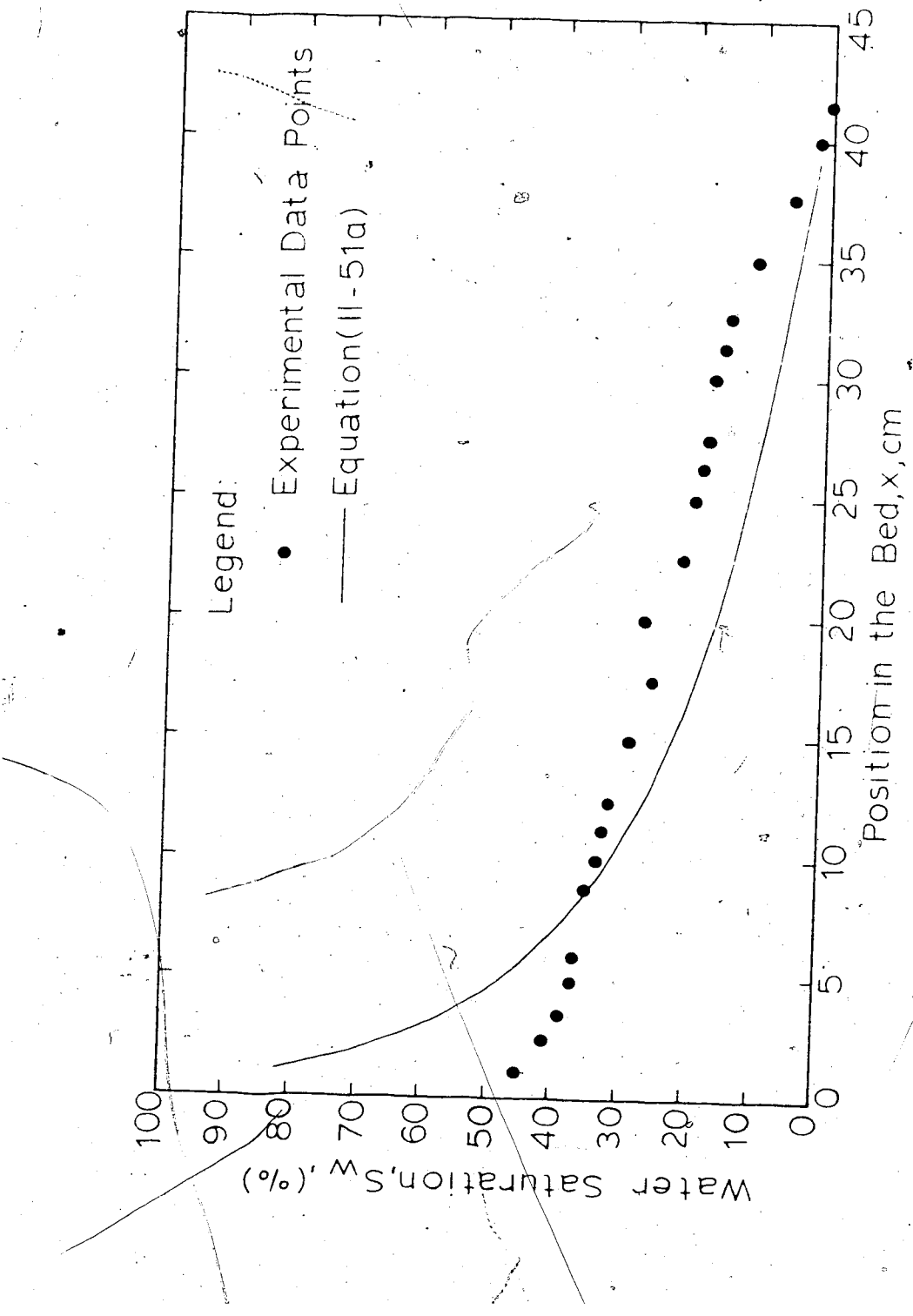


FIGURE V-26: BREAKTHROUGH SATURATION PROFILE  
OF RUN NO.2,ROLL NO.11,(WATERFLOOD)

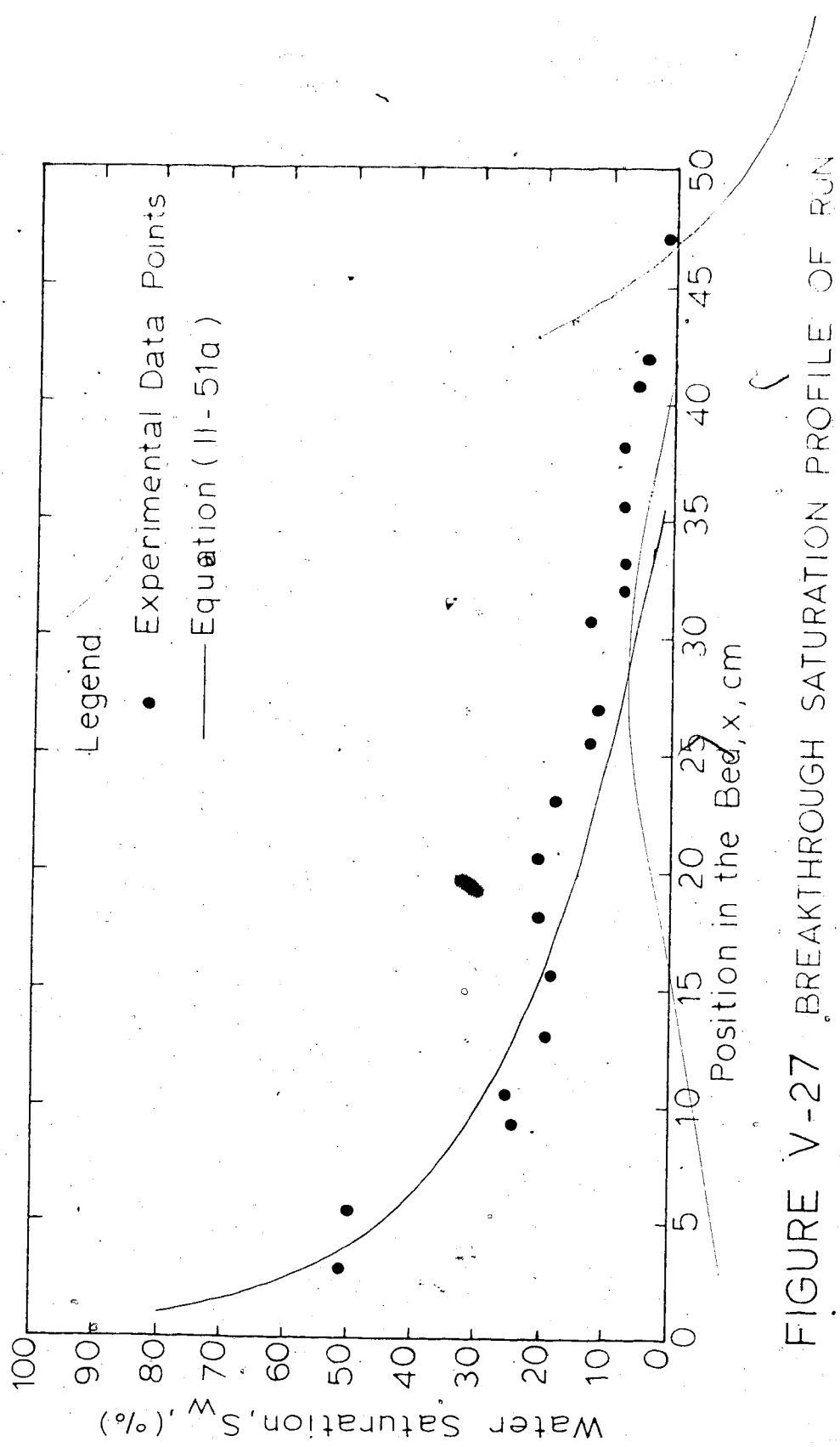


FIGURE V-27 BREAKTHROUGH SATURATION PROFILE OF RUN NO. 3, ROLL NO. 11 (WATERFLOOD)

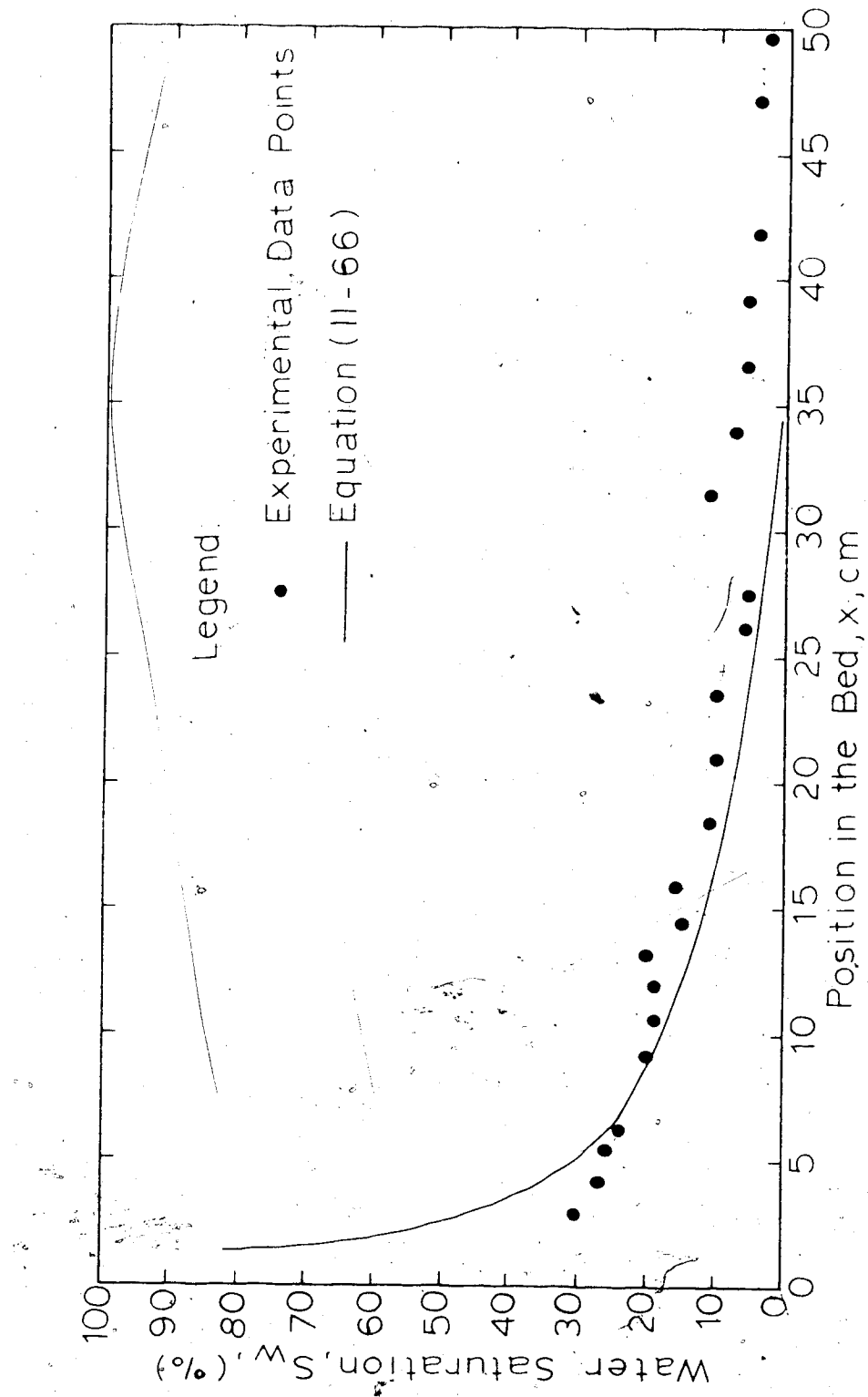
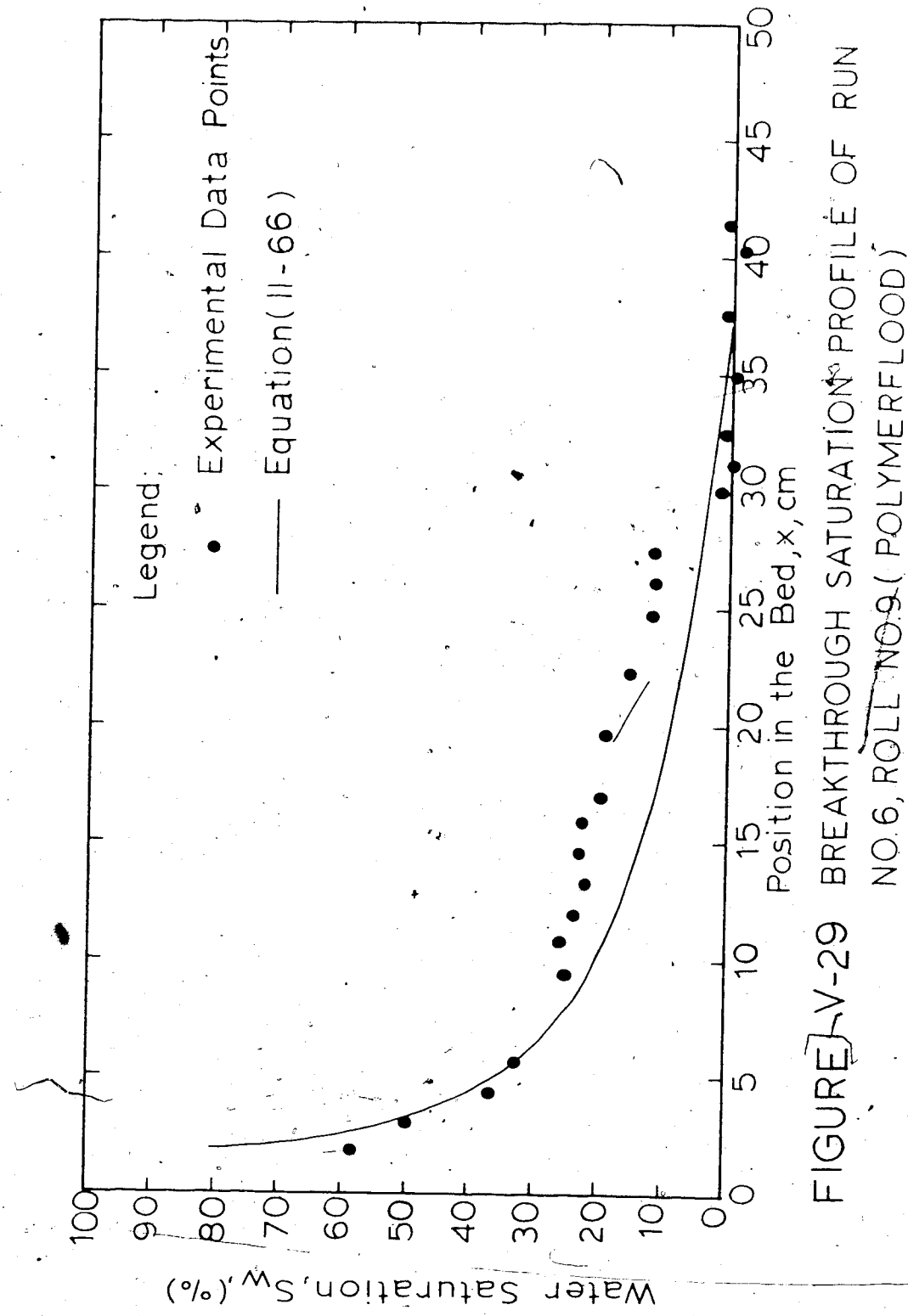


FIGURE V-28 BREAKTHROUGH SATURATION PROFILE OF  
RUN NO. 5, ROLL NO. 9 (POLYMERFLOOD)



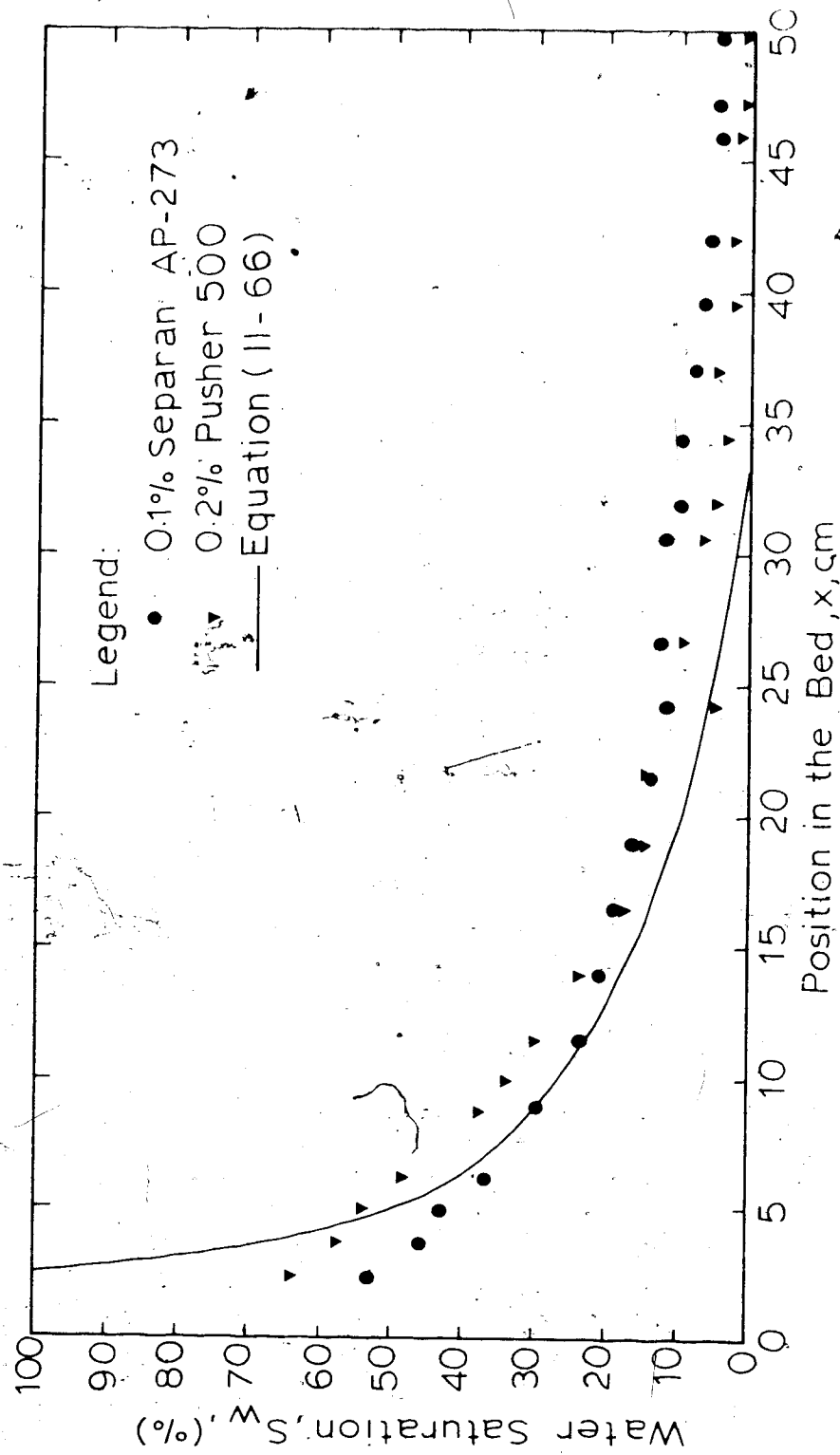


FIGURE V-30 BREAKTHROUGH SATURATION PROFILE OF RUN  
NO. 2 AND 4, ROLL NO. 13. ( POLYMERFLOOD )

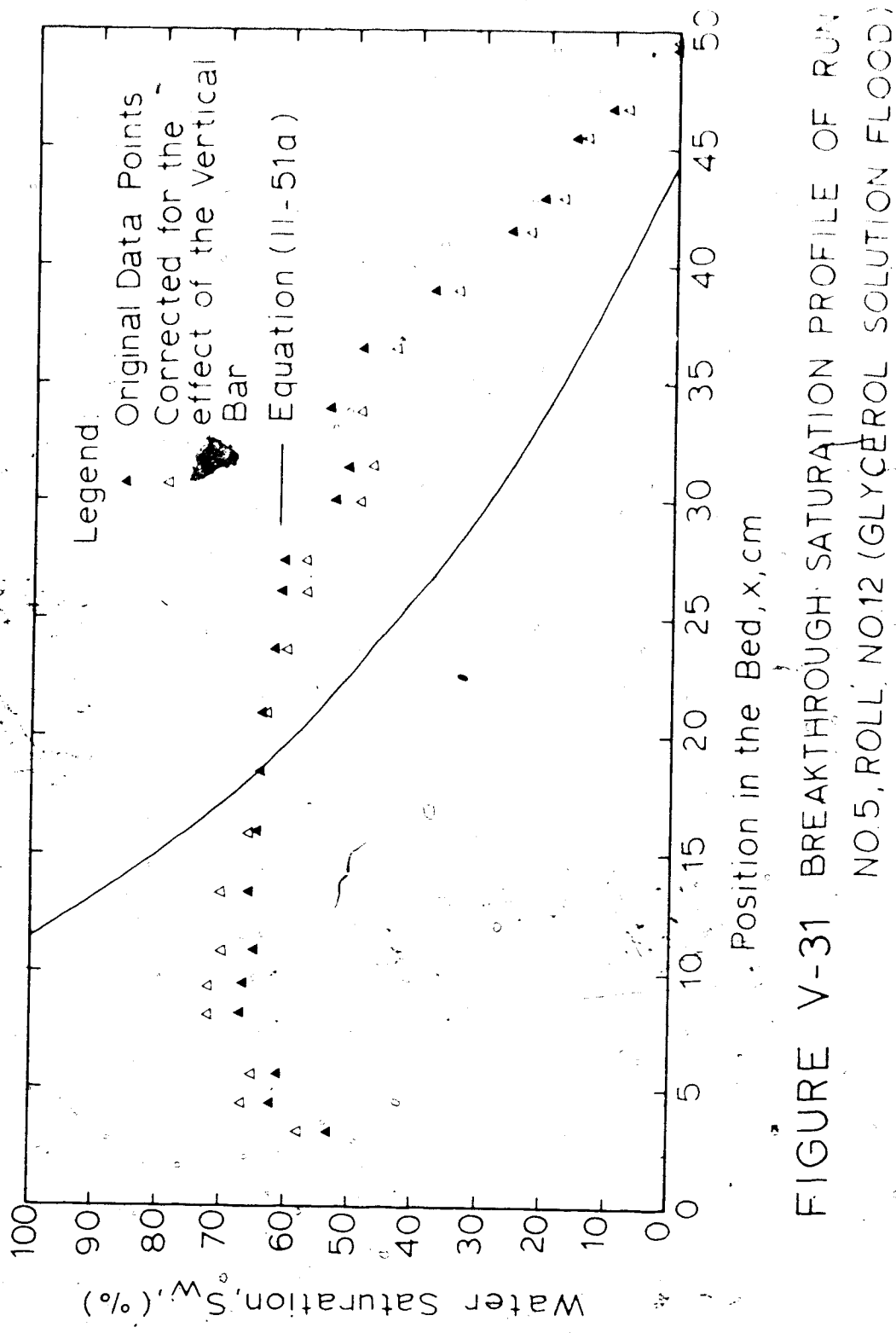


FIGURE V-31 BREAKTHROUGH SATURATION PROFILE OF RUN NO. 5, ROLL NO. 12 (GLYCEROL SOLUTION FLOOD)

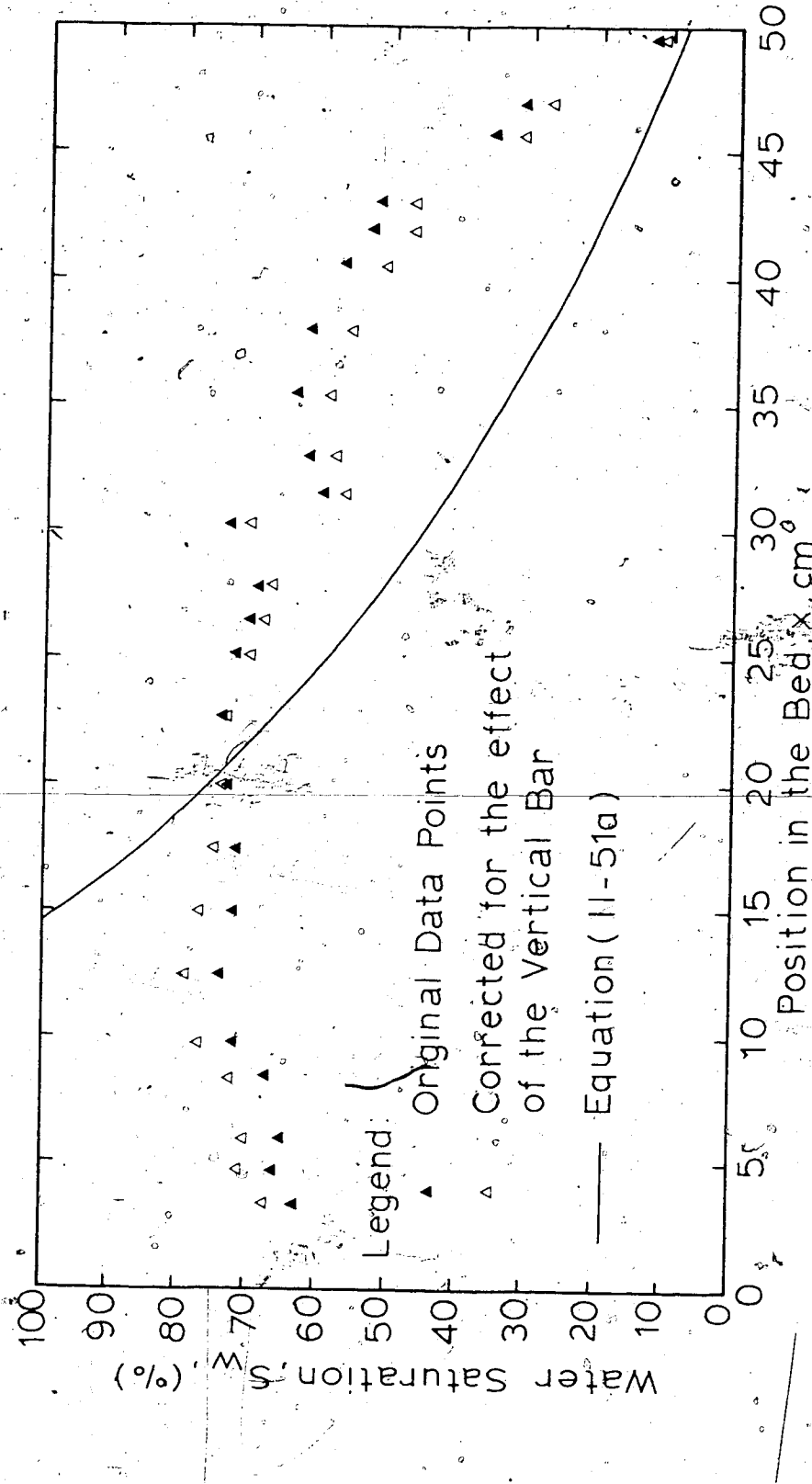


FIGURE V-32 BREAKTHROUGH SATURATION PROFILE OF RUN NO.6, ROLL NO.12 (GLYCEROL SOLUTION FLOOD)

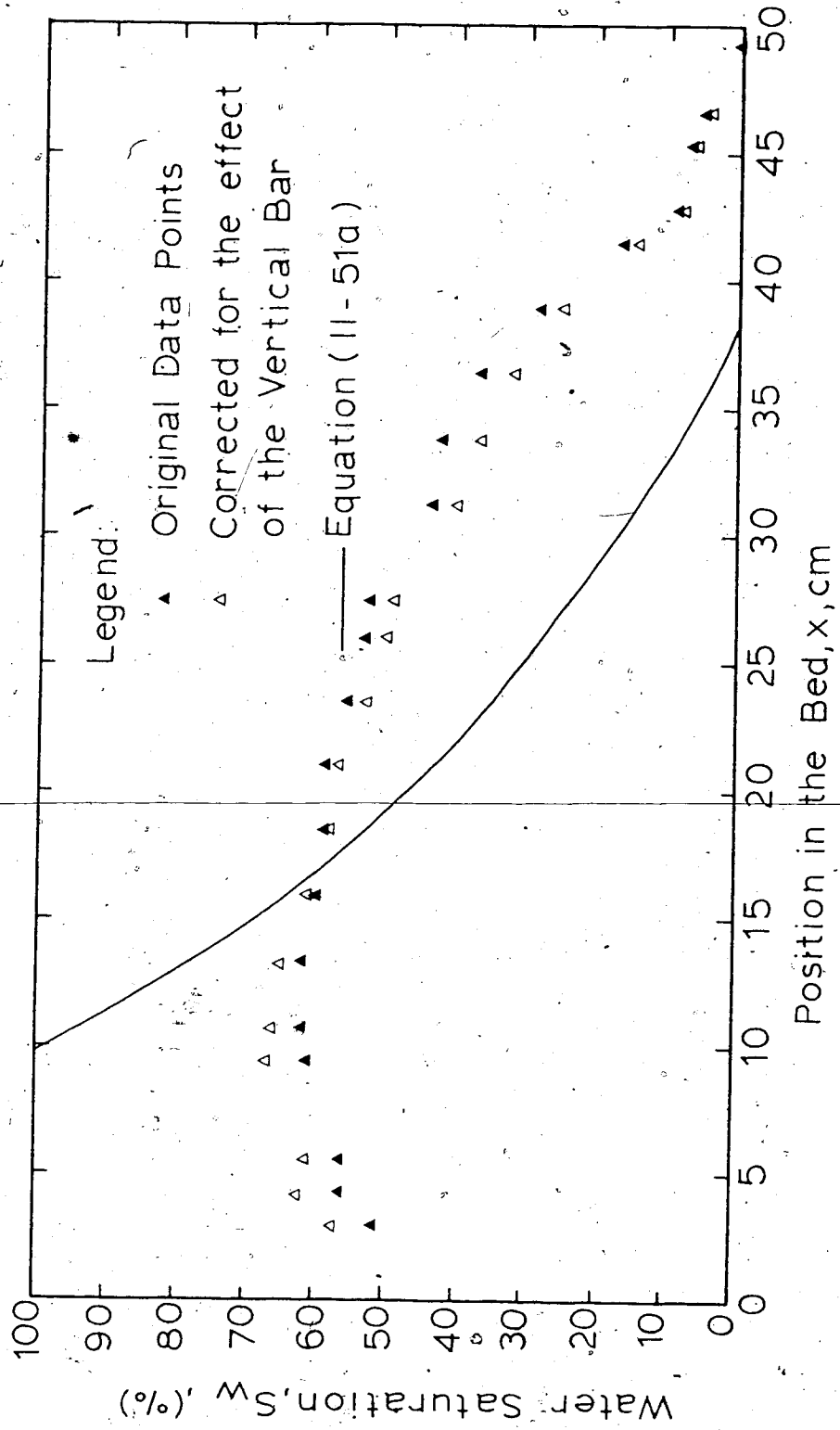


FIGURE V-33 BREAKTHROUGH SATURATION PROFILE OF RUN  
NO. 7, ROLL NO. 12 (GLYCEROL SOLUTION FLOOD)

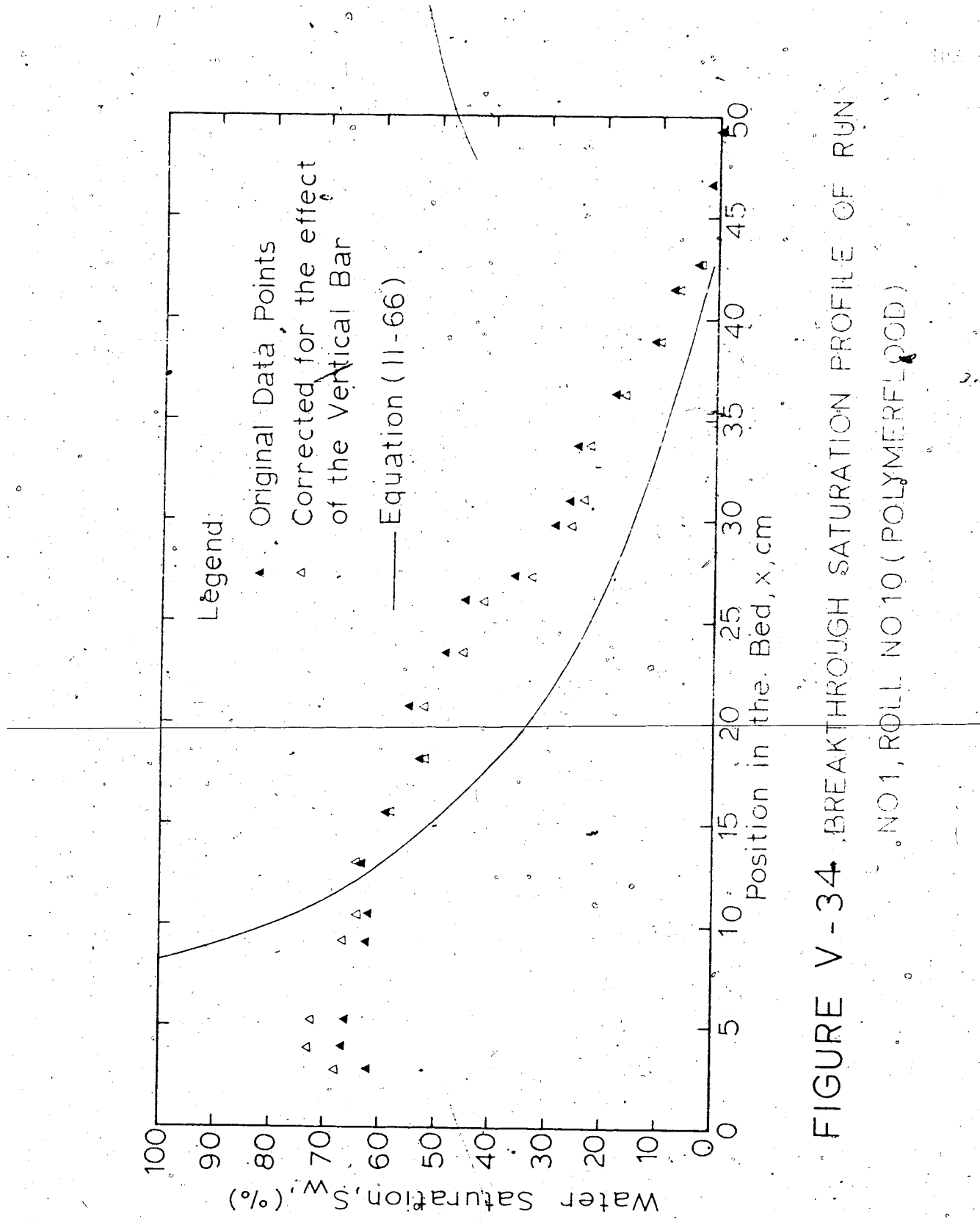


FIGURE V-34, BREAKTHROUGH SATURATION PROFILE OF RUN NO 1, ROLL NO 10 (POLYMER PCD)

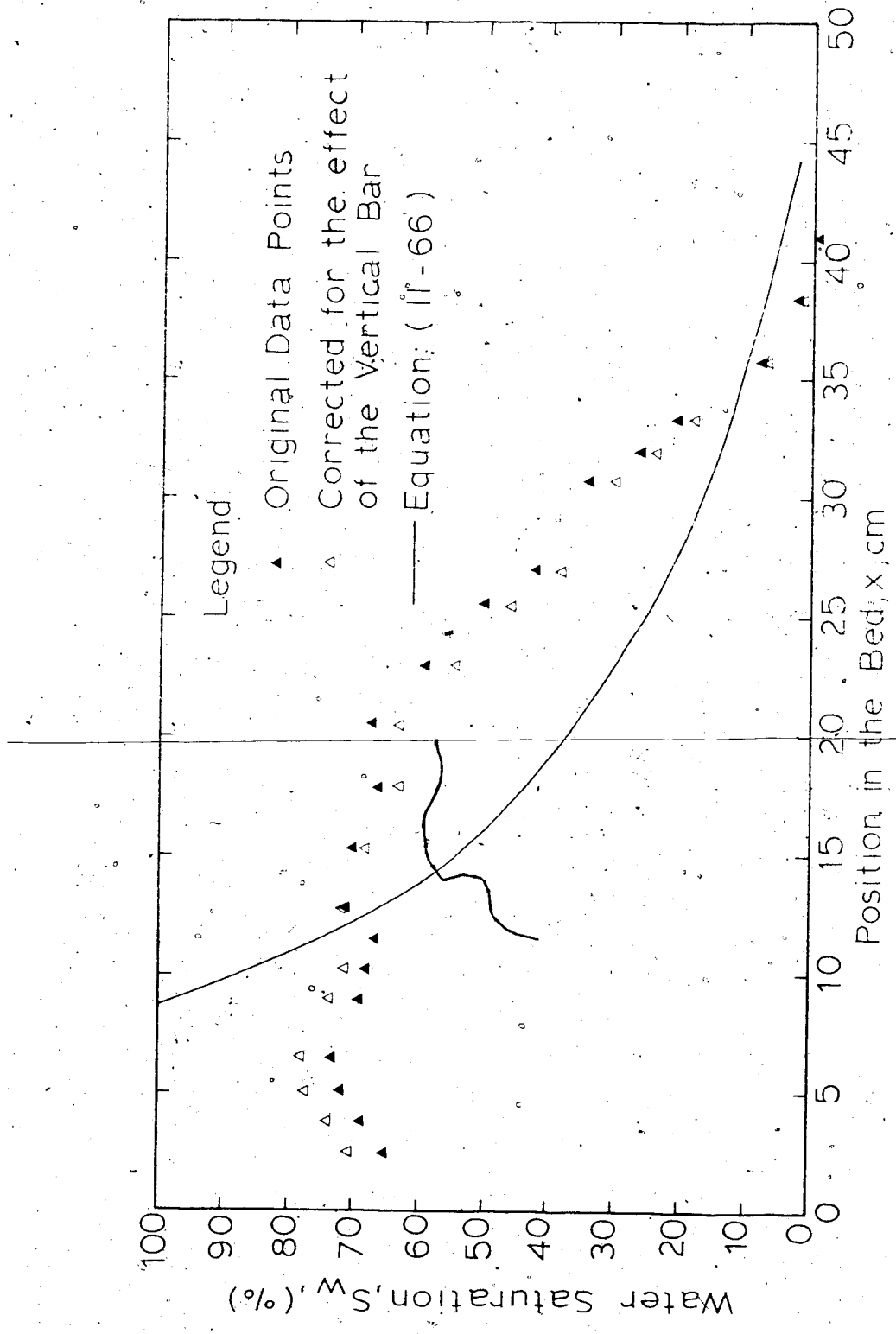


FIGURE V-35 BREAKTHROUGH SATURATION PROFILE OF RUN NO. 5, ROLL NO. 10 (POLYMER FLOOD)

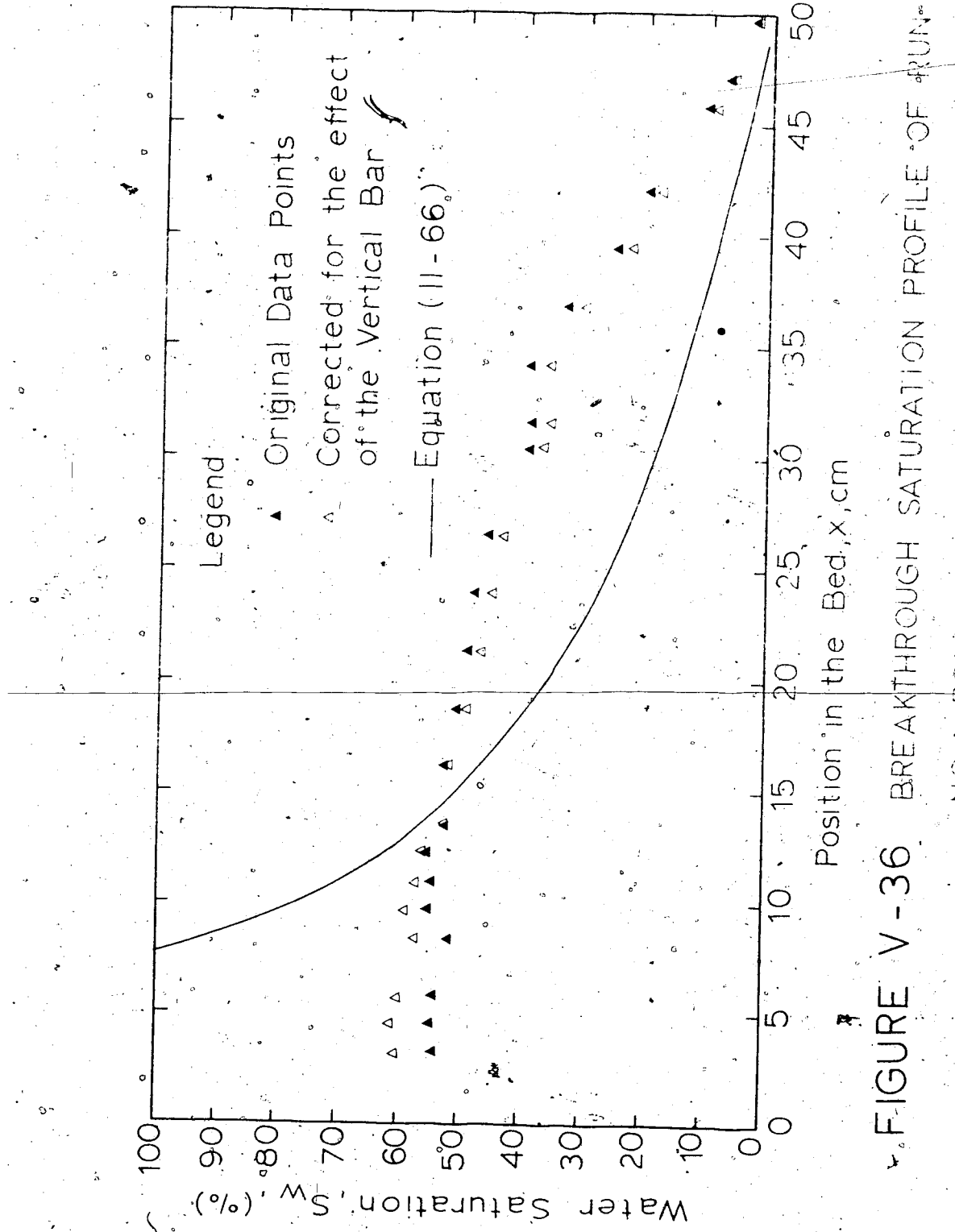


FIGURE V - 36.

BREAKTHROUGH SATURATION PROFILE OF RUN  
NO. 4, ROLL NO. 11 (POLYMER LOGO)

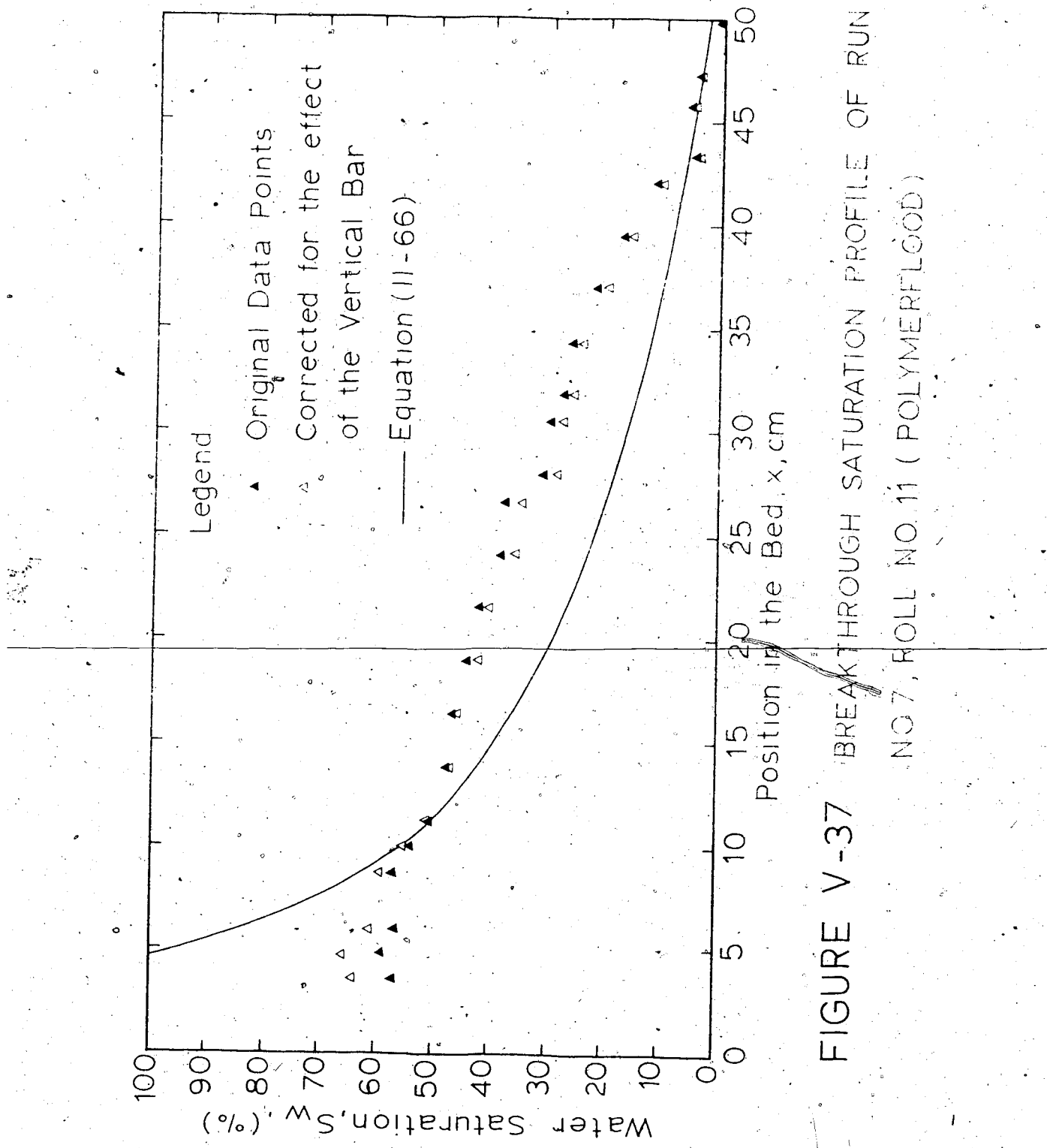


FIGURE V-37 BREAKTHROUGH SATURATION PROFILE OF RUN NO. 11 (POLYMER FLOOD)

## CHAPTER VI

## DISCUSSION OF THE RESULTS

VI.1 Pressure Drop

It was mentioned in Section (V.1) that the arithmetic average of the absolute permeability values in Tables (F-3, 4) was chosen to approximate the permeabilities of the beds. In Figure (VI-1)  $\Delta P/\mu L$  is plotted against superficial velocity,  $U$ , to show the quality of the data and also the applicability of the Darcy's law. The slopes of the lines shown in this Figure are the inverse of the corresponding average absolute permeabilities.

The absolute permeability predicted by Equation (B-21) with the commonly used value (see Appendix B)  $C_t = 25/12 = 2.08$  was very close to the measured value in the case of the small beads, while a different geometrical constant is necessary to fit the data for the large beads. This discrepancy is probably due to a wall effect. The ratio of bead depth to diameter of beads was approximately three in the case of the large beads. The minimum ratio of column diameter to bead size for a packed column free from wall effects is reported (58) to be eight; thus some wall effect is expected with the large beads.

The geometric constant calculated for the large beads based on the absolute permeability measurements was  $C_t = 3.45$ . This value was used in calculating the Reynolds number from Equations (B-27, 28) for the large beads.

The linearity of the friction factor v.s. Reynolds number for Newtonian fluids is evident from Figure (V-1) which also shows the applicability of Darcy's law.

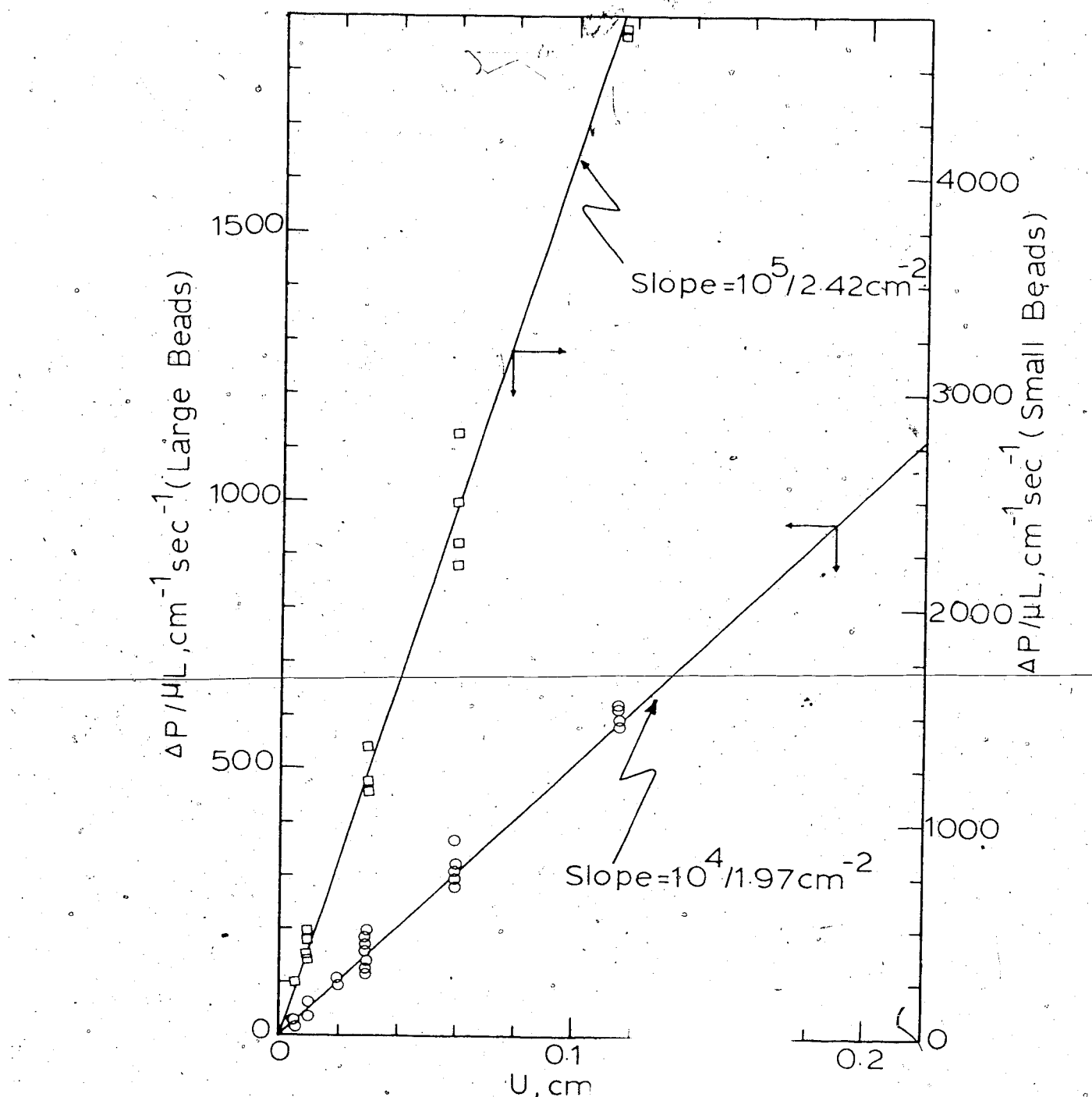


FIGURE VI-1 PRESSURE DATA FOR ABSOLUTE PERMEABILITY MEASUREMENT

For the three different polymer solutions, upward deviation of the data points from the straight line is observed. This upward deviation could be attributed to the effect of elasticity, adsorption and plugging as has been discussed in the previous work (34, 59).

Deviation from linearity can also be demonstrated as in an earlier work (68), by plotting  $f_k N_{Re}$  against the Deborah number. This is performed in Figure (VI.2).

The Deborah number is defined and calculated for the polymer solutions in Appendix C. The upward deviation at high flow rates is emphasized in this Figure. Different concentrations of the polymer solution tend to show independent trends of upward deviation.

That is 0.05% Separan solution shows a significant effect of elasticity at a Deborah number of  $10^{-1}$  while the 0.2% Separan solution does not seem to show any elasticity effect even at a Deborah number of unity. The early occurrence of the upward deviation is not due to adsorption or plugging effects. Because, if this was the case, the more concentrated solutions would have appeared to show higher upward deviation at an even smaller Deborah number. It is observed from Figure (VI-2) that this is not the case.

Figure (V-2) is similar to Figure (V-1) but is for the displacement process. The Reynolds number and friction factor were calculated from the same equations as for single phase flow, Equation (B-27, 28) and (B-25), except for the modification of viscosity. The viscosity used was the effective viscosity defined by Equation (II-33). In the case of polymer floods,  $\mu_w$  in Equation (II-33) was replaced by  $\bar{\eta}_w$ . The arithmetic average of the pressure gradients with asterisk in Table (F-7) was used in calculating the friction factor of the mixed zone. Figure (V-2) shows that a single valued viscosity correlates the data points satisfactorily.

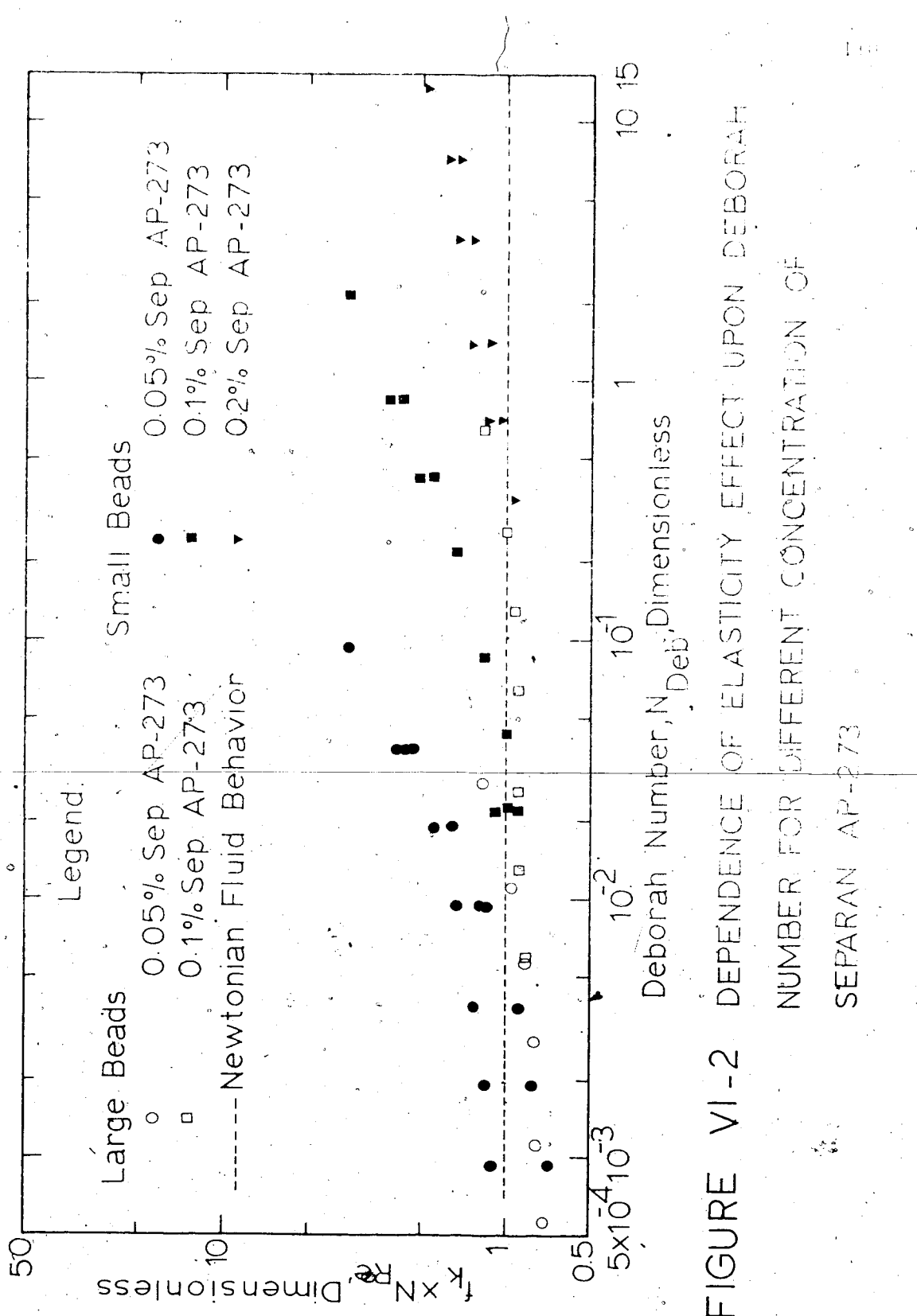


FIGURE VI-2 DEPENDENCE OF ELASTICITY EFFECT UPON DEBORAH NUMBER FOR DIFFERENT CONCENTRATION OF SEPARAN AP-273

Although the data points of the polymer solutions scatter above the Newtonian line, there is no consistent upward deviation as was observed for the single phase flow polymer solution data. As a matter of fact, the range of the flow rates studied for the displacement tests is not sufficient to make any conclusive statement on this matter. Figure (V-2) is an indication that the chosen effective viscosity gives a reasonable reproduction of the data points.

#### VI.2 Frontal Plane Advance

The linear advance of the frontal plane, or plane of zero water saturation, is predicted by Equation (II-26). The experimental data of Figures (V-3) to (V-18) support this prediction. The linearity is observed in waterflood, glycerolflood, as well as polymerflood. Figures (V-5, 8 and 10) show reproducibility of the data points when different runs with the same conditions were conducted.

The slope of the eye-fit lines is equal to the first derivative of the fraction flow function evaluated at  $S_w = 0$ . It is also understood from Equation (II-32) that the inverse of this slope gives the breakthrough recovery efficiency. Therefore higher slope indicates less recovery or more severe fingering. The data points of different flow rates tend to behave similarly in a reasonable range of flow rates. The effect of flow rate is being shown in Figures (V-3) and (V-4) for the large and small beads respectively. It is observed in Figure (V-4) that the data points of the different flow rates ranging from  $q = 0.32$  to  $3.2 \text{ cc/sec}$  could be presented by a single line while the highest flow rate  $q = 6.35 \text{ cc/sec}$  and smallest  $q = 0.16 \text{ cc/sec}$ , tend to have smaller slope which means better efficiency. More stable displacement at very low flow rate is not surprising because in the present experiments there exists some small

effect of capillary and gravity forces which become important at very low flow rate. This tends to stabilize the displacement process. However the better recovery at high flow rate was not expected. Referring to the motion pictures of the different cases, it was noticed that in the case of high flow rate many small fingers were created which helped to sweep the area more efficiently. A similar behaviour was observed for large beads. This behaviour can be observed in the sample photographs presented in Figures (IV-7) and (IV-8).

The effect of flow rate on the slope of the frontal advance lines was more pronounced for glycerol solution floods. This is shown in Figure (V-7) which reveals that the smaller flow rates have less slope corresponding to higher efficiency. The effect of flow rate on recovery is presented in Figure (VI-3) for water and glycerol floods.

The effect of viscosity ratio becomes evident by comparing the results of the different concentration glycerol solutions and also the results for waterflood. Higher viscosity ratio defined by Equation (II-45) produces less stable displacement which is in the same direction as predicted by the mobility ratio considerations (41). This will be further explored in the next section.

From the present data points some effect of the bead size is noticeable. The slopes of the eye-fit lines in Figure V-3 are smaller than those of the corresponding lines in Figure V-4 which means smaller recovery for the smaller beads. This can be verified with the visual observation. While fingering patterns were similar in the axial direction, in the case of the small beads the fingers did not cover the depth of the bed. This effectively caused smaller concentration of displacing

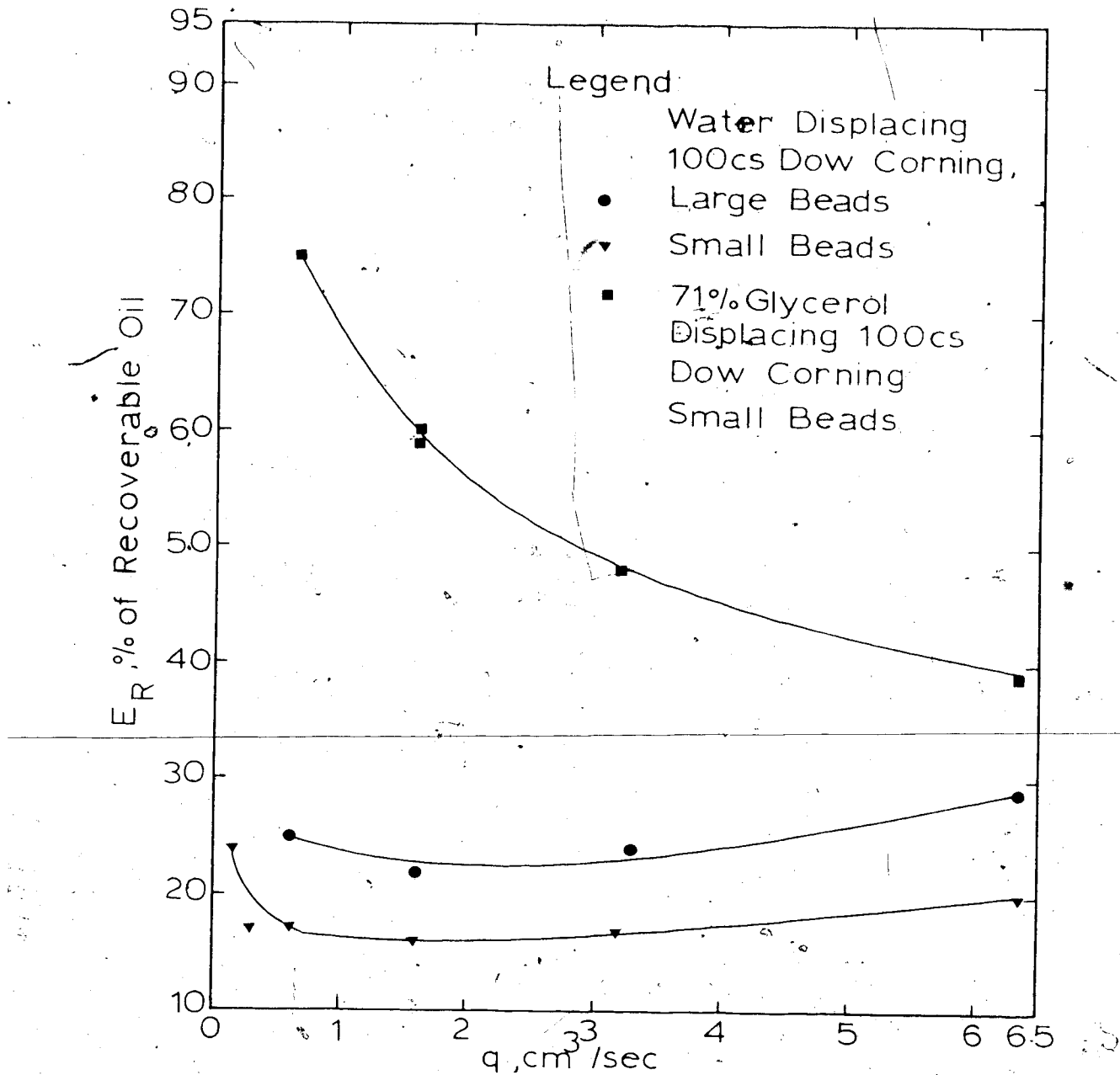


FIGURE VI-3 EFFECT OF FLOW RATE ON RECOVERY

fluid than if the fingers were the thickness of the bed. For the large beads fingers were nearly the thickness of the bed causing a higher concentration of displacing fluid. This can be attributed to the effect of the front and back walls on finger configuration which forced the bed to behave more like a narrow open channel.

In their study of viscous fingering in miscible displacement, Benham, et al. (38) showed that the displacement in an open channel is more stable than in a packed bed. Therefore, the behaviour of the bed with larger beads is in the expected direction. Indeed, as already discussed the pressure drop measurements for the same bed showed some wall effect indicating that the bed did not fully represent a packed bed free from wall effects. The effect of the bead size is much less pronounced for polymerflood than waterflood.

It is understood that the term  $qt/\delta A$  is the position of the average interface. That is the position of the hypothetical interface of a completely stable displacement. Therefore, for a complete piston-like displacement, the zero saturation plane would coincide with the position of the average interface. Or in terms of the displacement figures, a plot of  $x_0$  vs.  $qt/\delta A$  is a line with slope unity which is the limiting case. The limiting case of slope unity was shown experimentally by displacing water with oil. The data points of this experiment are shown in Figure (V-17). Due to the highly favourable viscosity ratio a complete piston-like displacement was expected which is not surprising.

It is evident from Figures (V-9 to 16) that all the polymer runs have smaller slopes than the waterflood which indicates better efficiency.

Higher concentration of polymer produces better efficiency. This is shown in Figure V-16. However, the increase in recovery from 0.1% Separan to 0.2% was not as large as that from 0.05% to 0.1% Separan.

This suggests a limiting effectiveness of increasing the polymer concentration.

### VI.3 Volumetric Recovery Efficiency at Breakthrough

The slope of the frontal plane advance lines, as discussed in the former section, was inversely related to the volumetric recovery efficiency at or before breakthrough. To further examine the effect of viscosity ratio on the volumetric efficiency, the latter was plotted against viscosity ratio in Figures (V-19) and (V-20) for Newtonian and non-Newtonian floods respectively. The theoretically predicted curves of Equations (II-52, 63) are also presented. For the waterflood some available literature data points have also been included to show the consistency of the theoretical prediction discussed in Chapter II. Considering the fact that the experimental work of the other investigators has been performed with quite different and diversified situations such as the size and type of the bed, beads, etc., the data points fit the theoretical curve in a satisfactory manner. The effect of the flow rate, which has not been reflected in the analysis seems to be inevitable. This effect has already been discussed in the preceding section.

The data points of the polymerfloods in Figure (V-20) are without exception below the theoretical curve of Newtonian displacing fluids.

This means that at the same viscosity ratio, as defined by Equation (II-64), the recovery of the polymer solution is less than Newtonian fluids.

This is in contrast to conclusions that one might arrive at by reviewing the abundant literature material on this subject (42, 43, 45, 57).

Improving the mobility ratio of waterflood via increasing the viscosity of the displacing fluid has shown increased recovery efficiency. Also, it is well documented (42, 43, 60-62) that the addition of polymer to water may decrease its mobility many times more than would be expected from the solution viscosity alone. However, this by itself does not justify the claim that the recovery efficiency would also increase as many times as the mobility reduction. The earlier literature attributes mobility reduction of the polymer solution to viscosity as well as the entrapment or adsorption of the polymer molecules, and possibly the effect of polymer solution elasticity. Only that portion of mobility reduction due to the viscosity can be safely considered for recovery increase. Adsorption, pore blockage and any elasticity effect may or may not change recovery efficiency. No evidence or direct comparison has been made to show that the recovery efficiency of the polymerflood will increase as many times as its mobility has been reduced. Different arguments may be necessary for heterogeneous porous media. As shown in former work (34), due to the effect of elasticity of the polymer solution, the effect of heterogeneity seems to be suppressed by adding polymers.

Lee, et al. (71) in studying a Five-Spot Hele-Shaw model, also reported a lower areal sweep at breakthrough with polymer solutions than with Newtonian fluids of comparable viscosity. Their analysis only allows for an effect of polymer through a variation of viscosity with shear rate due to the radial flow. In linear flow, therefore, they would predict no

effect. They did not include the additional dependency of the polymer solution apparent viscosity on the saturation distribution as discussed in Section II-9.

#### VI.4 Saturation Profile

Saturation profiles presented in Figures (V-21) to (V-37) are the profiles obtained at breakthrough. Due to the physical difficulties encountered in obtaining the correct data of water saturation, some correction had to be applied. The procedure and its justification is discussed in Appendix (G.3).

From the experimental measurements of the saturation profiles presented in Figures (V-21) to (V-37) two different types of saturation distribution are observed. In the case of waterfloods a sharp decrease in water saturation is noticed at the beginning of the bed, then the change in saturation becomes more gradual. Refer to Figures (V-21) to (V-27). A sharp decrease in saturation corresponds to high slope in frontal plane advance lines which is an indication of severe fingering. The sharp decrease in saturation is consistent with the theoretical prediction. This behavior is not restricted to waterflood but occurs whenever the fingering is severe such as Figures (V-28) to (V-30).

In the case of more uniform sweeping such as Figures (V-31) to (V-37), a gradual decrease followed by a sharp decrease of saturation is noticed from the experimental data points. There is no apparent major difference between Newtonian and non-Newtonian displacing fluid. In this group the predicted saturation profiles are qualitatively different from the experimental data points. This difference can not be justified from

the error analysis which is presented in Appendix (G.3). Therefore, the experimental data points indicate a different regime of saturation distribution compared to the prediction of the present theoretical analysis.

The shape of the experimental profiles is similar to the Buckley-Leverett profile with frontal transition zone. The assumption of having a mixed zone being characterized by a mixture of two immiscible fluids may not hold for a uniform displacement.

As mentioned earlier in section 1.2.2, Hagoort (32) showed that the analysis based on shock front or a relatively small frontal transition zone was not justified for  $M_R \geq 57$  where  $M_R$  is the conventional mobility ratio. Taking the viscosity ratio  $M$ , of the present analysis, equivalent to  $M_R$ , it is understood that the displacement tests of Figures (V-21 to 27) lie in the group that shock front analysis is not justified, while the glycerol solution floods, i.e. Figures (V-31 to 35) remain in the domain of the shock front analysis.

It is concluded that in the case of severe fingering the present analysis predicts the saturation distribution very accurately while the experimental data points of the more uniform swept displacement tests resemble the Buckley-Leverett profile with frontal transition zone.

#### VI.5 Effect of Polymer Solution Elasticity on Displacement Process

The theoretical analysis of Chapter II is based on purely viscous behaviour of the displacing fluid. To independently explore the possible effect of the polymer solution elasticity on the displacement process, the following approach was undertaken. Two polymers, one more elastic than the other were chosen. These polymers were Separan AP-273 and Pusher 500.

The former one having a molecular weight in the range of 10 million is more elastic than the latter with molecular weight approximately 2-3 million. (Approximate values quoted by Dow Chemical - it is not known how they were estimated). Independent normal force measurements support the relative magnitudes).

The concentrations of the two polymer solutions were adjusted to obtain a similar viscosity level at shear rates encountered in the displacement tests. Their apparent viscosity and shear stress - shear rate behaviour is compared in Table A-3 and Figure A-5. The relaxation time defined by Bueches' theory (63a) is chosen as a criterion to compare the elasticity effect of the two polymer solutions so that,

$$\theta = \frac{12(\mu_\ell - \mu_{S_0})M_1}{\pi^2 C R_g T_a} \quad (VI-1)$$

where  $\theta$  represents the relaxation time.

Writing Equation (VI-1) for both polymer solutions and dividing the respective equations, one obtains,

$$\frac{\theta_s}{\theta_p} = \frac{C_p M_{1,s}}{C_s M_{1,p}} \cdot \frac{\mu_{\ell,s}}{\mu_{\ell,p}} \quad (VI-2)$$

where the subscripts "s" and "p" stand for Separan and Pusher respectively.

In obtaining Equation (VI-2) the viscosity of the solvent has been neglected compared to the viscosity of the polymer solution at zero shear rate.

Relative viscosity,  $\mu_r$ , defined by the ratio of the polymer solution viscosity at zero shear rate to the viscosity of the solvent for large values of molecular weight is given (63b) by,

$$\mu_r = \frac{\mu_\ell}{\mu_{S_0}} = C^5 M_1^{3.4} \quad (VI-3)$$

Therefore,

120

$$\frac{\mu_{\ell,s}}{\mu_{\ell,p}} = \frac{C_s^5 M_{1,s}^{3.4}}{C_p^5 M_{1,p}^{3.4}} \quad (VI-4)$$

By substituting (VI-4) into (VI-2) and simplifying,

$$\frac{\theta_s}{\theta_p} = \left( \frac{C_s}{C_p} \right)^4 \left( \frac{M_{1,s}}{M_{1,p}} \right)^{4.4} \quad (VI-5)$$

In the present investigation the concentration of the Separan solution was chosen to be 0.1 percent and that of Pusher 0.2 percent. Therefore, by taking  $M_{1,s}/M_{1,p} \approx 3$  one obtains,

$$\frac{\theta_s}{\theta_p} = \left( \frac{1}{2} \right)^4 (3)^{4.4} = 7.86$$

That is, the relaxation time of 0.1% Separan solution is approximately eight times larger than the 0.2% Pusher 500 solution while the viscosities are approximately equal. If the elasticity of the polymer solution has any significant effect on the displacement behavior it should be evident from comparison of the results of these two displacements. If the displacement behavior, such as the advancing rate of the zero saturation plane, breakthrough recovery, and saturation profile are similar, it should be safe to conclude that the polymer solution elastic behavior has no significant effect on the behavior of the displacement process.

Figure (V-18) gives a comparison of the advancing rate of the zero saturation plane at two different flow rates. The slopes of the two eye-fit lines are very nearly identical. The small difference in the slope is

attributed to the small difference in viscosity level.

The breakthrough recovery efficiency evaluated from the slope of the eye-fit lines of Figure (V-18), also, by using a stop watch to measure the time of the injection period till breakthrough is compared in Table (F-9) which is reproduced below:

Table VI-1 Comparison of the Separan  
and Pusher Displacement Recoveries

Flow Rate $q$ $\text{cm}^3/\text{sec}$	$E_R$ , % of Recoverable Oil			
	Separan AP-273		Pusher 500	
	Slope	Stop Watch	Slope	Stop Watch
0.15885	30	28	33	31
0.6354	18	18	17	17

Obviously the breakthrough recovery efficiencies of Separan are closely in agreement with those of pusher.

Figure (V-30) compares the breakthrough saturation profiles of the two fluids at a flow rate of  $q = 0.6354 \text{ cc/sec}$ . The theoretical curve predicted by Equation (II-66) with  $n = 0.53$  for 0.1% Separan AP-273 is also included in this Figure. The experimental data points of the two different displacements are surprisingly close to each other which leads to the conclusion that elasticity has little if any effect on the displacement. This is in agreement with the earlier conclusion concerning the effect of polymer as shown in Figure (V-20).

## CHAPTER VII

## CONCLUSIONS AND RECOMMENDATIONS

VII.1 Conclusions

A new analytical approach has been presented to describe displacement behavior in porous media. This analysis differs in a major way from conventional methods in that relative permeability is eliminated. The present analysis and the experimental investigation afford the following conclusions.

1. The pressure drop of the mixed zone can be adequately predicted by assuming an effective viscosity which is obtained to be equal to an arithmetic average of the displacing and displaced fluid viscosities.
2. The progress of the zero saturation plane was found to be linear with time. This linearity holds for waterflood as well as polymerflood.
3. The experimental relative permeability data obtained from steady state conditions does not reflect the phenomenon of channeling faithfully. This deviation tends to be worse at larger viscosity ratios.
4. Estimation of the breakthrough recovery from Equations (II-52, 63) for water and polymer flood respectively is satisfactory compared to predictions based on presently used methods.
5. Saturation distributions predicted by Equations (II-51, 66) for water and polymer flood respectively are very close to the experimental profiles in the case of severe fingering. However, the

experimentally measured saturation distributions, for the cases of viscosity ratios less than about ten, more closely resemble the Buckley-Leverett profile with a frontal transition zone.

6. Over a range of flow rates recovery efficiency goes through a minimum. At low flow rates no growing fingers occur, while at high flow rates many fingers are created which help sweep the cross section area of the bed more uniformly.
7. The displacement behavior of a polymer flood can be adequately described by power-law model with power-law indices measured from the viscometric behavior of the polymer fluid. The effect of the polymer solution elasticity on the displacement behavior was independently checked by doing tests with two different molecular weight polymer solutions. These showed almost identical behavior. This, of course, does not overrule what might be the controlling effect of polymer solution on inception of the fingers due to the local heterogeneity or, in general, on the fingering behavior in a heterogeneous porous media.
8. The recovery efficiency of the polymer flood is very much higher than for a conventional water-flood. However, in spite of the general expectations, it is less than the case of Newtonian displacing fluid with comparable viscosity. This behavior is reflected in Equation (II-63) via the power-law exponent,  $n$ . A smaller  $n$ , which corresponds to the more non-Newtonian behavior of the polymer solution, results in smaller recovery efficiency.

9. Initiation of an individual finger does not guarantee its growth even at an unfavorable viscosity ratio. From the photographs both acceleration and deceleration of a single finger along its path in the bed was noticed.

#### VII.2 Recommendations

1. The present theoretical analysis can be adapted to the polymer slug flood to predict the minimum slug size. Experimental slug flood should be undertaken to justify the prediction. Modification of the present analysis to the polymer slug flood is simply achieved by considering a non-Newtonian slug followed and preceded by Newtonian fluids. Slug breakdown occurs when the plane of zero water saturation meets the mixed zone of polymer and oil.
2. Inclusion of the gravity and capillary forces in the present analysis could give an interesting insight of the gravity and capillary effect if the resultant equations are amenable to the analytical treatment.
3. The present approach should be adapted to the radial flow case and ultimately to pattern flooding, especially five-spot patterns, and comparisons made with the available literature data.
4. An experimental study of the different kind of polymers with different degrees of elastic effect performed on a more heterogeneous porous bed might establish useful information about the effect of the polymer solution elasticity on displacement behavior.
5. This study did not reveal a large effect of bead size, however, a more systematic approach to study the effect of bead size, if any, on

fingering phenomenon would be useful. Studies by reducing bead size should be performed cautiously so as not to include the effect of capillary forces. Alternatively a proper treatment to consider the capillary effects must be undertaken.

## BIBLIOGRAPHY

1. Debanne, J. G., "The New Oil Price Leadership and North America's Posture," paper prepared for the 26th Annual Technical Meeting of the Petroleum Society of AIME in Banff, Alberta (1975).
2. Engelberts, W. F., and Klinkenberg, L. J., "Laboratory Experiments on the Displacement of Oil by Water from Packs of Granular Material," Proceedings Third World Petroleum Congress Section II, 544 (1950).
3. Chuoke, R. L., van Meurs, P., and van der Poel, C., "The Stability of Slow, Immiscible, Viscous Liquid - Liquid Displacements in Permeable Media," AIME Petroleum Trans., 216, 188 (1959).
4. Perrine, R. L., "Stability Theory and Its Use to Optimize Solvent Recovery of Oil," Soc. of Pet. Eng of AIME J., 1, 9 (1961).
5. Perrine, R. L., "The Development of Stability Theory for Miscible Liquid - Liquid Displacement," Soc. of Pet. Eng of AIME J., 1, 17 (1961).
6. Scheidegger, A. E., "General Spectral Theory for the Onset of Instabilities in Displacement Processes in Porous Media," Geofisica Pura e Applicata, 47, 41 (1960).
7. Scheidegger, A. E., "Growth of Instabilities in Displacement Fronts in Porous Media," Physics of Fluids, 3, 94 (1960).
8. Rachford, JR., H. H., "Instability in Water Flooding Oil from Water - Wet Porous Media Containing Connate Water," Soc. of Pet. Eng of AIME J., 4, 153 (1964).
9. Outmans, H. D., "Transient Interfaces During Immiscible Liquid - Liquid Displacement in Porous Media," Soc. of Pet. Eng of AIME J., 225, 156 (1962).
10. Outmans, H. D., "Non-linear Theory for Frontal Stability and Viscous Fingering in Porous Media," Soc. of Pet. Eng of AIME J., 225, 165 (1962).
11. Scheidegger, A. E., "Stability Conditions for Displacement Processes in Porous Media," Canadian Journal of Physics, 47, 209 (1969).
12. Cellia Chung Chow and Scheidegger, A. E., "Stability Conditions for Fingering Processes in Porous Media," Journal of Hydrology, 15, 1 (1972).
13. Buckley, S. E., and Leverett, M. C., "Mechanism of Fluid Displacement in Sands," AIME Trans., 146, 107 (1942).

14. Hill, S., "Channelling in Packed Columns," Chem. Engg. Sci., 1, 1 (6), 242 (1952).
15. Blackwell, R. J., Rayne, J. R., and Terry, W. M., "Factors Influencing the Efficiency of Miscible Displacement," AIME Trans., 216, T (1959).
16. Hawthorne, R. G., "Two-phase Flow in Two-dimensional Systems. Effect of Rate, Viscosity and Density of Fluid Displacement in Porous Media," AIME Trans., 219, 81 (1960).
17. Holmgren, C. R., and Morse, R. A., "Effect of Free Gas Saturation on Oil Recovery by Water Flooding," AIME Trans., 192, 15 (1951).
18. Terwilliger, P. L., Wilsey, L. L., Hall, H. N., Bridges, P. M., and Morse, R. A., "An Experimental and Theoretical Investigation of Gravity Drainage Performance," AIME Trans., 192, 285 (1951).
19. Welge, H. J., "A Simplified Method for Computing Oil Recovery by Gas or Water Drive," AIME Trans., 195, 91 (1952).
20. Rapoport, L. A., and Leas, W. J., "Properties of Linear Water Floods," AIME Trans., 189, 139 (1953).
21. Fayers, E. J., and Sheldon, J. W., "The Effect of Capillary Pressure and Gravity on Two-Phase Fluid Flow in a Porous Medium," AIME Pet. Trans., 216, 147 (1959).
22. Havanessian, S. A., and Fayers, E. J., "Linear Water Flood with Gravity and Capillary Effects," Soc. of Pet. Eng. of AIME J., 1, 52 (1961).
23. Sheldon, J. W., Zondek, B., and Cardwell, JR., E. T., "One-Dimensional, Incompressible, Non-capillary, Two-Phase Fluid Flow in a Porous Medium," AIME Pet. Trans., 216, 290 (1959).
24. Cardwell, JR., E. T., "The Meaning of the Triple Value in Non-capillary Buckley-Leverett Theory," AIME Pet. Trans., 216, 271 (1959).
25. van Meurs, P., and van der Poel, C., "A Theoretical Description of Water-Drive Processes Involving Viscous Fingering," AIME Pet. Trans., 213, 105 (1958).
26. van Meurs, P., "The Use of Transparent Three - Dimensional Model for Studying the Mechanism of Flow Processes in Oil Reservoirs," AIME Pet. Trans., 210, 295 (1957).
27. Scheidegger, A. E., and Johnson, E. F., "The Statistical Behavior of Instabilities in Displacement Processes in Porous Media," Canadian Journal of Physics, 39, 326 (1961).

28. Koval, E. J., "A Method for Predicting the Performance of Unstable Miscible Displacement in Heterogeneous Media." Soc. of Pet. Eng. of AIME J., 3, 145 (1963).
29. Verma, A. P., "Statistical Behavior of Fingering in a Displacement Process in Heterogeneous Porous Medium with Capillary Pressure." Canadian Journal of Physics, 47, 319 (1969).
30. Dougherty, E. L., "Mathematical Model of an Unstable Miscible Displacement." Soc. of Pet. Eng. of AIME J., 3, 155 (1963).
31. Peaceman, D. W., and Rachford, JR., H. H., "Numerical Calculation of Multidimensional Miscible Displacement." Soc. of Pet. Eng. of AIME J., 2, 327 (1962).
32. Hagoort, J., "Displacement Stability of Water Drives in Water + Wet Connate Water-Bearing Reservoirs." Soc. of Pet. Eng. of AIME J., 14, 63 (1974).
33. Scheidegger, A. E., "The Physics of Flow Through Porous Media." University of Toronto Press, Third Edition, Chapter 9 (1974).
34. Vossoughi, S., "Non-Newtonian Flow Distribution in a Porous Bed." M.Sc. Dissertation, University of Alberta, Alberta, (1973).
35. Abbott, M. B., "An Introduction to the Method of Characteristics." American Elsevier, New York, (1966).
36. Richardson, J. G., Kerner, J. K., Hafford, J. A., and Osoba, J. S., "Laboratory Determination of Relative Permeability." AIME Pet. Trans., 195, 187 (1952).
37. Jennings, JR., H. Y., "Effect of Laboratory Core Cleaning on Water-Oil Relative Permeability." Producers Monthly, 22 (10), 26 (1958).
38. Benham, A. L., and Olson, R. W., "A Model Study of Viscous Fingering" Soc. of Pet. Eng. of AIME J., 3, 138 (1963).
39. Hatschek, E., "The Viscosity of Liquids." G. Bell and Sons, Ltd., London, (1928).
40. Christopher, R. H., and Middleman, S., "Power-Law Flow Through a Packed Tube." I. & E. C. Fundamentals, 4 (4), 422 (1965).
41. Craig, JR., F. F., "The Reservoir Engineering Aspects of Water Flooding." Monograph Volume 3, Soc. of Pet. Eng. of AIME, New York, (1971).
42. Sandiford, B. B., "Laboratory and Field Studies of Water Floods Using Polymer Solutions to Increase Oil Recoveries." Journal of Petroleum Technology, 16, 917 (1964).

43. Pye, D. J., "Improved Secondary Recovery by Control of Water Mobility." Journal of Petroleum Technology, Petroleum Transactions, 16, 911 (1964).
44. Jewett, R. L., and Schwarz, G. F., "Polymer Flooding - A Current Appraisal". Paper No. SPE 2545 prepared for the 44th Annual Fall Meeting of the Society of Petroleum Engineers of AIME to be held in Denver, Colo. (1969).
45. Patton, J. T., Coats, K. H., and Colegrave, G. T., "Prediction of Polymer Flood Performance." Soc. of Pet. Eng. of AIME J. 11, 72 (1971).
46. Birkhoff, G., "Hydrodynamics: A Study in Logic, Fact and Similitude." Princeton University Press, (1950).
47. Langhaar, H. L., "Dimensional Analysis and Theory of Models." John Wiley & Sons, Inc. New York (1951).
48. Focken, C.M., "Dimensional Methods and Their Applications." Edward Arnold & Co., London (1953).
49. Duncan, W. J., "Physical Similarity and Dimensional Analysis." Edward Arnold & Co., London, (1953).
50. Leverett, M. C., Lewis, W. B., and True, M. E., "Dimensional Model Studies of Oil - Field Behavior." AIME Trans., 146, 175 (1942).
51. Croes, G. A., and Schwarz, N., "Dimensionally Scaled Experiments and the Theories on the Water - Drive Process." AIME Pet. Trans., 204, 35 (1955).
52. Rapoport, I. A., "Scaling Laws for Use in Design and Operation of Water - Oil Flow Models." AIME Trans., 204, 143 (1955).
53. Geertsma, J., Croes, G. A., and Schwarz, N., "Theory of Dimensionally Scaled Models of Petroleum Reservoirs." AIME Trans., 207, 118 (1956).
54. Perkins, JR., F.M., and Collins, R. E., "Scaling Laws for Laboratory Flow Models of Oil Reservoirs." AIME Trans., 219, 583 (1960).
55. Nielsen, R. L., and Tek, M. R., "Evaluation of Scale-Up Laws for Two-Phase Flow Through Porous Media." Soc. of Pet. Eng. of AIME J., 5, 164 (1965).
56. Craig, JR., F. F., "Water Flooding." Chapter I of "Secondary and Tertiary Oil Recovery Process." Interstate Oil Compact Commission, Oklahoma City, Oklahoma, (1974).
57. Knight, E. L., "Reservoir Stability of Polymer Solutions." J. of Pet. Tech., 618 (May 1975).

58. Baker, T., Chilton, T. H., and Vernon, H.C., "The Course of Liquor Flow in Packed Towers." AIChE Trans., 31, 296 (1935).
59. Vossoughi, S., and Seyer, F. A., "Pressure Drop for Flow of Polymer Solution in a Model Porous Medium." The Can. J. of Chem. Eng., 52 (5), 666 (1974).
60. Mungan, N., Smith, F. W., and Thompson, J. L., "Some Aspects of Polymer Floods." J. Pet. Tech., 18, 1143 (1966).
61. Dauben, JR., D. L., and Menzie, D. E., "Flow of Polymer Solutions Through Porous Media." J. Pet. Tech. 19, 1065 (1967).
62. Burcik, E. J., "A Note on the Flow Behavior of Polyacrylamide Solutions in Porous Media." Prod. Monthly, 29 (6), 141 (1965).
63. Middleman, S., "The Flow of High Polymers, Continuum and Molecular Rheology." Interscience Publishers, John Wiley & Sons, Inc. New York, a. 148, b. 172, C. 24, (1968).
64. Massey, B. S., "Mechanics of Fluids." D. Van Nostrand Co. Ltd., London, 161 (1968).
65. Bird, R. B., Stewart, W. E., and Lightfoot E.N., "Transport Phenomena." John Wiley & Sons, Inc., New York, a. 95, b. 79, C. 197, d. 199 (1960).
66. Savins, J. G., "Non-Newtonian Flow Through Porous Media." Ind. & Eng. Chem. 61, 18 (1969).
67. Ergun, S., "Fluid Flow Through Packed Columns." Chem. Eng. Prog., 48 (2), 89 (1952).
68. Marshall, R. J., and Metzner, A. B., "Flow of Viscoelastic Fluids Through Porous Media." I&E.C. Fundamentals, 6 (3), 393 (1967).
69. Everett, J. P., Gooch, JR., F. W., Colhoun, JR., J. C., "Liquid - Liquid Displacement in Porous Media as Affected by the Liquid - Liquid Viscosity Ratio and Liquid - Liquid Miscibility." AIME Pet. Trans., 189, 215 (1950).
70. Jones-Parra, J., Stahl, C. D., and Colhoun, J. C., "A Theoretical and Experimental Study of Constant Rate Displacements in Water Wet Systems." Producers Monthly, 18 (5), 18 (1954).
71. Lee, K. S., and Claridge, E. L., "Areal Sweep Efficiency of Pseudoplastic Fluids in a Five-Spot Hele-Shaw Model." Soc. of Pet. Eng. of AIME J., 8, 52 (1968).
72. Lamb, H., "Hydrodynamics". Dover Publications, New York. (1945).

## APPENDIX A

RHEOLOGICAL PROPERTIES OF THE  
EXPERIMENTAL SOLUTIONS

A WEISSENBURG R-18 Rheogoniometer with cup and cylinder arrangement was used to measure viscosity of the glycerol and polymer solutions.

Consider two vertical coaxial cylinders, the outer one of which is rotating with an angular velocity  $\Omega$  by application of a torque  $T_o$ . This torque must balance the torque exerted by the fluid on the inner face of cup so that,

$$T_o = 2\pi b_1^2 h \tau_R \quad (A-1)$$

where,  $b_1$  represents the radius of the cup,  $h$ , the height of the cylinder in contact with the fluid, and  $\tau_R$  is wall shear stress.

The torque,  $T_o$ , is determined by measuring the torsion in a T-bar suspending the cylinder, so that,

$$T_o = S_1 \Delta t K_t \quad (A-2)$$

where,  $S_1$  represents the "torque transducer" sensitivity which was calibrated to be equal to 1.008 micron/volt,  $\Delta t$ , movement of torsion head transducer in volts, and  $K_t$ , torsion bar constant which was equal to 106.6 dyne cm per micron movement of the transducer. The dimensions of the cup and cylinders were as follows:

radius of the cup,  $a_1 = 2.747$  cm

radius of the cylinder,  $b_1 = 2.5$  cm

height of the cylinder,  $h = 5$  cm

therefore, equations (A-1, 2) become,

$$T_{\text{or}} = 196.55 \tau_R \text{ ergs} \quad (\text{A-4})$$

$$\tau_E = 107.35 \tau_R \text{ ergs} \quad (\text{A-5})$$

For Newtonian fluids, it can be shown (63, 65a) that the torque is related to the viscosity of the fluid by,

$$T_{\text{or}} = K_1 \dot{\gamma} \quad (\text{A-6})$$

where  $K_1$  is a constant for any given apparatus and equal to,

$$K_1 = \frac{4\pi h^2 b_1^2}{b_1^2 - b_1 a_1} = 2286.49 \text{ ergs} \quad (\text{A-7})$$

From equations (A-5, 6)  $\dot{\gamma}$  for Newtonian fluid is calculated by,

$$\dot{\gamma} = 0.5047 \frac{\tau_E}{\mu} \text{ peise} \quad (\text{A-8})$$

shear rate of Newtonian fluid in Couette flow is given (64) by,

$$\dot{\gamma} = \frac{2a_1^2 b_1^2}{r_m^2 (b_1^2 - b_1 a_1)} \quad (\text{A-9})$$

where  $r_m$  is the mean radius.

$$r_m = \frac{a_1 + b_1}{2} \quad (\text{A-10})$$

Therefore,

$$\dot{\gamma} = 10.57 \Omega \cdot \text{sec}^{-1} \quad (\text{A-11})$$

The shear rate of a power-law fluid in Couette flow is given (63C) by,

$$\dot{\gamma} = \frac{2\Omega}{n \left[ 1 - \left( \frac{b_1}{a_1} \right)^{2/n} \right]} \quad (\text{A-12})$$

The shear stress-shear rate relationship of the power-law model is given by equation (B-9). Therefore by plotting  $\log \tau$  v.s.  $\log \dot{\gamma}$ , the power-law exponent,  $n$ , is obtained from the slope. The Y-intercept of such a plot at  $\dot{\gamma} = 1$  is equal to,

$$\text{Y-intercept} = m \left[ \frac{2}{n \left[ 1 - \left( \frac{a_1}{a_2} \right)^{2/n} \right]} \right]^n \quad (\text{A-13})$$

from which  $m$  can be determined. Or, by knowing  $n$ ,  $\dot{\gamma}$  is calculated from equation (A-12). A plot of  $\log \tau$  v.s.  $\log \dot{\gamma}$  is constructed with the slope equal to  $n$  and Y-intercept at  $\dot{\gamma} = 1$  equal to  $m$ .

The apparent viscosity of the polymer solutions is calculated from the following equation,

$$\eta_a = m \dot{\gamma}^{n-1} \quad (\text{A-14})$$

Plots of shear stress v.s. shear rate are given in Figures (A-1), (A-3) and (A-5). Figure (A-1) is for the Glycerol solutions, while the viscometric behaviour of polymer solutions is presented in Figures (A-3) and (A-5). Figures (A-2) and (A-4) are plots of  $\tau$  v.s.  $\dot{\gamma}$  used to obtain  $n$  for the polymers. All of the data points of the viscometric measurements are included in Tables (A-1 to 3).

It should be mentioned that most of the polymer floods were performed on Separan solutions with rheological properties given by Figure A-3. A new batch of 0.1% Separan solution was prepared for the last few displacement tests to compare with 0.2% pusher 500. The rheological properties of this new solution with those of pusher 500 are presented in Figures (A-4, 5) and Table (A-3).

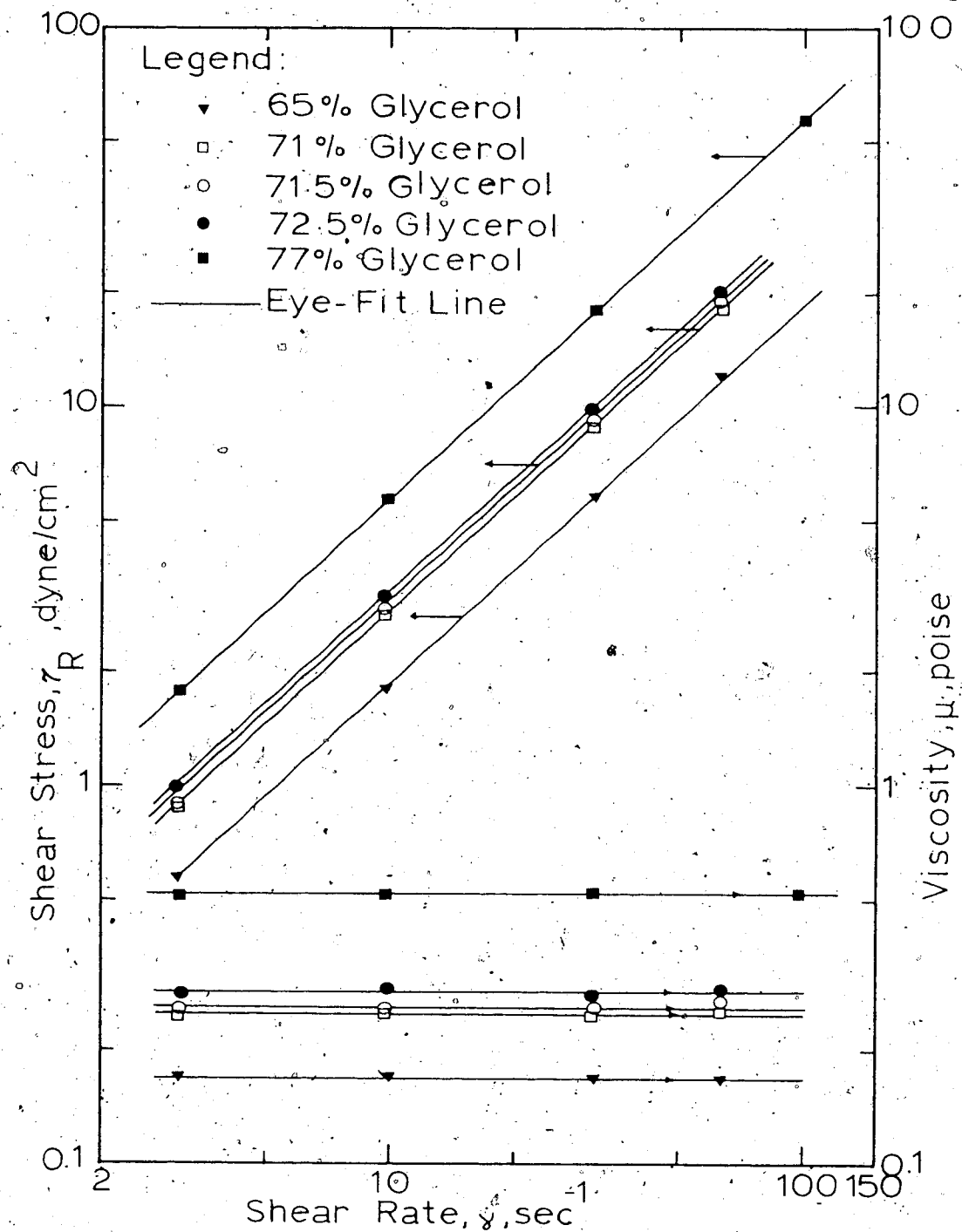


FIGURE A-1 VISCOMETRIC BEHAVIOR OF GLYCEROL SOLUTIONS

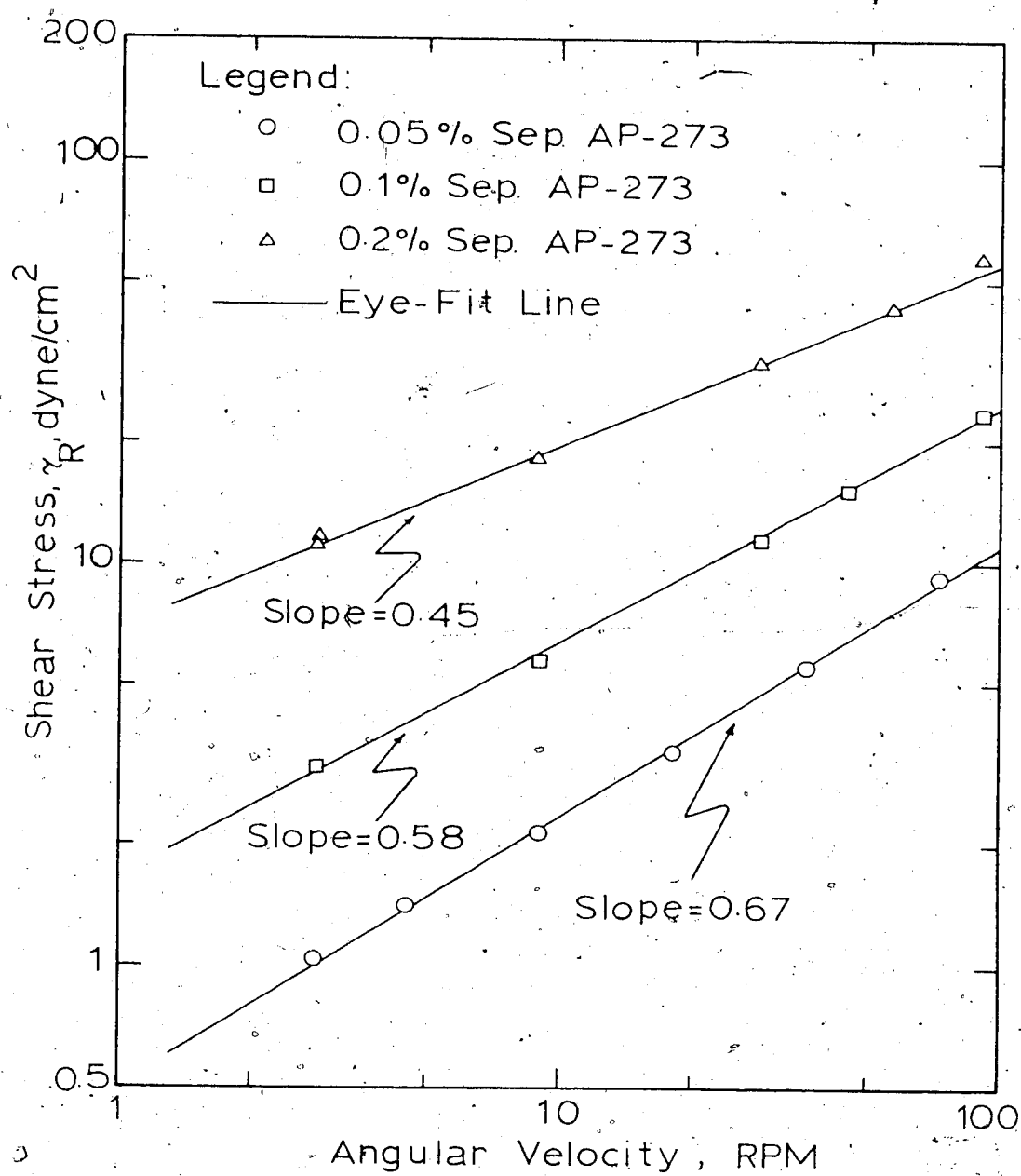


FIGURE A-2 SHEAR STRESS VS. ANGULAR VELOCITY FOR SEPARAN AP-273 SOLUTIONS

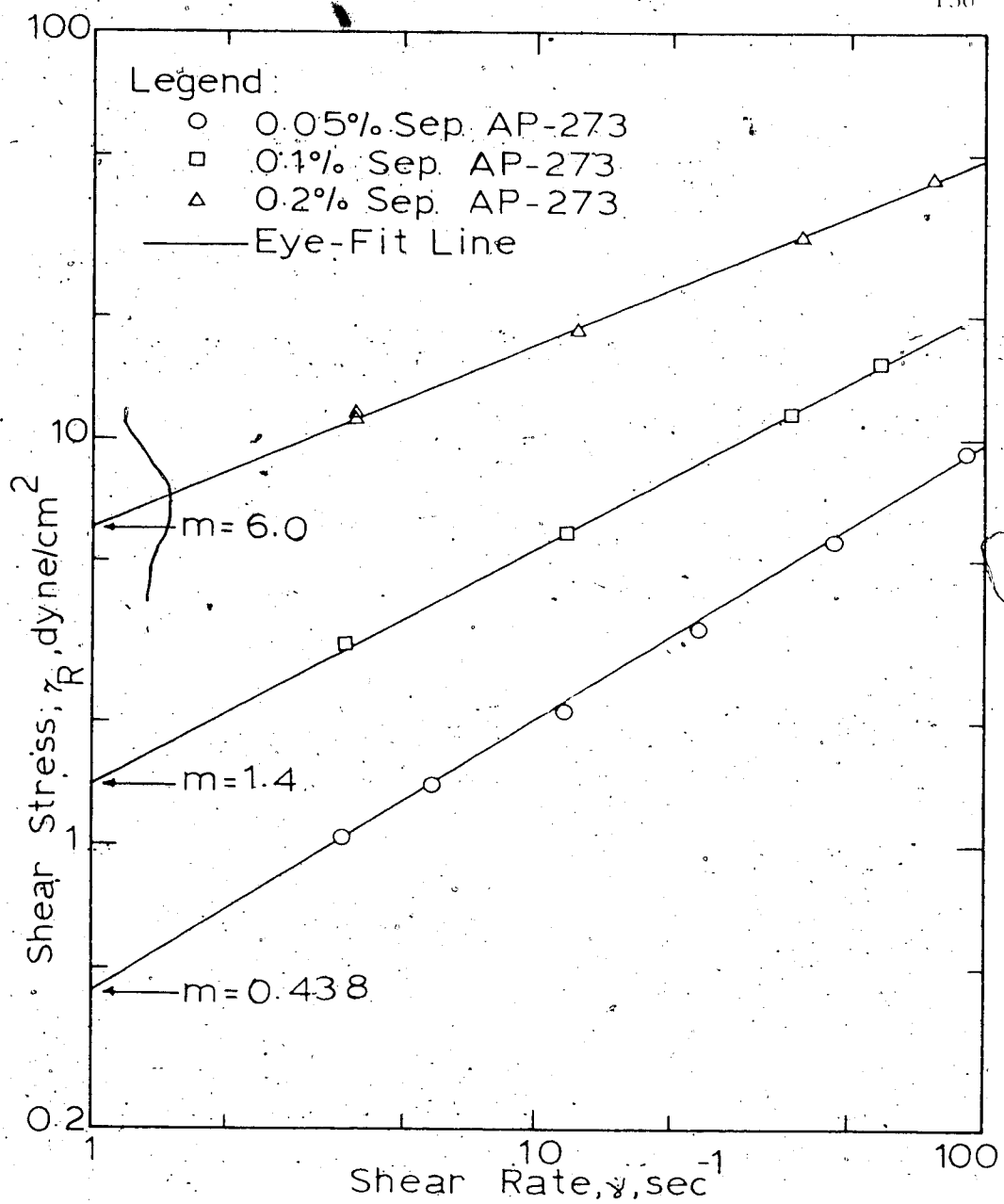


FIGURE A-3 SHEAR STRESS-SHEAR RATE BEHAVIOR OF SEPARAN AP-273 SOLUTIONS

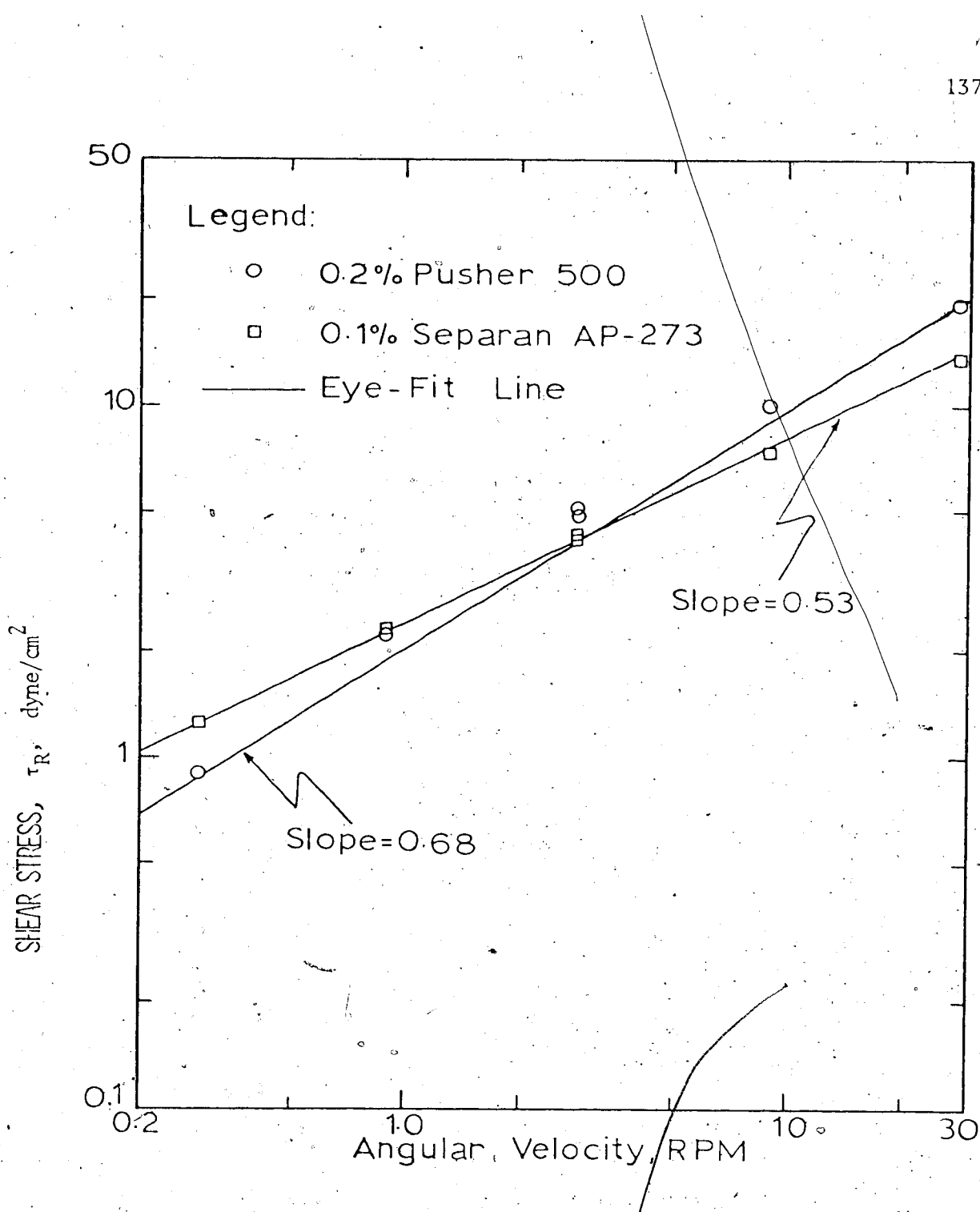


FIGURE A-4 SHEAR STRESS VS. ANGULAR VELOCITY FOR POLYMER SOLUTIONS

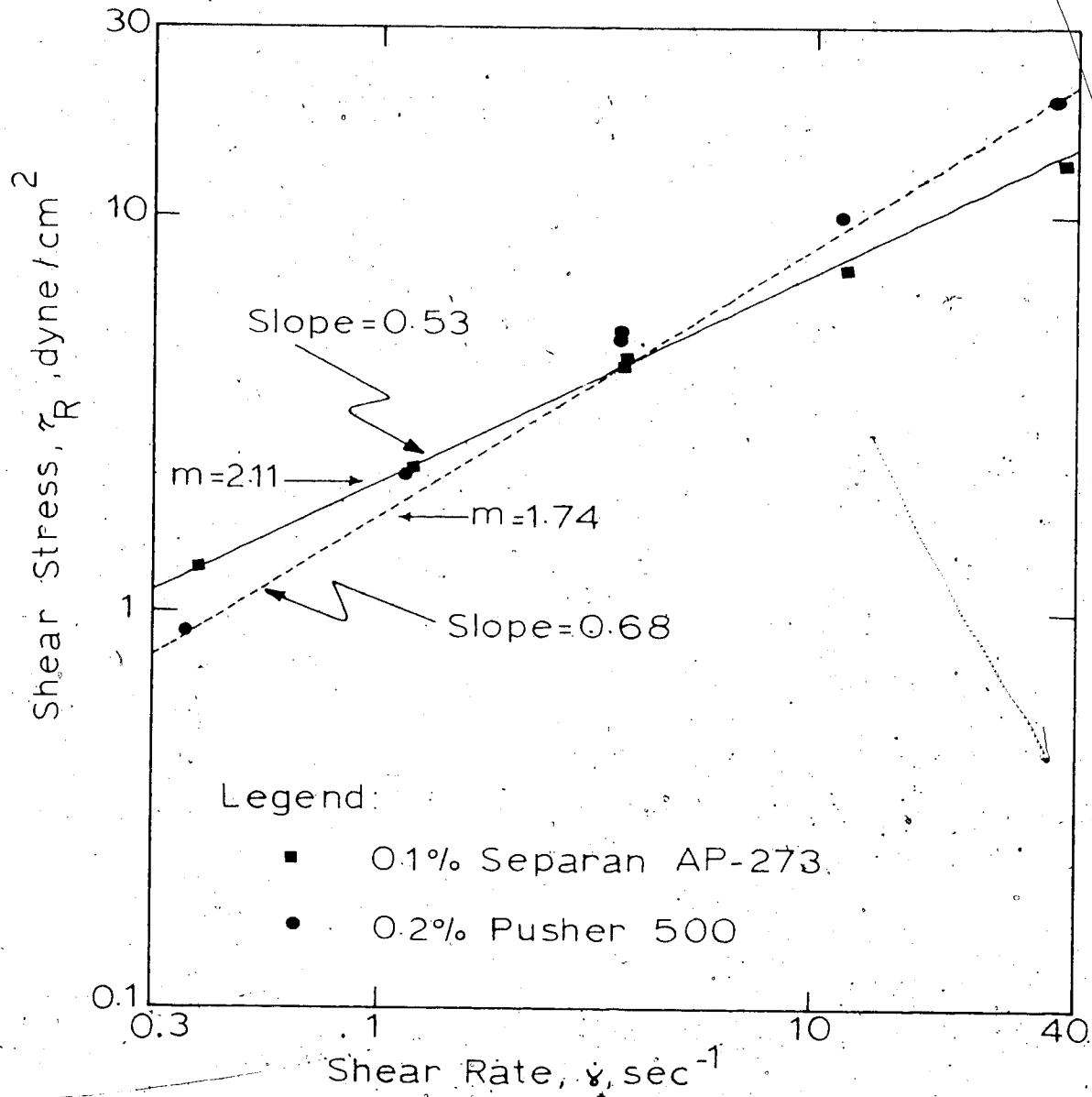


FIGURE A-5 SHEAR STRESS-SHEAR RATE BEHAVIOR OF POLYMER SOLUTIONS

TABLE A.1

179

 VISCOSIMETRIC MEASUREMENTS OF GLYCEROL  
 SOLUTIONS

Run No.	RPM	$\bar{V}$ sec <sup>-1</sup>	AT Volt	$\tau_R$ dynes/cm <sup>2</sup>	$\mu$ Poise
65% Glycerol solution, T = 20°C					
1	2.84	5.14	1.85	0.57	0.17
2	9.0	9.96	5.55	1.83	0.17
3	28.4	51.44	10.6	0.80	0.17
4	56.8	62.87	21.8	11.93	0.17
5	90.1	99.62	3.4	1.86	0.17
71% Glycerol Solution, T = 20°C					
1	2.84	5.14	1.6	0.88	0.20
2	9.0	9.96	5.1	2.59	0.20
3	28.4	51.44	10.0	8.76	0.20
4	56.8	62.87	32.3	17.68	0.20
5	92.84	5.14	1.6	0.88	0.20
71.5% Glycerol Solution, T = 20.5°C					
1	2.84	5.14	1.65	0.9	0.20
2	9.0	9.96	5.50	2.9	0.20
3	28.4	51.44	10.6	9.88	0.20
4	56.8	62.87	35.7	18.44	0.20
5	92.84	5.14	1.65	0.9	0.20
72.5% Glycerol Solution, T = 20°C					
1	2.84	5.14	1.8	0.99	0.23
2	9.0	9.96	5.75	5.15	0.23
3	28.4	51.44	17.6	9.65	0.23
4	56.8	62.87	36.8	20.14	0.23
5	92.84	5.14	1.8	0.99	0.23
77% Glycerol Solution, T = 20°C					
1	2.84	5.14	3.25	1.78	0.51
2	9.0	9.96	10.5	5.75	0.52
3	28.4	51.44	32.9	18.0	0.52
4	90.1	99.62	105	57.46	0.52
5	92.84	5.14	3.25	1.78	0.51

TABLE A-2

VISCOMETRIC MEASUREMENTS OF SEPARAN  
AP-273 SOLUTIONS

Run No.	RPM	$\Delta t$ Volt	$\eta_{sp}$ Dynes/cm <sup>2</sup>	$\eta$ dl./sec. <sup>-1</sup>	$\eta_0$ dl./sec. <sup>-1</sup>
$0.05\%$ Separan AP-273, $T = 21^\circ C$					
1	2.84	1.9	1.04	5.62	0.81
2	4.52	3.6	1.42	5.76	0.85
3	9.0	5.9	2.15	11.48	0.89
4	17.99	10.25	5.42	22.94	0.93
5	36.8	10.25	5.61	45.90	0.97
6	71.6	17.	9.50	91.29	0.10
7	4.52	2.6	1.42	5.76	0.10
$0.1\%$ Separan AP-273, $T = 20^\circ C$					
1	2.84	7.8	5.15	5.7	0.81
2	9.0	5.77	11.72	0.58	0.58
3	28.4	11.27	36.97	0.34	0.34
4	45.2	15.21	58.84	0.21	0.21
5	90.0	23.75	117.16	0.19	0.19
$0.2\%$ Separan AP-273, $T = 20^\circ C$					
1	2.84	20.2	11.05	5.86	0.88
2	9.0	55.2	18.17	12.24	1.13
3	28.4	57.0	31.19	38.63	1.87
4	56.8	79.5	43.51	77.27	0.33
5	90.	106.	58.01	122.43	0.45
6	2.84	21.2	11.6	3.86	2.85

TABLE A-3  
COMPARISON OF THE VISCOMETRIC BEHAVIOUR  
OF 0.2% PUSHER 500 AND 0.1% SEPARAN  
AP-273, T = 20°C

Run No.	Speed, RPM	$\Delta t_0$ , volt	$f_R$ , dyne/cm <sup>2</sup>	$\dot{\gamma}$ , sec <sup>-1</sup>	Pusher 500	Separan AP-273						
1	2.84	2.9	7.16	4.95	4.16	5.01	5.75	1.15	1.15	1.15	1.15	1.15
2	6.9	4.05	4.25	2.22	2.55	1.15	1.12	1.04	1.04	1.04	1.04	1.04
3	0.284	1.65	2.5	0.90	1.20	0.56	0.56	0.41	0.41	0.41	0.41	0.41
4	0.09	0.6	1.2	0.55	0.66	0.11	0.11	0.05	0.05	0.05	0.05	0.05
5	9.9	48.4	15.5	10.07	7.59	11.45	11.32	0.81	0.81	0.81	0.81	0.81
6	28.4	55.8	25.7	19.59	15.68	36.14	35.51	0.55	0.55	0.55	0.55	0.55
7	90.	68.75	49	57.62	26.81	114.55	118.87	0.38	0.38	0.38	0.38	0.38
8	2.84	2.25	7.9	5.06	4.52	5.01	5.75	1.15	1.15	1.15	1.15	1.15

## APPENDIX B

## MODIFIED FRICTION FACTOR

 $\phi$  AND REYNOLDS NUMBER

The capillary tube model, has been successfully applied to porous media to predict the pressure drop or friction factor Reynolds number relation of purely viscous flow (40,66). The model is based on cylindrical poiseuille flow using hydraulic radius of the medium instead of radius of the cylinder. Consider the flow of a fluid through a circular tube in the z-direction as shown in Figure (B-1).

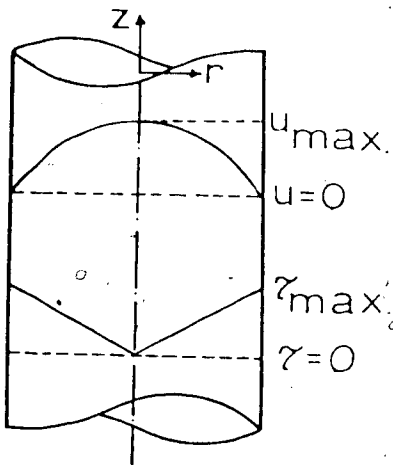


FIGURE B-1 FLOW IN CYLINDRICAL TUBE

One can write,

$$q_o = 2\pi \int_0^R u_z r dr \quad (B-1)$$

where  $q$  is volumetric flow rate,  $u_z$  velocity in the  $z$ -direction,  $r$ , radial distance and  $R$ , radius of the tube. Integrating equation (B-1) by parts and assuming no-slip at the wall yields,

$$\frac{q}{\pi R^2} = - \int_0^R r^2 \frac{du_z}{dr} dr$$

From the equation of motion (65 b),

$$\tau_z = \left( \frac{3D}{2L} \right) r \quad (B-3)$$

where  $\tau_z$  represents  $\tau_{rg}$ , and  $\Delta p$  is pressure drop along the length  $L$  of the tube. From equation (B-3) the wall shear stress,  $\tau_R$ , is obtained,

$$\tau_R = \frac{3D}{2L} R \quad (B-4)$$

It is evident from equations (B-3, 4) that,

$$dr = \frac{R}{\tau_R} d\tau \quad (B-5)$$

substituting equation (B-5) into (B-2) yields,

$$\Gamma = \frac{1}{\tau_R^3} \int_0^{\tau_R} \dot{\gamma} \tau^2 d\tau \quad (B-6)$$

where  $\Gamma$  is defined as an average nominal shear rate, i.e.

$$\Gamma = \frac{u_m}{R} \quad (B-7)$$

and  $\bar{u}_m$  is average velocity,  $\dot{\gamma} = \frac{du}{dr}$  represents true shear rate. For the assumed steady flow  $\dot{\gamma}$  is a function only of  $\tau$ . For Newtonian fluids,

$$\dot{\gamma} = \frac{\tau}{\mu} \quad (B-8)$$

and for the power law model,

$$\dot{\gamma} = m \cdot |\dot{\gamma}|^{n-1} \quad (B-9)$$

where  $|\dot{\gamma}|$  is the absolute value of  $\dot{\gamma}$ ,  $m$  and  $n$  are power-law parameters.

To modify equation (B-6) for a porous media, it is sufficient to introduce  $U/\phi$  in place of  $\dot{\gamma}$ , i.e.,

$$u_m = \frac{U}{\phi} \quad (B-10)$$

Also  $R$  should be replaced by  $2R_H$ , where  $R_H$  is hydraulic radius and  $L$  by  $L_t$ , the length of the tortuous path of the fluid. Taking  $C_t$  as the tortuosity factor or geometric constant,

$$L_t = C_t L \quad (B-11)$$

in which  $C_t$  should be obtained experimentally. Analysis of a great deal of data in the literature has led to the value 25/12 for packed columns (40, 65d).

The modified form of equations (B-4, 6) are respectively,

$$\frac{1}{\phi} = \frac{\Delta p}{C_t L} R_H \quad (B-12)$$

$$\frac{1}{\phi} = \frac{U}{2\phi R_H} = \frac{U}{\tau_\phi} \cdot \frac{1}{3} \int_0^{\tau_\phi} \dot{\gamma}^2 \tau^2 d\tau \quad (B-13)$$

where the subscript  $\phi$  indicates that the equation has been modified for the porous bed.

Following Bird, et al (65C), the hydraulic radius may be expressed in terms of the porosity and the mean particle diameter,  $D_p$ .

$$R_H = \frac{D_p \phi}{6(1-\phi)} \quad (B-14)$$

consequently,

$$\Gamma_\phi = \frac{3(1-\phi)^2 U}{D_p \phi^2} = -\frac{1}{\tau_\phi^3} \int_0^{\tau_\phi} \gamma \tau^2 d\tau \quad (B-15)$$

where,

$$\tau_\phi = \frac{\omega \Delta P}{6 C_t L} \quad (B-16)$$

$$\omega = \frac{D_p \phi}{1-\phi} \quad (B-17)$$

For a Newtonian fluid by using equation (B-8), equation (B-15) becomes,

$$\Gamma_\phi = \frac{\tau_\phi}{4\mu} \quad (B-18)$$

Solving for  $\mu$  and substituting (B-15, 16, 17) gives,

$$\mu = \frac{D_p^2 \phi^3}{72 C_t (1-\phi)^2} \frac{\Delta P}{L U} \quad (B-19)$$

From Darcy's law,

$$\mu = \frac{K}{U} \frac{\Delta P}{L} \quad (B-20)$$

Therefore,

$$K = \frac{D^2 \cdot \varphi^3}{72C_t (1-\varphi)^2} \quad (B-21)$$

Applying equation (B-9) to the equation (B-15) gives,

$$\tau_{\phi} = C_m \left( \frac{1 + 5n}{n} - \frac{1}{R} \right)^{n-1} \quad (B-22)$$

Further, equation (B-22) can be transformed into,

$$U^n = \frac{K \Delta p}{H L} \quad (B-23)$$

where  $B$  denotes a viscosity model parameter defined by

$$B = \frac{11}{12} \left( 72C_t K \right)^{1/2} \left( \frac{5}{n} + 9 \right)^{1/2} \quad (B-24)$$

Equation (B-24) is identical to that presented by Christopher, et al. (10) choosing  $C_t = 25/12$  for the spherical beads. It is evident that  $B = 1$  when  $n = 1$  as for a Newtonian fluid. Equation (B-23) is the modified form of Darcy's law for a power-law model fluid.

Let us use Ergun's definition (67) of the friction factor; therefore,

$$f_K = \frac{D_p \varphi^3}{2 U^2 (1-\varphi)} \frac{\Delta p}{L} \quad (B-25)$$

The Reynolds number is arbitrarily defined so that,

$$f_{K_1} = \frac{1}{N_{Re}} \quad (B-26)$$

After straight forward algebraic manipulation of the preceding equations

$$N_{Re} = \frac{\rho D u^2 n}{72 C_t (1-\eta) \mu} \quad (B-27)$$

For a Newtonian fluid  $n = 1$ ; therefore,

$$N_{Re} = \frac{\rho D u^2}{72 C_t (1-\eta) \mu} \quad (B-28)$$

## APPENDIX C

## DEBORAH NUMBER

The dimensionless group Deborah number represents a ratio of time scales of the material and the flow process. It may be defined (68) as,

$$N_{\text{Deb}} = \frac{\theta_f}{\theta_{\text{pr}}} \quad (\text{C-1})$$

where  $\theta_f$  is the relaxation time of the fluid, and  $\theta_{\text{pr}}$ , the duration of a process which represents either the duration of a given deformation state or, equivalently, the reciprocal of the rate at which the deformation process changes. Marshall and Metzner (68) applied the convected Maxwell model to approximate the behavior of the viscoelastic fluid and showed that the appropriate measure of the process time in a packed bed of spheres was the reciprocal of the deformation or stretch rate in the flow direction. They showed that in this special case of a porous medium the Deborah number then had the following form,

$$N_{\text{Deb}} = 2.5 \cdot \frac{u}{D_p} \quad (\text{C-2})$$

where,

$$u = \frac{q}{A_p} \quad (\text{C-3})$$

is an average velocity in the pores.

The relaxation time,  $\theta_f$ , for the present study was estimated from Bueches' theory, Equation (VI-1). Viscosity at zero shear rate of 0.2% Separan AP-273 solution was taken equal to 42 poise - Refer to Fig. A-3 of reference (34). The limiting viscosity at zero shear rate of 0.1% and 0.05% Separan was estimated by using Equation VI-3 such that,

$$\frac{\mu_{\infty,1}}{\mu_{\infty,2}} = \left( \frac{C_1}{C_2} \right)^5 \quad (C-4)$$

where subscripts 1 and 2 indicate the different concentration of the Separan solutions. Therefore,

$$\mu_{\infty} (0.1\% \text{ Sep.}) = 1.31 \text{ poise} \quad (C-5)$$

$$\mu_{\infty} (0.05\% \text{ Sep.}) = 4.1 \text{ cp} \quad (C-6)$$

Consequently,  $\theta_f$  was estimated to be,

$$\theta_f (0.2\% \text{ Sep.}) = 3.126 \text{ sec} \quad (C-7)$$

$$\theta_f (0.1\% \text{ Sep.}) = 0.19 \text{ sec} \quad (C-8)$$

$$\theta_f (0.05\% \text{ Sep.}) = 8.34 \text{ mili. sec} \quad (C-9)$$

Calculated Deborah numbers for the three different concentrations of polymer solutions are presented in Tables (F-5, 6).

## APPENDIX D

BREAKTHROUGH RECOVERY WITH  
CONNATE WATER AND/OR RESIDUAL  
OIL SATURATION

The procedure for calculating the breakthrough recovery with non-zero connate water and/or residual oil saturation is exactly the same as presented in Chapter II. The only modification needed to be taken into account is the fact that the total gross sectional area of the porous bed available for flow is now reduced because of the connate water or residual oil. Assuming that the distribution of the connate water saturation and/or residual oil saturation is uniform along the bed, one can write,

$$\Lambda = \Lambda_w + \Lambda_o + \Lambda_r \quad (D-1)$$

where  $\Lambda_r$  indicates that portion of the cross sectional area occupied by connate water and/or residual oil. Solving  $\Lambda_w$  and  $\Lambda_o$  from Equations (II-50) and (D-1) and applying Equation (II-54) yields,

$$\Lambda_w = \frac{M^2 - 1}{M - 1} \Lambda + \frac{\Lambda_r}{M - 1} \quad (D-2)$$

$$\Lambda_o = \frac{M - M^{2-S_w}}{M - 1} \Lambda + \frac{M \Lambda_r}{1 - M} \quad (D-3)$$

Therefore the new expression for  $f_{w,i}$  will be,

$$f_{w,i} = \frac{M - M^{1-S_w}}{M - 1} + \frac{M^{1-S_w} - \Lambda_r}{M - 1} / \bar{\Lambda} \quad (D-4)$$

Consequently, breakthrough recovery efficiency is obtained by,

$$E_R = \frac{M-1}{M \ln M} \left( 1 - \frac{\lambda_r}{\lambda} \right) \quad (D-5)$$

This shows that the effect of the connate water and/or residual oil saturation is simply a parallel downward shift of the breakthrough recovery curve.

APPENDIX E  
PRESSURE TRANSDUCER CALIBRATION

The calibration of transducers was accomplished through the use of the scheme presented in Figure (E-1). The calibration vessel was a cylindrical bomb which could be connected to either a mercury or a water manometer depending upon the desired calibration range. Valve  $V_1$  connects the bomb to the positive side of transducer while the negative side was open to the atmosphere. Valve  $V_2$  connects the bomb through a regulator to an air pressure supply. Prior to the calibration, valve  $V_2$  was closed, the others were opened, and the transducer zeroed. Calibration was performed by pressurizing the bomb to various levels and reading the manometer and corresponding signal on the recorder.

Table (E-1) presents the calibration data of all the transducers used during the course of the experiments and Figure (E-2) is to obtain the pertinent equations of the transducers. The working equations derived from Figure (E-2) are as follows:

Trans. No. 2221 with 5 psi Diaphragm:

$$P_{\text{in } H_2O} \approx 0.05 R$$

Trans. No. 2010 with 5 psi Diaphragm:

$$P_{\text{in } H_2O} = 0.04 R$$

Trans. No. 2012 with 1 psi Diaphragm:

$$P_{\text{in } H_2O} \approx 0.016 R$$

Trans. No. 2223 with 5 psi Diaphragm:

$$P_{\text{in } Hg} = 0.0037 R$$

Trans. No. 2221 with 20 psi Diaphragm:

$$P_{\text{in } Hg} = 0.015 R$$

where,  $p$  represents pressure and  $R_s$  reading on the recorder at attenuation 1 in inches.

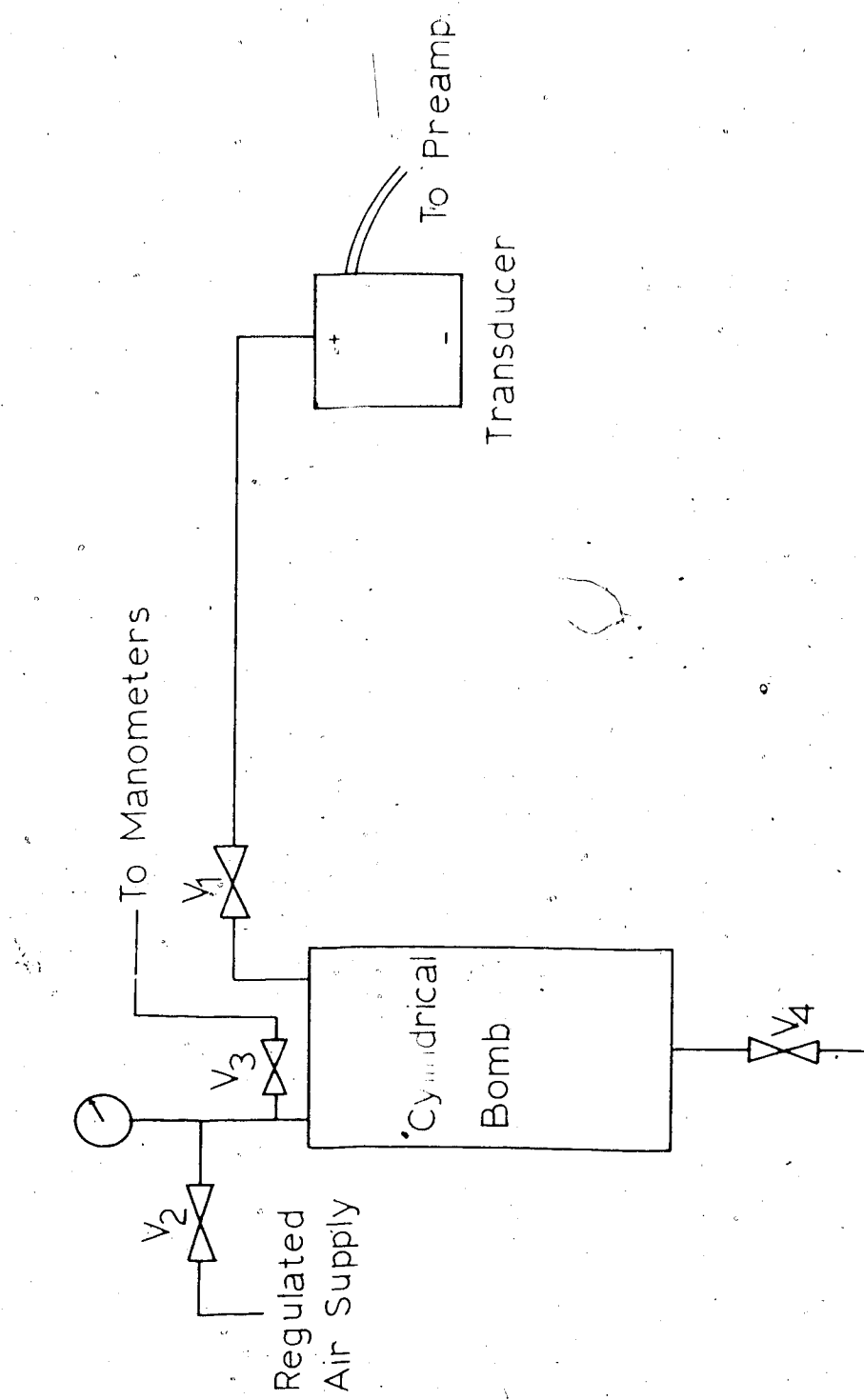


FIGURE E-1 SCHEMATIC OF PRESSURE TRANSDUCER CALIBRATION

TABLE E-1  
PRESSURE TRANSDUCER CALIBRATION DATA

Run No.	Manometer In. of H <sub>2</sub> O	Recorder In. at X1
------------	--------------------------------------	-----------------------

Trans. No. 2221 with 5 psi Diaphragm

1	24.5	488
2	6.3	126.5
3	11.1	223
4	17.5	348
5	30.8	610
	37.85	750
	50.6	1006
	67.9	1364
	5.6	114.4
	11.07	225
11	16.55	336.5
12	26.12	530

Trans. No. 2010 with 5 psi Diaphragm

1	5.6	136
2	11.07	271.5
3	16.55	404
4	26.12	638

Trans. No. 2012 with 1 psi Diaphragm

1	7.1	363
2	9.65	604
3	15.05	940
4	21.54	1450

Trans. No. 2223 with 5 psi Diaphragm (In. of Hg)

1	1.85	493
2	1.6	413
3	2.8	741
4	4.12	1100

Trans. No. 2221 with 20 psi Diaphragm (In. of Hg)

1	2.45	165
2	5.7	247
3	5.65	384
4	7.65	522
5	9.2	626
6	11.36	782
7	17.5	1208

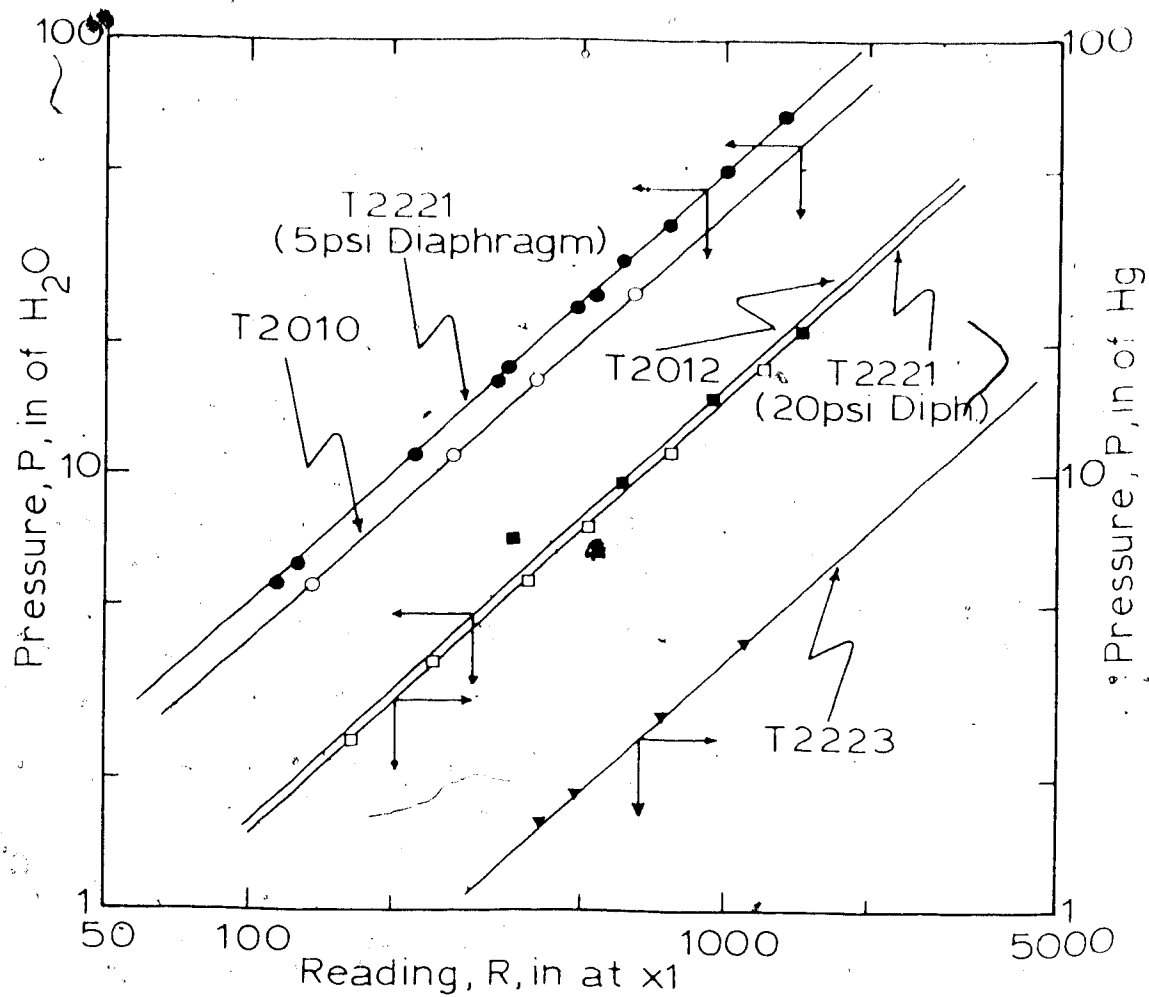


FIGURE E-2 PRESSURE TRANSDUCER CALIBRATION

APPENDIX F  
EXPERIMENTAL DATA

F.1 Specification of the Experimental Runs

The specifications of all the experimental runs reported in this study are given in this section. The experimental runs are labelled by two numbers, namely Roll No. and Run No. Roll number reflects the consecutive number recorded on the original rolls of film on which the pertinent runs were recorded. These are the same numbers recorded in the note book of the raw data during the course of the experimental work. Therefore, reference to the raw data and also unreported data of the glass rods bed is directly viable without any confusion.

TABLE F-1  
Specification of Experimental Runs

1. Runs being performed with the large beads,

Bead Diameter = 4.7 mm

<u>Label</u>	<u>Specification</u>
Roll No. 8	Water Displacing 100 cs Dow Corning
Run No. 1	$q = 1.5885 \text{ cm}^3/\text{sec}$
Roll No. 8	Water Displacing 100 cs Dow Corning
Run No. 2	$q = 3.177 \text{ cm}^3/\text{sec}$
Roll No. 8	Water Displacing 100 cs Dow Corning
Run No. 3	$q = 6.354 \text{ cm}^3/\text{sec}$
Roll No. 8	Water Displacing 100 cs Dow Corning
Run No. 4	$q = 6.354 \text{ cm}^3/\text{sec}$
Roll No. 8	Water Displacing 100 cs Dow Corning
Run No. 5	$q = 0.6354 \text{ cm}^3/\text{sec}$

<u>Label</u>	<u>Specification</u>
Roll No. 8	100 cs Dow Corning Displacing Water
Run No. 6	$q = 3.4 \text{ cm}^3/\text{sec}$
Roll No. 9	0.2% Sep. Displacing 100 cs Dow Corning
Run No. 1	$q = 1.5885 \text{ cm}^3/\text{sec}$
Roll No. 9	0.2% Sep. Displacing 100 cs Dow Corning
Run No. 2	$q = 3.177 \text{ cm}^3/\text{sec}$
Roll No. 9	0.2% Sep. Displacing 100 cs Dow Corning
Run No. 3	$q = 6.354 \text{ cm}^3/\text{sec}$
Roll No. 9	0.2% Sep. Displacing 100 cs Dow Corning
Run No. 4	$q = 15.885 \text{ cm}^3/\text{sec}$
Roll No. 9	0.2% Sep. Displacing 12500 cs Dow Corning
Run No. 5	$q = 0.6354 \text{ cm}^3/\text{sec}$
Roll No. 9	0.2% Sep. Displacing 12500 cs Dow Corning
Run No. 6	$q = 0.3177 \text{ cm}^3/\text{sec}$
Roll No. 9	0.1% Sep. Displacing 100 cs Dow Corning
Run No. 7	$q = 6.354 \text{ cm}^3/\text{sec}$
Roll No. 9	0.1% Sep. Displacing 100 cs Dow Corning
Run No. 8	$q = 15.885 \text{ cm}^3/\text{sec}$
Roll No. 10	0.05% Sep. Displacing 100 cs Dow Corning
Run No. 1	$q = 6.354 \text{ cm}^3/\text{sec}$
Roll No. 10	0.05% Sep. Displacing 100 cs Dow Corning
Run No. 3	$q = 1.5885 \text{ cm}^3/\text{sec}$
Roll No. 10	0.05% Sep. Displacing 100 cs Dow Corning
Run No. 4	$q = 6.354 \text{ cm}^3/\text{sec}$
Roll No. 10	0.05% Sep. Displacing 100 cs Dow Corning
Run No. 5	$q = 15.885 \text{ cm}^3/\text{sec}$

LabelSpecification

Roll No. 10            0.05% Sep. Displacing 100 cs Dow Corning  
 Run No. 6             $q = 6.354 \text{ cm}^3/\text{sec}$

2. Runs being performed with the small beads,

Bead Diameter = 1.5 mm

Roll No. 10            Water Displacing 100 cs Dow Corning  
 Run No. 7             $q = 1.5885 \text{ cm}^3/\text{sec}$

Roll No. 10            Water Displacing 100 cs Dow Corning  
 Run No. 8             $q = 0.6354 \text{ cm}^3/\text{sec}$

Roll No. 10            Water Displacing 100 cs Dow Corning  
 Run No. 9             $q = 0.3177 \text{ cm}^3/\text{sec}$

Roll No. 10            Water Displacing 100 cs Dow Corning  
 Run No. 10             $q = 3.177 \text{ cm}^3/\text{sec}$

Roll No. 11            Water Displacing 100 cs Dow Corning  
 Run No. 1             $q = 0.15885 \text{ cm}^3/\text{sec}$

Roll No. 11            Water Displacing 100 cs Dow Corning  
 Run No. 2             $q = 6.354 \text{ cm}^3/\text{sec}$

Roll No. 11            Water Displacing 100 cs Dow Corning  
 Run No. 3             $q = 1.5885 \text{ cm}^3/\text{sec}$

Roll No. 11            0.05% Sep. Displacing 100 cs Dow Corning  
 Run No. 4             $q = 3.177 \text{ cm}^3/\text{sec}$

Roll No. 11            0.05% Sep. Displacing 100 cs Dow Corning  
 Run No. 5             $q = 6.354 \text{ cm}^3/\text{sec}$

Roll No. 11            0.05% Sep. Displacing 100 cs Dow Corning  
 Run No. 6             $q = 1.5885 \text{ cm}^3/\text{sec}$

<u>Label</u>	<u>Specification</u>
Roll No. 11	0.05% Sep. Displacing 100 cs Dow Corning
Run No. 7	$q = 15.885 \text{ cm}^3/\text{sec}$
Roll No. 11	0.1% Sep. Displacing 100 cs Dow Corning
Run No. 8	$q = 6.354 \text{ cm}^3/\text{sec}$
Roll No. 11	0.1% Sep. Displacing 100 cs Dow Corning
Run No. 9	$q = 3.177 \text{ cm}^3/\text{sec}$
Roll No. 11	0.2% Sep. Displacing 100 cs Dow Corning
Run No. 10	$q = 3.177 \text{ cm}^3/\text{sec}$
Roll No. 12	26 cp Glycerol Displacing 100 cs Dow Corning
Run No. 1	$q = 1.5885 \text{ cm}^3/\text{sec}$
Roll No. 12	17 cp Glycerol Displacing 100 cs Dow Corning
Run No. 2	$q = 3.177 \text{ cm}^3/\text{sec}$
Roll No. 12	17 cp Glycerol Displacing 100 cs Dow Corning
Run No. 3	$q = 3.177 \text{ cm}^3/\text{sec}$
Roll No. 12	52 cp Glycerol Displacing 100 cs Dow Corning
Run No. 4	$q = 3.177 \text{ cm}^3/\text{sec}$
Roll No. 12	25 cp Glycerol Displacing 100 cs Dow Corning
Run No. 5	$q = 3.177 \text{ cm}^3/\text{sec}$
Roll No. 12	25 cp Glycerol Displacing 100 cs Dow Corning
Run No. 6	$q = 1.5885 \text{ cm}^3/\text{sec}$
Roll No. 12	25 cp Glycerol Displacing 100 cs Dow Corning
Run No. 7	$q = 6.354 \text{ cm}^3/\text{sec}$
Roll No. 12	28.5 cp Glycerol Displacing 100 cs Dow Corning
Run No. 8	$q = 0.6354 \text{ cm}^3/\text{sec}$

<u>Label</u>	<u>Specification</u>
Roll No. 13	0.2% Pusher 500 Displacing 1000 cs Dow Corning
Run No. 1	$q = 0.15885 \text{ cm}^3/\text{sec}$
Roll No. 13	0.2% Pusher 500 Displacing 1000 cs Dow Corning
Run No. 2	$q = 0.6354 \text{ cm}^3/\text{sec}$
Roll No. 13	0.1% Sep. Displacing 1000 cs Dow Corning
Run No. 3	$q = 0.15885 \text{ cm}^3/\text{sec}$
Roll No. 13	0.1% Sep. Displacing 1000 cs Dow Corning
Run No. 4	$q = 0.6354 \text{ cm}^3/\text{sec}$

## E.2. Frontal Plane Advance

The procedure undertaken to obtain the data points of Figures (V-3) to (V-18) is described in the following. The position,  $x_0$ , of the frontal plane or the plane of zero saturation was determined by projecting the movie pictures frame by frame onto a white wall. The distance of the projector from the wall was set so that a magnification of 1:1 with respect to the actual dimensions of the bed was obtained. The number of the frames was counted to calculate the time elapsed,  $t$ , by using the previously determined camera calibration factor. The time of breakthrough was checked by a stopwatch which determined the time period between when the displacing fluid reached the inlet screen and breakthrough. The distance from the screen to the tip of the longest finger,  $x_0$ , was measured from the projections by a precision steel ruler with 1mm divisions. In the case of low rates to reduce film consumption, the camera was stopped after taking two pictures, then restarted again. The time lapse between every two sets of pictures was measured by a stop watch and added to the time calculated from counting the number of the frames.

TABLE F-2  
POSITION OF THE ZERO SATURATION PLANE

$x_0$ cm	t sec	$qt/\phi\Lambda$ cm	$x_0$ cm	t sec	$qt/\phi\Lambda$ cm
Roll No. 8, Run No. 1					
3.0	9.52	0.66	23.0	23.81	6.57
5.5	19.05	1.31	26.5	28.57	7.88
8.0	28.57	1.97	30.0	33.33	9.2
11.5	38.10	2.63	35.5	38.10	10.51
13.5	47.62	3.28	38.7	42.86	11.82
16.5	57.14	3.94	44.7	47.62	13.14
18.7	66.67	4.60	47.5	52.38	14.45
22.0	76.19	5.25	53.5	59.05	16.29
24.5	85.71	5.91			
28.5	95.24	6.57			
33.0	104.76	7.23			
35.5	114.29	7.88			
39.0	123.81	8.54			
43.0	133.33	9.20			
47.0	142.86	9.85			
50.5	152.38	10.51			
53.5	155.71	10.74			
Roll No. 8, Run No. 2					
4.5	7.14	0.99	42.2	38.10	10.51
8.0	14.29	1.97	45.0	42.86	11.82
11.7	21.43	2.96	47.2	47.62	13.14
18.0	28.57	3.94	53.5	53.81	14.84
22.0	35.71	4.93			
23.7	42.86	5.91			
28.0	50.00	6.90			
31.0	57.14	7.88			
36.4	64.29	8.87			
44.3	71.43	9.95			
48.0	78.57	10.84			
53.5	91.43	12.61			
Roll No. 8, Run No. 3					
5.7	4.76	1.31	28.7	276.61	7.63
10.8	9.52	2.63	44.5	408.41	11.27
13.5	14.29	3.94	49.0	443.17	12.25
18.0	19.05	5.25	52.0	472.97	13.05
			53.5	484.40	13.56

TABLE F-2 (Continued)

$x_0$ cm	t sec	qt/ $\phi\Lambda$ cm	$x_0$ cm	t sec	qt/ $\phi\Lambda$ cm
RoII No. 8, Run No. 6					
4.0	23.81	3.51	3.4	9.52	2.63
7.5	47.62	7.03	5.4	14.29	5.94
11.2	71.43	10.54	8.5	23.81	6.37
14.5	95.24	14.06	11.5	33.33	9.22
17.2	119.05	17.57	14.8	42.86	11.82
20.5	142.86	21.09	17.5	52.38	11.43
27.5	190.48	28.12	20.8	61.00	15.08
35.2	238.10	35.15	23.8	71.43	19.70
43.0	285.71	42.18	29.0	85.71	25.65
51.8	333.53	49.21	31.5	95.24	26.27
53.3	346.19	51.10	37.0	107.14	29.56
			41.5	119.05	32.84
			47.0	130.93	36.15
			53.5	147.62	40.72
RoII No. 9, Run No. 1					
2.8	23.81	1.64	RoII No. 9, Run No. 4		
5.0	47.62	3.28	2.5	2.58	1.64
6.0	71.43	4.95	5.5	4.76	5.28
8.0	95.24	6.57	7.5	7.14	9.95
9.5	112.86	7.78	9.0	9.52	6.57
22.5	297.96	20.55	11.0	11.9	8.21
25.5	329.86	22.75	13.5	14.29	9.85
33.3	429.06	29.59	17.5	19.05	13.14
35.5	456.20	31.46	21.5	23.81	16.42
42.0	530.60	36.59	25.0	28.57	19.70
45.5	571.08	39.39	29.5	33.33	22.39
52.0	652.78	43.64	36.5	38.10	26.27
53.5	651.83	44.95	42.0	42.86	29.56
			49.5	47.62	32.84
			53.5	51.43	35.47
RoII No. 9, Run No. 2					
4.5	23.81	3.28	RoII No. 9, Run No. 5		
8.0	46.62	6.57	5.5	9.52	0.26
12.5	71.43	9.85	5.5	19.05	0.53
16.5	94.76	13.07	11.5	42.86	1.18
32.0	194.96	26.89	18.0	66.67	1.84
36.5	219.25	30.24	19.0	71.43	1.97
38.5	228.77	31.55	33.5	134.55	5.71
51.0	294.57	40.65	40.0	158.54	4.37
53.5	305.52	42.14	47.0	182.15	5.02
			53.5	212.62	5.87
RoII No. 9, Run No. 3					
2.0	4.76	1.51			

TABLE E-2 (Continued)

$x_0$ cm	t sec	qt/ $\phi\Lambda$ cm	$x_0$ cm	t sec	qt/ $\phi\Lambda$ cm
Roll No. 9, Run No. 6					
5.0	47.62	0.66	43.5	3.55	22.90
8.0	95.24	1.51	49.5	55.71	21.65
11.5	142.86	1.97	53.5	58.10	26.27
16.0	173.53	1.59			
20.0	328.55	4.55			
23.5	363.57	5.01			
27.0	448.07	6.18			
33.5	495.69	6.84			
Roll No. 9, Run No. 7					
4.0	7.14	1.97	43.5	4.76	1.51
8.0	14.29	3.94	49.5	9.82	2.65
11.5	21.43	5.91	53.5	14.29	3.94
15.5	28.57	7.88	11.4	19.05	5.25
18.5	35.71	9.85	18.5	25.81	6.57
23.0	42.86	11.82	22.5	28.57	7.88
25.5	50.00	13.79	25.7	33.33	9.2
28.5	57.14	15.76	29.4	38.09	10.51
31.0	64.29	17.73	33.0	42.86	11.82
34.0	71.43	19.70	33.7	47.62	13.14
36.5	78.57	21.68	38.9	52.58	14.45
39.0	85.71	23.65	42.8	57.14	15.76
43.0	92.86	25.62	47.2	61.90	17.08
50.0	100.00	28.59	51.2	66.67	18.59
53.5	105.71	29.16	55.5	70.00	19.51
Roll No. 9, Run No. 8					
5.5	2.58	1.64	4.1	25.81	1.64
7.5	4.46	3.28	7.5	48.57	3.55
12.0	7.14	4.93	14.9	114.67	7.91
14.5	9.52	6.57	17.6	157.53	9.45
18.0	11.90	8.21	24.6	215.43	14.86
20.0	14.29	9.85	28.7	259.24	16.50
22.0	16.67	11.49	31.5	247.81	17.09
25.5	19.03	13.14	37.0	301.11	20.77
26.0	21.43	14.78	41.6	324.92	22.41
31.0	23.81	16.42	43.0	348.75	24.05
32.0	26.19	18.06	44.0	357.78	24.67
35.5	28.57	19.70	49.8	404.08	27.87
39.0	30.95	21.35	53.5	449.79	31.02
Roll No. 10, Run No. 4					
			1.9	2.58	0.60
			4.1	4.76	1.51

TABLE F-2 (Continued)

$x_0$	t	qt/φA	$x_0$	t	qt/φA
cm	sec	m	cm	sec	cm
Roll No. 10, Run No. 4					
5.4	7.14	1.97	31.7	58.09	10.51
8.5	11.90	3.28	29.4	42.86	11.82
11.1	16.67	4.60	33.7	47.02	13.14
14.1	21.43	5.91	36.8	52.58	14.45
17.5	26.19	7.22	43.3	57.14	15.76
20.8	30.95	8.54	47.0	61.90	17.08
23.1	35.71	9.85	53.5	70.48	19.44
26.3	40.48	11.17			
30.5	45.24	12.48			
33.4	50.00	13.79			
40.5	54.76	15.11			
42.5	59.52	16.42			
45.0	64.29	17.73			
50.0	69.05	19.05			
53.5	74.76	20.62			
Roll No. 10, Run No. 5					
4.5	2.58	4.64	23.5	50.0	5.69
10.6	4.76	3.28	28.5	57.14	4.22
14.5	7.14	4.93	32.6	64.29	4.75
17.5	9.52	6.57	34.7	71.43	5.28
21.0	11.90	8.21	39.5	78.57	5.81
24.0	14.29	9.85	44.0	85.71	6.35
28.5	16.67	11.49	47.5	92.86	6.86
32.1	19.05	13.14	51.0	100.0	7.39
38.1	21.43	14.78	53.5	105.71	7.84
42.5	25.81	16.42			
46.5	26.19	18.06			
50.8	28.57	19.70			
53.5	30.48	21.02			
Roll No. 10, Run No. 6					
14.0	4.76	1.51	23.7	165.47	4.89
16.9	9.32	2.65	26.0	172.14	5.09
10.7	14.29	3.94	28.5	194.04	5.73
14.0	19.05	5.25	30.0	251.54	7.45
16.6	25.81	6.57			
19.1	28.57	7.88			
23.6	33.35	9.2			
Roll No. 10, Run No. 6					
5.0	7.14	0.53			
9.0	11.90	1.28			
13.0	16.67	2.03			
17.0	21.43	2.78			
21.0	26.19	3.53			
25.0	30.95	4.28			
29.0	35.71	5.03			
33.0	40.48	5.78			
37.0	45.24	6.53			
41.0	50.00	7.28			
45.0	54.76	8.03			
49.0	59.52	8.78			
53.0	64.29	9.53			
57.0	69.05	10.28			
61.0	74.76	11.03			
65.0	79.52	11.78			
69.0	84.29	12.53			
73.0	89.05	13.28			
77.0	93.81	14.03			
81.0	98.57	14.78			
85.0	103.35	15.53			
89.0	108.11	16.28			
93.0	112.88	17.03			
97.0	117.64	17.78			
101.0	122.40	18.53			
105.0	127.16	19.28			
109.0	131.92	20.03			
113.0	136.68	20.78			
117.0	141.44	21.53			
121.0	146.20	22.28			
125.0	150.96	23.03			
129.0	155.72	23.78			
133.0	160.48	24.53			
137.0	165.24	25.28			
141.0	169.90	26.03			
145.0	174.66	26.78			
149.0	179.42	27.53			
153.0	184.18	28.28			
157.0	188.94	29.03			
161.0	193.70	29.78			
165.0	198.46	30.53			
169.0	203.22	31.28			
173.0	207.98	32.03			
177.0	212.74	32.78			
181.0	217.50	33.53			
185.0	222.26	34.28			
189.0	226.92	35.03			
193.0	231.68	35.78			
197.0	236.44	36.53			
201.0	241.20	37.28			
205.0	245.96	38.03			
209.0	250.72	38.78			
213.0	255.48	39.53			
217.0	260.24	40.28			
221.0	264.90	41.03			
225.0	269.66	41.78			
229.0	274.42	42.53			
233.0	279.18	43.28			
237.0	283.94	44.03			
241.0	288.70	44.78			
245.0	293.46	45.53			
249.0	298.22	46.28			
253.0	302.98	47.03			
257.0	307.74	47.78			
261.0	312.50	48.53			
265.0	317.26	49.28			
269.0	321.92	50.03			
273.0	326.68	50.78			
277.0	331.44	51.53			
281.0	336.20	52.28			
285.0	340.96	53.03			
289.0	345.72	53.78			
293.0	350.48	54.53			
297.0	355.24	55.28			
301.0	359.90	56.03			
305.0	364.66	56.78			
309.0	369.42	57.53			
313.0	374.18	58.28			
317.0	378.94	59.03			
321.0	383.70	59.78			
325.0	388.46	60.53			
329.0	393.22	61.28			
333.0	397.98	62.03			
337.0	402.74	62.78			
341.0	407.50	63.53			
345.0	412.26	64.28			
349.0	416.92	65.03			
353.0	421.68	65.78			
357.0	426.44	66.53			
361.0	431.20	67.28			
365.0	435.96	68.03			
369.0	440.72	68.78			
373.0	445.48	69.53			
377.0	450.24	70.28			
381.0	454.90	71.03			
385.0	459.66	71.78			
389.0	464.42	72.53			
393.0	469.18	73.28			
397.0	473.94	74.03			
401.0	478.70	74.78			
405.0	483.46	75.53			
409.0	488.22	76.28			
413.0	492.98	77.03			
417.0	497.74	77.78			
421.0	502.50	78.53			
425.0	507.26	79.28			
429.0	511.92	80.03			
433.0	516.68	80.78			
437.0	521.44	81.53			
441.0	526.20	82.28			
445.0	530.96	83.03			
449.0	535.72	83.78			
453.0	540.48	84.53			
457.0	545.24	85.28			
461.0	549.90	86.03			
465.0	554.66	86.78			
469.0	559.42	87.53			
473.0	564.18	88.28			
477.0	568.94	89.03			
481.0	573.70	89.78			
485.0	578.46	90.53			
489.0	583.22	91.28			
493.0	587.98	92.03			
497.0	592.74	92.78			
501.0	597.50	93.53			
505.0	602.26	94.28			
509.0	606.92	95.03			
513.0	611.68	95.78			
517.0	616.44	96.53			
521.0	621.20	97.28			
525.0	625.96	98.03			
529.0	630.72	98.78			
533.0	635.48	99.53			
537.0	640.24	100.28			
541.0	644.90	101.03			
545.0	649.66	101.78			
549.0	654.42	102.53			
553.0	659.18	103.28			
557.0	663.94	104.03			
561.0	668.70	104.78			
565.0	673.46	105.53			
569.0	678.22	106.28			
573.0	682.98	107.03			
577.0	687.74	107.78			
581.0	692.50	108.53			
585.0	697.26	109.28			
589.0	701.92	110.03			
593.0	706.68	110.78			
597.0	711.44	111.53			
601.0	716.20	112.28			
605.0	720.96	113.03			
609.0	725.72	113.78			
613.0	730.48	114.53			
617.0	735.24	115.28			
621.0	739.90	116.03			
625.0	744.66	116.78			
629.0	749.42	117.53			
633.0	754.18	118.28			
637.0	758.94	119.03			
641.0	763.70	119.78			
645.0	768.46	120.53			
649.0	773.22	121.28			
653.0	777.98	122.03			
657.0	782.74	122.78			
661.0	787.50	123.53			
665.0	792.26	124.28			
669.0	796.92	125.03			
673.0	801.68	125.78			
677.0	806.44	126.53			
681.0	811.20	127.28			
685.0	815.96	128.03			
689.0	820.72	128.78			
693.0	825.48	129.53			
697.0	830.24	130.28			
701.0	834.90	131.03			
705.0	839.66	131.78			
709.0	844.42	132.53			
713.0	849.18	133.28			
717.0	853.94	134.03			
721.0	858.70	134.78			
725.0	863.46	135.53			
729.0	868.22	136.28			
733.0	872.98	137.03			
737.0	877.74	137.78			
741.0	882.50	138.53			
745.0	887.26	139.28			</td

TABLE E-2 (Continued)

$x_0$	t	qt/ $\phi\Lambda$	$x_0$	t	qt/ $\phi\Lambda$
cm	sec	cm	cm	sec	cm
ROLL No. 10, Run No. 9					
3.7	33.81	0.55	11.0	546.58	2.56
4.8	47.62	0.70	11.5	560.39	2.66
6.0	74.29	1.10	15.0	153.49	5.20
12.5	141.19	3.09	15.5	148.72	5.51
14.4	165.00	3.44	17.5	526.52	5.89
21.0	246.20	5.64	17.6	541.76	4.00
22.7	269.05	5.98	19.4	624.56	4.61
30.0	344.65	5.09	20.0	647.42	4.78
33.0	369.41	5.46	22.0	732.52	5.41
37.3	452.01	6.68	22.0	748.23	5.53
42.7	474.87	7.02	24.0	842.55	6.22
47.5	552.97	8.17	24.5	859.48	6.55
50.3	573.55	8.50	26.0	941.28	6.95
52.0	652.75	9.65	27.0	958.42	7.08
52.5	672.28	9.93	29.5	1096.82	8.10
53.5	731.98	10.83	30.0	1116.82	8.25
ROLL No. 10, Run No. 10					
3.0	4.76	1.70	11.5	1252.12	9.25
9.5	9.52	1.41	11.8	1265.95	9.35
14.0	14.29	2.11	11.8	1403.75	10.57
17.0	19.05	2.81	14.5	1419.92	10.49
21.5	25.81	3.52	14.8	1550.62	11.45
24.0	28.57	4.22	14.8	1568.71	11.59
28.0	53.55	4.93	15.5	1691.21	12.49
33.5	58.09	5.65	15.5	1715.02	12.67
38.5	42.80	6.35	17.0	ROLL No. 11, Run No. 2	
42.5	47.62	7.04	17.0	2.38	0.70
45.5	52.58	7.74	17.5	4.76	1.41
48.5	57.14	8.44	11.0	7.14	2.11
50.0	61.90	9.15	11.0	9.52	2.81
53.5	66.67	9.85	17.0	11.90	3.52
ROLL No. 11, Run No. 1					
3.6	96.67	0.71	20.5	14.29	4.22
4.6	160.97	1.19	23.5	16.67	4.95
5.5	182.87	1.55	28.5	19.05	5.65
7.2	255.57	1.87	53.5	21.43	6.55
7.7	275.48	2.05	53.5	23.81	7.04
			58.0	26.19	7.74
			42.5	28.57	8.44
			45.5	30.95	9.15
			49.0	33.33	9.85
			53.5	36.67	10.84

TABLE E-2 (Continued)

$x_0$	$t$	$qt/\phi A$	$x_0$	$t$	$qt/\phi A$			
cm	sec	cm	cm	sec	cm			
Roll No. 11, Run No. 3								
3.4	7.14	20.55	3.5	4.76	1.41			
6.5	14.29	14.06	8.0	9.52	1.81			
12.0	21.43	1.58	12.5	14.29	1.17			
15.2	28.57	2.11	16.0	19.05	1.07			
19.3	35.71	2.64	20.5	25.81	1.04			
21.5	42.86	3.17	25.0	28.57	1.44			
22.7	50.00	3.69	29.0	55.33	1.83			
27.0	57.14	4.22	32.5	58.10	11.76			
34.0	64.29	4.75	38.0	42.86	11.67			
36.2	71.43	5.28	42.5	47.62	11.07			
40.0	78.57	5.81	47.0	52.38	15.48			
42.5	85.71	6.33	50.5	57.14	16.89			
44.0	92.86	6.86	53.5	61.90	18.50			
45.0	100.00	7.39	Roll No. 11, Run No. 6					
47.5	107.14	7.92	5.0	25.81	1.76			
49.7	114.29	8.44	8.0	47.62	5.52			
53.5	121.43	9.52	11.0	62.58	1.61			
Roll No. 11, Run No. 4								
3.5	7.14	1.05	19.0	131.78	9.74			
6.0	14.29	2.11	22.5	156.54	11.57			
10.5	21.43	3.17	34.0	225.04	16.48			
13.0	28.57	4.22	37.2	246.38	18.24			
15.4	35.71	5.28	45.5	286.28	21.35			
18.0	42.86	6.33	48.7	303.42	22.42			
20.2	50.00	7.39	53.5	325.72	24.07			
24.0	57.14	8.44	Roll No. 11, Run No. 5					
26.5	64.29	9.50	6.5	2.58	1.76			
29.5	71.43	10.56	11.5	4.76	5.52			
33.5	78.57	11.61	15.0	7.14	5.28			
37.0	85.71	12.67	19.0	9.52	7.04			
40.0	92.86	13.72	25.5	11.90	8.80			
42.5	100.00	14.78	29.5	14.29	10.56			
46.2	107.14	15.83	36.0	16.67	12.32			
48.0	114.29	16.89	41.0	19.05	14.07			
51.0	121.43	17.95	48.0	21.45	15.85			
51.8	128.57	19.00	50.0	23.81	17.50			
53.5	135.81	19.78	53.5	25.24	18.65			

TABLE E-2 (Continued)

$x_0$	t	qt/ $\phi A$	$x_0$	t	qt/ $\phi A$
cm	sec	cm	cm	sec	cm
RoII No. 11, Run No. 8					
RoII No. 11, Run No. 9					
5.0	4.76	1.41	5.5	23.81	13.52
5.5	9.52	2.81	6.0	47.62	7.04
8.0	14.29	4.22	14.0	69.52	10.77
9.5	19.05	5.63	21.7	120.72	17.84
12.0	25.81	7.04	35.0	152.65	19.60
15.0	28.57	8.44	34.8	197.73	29.72
18.0	35.33	9.85	39.0	224.39	53.16
21.0	38.10	11.26	49.8	252.99	57.39
22.5	42.86	12.67	53.5	301.09	44.50
26.0	47.62	14.07			
27.5	52.38	15.48			
30.0	57.14	16.89			
33.0	61.90	18.30			
36.0	66.67	19.70			
38.5	71.43	21.11			
39.5	76.19	22.52			
41.5	80.95	23.93			
46.0	85.71	25.33			
49.5	90.48	26.74			
53.5	97.14	28.71			
RoII No. 11, Run No. 10					
5.5	23.81	13.52			
6.0	47.62	7.04			
7.4	71.43	8.28			
12.5	95.24	7.04			
15.0	119.05	8.80			
17.5	142.86	10.56			
20.6	166.67	12.52			
21.5	172.86	12.52			
29.7	239.16	17.67			
32.0	256.78	18.97			
35.2	280.59	20.75			
36.2	286.78	21.19			
45.6	367.78	27.13			
49.3	391.59	28.94			
55.5	421.59	31.15			
RoII No. 12, Run No. 1					
5.0	23.81	13.52			
6.8	47.62	7.04			
9.3	71.43	8.28			
12.5	95.24	7.04			
15.0	119.05	8.80			
17.5	142.86	10.56			
20.6	166.67	12.52			
21.5	172.86	12.52			
29.7	239.16	17.67			
32.0	256.78	18.97			
35.2	280.59	20.75			
36.2	286.78	21.19			
45.6	367.78	27.13			
49.3	391.59	28.94			
55.5	421.59	31.15			
RoII No. 12, Run No. 2					
5.0	4.76	0.70			
5.0	9.52	1.41			
7.4	14.29	2.11			
8.6	19.05	2.81			
11.5	26.19	3.87			
15.0	33.33	4.93			
17.7	40.48	5.98			
20.6	47.62	7.04			
23.4	57.14	8.44			
26.3	66.67	9.85			
30.0	76.19	11.26			
32.0	84.44	12.52			
35.2	92.73	13.52			
36.2	97.14	14.07			
45.6	119.05	17.67			
49.3	142.86	20.75			
55.5	172.86	27.13			
56.1	239.16	31.15			
58.3	256.78	34.44			
61.4	280.59	38.94			
64.3	286.78	42.52			
71.4	367.78	47.62			
74.3	391.59	51.15			
76.1	421.59	55.50			
81.4	476.20	60.70			
84.4	57.14	64.44			
87.5	66.67	69.85			
91.4	76.19	74.26			
94.3	84.44	78.94			
97.1	92.73	83.52			
101.4	119.05	90.70			
104.3	142.86	94.44			
107.1	172.86	98.94			
111.4	239.16	105.50			
114.3	256.78	110.70			
117.1	280.59	115.50			
121.4	286.78	120.70			
124.3	367.78	125.50			
127.1	391.59	130.70			
131.4	421.59	135.50			
134.3	476.20	140.70			
137.1	57.14	144.44			
141.4	66.67	148.94			
144.3	76.19	153.50			
147.1	84.44	158.94			
151.4	92.73	163.50			
154.3	119.05	168.94			
157.1	142.86	173.50			
161.4	172.86	178.94			
164.3	239.16	185.50			
167.1	256.78	190.70			
171.4	280.59	195.50			
174.3	286.78	200.70			
177.1	367.78	205.50			
181.4	391.59	210.70			
184.3	421.59	215.50			
187.1	476.20	220.70			
191.4	57.14	224.44			
194.3	66.67	228.94			
197.1	76.19	233.50			
201.4	84.44	238.94			
204.3	92.73	243.50			
207.1	119.05	248.94			
211.4	142.86	253.50			
214.3	172.86	258.94			
217.1	239.16	263.50			
221.4	256.78	268.94			
224.3	280.59	273.50			
227.1	286.78	278.94			
231.4	367.78	283.50			
234.3	391.59	288.94			
237.1	421.59	293.50			
241.4	476.20	298.94			
244.3	57.14	302.44			
247.1	66.67	306.94			
251.4	76.19	311.50			
254.3	84.44	316.94			
257.1	92.73	321.50			
261.4	119.05	326.94			
264.3	142.86	331.50			
267.1	172.86	336.94			
271.4	239.16	341.50			
274.3	256.78	346.94			
277.1	280.59	351.50			
281.4	286.78	356.94			
284.3	367.78	361.50			
287.1	391.59	366.94			
291.4	421.59	371.50			
294.3	476.20	376.94			
297.1	57.14	380.44			
301.4	66.67	386.94			
304.3	76.19	391.50			
307.1	84.44	396.94			
311.4	92.73	401.50			
314.3	119.05	406.94			
317.1	142.86	411.50			
321.4	172.86	416.94			
324.3	239.16	421.50			
327.1	256.78	426.94			
331.4	280.59	431.50			
334.3	286.78	436.94			
337.1	367.78	441.50			
341.4	391.59	446.94			
344.3	421.59	451.50			
347.1	476.20	456.94			
351.4	57.14	460.44			
354.3	66.67	466.94			
357.1	76.19	471.50			
361.4	84.44	476.94			
364.3	92.73	481.50			
367.1	119.05	486.94			
371.4	142.86	491.50			
374.3	172.86	496.94			
377.1	239.16	501.50			
381.4	256.78	506.94			
384.3	280.59	511.50			
387.1	286.78	516.94			
391.4	367.78	521.50			
394.3	391.59	526.94			
397.1	421.59	531.50			
401.4	476.20	536.94			
404.3	57.14	540.44			
407.1	66.67	546.94			
411.4	76.19	551.50			
414.3	84.44	556.94			
417.1	92.73	561.50			
421.4	119.05	566.94			
424.3	142.86	571.50			
427.1	172.86	576.94			
431.4	239.16	581.50			
434.3	256.78	586.94			
437.1	280.59	591.50			
441.4	286.78	596.94			
444.3	367.78	601.50			
447.1	391.59	606.94			
451.4	421.59	611.50			
454.3	476.20	616.94			
457.1	57.14	620.44			
461.4	66.67	626.94			
464.3	76.19	631.50			
467.1	84.44	636.94			
471.4	92.73	641.50			
474.3	119.05	646.94			
477.1	142.86	651.50			
481.4	172.86	656.94			
484.3	239.16	661.50			
487.1	256.78	666.94			
491.4	280.59	671.50			
494.3	286.78	676.94			
497.1	367.78	681.50			
501.4	391.59	686.94			
504.3	421.59	691.50			
507.1	476.20	696.94			
511.4	57.14	700.44			
514.3	66.67	706.94			
517.1	76.19	711.50			
521.4	84.44	716.94			
524.3	92.73	721.50			
527.1	119.05	726.94			
531.4	142.86	731.50			
534.3	172.86	736.94			
537.1	239.16	741.50			
541.4	256.78	746.94			
544.3	280.59	751.50			
547.1	286.78	756.94			
551.4	367.78	761.50			
554.3	391.59	766.94			
557.1	421.59	771.50			
561.4	476.20	776.94			
564.3	57.14	780.44			
567.1	66.67	786.94			
571.4	76.19	791.50			

TABLE E-2 (Continued)

$x_0$	t	$qt/\phi\Lambda$	$x_0$	t	$qt/\phi\Lambda$
cm	sec	cm	cm	sec	cm
ROLL NO. 12, Run No. 2					
35.6	85.71	13.67	53.2	142.86	31.41
56.6	95.24	14.07	53.2	153.76	32.38
40.0	104.76	15.48	57.5	166.67	31.66
43.7	114.29	16.89	40.3	178.57	36.59
45.7	125.81	18.50	43.5	191.86	38.50
49.7	135.33	19.70	47.5	202.58	39.91
55.5	145.84	21.78	53.5	225.24	55.29
ROLL NO. 12, Run No. 4					
3.7	7.14	1.06	5.0	4.76	0.70
7.5	14.29	2.11	4.5	9.52	1.11
9.5	21.43	3.17	5.0	16.67	2.46
13.4	28.57	4.22	9.0	3.84	3.32
13.9	35.71	5.28	11.5	53.55	4.95
18.7	42.86	6.33	14.5	42.86	6.35
20.6	50.00	7.39	16.5	52.38	7.74
23.7	57.14	8.44	19.2	61.90	9.45
25.6	64.29	9.50	22.7	71.43	10.56
28.6	71.43	10.56	26.0	83.53	12.52
31.7	80.95	11.96	29.0	95.24	14.07
35.6	90.48	13.57	32.5	107.14	15.85
39.0	100.00	14.78	36.0	119.05	17.59
42.5	109.52	16.19	39.7	130.95	19.33
46.6	119.05	17.59	45.6	147.02	21.82
53.5	132.58	19.56	47.8	154.76	22.87
			53.5	169.05	24.98
ROLL NO. 12, Run No. 5					
3.0	7.14	1.06	2.8	14.90	0.88
4.6	14.29	2.11	4.5	23.81	1.76
6.8	23.81	3.52	7.4	40.48	2.99
8.5	33.55	4.93	8.5	52.38	3.87
10.7	42.86	6.33	9.2	58.10	4.29
13.5	52.38	7.74	13.0	114.60	8.47
15.0	61.90	9.15	16.5	127.95	9.45
17.0	71.43	10.56	17.5	135.55	10.02
19.6	83.53	12.52	24.0	190.71	11.09
22.5	95.24	14.07	26.5	205.68	12.45
24.6	107.14	15.83	33.0	287.55	20.94
30.2	130.95	19.55			

TABLE F-2 (Continued)

$x_0$	t	qt/sA
cm	sec	cm
R611 No. 12, Run No. 6		
37.0	297.18	328.06
58.6	305.24	22.55
46.1	363.74	261.88
47.7	379.45	18.74
49.3	391.56	28.92
51.0	403.26	20.80
55.6	418.50	30.92

Roll No.	Row No.	Run No.	Time
15.6	4.76	1.41	
9.2	9.52	1.81	
12.8	14.29	1.22	
15.6	19.05	3.63	
18.7	23.81	7.04	
22.8	28.57	8.44	
26.3	33.33	9.85	
30.3	38.10	11.26	
33.3	42.86	12.67	
36.2	47.62	14.07	
39.8	52.38	15.48	
43.0	57.14	16.89	
46.0	61.90	18.30	
49.5	66.67	19.70	
53.5	74.29	21.06	

Roll No.	Run No.	Time
1, 2		23.81
2, 8		47.62
2, 8		54.76
8, 0		193.46
9, 0		218.22
13, 0		325.82
15, 15		348.68
19, 7		494.18
20, 7		520.85
25, 2		654.05
26, 0		674.52
31, 4		807.82
32, 2		825.44
		0.70
		11.41
		1.62
		5.72
		6.45
		9.65
		10.51
		14.61
		15.59
		19.33
		19.94
		23.88
		24.40

$x_0$ cm	$t$ sec	qt/ $\mu$ A cm
<b>Roll No. 12, Print No. 18</b>		
57.5	964.24	38.00
58.3	979.48	38.00
59.1	1155.58	34.09
59.9	1175.58	34.68
61.9	1257.58	57.17
63.5	1286.13	58.02

R-111 No.	R-111 No.
2,6	21.43
4,6	146.19
8,2	285.39
8,6	300.06
10,8	132.26
11,2	464.64
14,5	600.04
14,8	615.28
17,4	757.68
17,8	784.96
20,3	925.56
20,7	942.7
23,2	1074.15
23,5	1091.65
26,0	1218.65
26,3	1232.46

26.5	1252.46	9.11
51.0	1423.86	10.52
55.5	1625.8	12.01
39.3	1779.06	15.15
46.5	2003.62	14.81
51.5	2152.03	15.90
53.5	2246.79	16.6
ROLL No. 13, Run No. 2		
41.7	25.81	0.70
8.7	47.62	1.44
11.8	71.43	2.11
13.5	77.14	2.28
24.2	140.04	4.14
30.0	175.28	5.18
41.5	238.88	7.06

TABLE E-2 (Continued)

$x_O$	$t$	$qt/\lambda^*$	$x_O$	$t$	$qt/\lambda^*$
cm	sec	cm	cm	sec	cm
<b>ROLL NO. 15, RUN NO. 2</b>					
45.6	262.69	7.76	50.5	1947.14	14.39
49.0	286.5	8.42	53.5	2005.69	14.82
53.5	312.21	9.23			
<b>ROLL NO. 15, RUN NO. 3</b>					
3.5	95.24	0.70	5.5	23.81	0.70
4.7	170.00	1.26	7.5	47.62	1.41
8.0	299.80	2.22	11.0	71.43	2.11
10.5	444.87	3.29	14.5	95.24	2.81
14.0	589.41	4.36	18.0	119.05	5.52
19.0	793.28	5.86	22.0	142.86	4.22
21.8	936.71	6.92	26.5	166.67	4.93
24.2	1082.95	8.00	34.5	213.82	6.32
30.0	1512.24	9.70	38.5	237.63	7.02
34.5	1460.74	10.79	42.0	261.44	7.73
38.0	1614.23	11.95	46.0	285.25	8.43
45.5	1788.62	13.22	50.0	309.06	9.14
			53.5	330.01	9.75

### 1. Treading Drop Requirement of Angle of Friction

The treading drop experiments were performed to determine the perpendicular distance

from the bed and floor to establish the friction factor to provide guidance in the design of ships.

The fire drop was measured either from the tilted position of the ship or from the

horizontal position of the ship. The first part of the experiment was to determine

the friction coefficient of the ship's hull at the time of the fire drop, i.e., the friction

coefficient of the ship's hull at the time of the fire drop, i.e., the friction coefficient

of the ship's hull at the time of the fire drop, i.e., the friction coefficient of the ship's

hull at the time of the fire drop, i.e., the friction coefficient of the ship's hull at the

time of the fire drop, i.e., the friction coefficient of the ship's hull at the time of the

fire drop, i.e., the friction coefficient of the ship's hull at the time of the fire drop,

which was determined by the formula given below:

Friction coefficient =  $\mu = \frac{W}{F}$  where  $W$  is the weight of the ship and  $F$  is the force

of friction, which was determined by the formula given below:

Friction coefficient =  $\mu = \frac{W}{F}$  where  $W$  is the weight of the ship and  $F$  is the force

of friction, which was determined by the formula given below:

Friction coefficient =  $\mu = \frac{W}{F}$  where  $W$  is the weight of the ship and  $F$  is the force

of friction, which was determined by the formula given below:

Friction coefficient =  $\mu = \frac{W}{F}$  where  $W$  is the weight of the ship and  $F$  is the force

of friction, which was determined by the formula given below:

Friction coefficient =  $\mu = \frac{W}{F}$  where  $W$  is the weight of the ship and  $F$  is the force

of friction, which was determined by the formula given below:

Friction coefficient =  $\mu = \frac{W}{F}$  where  $W$  is the weight of the ship and  $F$  is the force

of friction, which was determined by the formula given below:

Friction coefficient =  $\mu = \frac{W}{F}$  where  $W$  is the weight of the ship and  $F$  is the force

of friction, which was determined by the formula given below:

Friction coefficient =  $\mu = \frac{W}{F}$  where  $W$  is the weight of the ship and  $F$  is the force

of friction, which was determined by the formula given below:

Friction coefficient =  $\mu = \frac{W}{F}$  where  $W$  is the weight of the ship and  $F$  is the force

of friction, which was determined by the formula given below:

TABLE F-3  
PRESSURE DROP MEASUREMENT OF SINGLE  
PHASE NEWTONIAN FLUID FLOW, LARGE BEADS

$q$ $\text{cm}^3/\text{sec}$	$U$ $\text{cm/sec}$	$\Delta P$ $\text{cm of H}_2\text{O}$	$L$ $\text{cm}$	$\Delta P/\mu\text{L}$ $\text{cm}^{-1}\text{sec}^{-1}$	$K \times 10^4$ $\text{cm}^2$	$f_K \times 10^{-3}$	$N_{Re} \times 10^5$
1.588	0.029	0.0610	49	122.08	2.57	0.0673	940
3.177	0.058	0.1422	49	284.58	2.03	0.0509	1890
6.354	0.116	0.3048	49	610.0	1.9	0.0275	3780
100	cs	TAP WATER					
1.717	0.031	5.82	24.5	159.27	1.97	9.75	10.21
1.717	0.031	7.96	49	165.94	1.89	10.16	10.21
1.588	0.029	3.49	24.5	145.51	1.99	10.41	9.45
1.588	0.029	7.2	49	150.10	1.93	10.73	9.45
1.717	0.031	4.72	24.5	196.79	1.59	12.04	10.21
1.717	0.031	4.0	24.5	166.77	1.88	10.21	10.21
3.177	0.058	8.8	24.5	366.91	1.58	6.56	18.9
3.177	0.058	7.7	24.5	321.04	1.81	5.74	18.9
6.354	0.116	14.75	24.5	614.98	1.89	2.75	37.8
1.717	0.031	4.66	24.5	194.13	1.61	11.88	10.21
6.354	0.116	14.9	24.5	621.24	1.87	2.78	37.8
1.717	0.031	3.8	24.5	158.44	1.98	9.70	10.21
6.554	0.116	14.88	24.5	620.40	1.87	2.72	37.8
1.717	0.031	3.96	24.5	165.11	1.90	10.11	10.21
1.717	0.031	4.15	24.5	173.03	1.81	10.59	10.21
0.685	0.012	1.56	24.5	65.04	1.92	25.01	4.07
0.685	0.012	1.65	24.5	68.79	1.82	26.45	4.07
1.07	0.020	2.48	24.5	105.4	1.89	16.50	6.37
1.07	0.020	2.6	24.5	108.4	1.80	17.08	6.57
0.635	0.012	1.44	24.5	60.04	1.93	26.85	5.78
Q. 635	0.012	1.5	24.5	62.54	1.85	27.95	5.78

TABLE F-3 (Continued)

$q$ $\text{cm}^3/\text{sec}$	$U$ $\text{cm/sec}$	$\Delta P$ $\text{cm. dH}_2\text{O}$	$L$ $\text{cm}$	$\frac{\Delta P/\mu L}{\text{sec}^{-1}}$	$K \times 10^4$ $\text{cm}^2$	$f_K \times 10^{-5}$	$N_{Re} \times 10^5$
1.588	0.029	5.63	24.5	151.35	1.92	10.8	9.45
1.588	0.029	5.6	24.5	150.19	1.93	10.7	9.45
3.177	0.058	7.6	24.5	316.87	1.85	5.7	18.9
3.177	0.058	7.1	24.5	296.03	1.96	5.5	18.9
6.354	0.116	14.0	24.5	583.71	1.99	6.61	37.8
6.354	0.116	14.2	24.5	592.05	1.96	6.65	37.8
15.885	0.290	38.4	24.5	1601.04	1.81	1.14	94.49
15.885	0.290	37.0	24.5	1542.67	1.88	1.10	94.49
6.354	0.116	14.25	24.5	594.14	1.95	2.66	37.8
1.717	0.031	3.73	24.5	155.52	2.01	9.52	10.21
1.717	0.031	3.24	24.5	135.09	2.32	8.27	10.21
1.717	0.031	6.68	49	159.26	2.35	8.52	10.21
1.717	0.031	6.6	49	137.59	2.38	8.42	10.21
12500 CS DOW CORNING FLUID							
0.635	0.012	189.07	24.5	60.54	1.92	3500	0.0305
0.635	0.012	129.0	24.5	41.51	2.81	2400	0.0305
0.172	0.003	42.0	24.5	13.45	2.35	10720	0.0082
0.172	0.003	39.5	24.5	12.65	2.48	10080	0.0082
0.172	0.003	48.69	24.5	15.59	2.01	12450	0.0082
0.273	0.005	70.4	24.5	22.54	2.21	7150	0.0151
0.273	0.005	87.02	24.5	27.86	1.78	8820	0.0151
0.318	0.006	80.81	24.5	25.88	2.24	6020	0.0153
0.318	0.006	107.74	24.5	34.50	1.68	8050	0.0153

$$\frac{\sum_{i=1}^n K_i}{n} = \frac{1.97 \times 10^{-4}}{cm^2}$$

TABLE F-4  
PRESSURE DROP MEASUREMENT OF SINGLE  
PHASE NEWTONIAN FLUID FLOW, SMALL BEADS

$q$ $\text{cm}^3/\text{sec}$	$U$ $\text{cm/sec}$	$\Delta P$ $\text{cm of H}_2\text{O}$	$L$ $\text{cm}$	$\Delta P/\mu L$ $\text{cm}^{-1} \text{sec}^{-1}$	$K \times 10^5$ $\text{cm}^2$	$f_K \times 10^{-3}$	$N_{Re} \times 10^5$
TAP WATER							
0.635	0.012	0.11	24.5	440.29	2.63	0.487	191
1.588	0.029	0.285	24.5	1140.74	2.54	0.202	476
3.177	0.058	0.575	24.5	2301.50	2.52	0.102	955
6.354	0.116	1.17	24.5	4683.05	2.47	0.052	1906
15.885	0.290	3.19	24.5	12768.51	2.27	0.023	4764
15.885	0.290	3.14	24.5	12568.18	2.30	0.022	4764
100 CS DOW CORNING FLUID							
0.544	0.010	8.95	24.5	575.16	2.66	54.1	1.7
0.544	0.010	8.4	24.5	550.25	2.85	50.7	1.7
1.588	0.029	27.73	24.5	1156.18	2.51	19.6	4.96
0.635	0.012	11.0	24.5	458.65	2.55	48.7	1.99
0.635	0.012	11.76	24.5	490.52	2.56	52.1	1.99
0.318	0.006	6.07	24.5	253.08	2.29	107.5	0.99
3.177	0.058	60.07	24.5	2504.55	2.31	10.6	9.95
3.177	0.058	52.6	24.5	2195.09	2.64	9.5	9.95
6.354	0.116	112.0	24.5	4669.71	2.48	15.0	19.85
3.177	0.058	67.73	24.5	2825.92	2.05	12.0	9.95
6.354	0.116	132.91	24.5	5541.52	2.09	5.9	19.85
1.588	0.029	32.59	24.5	1558.80	2.15	25.1	4.96
1.588	0.029	28.5	24.5	1188.27	2.44	20.2	4.96

$$K = \frac{\sum_{i=1}^n K_i}{n} = 2.42 \times 10^{-5} \text{ cm}^2$$

TABLE II  
PRESSURE DROP MEASUREMENT OF SINGLE PHASE  
NON-NEWTONIAN FLUID FLOW, LARGE PLATE

$q$ $\text{cm}^3/\text{sec}$	$d_p$ $\text{cm}$	$N_{Re} \times 10^5$	Flow Type	$\Delta P \times 10^5$	Flow Type
0.15885	0.555	0.05	Separate	0.15	Separate
0.317	0.65	5.14	5.15	0.56	0.56
0.6554	1.1	7.89	7.84	1.15	1.15
1.5885	1.1	20.70	20.61	2.81	2.81
3.17	1.55	6.11	6.11	1.15	1.15
6.354	0.8	168.75	168.75	11.36	11.36
15.885	1.55	570.74	570.74	18.15	18.15
0.15885	0.555	1.25	50.1	0.15	0.15
0.6554	1.0	7.89	7.89	1.35	1.35
3.17	5.11	6.11	6.11	1.35	1.35
0.05	Separate	0.15	Separate	0.15	Separate
0.15885	0.555	0.558	0.558	0.15	0.15
0.317	0.65	0.905	0.905	0.15	0.15
0.6554	1.1	2.47	2.47	0.15	0.15
1.5885	1.1	8.99	8.99	0.15	0.15
3.17	1.55	15.80	15.80	0.15	0.15
6.354	1.55	65.70	65.70	0.15	0.15
15.885	1.55	155.00	155.00	0.15	0.15
0.354	1.55	65.70	65.70	0.15	0.15

SINIS TAKS, VED ALV NÖNMIN-NÖN ASVAN  
JENIS A. INGEMARSK JÖRK FÜSS RID  
S-A HEVI

$\omega$ cm <sup>-1</sup> /sec	cm <sup>2</sup> of film	$N_{H_2} \times 10^5$	$N_{D_2} \times 10^5$	Separation (cm)
0.5177	0.655	15.56	15.51	0.02
0.6554	0.5	15.56	15.51	0.02
0.6554	0.6	15.56	15.51	0.02
1.5885	15.91	15.51	15.51	0.02
1.5885	15.91	15.51	15.51	0.02
5.17	35.1	15.51	15.51	0.02
5.17	35.1	15.51	15.51	0.02
3.17	15.4	15.51	15.51	0.02
3.17	15.4	15.51	15.51	0.02
0.554	15.54	15.51	15.51	0.02
0.554	15.54	15.51	15.51	0.02
15.885	15.51	15.51	15.51	0.02
15.885	15.51	15.51	15.51	0.02
0.554	15.54	15.51	15.51	0.02
0.554	15.54	15.51	15.51	0.02
3.17	15.4	15.51	15.51	0.02
3.17	15.4	15.51	15.51	0.02
0.554	15.54	15.51	15.51	0.02
0.554	15.54	15.51	15.51	0.02
1.5885	15.51	15.51	15.51	0.02
1.5885	15.51	15.51	15.51	0.02
0.554	15.54	15.51	15.51	0.02
0.554	15.54	15.51	15.51	0.02
0.15885	0.317	0.02	0.02	0.02

TABLE IV-Continued

$\frac{d}{q}$ cm. <sup>-5</sup> /sec.	$D$ cm. of H <sub>2</sub> O	$N_{RE} \times 10^5$	0.1% Separation
0.15885	2.58	0.29	8.1
0.554	191.69	55.05	8.1
0.15885	10.62	0.29	8.1
0.15885	8.81	0.29	8.1
0.517	14.92	0.29	8.1
0.654	26.42	0.29	8.1
0.654	26.91	0.29	8.1
1.5885	55.57	0.29	8.1
5.17	100.49	20.5	8.1
5.17	111.89	20.5	8.1
6.554	205.06	25.05	8.1
15.885	515.86	30.25	8.1
0.15885	40.92	0.000	8.1
0.517	61.64	0.105	8.1
0.654	90.65	0.566	8.1
1.5885	156.44	2.57	8.1
5.17	250.71	6.858	8.1
6.554	426.85	20.085	8.1
5.17	267.28	6.358	8.1
1.5885	174.5	2.57	8.1
0.654	106.71	0.566	8.1
0.517	61.15	0.105	8.1

#### E.4 Pressure Drop Measurement of the Displacement Tests

It was mentioned in Section (IV-6) that the pressure drop history of each displacement test was recorded on a Strip Chart recorder. The pressure drop recorded on the chart,  $\Delta P_T$ , was the total pressure drop which consisted of pressure drop of the flooded zone,  $\Delta P_F$ , plus pressure drop of the oil zone,  $\Delta P_O$ . The value of  $\Delta P_O$  for the single phase region could be calculated by knowing the length of the bed above the plane of zero saturation. This was obtained as described in the following paragraph.

The time when the displacing fluid passed the inlet screen was marked on the pressure drop chart. Therefore, by knowing the speed of the chart; the corresponding time,  $t_i$ , of each point on the chart could be obtained. This value of  $t$  was used to calculate  $q_t/t\lambda$ . From the eye-fit line of Figures (V-3) to (V-18) the value of  $x_i$  or length of flooded zone was determined. Therefore the length of the unswept portion of the bed could be easily calculated by difference and subsequently used to determine  $\Delta P_O$ .

Table (F-7) includes the pressure drop measurements of the flooded zone and the overall pressure gradient of the flooded area,  $\left(\frac{dp}{dx}\right)_F$ .

Volumetric average water saturation,  $\bar{S}_w$ , which has already been defined in Section II.3 was calculated at each position in the bed. This is included in column four of the Table (F-7). Correction of the pressure drop reading due to the small difference in specific gravity of the displacing and displaced fluid has also been considered. Occurrence of the breakthrough is marked by B. T. which appeared in Columns 3 and 4 of Table (F-7).

Table F-8 presents the friction factor-Reynolds number relationship of the flooded zone. Friction factor and Reynolds number were calculated from Equations (B-25, 28) respectively. The only modification involved was

replacement of the viscosity in the Reynolds number by effective viscosity, defined by Equation (II-33). For the polymerflood, Equation (II-33) with apparent viscosity of the polymer solution instead of  $\mu_w$  was used to obtain the average viscosity for the Reynolds number calculation. Estimation of the apparent viscosity of the polymer solution was based on the shear rate in the bed. The reason behind this choice is discussed in Appendix II.

To calculate the friction factor of the flooded zone the arithmetic average of the overall pressure gradients with a star in Table (E-7) were used. The initial data points were ignored to minimize the error contribution due to the initial segment of the bed which is discussed in Appendix G.L.

For the sake of comparison, in addition to the experimental values of the overall pressure gradient of the flooded zone its predicted values based on the effective viscosity and Darcy's law are also reported in Table (E-8).

TABLE E-7  
OVERALL PRESSURE GRADIENT OF THE FLOODED  
ZONE

\* The arithmetic average of asterisked overall gradients is being used to calculate friction factor of the mixed zone.

t sec	$\dot{q}t/\Delta A$ cm	$x_0$ cm	$\bar{s}_w$	$\Delta P_T$ cm of $H_2O$	$\Delta P_F$ cm of $H_2O$	$(dP/dx)_P$ cm of $H_2O/cm$
Roll No. 8, Run No. 1						
0.0	0.0	0.0	0.0	7.2	-	0.004
30	2.07	9.7	0.21	6.4	0.03	0.011*
60	4.14	18.8	0.22	5.8	0.16	0.043*
90	6.21	28	0.22	5.6	1.12	0.046*
120	8.28	37.7	0.22	5.0	1.65	0.044*
150	10.34	46.7	0.22	4.4	1.97	0.047*
180	12.4	55.5	0.23	4.2	2.2	0.047*
210	14.5	B.T.	B.T.	3.8	1.8	0.037
240	16.5	-	-	3.4	1.4	0.029
300	20.7	-	-	3.2	1.2	0.024
360	24.8	-	-	3.0	1.0	0.02
420	29	-	-	2.9	0.9	0.018
480	33.1	-	-	2.8	0.8	0.016
Roll No. 8, Run No. 2						
0.0	0.0	0.0	0.0	16.5	-	-
33	4.55	19	0.24	13.7	2.62	0.15*
48	6.62	28	0.24	12.1	3.85	0.15*
78	10.76	45.5	0.24	10.3	6.73	0.15*
108	14.9	B.T.	B.T.	8.7	6.74	0.14*
138	19.03	-	-	7.3	5.34	0.11
168	23.17	-	-	6.4	4.44	0.09
198	27.31	-	-	5.8	3.84	0.08
228	31.45	-	-	5.8	3.84	0.08
258	35.59	-	-	5.3	3.34	0.07
Roll No. 8, Run No. 3						
0.0	0.0	0.0	0.0	32.95	-	-
15	4.14	14	0.30	30.15	5.63	0.47*
30	8.28	29.2	0.28	25.95	11.74	0.45*
45	12.41	42.5	0.29	23.75	17.01	0.42*
60	16.55	B.T.	B.T.	20.55	18.59	0.38*
90	24.83	-	-	19.50	17.54	0.36
120	33.10	-	-	13.15	11.19	0.23
150	41.38	-	-	8.8	6.84	0.14
180	49.66	-	-	7.55	5.59	0.11

TABLE I (continued)

	Q <sub>1</sub> /A cm	Q <sub>2</sub> /A cm	Q <sub>3</sub> /A cm	W <sub>1</sub> cm <sup>-1</sup>	W <sub>2</sub> cm <sup>-1</sup>	W <sub>3</sub> cm <sup>-1</sup>	P <sub>1</sub> cm of H <sub>2</sub> O	P <sub>2</sub> cm of H <sub>2</sub> O	P <sub>3</sub> cm of H <sub>2</sub> O
RgII sec S <sub>1</sub> Run No. 4									
0.0	0.0	0.0	0.0	29.38*					
15	1.14	2.14	0.0	0.10	26.41	0.15	0.19*		
30	8.78	19.17	0.0	0.10	23.17	0.37	0.14*		
45	19.11	38.11	0.0	0.10	22.17	1.53	0.18*		
60	36.53	78.11	0.0	0.10	20.67	1.71	0.18*		
90	74.85	14.85	0.0	0.10	19.47	1.16	0.16*		
120	55.10	0	0	0	16.57	1.16	0.16*		
135	55.24	0	0	0	14.57	0.49	0.15*		
150	44.38	0	0	0	12.57	0.49	0.15*		
180	49.66	0	0	0	11.04	0.08	0.10		
210	55.05	0	0	0	6.39	1.15	0.10		
240	66.24	0	0	0	6.17	1.06	0.13*		
270	74.48	0	0	0	5.69	0.88	0.18		
RgII sec S <sub>1</sub> Run No. 5									
0.0	0.0	0.0	0.0	2.94					
21	0.58	2.5	0.0	0.25	5.56	0.45	0.86		
31	21.31	5.7	0	0.25	5.20	0.35	0.10		
81	2.25	9.0	0	0.25	5.18	0.37	0.03		
111	51.06	12.5	0	0.24	5.18	0.44	0.04*		
141	5.89	15.7	0	0.25	5.16	0.48	0.04*		
171	4.72	19.7	0	0.25	5.10	0.48	0.05*		
201	5.54	22.3	0	0.25	5.08	0.41	0.02*		
216	5.96	24.2	0	0.25	5.05	0.42	0.02*		
231	6.57	26.0	0	0.25	5.03	0.35	0.01*		
246	6.79	27.5	0	0.25	2.84	0.37	0.01*		
261	7.20	29.49	0	0.25	2.83	0.37	0.01*		
291	8.05	32.5	0	0.25	2.80	0.37	0.014*		
321	8.80	36.0	0	0.25	2.88	0.53	0.017*		
381	10.51	42.2	0	0.25	2.81	0.56	0.016*		
441	12.17	49.0	0	0.25	2.74	0.71	0.015*		
501	13.82	51.1	0	0.25	2.42	0.16	0.009		
561	15.48	0	0	0	2.48	0.13	0.010		
621	17.13	0	0	0	2.53	0.39	0.012		
681	18.79	0	0	0	2.01	0.38	0.002		
741	20.44	0	0	0	2.52	0.36	0.007		
801	22.60	0	0	0	1.92	0.02	0.000		
861	23.75	0	0	0	2.12	0.16	0.003		
921	25.41	0	0	0	2.54	0.38	0.008		
981	27.06	0	0	0	2.18	0.22	0.004		
1041	28.72	0	0	0	2.15	0.17	0.003		

TABLE E-7 (Continued)

t sec.	qt./#A cm	$x_0$ cm	$\bar{S}_w$	$\Delta P_T$ cm of $H_2O$	$\Delta P_F$ cm of $H_2O$	$(dP/dx)_F$ cm of $H_2O/cm$
-----------	--------------	-------------	-------------	------------------------------	------------------------------	--------------------------------

1101	30.37	-	-	1.96	0.02	0.0004
1221	35.68	-	-	1.96	0.02	0.0004
1341	36.99	-	-	1.96	0.02	0.0004
1461	40.30	-	-	1.86	0.0	0.0
1581	43.61	-	-	1.91	0.0	0.0

## Roll No. 9, Run No. 1

0.0	0.0	0.0	0.0	7.23	-	-
21	1.45	1.6	0.91	7.23	-	-
51	3.52	4.1	0.86	9.6	2.6	1.24
81	5.59	6.6	0.85	11.08	4.36	0.95
111	7.66	9.1	0.84	13.08	6.62	0.93
141	9.72	11.5	0.84	14.88	8.67	0.91*
171	11.79	14.1	0.84	16.28	10.36	0.86*
231	15.93	18.8	0.85	18.64	13.22	0.79*
291	20.07	23.8	0.84	21.36	16.48	0.76*
351	24.21	28.7	0.84	24.36	20.00	0.75*
411	28.35	33.6	0.84	26.96	23.13	0.73*
471	32.48	38.6	0.84	29.56	26.27	0.72*
531	36.62	43.5	0.84	32.36	29.59	0.71*
591	40.76	48.4	0.84	35.76	33.68	0.73*
651	44.90	53.5	0.84	36.76	34.80	0.71*
711	49.04	B.T.	B.T.	36.26	34.80	0.70
771	53.17	-	-	36.26	34.30	0.70

## Roll No. 9, Run No. 2

0.0	0.0	0.0	0.0	14.35	-	-
30	4.14	5.2	0.80	18.6	5.06	1.58
60	8.28	9.7	0.85	22.05	9.64	1.25
90	12.41	14.6	0.85	25.1	13.94	1.11*
120	16.55	19.6	0.84	28.3	18.4	1.05*
150	20.69	24.5	0.84	31.5	22.84	1.02*
180	24.83	29.5	0.84	35.2	27.8	1.01*
210	28.97	34.5	0.84	37.8	31.67	0.97*
240	33.10	39.3	0.84	41.45	36.53	0.98*
270	37.24	44.1	0.84	44.60	40.90	0.97*
300	41.38	49.0	0.84	46.60	44.13	0.94*
360	49.66	B.T.	B.T.	46.25	44.29	0.90
420	57.93	-	-	46.84	44.88	0.92

TABLE F-7 (Continued)

t sec	qt/ $\mu$ A cm <sup>2</sup>	$x_0$ cm	$\bar{S}_w$	$\Delta P_T$ cm of H <sub>2</sub> O	$\Delta P_F$ cm of H <sub>2</sub> O	$(dP/dx)_F$ cm of H <sub>2</sub> O/cm.
Roll No. 9, Run No. 3						
0.0	0.0	0.0	0.0	28.20		
24	6.62	8.5	0.78	57.40	12.68	1.95
54	14.90	18.8	0.79	43.80	24.60	1.46*
84	23.17	29.5	0.79	53.20	39.73	1.44*
114	31.45	39.6	0.79	58.60	51.54	1.37*
138	38.07	48.1	0.79	64.60	61.09	1.33*
156	43.04	53.5	0.80	64.80	62.84	1.28*
174	48.00	B.T.	B.T.	63.40	61.44	1.25
204	56.28			63.70	61.74	1.26
Roll No. 9, Run No. 4						
0.0	0.0	0.0	0.0	75.4		
9	6.21	8.7	0.71	88.2	22.84	3.41
15	10.35	14.3	0.72	94.5	37.54	3.05*
21	14.48	20.2	0.72	99.7	51.58	2.83*
27	18.62	25.8	0.72	109.2	69.01	2.9*
33	22.76	31.8	0.72	114.4	83.67	2.81*
39	26.90	37.4	0.72	116.8	94.45	2.67*
45	31.04	43.0	0.72	119.6	105.65	2.58*
51	35.17	48.7	0.72	121.6	116.19	2.49*
57	39.31	B.T.	B.T.	115.7	113.74	2.32
63	43.45			113.7	111.74	2.28
69	47.59			114.0	112.04	2.29
75	51.73			113.6	111.64	2.28
105	72.42			113.7	111.74	2.28
Roll No. 9, Run No. 5						
0.0	0.0	0.0	0.0	278.22		
50	0.85	7.5	0.11	294.76	47.55	8.65
48	1.52	11.7	0.11	287.76	64.23	6.62*
78	2.15	19.0	0.11	281.53	99.16	5.83*
108	2.98	26.5	0.11	275.89	135.80	5.54*
138	3.81	33.7	0.11	269.07	169.57	5.35*
168	4.63	41.2	0.11	257.30	200.09	5.10*
198	5.46	48.7	0.14	248.12	233.19	4.99*
228	6.29	B.T.	B.T.	236.12	234.16	4.78
258	7.12			231.30	229.34	4.68
318	8.77			211.76	209.80	4.28
378	10.43			191.04	189.08	3.86
438	12.08			179.86	177.90	3.63

TABLE E-7 (Continued)

t sec	qt/ $\phi\lambda$ cm	x cm	$S_w$	$\Delta P_T$ cm of $H_2O$	$\Delta P_F$ cm of $H_2O$	$(dP/dx)_F$ cm of $H_2O/cm$
558	15.39			166.32	164.56	3.55
678	18.70			148.78	146.82	3.00
918	25.32			129.24	127.28	2.60
1158	31.95			120.06	118.1	2.41
1398	38.57			113.88	111.92	2.28
1638	45.19			102.52	100.56	2.05
1938	53.46			92.16	90.2	1.84
2238	61.74			88.16	86.2	1.76
2838	78.29			78.98	77.02	1.57
3438	94.84			66.62	64.66	1.32
4038	111.40			57.44	55.48	1.13
RoII No. 9, Run No. 6						
0.0	0.0	0.0	0.0	175.60		
30	0.41	5.0	0.14	176.07	4.01	4.01
60	0.83	6.0	0.14	172.94	11.51	2.88
120	1.66	12.0	0.14	166.16	26.08	2.61*
180	2.48	18.0	0.14	160.64	41.74	2.61*
240	3.31	24.0	0.14	153.74	56.10	2.55*
300	4.14	30.2	0.14	147.74	72.07	2.56*
360	4.97	36.5	0.14	137.94	84.63	2.45*
420	5.79	42.5	0.14	126.79	94.71	2.34*
480	6.62	48.5	0.14	119.61	108.79	2.34*
540	7.45	B.T.	B.T.	110.84	108.88	2.22
600	8.28			100.48	98.52	2.01
660	9.10			94.30	92.34	1.88
780	10.76			82.48	80.52	1.64
900	12.41			74.73	72.77	1.49
1020	14.07			68.48	66.52	1.36
1140	15.72			65.40	63.44	1.29
1260	17.38			67.12	65.16	1.33
1340	19.86			56.26	54.30	1.11
1620	22.55			52.15	50.19	1.02
1920	26.48			48.58	46.62	0.95
2220	30.62			45.94	44.98	0.86
RoII No. 9, Run No. 7						
0.0	0.0	0.0	0.0	25.85		
21	5.79	10.5	0.55	26.29	4.58	0.54*
36	9.93	18.5	0.54	26.49	8.68	0.53*
51	14.07	26.0	0.54	26.85	12.70	0.53*
66	18.21	33.5	0.55	26.69	16.10	0.51*

TABLE F-7 (Continued)

t sec	qt/φA cm	x cm	$\bar{S}_w$	$\Delta P_T$ cm of $H_2O$	$\Delta P_F$ cm of $H_2O$	$(dP/dx)_F$ cm of $H_2O/cm$
81	22.35	40.8	0.55	25.96	19.03	0.40*
96	26.48	48.6	0.54	25.32	22.19	0.48*
111	30.62	B.T.	B.T.	24.19	23.23	0.47*
126	34.76			23.51	21.35	0.44
141	38.90			23.57	21.41	0.44
171	47.17			22.89	20.95	0.43
201	55.45			22.89	20.93	0.43
Roll No. 9, Run No. 8						
0.0	0.0	0.0	0.0	65.05	-	-
12	8.28	15.6	0.53	66.57	19.03	1.4*
24	16.55	30.2	0.55	65.81	37.07	1.51*
36	24.83	45.5	0.55	64.92	55.88	1.28*
48	33.10	B.T.	B.T.	57.81	55.85	1.14*
66	45.52			46.71	44.75	0.91
84	57.93			45.40	43.44	0.89
102	70.35			45.38	43.42	0.89
Roll No. 10, Run No. 1						
0.0	0.0	0.0	0.0	24.8	-	-
24	6.62	17.6	0.58	23.0	5.48	0.55*
54	14.90	39.6	0.58	20.0	12.75	0.54*
84	23.17	B.T.	B.T.	15.0	13.04	0.27
114	31.45			13.75	11.79	0.24
144	39.72			15.0	11.04	0.23
162	44.69			12.5	10.54	0.22
Roll No. 10, Run No. 3						
0.0	0.0	0.0	0.0	6.1	-	-
35	2.28	4.0	0.57	6.5	0.57	0.29
63	4.54	7.6	0.57	6.6	0.98	0.18
95	6.41	11.4	0.56	6.7	1.59	0.15*
125	8.48	15.1	0.56	6.8	1.81	0.14*
183	12.62	22.5	0.56	6.9	2.53	0.12*
243	16.76	30.0	0.56	7.0	3.27	0.12*
303	20.90	37.4	0.56	7.06	3.95	0.11*
363	25.03	44.7	0.56	7.0	4.51	0.11*
423	29.17	52.2	0.56	6.9	4.94	0.10*
483	35.31	B.T.	B.T.	6.6	4.64	0.09
543	37.45			6.0	4.04	0.08

TABLE T-7 (Continued)

t sec	qt/ $\phi\Lambda$ cm.	x cm	$S_w$	$\Delta P_T$ cm. of H <sub>2</sub> O	$\Delta P_F$ cm. of H <sub>2</sub> O	(dP/dx) cm. of H <sub>2</sub> O/cm.
Roll No. 10, Run No. 4						
0.0	0.0	0.0	0.0	24.9		
15	4.14	11.0	0.38	24.75	4.06	0.45*
30	8.28	22.4	0.37	24.0	8.65	0.42*
45	12.41	33.1	0.37	23.5	13.16	0.42*
60	16.55	44.0	0.38	22.25	17.01	0.41*
75	20.69	B.T.	B.T.	20.5	18.54	0.38
90	24.83			19.0	17.04	0.35
105	28.97			16.5	14.54	0.30
120	33.10			15.75	13.79	0.28
135	37.24			15.5	13.54	0.28
150	41.38			15.25	13.29	0.27
180	49.66			14.75	12.79	0.26
204	56.28			14.9	12.94	0.26
Roll No. 10, Run No. 5						
0.0	0.0	0.0	0.0	61.0*		
7.5	5.17	14.7	0.35	55.0	9.50	0.75*
45	10.35	27.5	0.38	45.0	14.49	0.57*
22.5	15.52	40.7	0.38	30.0	15.65	0.40*
50	20.69	B.T.	B.T.	25.0	25.04	0.47
57.5	25.86			25.0	25.04	0.47
52.5	36.21			25.0	25.04	0.47
Roll No. 10, Run No. 6						
0.0	0.0	0.0	0.0	24.7		
15	4.14	10.8	0.38	24.7	4.09	0.46*
30	8.28	22.2	0.37	23.5	8.17	0.40*
45	12.41	33.0	0.38	22.5	12.49	0.39*
60	16.55	44.0	0.38	21.25	16.94	0.38*
75	20.69	B.T.	B.T.	19.5	17.54	0.36*
90	24.83			17.0	15.04	0.31
105	28.97			15.75	13.79	0.28
120	33.10			15.0	13.04	0.27
135	37.24			13.0	13.04	0.27
150	41.38			14.5	12.54	0.26
165	45.52			14.5	12.54	0.26
195	53.79			14.25	12.29	0.25

TABLE E-7 (Continued)

$t$ sec	$qt/\phi A$ cm	$x$ cm	$\bar{s}_w$	$\Delta P_T$ cm of $H_2O$	$\Delta P_F$ cm of $H_2O$	$(dP/dx)_F$ cm of $H_2O/cm$
Roll No. 10, Run No. 7						
0.0	0.0	0.0	0.0	52.48	52.48	0.59
21	1.55	9.0	0.17	49.98	44.11	0.59
56	2.66	18.5	0.16	47.73	8.71	0.60*
66	4.88	30.0	0.16	42.22	17.53	0.62*
96	7.09	43.5	0.16	36.28	26.15	0.63*
126	9.31	B.T.	B.T.	29.17	27.21	0.56*
156	11.53			24.98	25.02	0.47
216	15.96			20.78	18.62	0.58
276	20.39			18.75	16.79	0.54
336	24.83			16.98	15.02	0.51
456	33.70			15.46	13.50	0.28
576	42.56			14.18	12.23	0.25
696	51.43			13.47	11.51	0.23
816	60.30			12.95	10.97	0.22
936	69.16			12.09	10.13	0.21
Roll No. 10, Run No. 8						
0.0	0.0	0.0	0.0	22.76	22.76	0.41
50	0.89	5.5	0.16	22.76	1.45	0.41
60	1.77	10.5	0.17	21.55	2.78	0.53*
90	2.66	16.0	0.17	20.72	4.33	0.51*
120	3.55	21.5	0.17	19.66	5.78	0.27*
150	4.43	26.0	0.17	18.55	6.82	0.28*
180	5.32	31.2	0.17	17.44	6.77	0.23*
210	6.21	36.5	0.17	16.55	8.01	0.23*
240	7.09	41.7	0.17	15.85	9.78	0.25*
270	7.98	47.2	0.17	14.84	11.21	0.25*
300	8.87	52.2	0.17	14.25	12.27	0.25*
330	9.75	B.T.	B.T.	13.25	11.27	0.25
360	10.64			12.95	10.99	0.22
420	12.41			12.57	10.61	0.22
480	14.19			11.98	10.92	0.20
540	15.96			11.86	9.90	0.20
660	19.51			11.76	9.80	0.20
720	21.28			10.79	8.85	0.18



TABLE E-7 (Continued)

t sec	qt/ΦΔ cm	x cm	$\bar{S}_w$	$\Delta P_T$ cm of H <sub>2</sub> O	$\Delta P_F$ cm of H <sub>2</sub> O	$(dP/dx)_F$ cm of H <sub>2</sub> O/cm
Roll No. 10, Run No. 10						
0.0	0.0	0.0	0.0	112.47		
18	2.66	16.0	0.17	105.67	22.50	1.61*
33	4.88	29.0	0.17	94.39	36.37	1.35*
48	7.09	41.7	0.17	77.22	52.83	1.35*
63	9.31	B.T.	B.T.	64.14	62.48	1.28*
78	11.53			48.78	46.82	0.96
93	13.74			38.20	36.24	0.74
108	15.96			34.57	32.41	0.66
138	20.39			29.75	27.77	0.57
198	29.26			25.54	23.58	0.48
258	38.15			22.79	20.83	0.45
318	47.00			20.50	18.34	0.37
378	55.86			18.62	16.66	0.34
438	64.73			16.55	14.59	0.30
498	73.60			15.91	13.95	0.28
618	91.33			14.00	12.04	0.25
738	109.07			12.75	10.77	0.22
Roll No. 11, Run No. 2						
0.0	0.0	0.0	0.0	250.02		
9.0	2.66	15.5	0.20	252.25	44.11	3.84*
16.5	4.88	24.5	0.20	228.80	67.96	3.02*
24.0	7.09	33.5	0.20	201.53	104.79	3.13*
31.5	9.31	46.5	0.20	156.13	126.65	2.85*
39.0	11.53	B.T.	B.T.	112.09	110.13	2.22*
46.5	13.74			84.81	82.85	1.69
54.0	15.96			66.92	64.96	1.53
61.5	18.18			60.53	58.57	1.20
76.5	22.61			54.14	52.18	1.06
106.5	31.48			47.23	45.27	0.92
136.5	40.35			44.27	42.31	0.86
166.5	49.21			41.92	39.96	0.82
Roll No. 11, Run No. 4						
0.0	0.0	0.0	0.0	126.43		
30	4.43	11.8	0.38	123.43	21.90	2.23*
60	8.87	23.7	0.37	118.43	47.12	2.17*
90	13.50	35.5	0.37	115.22	71.89	2.15*
120	17.73	47.2	0.38	106.54	94.75	2.10*
150	22.17	B.T.	B.T.	100.93	98.97	2.02
180	26.60			96.74	94.78	1.93

TABLE E-7 (Continued)

t sec	qt/φA cm	x cm	$\bar{S}_w$	$\Delta P_T$ , cm of $H_2O$	$\Delta P_F$ , cm of $H_2O$	$(dP/dx)_F$ , cm of $H_2O/cm$
210	31.04	-	-	94.82	92.86	1.90
240	35.47	-	-	92.8	90.84	1.85
270	39.90	-	-	90.93	88.97	1.82
300	44.34	-	-	89.35	87.39	1.78
330	48.77	-	-	88.93	86.99	1.78
360	53.20	-	-	88.21	86.25	1.76
390	57.64	-	-	87.73	85.77	1.75
Roll No. 11, Run No. 5						
0.0	0.0	0.0	0.0	243.91	-	-
15	4.43	15.1	0.34	235.42	44.78	4.05*
30	8.87	26.2	0.34	225.42	97.99	4.05*
45	13.30	39.5	0.34	210.29	151.08	4.05*
60	17.73	52.2	0.34	190.40	188.44	3.85*
75	22.17	B.T.	B.T.	171.34	169.58	3.46
90	26.60	-	-	163.20	161.24	3.29
105	31.04	-	-	157.88	155.92	3.18
135	39.90	-	-	150.00	148.04	3.02
165	48.77	-	-	145.17	143.21	2.92
195	57.64	-	-	142.61	140.65	2.87
225	66.50	-	-	140.57	138.61	2.85
Roll No. 11, Run No. 6						
0.0	0.0	0.0	0.0	62.59	-	-
60	4.43	9.5	0.47	62.21	8.90	1.19
120	8.87	19.0	0.47	61.43	19.88	1.17*
180	13.30	28.1	0.47	60.17	29.88	1.14*
240	17.73	37.6	0.47	58.02	39.48	1.11*
300	22.17	47.5	0.47	56.62	50.53	1.11*
360	26.60	B.T.	B.T.	54.98	53.02	1.08
420	31.04	-	-	53.7	51.74	1.06
480	35.47	-	-	52.56	50.60	1.03
540	39.90	-	-	51.1	49.14	1.00
660	48.77	-	-	49.25	47.29	0.97
780	57.64	-	-	48.37	46.41	0.95
900	66.50	-	-	47.73	45.77	0.93
1020	75.37	-	-	46.99	45.03	0.92
1140	84.24	-	-	45.95	43.99	0.90
1242	91.78	-	-	45.95	43.99	0.90

TABLE I (Continued)

t sec.	qt/φA cm	x cm	$\frac{S}{W}$	$\Delta P_T$ cm of $H_2O$	$\Delta P_F$ cm of $H_2O$	$(dP/dx)_F$ cm of $H_2O/cm$
ROLL No. 11, Run No. 8						
0.0	0.0	0.0	0.0	224.29		
15	4.43	8.1	0.55	227.92	31.23	5.12*
30	8.87	16.3	0.54	236.73	77.53	5.41*
45	13.30	24.5	0.55	245.01	121.90	5.47*
60	17.73	32.3	0.55	247.09	161.19	5.28*
90	26.60	48.7	0.55	250.71	238.31	5.10*
120	35.47	B.T.	B.T.	247.09	245.15	5.09
150	44.34			247.09	245.15	5.00
180	53.20			242.94	240.98	4.92
210	62.07			241.91	239.95	4.90
ROLL No. 11, Run No. 9						
0.0	0.0	0.0	0.0	112.52		
30	4.43	6.4	0.69	119.14	16.73	5.8
60	8.87	13.1	0.68	124.32	37.00	5.35*
90	13.30	19.7	0.68	128.46	56.00	5.16*
120	17.73	26.5	0.67	130.54	73.40	5.0 *
150	22.17	33.0	0.67	133.64	91.14	2.94*
180	26.60	39.8	0.67	137.27	110.09	2.91*
210	31.04	46.5	0.67	140.90	128.80	2.89*
240	35.47	53.2	0.67	140.90	138.94	2.84*
270	39.90	B.T.	B.T.	144.00	142.04	2.40
330	48.77			145.04	143.08	2.92
390	57.64			145.04	143.08	2.92
450	66.50			145.04	143.08	2.92
510	75.37			145.04	143.08	2.92
540	79.80			145.04	143.08	2.92
ROLL No. 11, Run No. 10						
0.0	0.0	0.0	0.0	111.59		
15	2.22	2.6	0.85	116.55	6.50	10.85
45	6.65	8.1	0.82	144.00	46.24	7.58
75	11.08	13.5	0.82	170.94	85.23	7.41*
105	15.52	19.6	0.79	195.80	125.72	7.05*
135	19.95	24.6	0.81	212.38	151.47	6.70*
165	24.38	30.1	0.81	230.51	181.88	6.47*
195	28.82	35.6	0.81	247.60	211.25	6.29*
225	33.25	41.0	0.81	268.32	244.03	6.20*
255	37.69	46.5	0.81	290.08	278.07	6.25*
285	42.12	51.7	0.81	313.39	311.43	6.36*
315	46.55	B.T.	B.T.	326.34	324.38	6.62

TABLE E-7 (Continued)

t sec	qt/φA cm	x cm	$\bar{S}_w$	$\Delta P_T$ cm of $H_2O$	$\Delta P_F$ cm of $H_2O$	$(dP/dx)_F$ cm of $H_2O/cm$
345	50.99			534.11	532.15	6.78
375	55.42			540.84	538.88	6.92
405	59.85			544.99	543.03	7.00
435	64.29			547.96	545.10	7.04
465	68.72			550.17	548.24	7.11
ReII No. 12, Run No. 1						
0.0	0.0	0.0	0.0	49.73		
60	4.43	7.2	0.62	49.21	5.56	0.68
120	8.87	15.0	0.59	48.69	9.16	0.70*
180	13.30	22.0	0.60	47.14	15.14	0.66*
240	17.73	29.5	0.60	46.10	17.95	0.65*
300	22.17	37.2	0.60	45.53	23.22	0.66*
360	26.60	44.6	0.60	44.29	27.99	0.66*
420	31.04	52.0	0.60	43.77	32.50	0.66*
480	35.47	B.T.	B.T.	42.99	31.72	0.65
540	39.90			41.44	30.47	0.62
600	44.34			41.44	30.47	0.62
660	48.77			40.92	29.65	0.61
720	53.20			40.15	28.88	0.59
780	57.64			39.57	28.10	0.57
ReII No. 12, Run No. 2						
0.0	0.0	0.0	0.0	98.42		
30	4.43	11.2	0.40	98.42	16.55	1.80*
60	8.87	22.7	0.59	95.24	32.05	1.55*
90	13.30	34.2	0.59	86.77	46.27	1.44*
120	17.73	45.8	0.59	80.29	60.65	1.38*
150	22.17	B.T.	B.T.	74.07	63.78	1.30*
180	26.60			68.64	58.35	1.19
210	31.04			65.27	54.98	1.12
ReII No. 12, Run No. 3						
0.0	0.0	0.0	0.0	99.72		
30	4.43	11.2	0.40	97.13	14.20	1.54*
60	8.87	22.7	0.59	93.24	31.30	1.51*
90	13.30	34.2	0.59	88.06	47.11	1.46*
120	17.73	45.8	0.59	82.10	62.32	1.42*
150	22.17	B.T.	B.T.	76.41	66.12	1.35*
180	26.60			71.23	60.94	1.24
210	31.04			67.54	57.05	1.16
240	35.47			64.75	54.46	1.11
270	39.90			62.16	51.87	1.06
300	44.34			60.87	50.58	1.03
330	48.77			59.57	49.28	1.01

TABLE E-7 (Continued)

t sec	qt/φA cm	x cm	φ <sub>w</sub>	ΔP <sub>T</sub> cm of H <sub>2</sub> O	ΔP <sub>E</sub> cm of H <sub>2</sub> O	(dR/dx) cm of H <sub>2</sub> O/cm
RoII No. 12, Run No. 4						
0.0	0.0	0.0	0.0	98.94		
30	4.43	7.0	0.63	99.46	9.57	1.87
60	8.87	14.0	0.63	100.49	22.78	1.9*
90	13.30	21.0	0.63	101.01	35.68	1.88*
120	17.73	28.0	0.63	101.53	48.59	1.87*
150	22.17	35.2	0.63	101.79	61.59	1.86*
180	26.60	42.2	0.63	103.08	75.26	1.87*
210	31.04	49.2	0.63	104.58	88.95	1.88*
240	35.47	B.T.	B.T.	106.97	94.72	1.93*
RoII No. 12, Run No. 5						
0.0	0.0	0.0	0.0	97.58		
30	4.43	9.2	0.48	95.83	11.18	1.55
60	8.87	18.5	0.48	92.72	24.50	1.48*
90	13.30	27.6	0.48	88.58	36.45	1.42*
120	17.73	37.1	0.48	85.47	50.15	1.43*
150	22.17	46.6	0.48	81.84	63.29	1.42*
180	26.60	B.T.	B.T.	78.74	67.96	1.39
210	31.04			76.15	65.37	1.35
240	35.47			71.45	60.70	1.24
270	39.90			67.86	57.08	1.16
RoII No. 12, Run No. 6						
0.0	0.0	0.0	0.0	48.07		
30	0.22	5.7	0.60	48.07	1.50	0.76
60	4.43	7.5	0.59	47.66	5.78	0.69
90	6.65	11.2	0.59	47.03	5.97	0.65*
120	8.87	15.1	0.59	46.41	8.31	0.63*
150	11.08	18.6	0.60	45.58	10.14	0.61*
180	13.30	22.6	0.59	44.76	12.37	0.60*
210	15.52	26.5	0.59	44.55	15.12	0.62*
240	17.73	30.1	0.59	43.93	17.25	0.61*
270	19.95	34.1	0.59	43.54	19.87	0.62*
300	22.17	38.1	0.58	42.89	22.29	0.62*
330	24.38	41.8	0.58	42.68	24.89	0.63*
390	28.82	49.4	0.58	41.96	29.96	0.63*
450	33.25	B.T.	B.T.	41.65	30.87	0.63*
510	37.69			40.61	29.83	0.61

TABLE I (Continued)

t sec	qt/ΦA cm	x cm	$\bar{S}_w$	$\Delta P_T$ cm of H <sub>2</sub> O	$\Delta P_F$ cm of H <sub>2</sub> O	$(dP/dx)_F$ cm of H <sub>2</sub> O/cm
R611 No. 12, Run No. 7						
0,0	0,0	0,0	0,0	195,80	-	-
15	4,43	11,3	0,39	189,59	28,90*	3,11*
30	8,87	25,0	0,39	180,26	65,75	3,04*
45	13,30	34,5	0,39	171,98	98,90	3,04*
60	17,73	45,8	0,39	162,65	132,23	3,02*
75	22,17	B.T.	B.T.	150,74	139,96	2,86*
90	26,60	-	-	142,97	132,19	2,70
105	31,04	-	-	131,57	120,79	2,47
120	35,47	-	-	127,43	116,65	2,38
135	39,90	-	-	122,25	111,47	2,27
150	44,34	-	-	118,10	107,52	2,19
165	48,77	-	-	115,51	104,75	2,14
R611 No. 12, Run No. 8						
0,0	0,0	0,0	0,0	19,57	-	-
60	1,77	2,4	0,74	18,86	-	-
120	5,55	4,6	0,77	19,57	0,43	0,17
180	9,52	7,1	0,75	19,68	1,16	0,25
240	17,09	9,4	0,75	19,89	1,75	0,24
300	9,75	13,0	0,75	19,99	2,44	0,22*
420	12,41	16,6	0,75	20,10	3,14	0,22*
510	15,07	20,2	0,75	20,20	3,83	0,21*
600	17,73	23,6	0,75	20,51	4,51	0,21*
690	20,39	27,4	0,74	20,41	5,24	0,21*
810	23,94	32,1	0,75	20,72	6,33	0,21*
930	27,49	37,1	0,74	21,24	7,68	0,22*
1050	31,04	41,9	0,74	21,96	9,18	0,23*
1170	34,58	46,6	0,74	23,31	11,51	0,25*
1290	38,13	51,5	0,74	24,55	13,28	0,27*
1410	41,68	B.T.	B.T.	25,00	11,75	0,24
1530	45,22	-	-	21,55	10,28	0,21
R611 No. 15, Run No. 1						
0,0	0,0	0,0	0,0	48,17	-	-
60	0,44	1,1	0,40	47,35	-	-
120	0,89	2,6	0,54	47,55	-	-
210	1,55	4,5	0,54	47,55	1,56	0,62
300	2,22	6,6	0,54	46,31	2,52	0,55
390	2,88	8,7	0,53	45,69	3,91	0,58
480	3,55	10,6	0,53	45,69	5,71	0,66*
600	4,43	15,5	0,53	44,76	7,55	0,66*

TABLE II (Continued)

t sec	qt/ΦA cm	x cm	$\xi_w$	$\Delta P_T$ cm of $H_2O$	$\Delta P_F$ cm of $H_2O$	$(dP/dx)_F$ cm of $H_2O/cm$
720	5.52	16.2	0.53	14.15	9.49	0.67*
840	6.21	19.1	0.53	14.31	12.57	0.72*
1020	7.54	23.1	0.53	15.20	15.14	0.75*
1200	8.87	27.3	0.52	14.96	18.09	0.71*
1380	10.20	31.6	0.52	10.92	10.96	0.71*
1360	11.53	35.7	0.52	89.58	85.53	0.70*
1740	12.86	40.7	0.52	58.54	26.68	0.70*
1920	14.19	44.2	0.52	37.50	29.35	0.70*
2100	15.52	47.7	0.53	53.95	51.51	0.69*
2280	16.85	52.5	0.52	54.91	53.44	0.68*
2520	18.62	B.T.	B.T.	55.15	51.68	0.65
2760	20.39	-	-	51.08	29.61	0.60
3060	22.61	-	-	29.42	27.95	0.57
3360	24.85	-	-	28.59	26.92	0.55
3660	27.04	-	-	27.66	26.19	0.53
3960	29.26	-	-	26.65	25.16	0.51
4260	31.48	-	-	25.90	24.45	0.50

## Run No. 15, Run No. 2

0.0	0.0	0.0	0.0	190.62	-	-
30	0.89	5.2	0.17	194.66	15.59	1.18
60	1.77	10.6	0.17	187.32	30.10	3.50*
90	2.66	16.0	0.17	183.80	47.31	3.58*
120	3.55	20.6	0.17	179.23	60.41	3.25*
150	4.43	25.9	0.17	173.55	75.17	3.15*
180	5.32	31.2	0.17	168.35	90.44	3.10*
210	6.21	36.4	0.17	162.15	104.50	3.05*
240	7.09	41.7	0.17	155.40	118.03	2.97*
270	7.98	47.0	0.17	149.18	132.27	2.94*
300	8.87	52.2	0.17	142.45	140.98	2.88*
360	10.64	B.T.	B.T.	130.54	129.07	2.65
420	12.41	-	-	118.10	116.03	2.38
480	14.19	-	-	108.78	107.51	2.19
540	15.96	-	-	99.97	98.50	2.01
660	19.51	-	-	92.20	90.75	1.85
780	23.05	-	-	82.88	81.41	1.66
960	26.60	-	-	78.74	77.27	1.58
1020	30.15	-	-	75.11	73.64	1.50
1140	33.70	-	-	72.52	71.05	1.45

TABLE I (Continued)

t sec	qt/φA cm	x cm	s <sub>w</sub>	ΔP <sub>T</sub> cm of H <sub>2</sub> O	ΔP <sub>F</sub> cm of H <sub>2</sub> O	(dP/dx) cm of H <sub>2</sub> O/cm
----------	-------------	---------	----------------	---	---	--------------------------------------

ROLL NO. 15, RUN NO. 3

0.0	0.0	0.0	0.0	19.1	19.1	1.0
60	0.44	1.5	0.29	19.4	19.4	1.0
120	0.89	3.0	0.50	19.7	19.7	1.0
180	1.33	4.4	0.63	19.9	19.9	1.0
240	1.77	5.8	0.74	19.9	19.9	1.0
300	2.06	8.2	0.74	18.4	18.4	1.0
480	3.55	11.6	0.51	17.6	17.6	1.0
600	4.45	14.4	0.51	16.6	16.6	1.0
720	5.35	17.4	0.51	15.8	15.8	1.0
900	6.05	21.7	0.51	14.5	14.5	1.0
1080	7.98	26.5	0.50	14.2	14.2	1.0
1520	9.75	31.0	0.50	14.4	14.4	1.0
1560	11.55	38.0	0.50	18.9	18.9	1.0
1860	13.74	45.2	0.50	17.0	17.0	1.0
2160	15.96	52.8	0.50	15.98	15.98	1.0
2460	18.18	6.4	1.4	30.23	38.78	0.33
2760	20.39			29.01	37.54	0.30
3060	22.61			27.97	36.37	0.34
3360	24.83			27.14	35.67	0.32

ROLL NO. 15, RUN NO. 4

0.0	0.0	0.0	0.0	170.94	170.94	1.0
30	0.89	4.9	0.18	185.89	22.08	7.92
60	1.77	9.9	0.18	185.89	40.27	5.10
90	2.66	14.9	0.18	180.04	55.68	4.11*
120	3.55	19.5	0.18	176.12	65.76	5.75*
180	5.32	29.5	0.18	164.47	87.05	5.22*
240	7.09	39.2	0.18	149.70	107.41	2.89*
300	8.87	49.2	0.18	137.68	126.98	2.69*
420	12.41	6.4	6.4	117.85	109.58	2.23
540	15.96			94.02	92.55	1.89
660	19.51			84.18	82.71	1.69
780	23.05			77.70	76.25	1.56
900	26.60			71.25	69.76	1.42
1020	30.15			67.86	66.39	1.35

TABLE F-8  
FRICTION FACTOR AND REYNOLDS NUMBER OF  
THE FLOODED ZONE

Roll No.	Run No.	$q$ $\text{cm}^3/\text{sec.}$	$S_w$	$\mu_e$ poise	$(dP/dx)$ $\frac{\text{cm. of H}_2\text{O}}{2}$	$N_{Re}$ $\times 10^5$	$f_K$ $\times 10^{-4}$
<b>Water Displacing 100 cs Dow Corning, Large Beads</b>							
8	1	1.5885	0.22	0.49	0.07	0.038	19.28
8	2	3.177	0.24	0.49	0.15	0.15	38.57
8	3	6.354	0.29	0.49	0.30	0.43	77.14
8	4	6.354	0.29	0.49	0.30	0.55	77.14
8	5	0.6354	0.25	0.49	0.03	0.02	7.71
<b>Water Displacing 100 cs Dow Corning, Small Beads</b>							
10	7	1.5885	0.16	0.49	0.60	0.60	9.69
10	8	0.6354	0.17	0.49	0.24	0.27	3.88
10	10	3.177	0.17	0.49	1.20	1.39	19.33
11	2	6.354	0.20	0.49	2.39	3.01	38.76
<b>Glycerol Solution Displacing 100 cs Dow Corning, Small Beads</b>							
12	1	1.5885	0.60	0.61	0.75	0.67	7.78
12	2	3.177	0.39	0.57	1.39	1.49	16.66
12	3	3.177	0.39	0.57	1.39	1.46	16.66
12	4	3.177	0.63	0.74	1.81	1.88	12.83
12	5	3.177	0.48	0.61	1.49	1.43	15.57
12	6	1.5885	0.59	0.61	0.75	0.62	7.78
12	7	6.354	0.39	0.61	2.98	3.01	31.14
12	8	0.6354	0.75	0.62	0.50	0.23	3.06
<b>0.05% Sep. Displacing 100 cs Dow Corning, Large Beads</b>							
10	1	6.354	0.38	0.58	0.35	0.35	65.17
10	3	1.5885	0.56	0.64	0.10	0.12	14.76
10	4	6.354	0.38	0.58	0.35	0.43	65.17
10	5	15.885	0.38	0.56	0.84	0.57	168.74
10	6	6.354	0.38	0.58	0.35	0.41	65.17
<b>0.05% Sep. Displacing 100 cs Dow Corning, Small Beads</b>							
11	4	3.177	0.38	0.56	1.57	2.16	16.96
11	5	6.354	0.34	0.55	2.69	3.99	34.53
11	6	1.5885	0.47	0.58	0.71	1.13	8.19

TABLE F-8 (Continued)

Roll No.	Run No.	$q$ $\text{cm}^3/\text{sec}$	$\bar{S}_w$	$\mu_e$ poise	(dP/dx) $\text{cm of H}_2\text{O F/cm}$	$N_{Re}$ Pred. Exp.	$f_K$ $\times 10^5$ $\times 10^{-4}$
<u>0.1% Sep. Displacing 100 cs Dow Corning, Large Beads</u>							
9	7	6.354	0.55	0.73	0.44	0.51	51.78
9	8	15.885	0.55	0.65	0.98	1.28	145.38
<u>0.1% Sep. Displacing 100 cs Dow Corning, Small Beads</u>							
11	8	6.354	0.55	0.63	3.08	5.32	30.15
11	9	3.177	0.67	0.67	1.64	3.01	14.17
<u>0.2% Sep. Displacing 100 cs Dow Corning, Large Beads</u>							
9	1	1.5885	0.84	2.07	0.31	0.77	4.56
9	2	3.177	0.84	1.57	0.47	1.01	12.04
9	3	6.354	0.79	1.23	0.74	1.38	30.73
9	4	15.885	0.72	0.93	1.40	2.76	101.61
<u>0.2% Sep. Displacing 100 cs Dow Corning, Small Beads</u>							
11	10	3.177	0.81	1.00	2.44	6.60	9.50
<u>0.2% Sep. Displacing 12500 cs Dow Corning, Large Beads</u>							
9	5	0.6354	0.11	63.57	3.83	5.57	$5.95 \times 10^2$
9	6	0.3177	0.14	64.81	1.95	2.49	$2.92 \times 10^2$
<u>0.1% Sep. Displacing 1000 cs Dow Corning, Small Beads</u>							
13	3	0.15885	0.30	5.85	0.71	0.71	$8.12 \times 10^2$
13	4	0.6354	0.18	5.38	2.63	3.34	0.35
<u>0.2% Pusher 500 Displacing 1000 cs Dow Corning, Small Beads</u>							
13	1	0.15885	0.33	5.72	0.70	0.69	$8.30 \times 10^2$
13	2	0.6354	0.17	5.41	2.64	3.13	0.35

#### F.5 Volumetric Recovery Efficiency at Breakthrough

Volumetric recovery efficiency at breakthrough was calculated either from the slope of the eye-fit lines in Figures (V-3) to (V-18) or directly from the time of breakthrough measured by a stop watch. Close agreement between the two methods is evident from Table (F-9). The data points of Figures (V-19, 20) are based on the first method.

TABLE F-9  
VOLUMETRIC RECOVERY EFFICIENCY AT BREAKTHROUGH

Roll No.	Run No.	$q^3/\text{sec}$	$\mu_0$	CP	$\mu_W$	$\mu_0/\mu_W$	$E_R, \%$ Recoverable Oil	
							from slope	from stop watch
8	1	1.5885	96	1	96	96	22	19
8	2	3.177	96	1	96	24	23	
8	3	6.354	96	1	96	29	30	
8	4	6.354	96	1	96	29	30	
8	5	0.6354	96	1	96	25	25	
8	6	3.4	96	0.01	100			
9	1	1.5885	96	0.23	84	83		
9	2	3.177	96	0.34	84	80		
9	3	6.354	96	0.49	79	78		
9	4	15.885	96	117	0.82	72	67	
9	5	0.6354	12187.50	688	17.71	11	12	
9	6	0.3177	12187.50	1007	12.10	14	15	
9	7	6.354	96	59	1.63	55	55	
9	8	15.885	96	40	2.40	55	51	
10	1	6.354	96	22	4.56	58	55	
10	3	1.5885	96	55	2.74	50	58	
10	4	6.354	96	22	4.56	38	39	
10	5	15.885	96	17	5.65	38	39	
10	6	6.354	96	22	4.56	58	58	
10	7	1.5885	96	1	16	15	16	
10	8	0.6354	96	1	17	16	16	

TABLE F-9 (Continued)

Run No.	Run No.	$\frac{d^3}{dt^3}$ cm/sec	$\frac{\mu_w}{\eta_p}$	$\frac{\mu_0}{\mu_w}$	$E_R \%$ Recoverable Oil	
					from slope	from stop watch
10	9	0.3177	96	1	96	17
10	10	3.177	96	1	96	18
11	1	0.15885	96	1	96	25
11	2	6.354	96	1	96	19
11	3	1.5885	96	1	96	16
11	4	3.177	96	18	5.33	17
11	5	6.354	96	14	6.86	34
11	6	1.5885	96	22	4.36	45
11	7	15.885	96	10	9.6	32
11	8	6.354	96	34	2.82	55
11	9	3.177	96	45	2.15	67
11	10	3.177	96	136	0.71	84
12	1	1.5885	96	26	3.69	60
12	2	3.177	96	17	5.65	39
12	3	3.177	96	17	5.65	39
12	4	3.177	96	52	1.85	63
12	5	3.177	96	25	3.84	48
12	6	1.5885	96	25	3.84	49
12	7	6.354	96	25	5.84	59
12	8	0.6354	96	28.5	3.37	75
13	1	0.15885	971	195	5.03	33
13	2	0.6354	971	124	7.85	17
13	3	0.15885	971	244	5.98	28
13	4	0.6354	971	127	7.65	18

In Figure IV-19, in addition to the experimental data of the present study, the data points of other investigators available in the literature are also included. These data points and the pertinent experimental conditions involved are briefly discussed below.

Verett, et al. (1954) studied the effect of viscosity ratio on displacement recovery for miscible as well as immiscible fluid injection. The waterflood experiments were performed on a linear system made of cemented silica sand grains having diameters between 65 and 170 microns. The permeability to air of the various linear portions was reported to be 2.77, 2.44, 2.54, and 2.00 darcies.<sup>13</sup> The average porosity of the system was 25.2 percent with a total pore volume of 980 cm<sup>3</sup>. The overall column was 115.8 cm long and 6.55 cm inside diameter. The oils used were standard grade lubricating oils. By varying the type of oil and the temperature during displacement the desired ratios of oil viscosity to water viscosity were obtained. The displacing liquid was always water.

All of the waterflood displacement tests were performed under a constant pressure drop of 20 psia. The data points reported in Table IV-19 are taken directly from the Table II of their paper.

TABLE F-10  
 BREAKTHROUGH RECOVERY VS. VISCOSITY  
 RATIO OBTAINED FROM TABLE II OF  
 EVERETT, et.al. (69)

$\mu_o/\mu_w$	$E_R (\%)$
1.04	81.6
2.41	56.1
3.51	41.8
15.49	41.8
48.53	34.5
98.6	29.0

2. Engelberts and Klinkenberg (2) studied the displacement of oil by water from a porous formation consisting of grains of sand between 20 and 30 mesh with a permeability of 200 darcies at a porosity of 38%. Kerosene and various white oils were employed together with sec. butyl alcohol or, for the more viscous oils, methyl ethyl ketone, to simulate the oil phase. Distilled water saturated with alcohol or ketone represented the water phase. In Figure 5 of their paper, they plotted the breakthrough recovery versus a dimensionless group  $\Delta gK/U_{\mu_w}$  for three different viscosity ratios. This dimensionless group which was obtained from dimensional analysis is the ratio of the hydrostatic pressure gradient,  $\Delta g$ , to the flow potential gradient  $U_{\mu_w}/K$  in the water phase. The breakthrough recovery efficiency at  $\Delta gK/U_{\mu_w} = 0$  was read off from their Figure 5 which corresponds to the absence of any gravity effect in the present study.

TABLE F-11  
 BREAKTHROUGH RECOVERY VS. VISCOSITY  
 RATIO OBTAINED FROM FIGURE 5 OF  
 ENGELBERTS, et al. (2)

$\mu_o/\mu_w$	R (%)
1	83
4	49
24	28

3. Jones-Parra, et al. (70) studied constant rate displacements in water wet systems. The porous matrices used were constructed from 2.5 inches inside diameter lucite tubes packed with unconsolidated glass beads. The packed tubes were of three different lengths, 19.0, 25.4 and 38 cm. The beads, of 140 - 170 mesh size were almost perfectly spherical. The permeability of the cores were reported to be approximately 7 darcies and porosity 35.5%. The displacing liquids were sodium chloride solutions blended with varying amounts of glycerol to produce different viscosities. The displaced-phase liquids were made up of inert water-white petroleum derivatives together with sufficient carbon tetra-chloride to adjust the liquid specific gravities to unity. Their results for floods performed on the core of 25.4 cm. length with unfavourable viscosity ratio are reproduced in Table F-12.

TABLE F-12  
 BREAKTHROUGH RECOVERY EFFICIENCY  
 OBTAINED FROM TABLE III OF  
 JONES-PARRA, et. al. (70)

$U$ cm/min	$\mu_o$ cp	$\mu_w$ cp	$\mu_o/\mu_w$	$E_R$ (%)
0.412	3.25	0.92	3.53	59.5
0.271	3.25	0.92	3.53	58.4
0.098	3.25	0.92	3.53	63.9
0.030	3.25	0.92	3.53	74.1
0.545	3.25	0.92	3.53	60.5
0.598	1.85	0.92	2.01	75.8
0.294	1.85	0.92	2.01	77.1
0.151	1.85	0.92	2.01	64.6
0.071	1.85	0.92	2.01	68.7
0.075	1.85	0.92	2.01	66.0
0.043	1.85	0.92	2.01	61.2
0.573	2.4	0.92	2.61	77.7
0.280	2.4	0.92	2.61	82.5
0.196	2.4	0.92	2.61	74.8
0.129	2.4	0.92	2.61	68.7
0.063	2.4	0.92	2.61	83.9
0.007	2.4	0.92	2.61	55.3
0.069	2.4	0.92	2.61	68.2
0.161	2.4	0.92	2.61	77.8
0.153	2.4	0.92	2.61	77.4
0.473	5.2	0.92	5.65	49.2
0.259	5.2	0.92	5.65	53.1
0.188	5.2	0.92	5.65	50.3
0.126	5.2	0.92	5.65	62.6
0.059	5.2	0.92	5.65	64.0
0.029	5.2	0.92	5.65	63.0
0.129	5.2	0.92	5.65	56.5
0.003	5.2	0.92	5.65	59.5
0.745	5.2	0.92	5.65	47.7

4. Croes and Schwarz (51) reported results in graphical form of a series of experiments carried out for measuring the efficiency of the water-drive process affected by the oil/water viscosity ratio. The model used in the experiments was a tube of 1 m length and 6.2 cm diameter, filled with unconsolidated sand. The sand was 20-30 mesh having a permeability of  $2 \times 10^5$  md and a porosity of 33 percent. The displacing phase was water and the displaced phase an SAE 30 lubricating oil blended with Kerosene to obtain the different viscosity ratios. The residual oil saturation was reported to be 15%. In this study they plotted the viscosity ratio vs. cumulative oil production as % of oil in place  $R_p$ , for various values of gross production including breakthrough recovery. The data points presented in Table F-13 were read off this graph and corrected for the residual oil saturation by dividing  $R_p$  by 0.85 - Refer to Appendix D.

TABLE F-13.  
 BREAKTHROUGH RECOVERY vs. VISCOSITY  
 RATIO OBTAINED FROM FIGURE 2 OF  
 CROES, et al. (51)

$\mu_o/\mu_w$	R <sub>P</sub> % of oil in place	E <sub>R</sub> % of Recoverable Oil
1.5	75	88.2
4.2	59	69.4
10	42	49.4
10	41	48.2
20	28	32.9
38	22	25.9
38	16	18.8
48	20	23.5
64	20	23.5
64	19	22.5
100	15	17.6
100	12	14
140	12	14
160	9	10.6
230	12	14
230	11	13
340	15	17.6
340	14	16.5
340	10	11.8

### F.6 Saturation Profiles

Saturation profiles were determined by the method of light scanning which was discussed in Section (IV-5). The difficulties involved and the error introduced during the course of converting the scanning readings into the saturation data are thoroughly analyzed in Appendix G.3. The data points of Figures (V-21) to (V-37) are presented in Tables (F-14, 15).

The net number of counts obtained from scanning of line  $i$  is presented as  $C_{N,i}$  and the water saturation of the plane corresponding to that line is taken as  $S_{w,i}$ . Assuming linear dependency of  $C_N$  and  $S_w$ , one can write,

$$S_{w,i} = K_{C,i} C_{N,i} \quad (F-1)$$

where  $K_{C,i}$  is the conversion factor. Since the displacement tests were not performed originally for the purpose of the saturation measurement, (the amount of the light and colour was not controlled) precalibration of the scanning instrument for water saturation was not possible. This means that the value of  $K_{C,i}$  was not known in advance and it was necessary to use material balance information to determine the  $K_{C,i}$  indirectly.

The area under the curve of  $S_w$  v.s.  $x$  at or before breakthrough is related to the cumulative volume of water injected by,

$$qt = A\phi \int_0^L S_w dx \quad (F-2)$$

or writing in difference form,

$$\frac{qt}{A\phi} = \sum_{i=1}^n S_{w,i} \Delta x_i \quad (F-3)$$

where  $\Delta x_i$  means  $(x_{i+1} - x_i)$ ,  $i = 1$  corresponds to the beginning of the bed and  $i = n$  the position of zero saturation plane. Substituting (E-1) into (E-3) and assuming  $K_{C,i}$  constant for all saturation levels and/or positions, the following expression is obtained for the conversion factor  $K_{C,i} = k_C$ .

$$k_C = \frac{q_t}{A} \left( \sum_{i=1}^n C_{N,i} - \Delta x_1 \right) \quad (E-4)$$

From Equations (E-1) and (E-4) it is concluded that,

$$k_{w,i} = \frac{q_t}{A} \frac{C_{N,i}}{\sum_{i=1}^n C_{N,i} - \Delta x_1} \quad (E-5)$$

The influence of the vertical bar on  $C_{N,i}$  for the case of more uniformly swept frames was significant and the procedure to correct this influence is given in Appendix G.5. These data points belong to Figures V-31 to V-37 which are presented in Table (E-15). Table (E-14) includes the data points of Figures V-21 to V-30 in which the effect of the vertical bar was insignificant so that no correction need to be considered.

TABLE I-11  
WATER SATURATION DISTRIBUTION FROM  
FILM SCANNING - EFFECT OF VERTICAL  
PAR IN SIGNIFICANT

$x_i$ , cm.	$\Delta x_i$ , cm.	$C_{N,i}$	$w_i$ , %
Roll No. 8, Run No. 1, $qt/\lambda = 10.71 \text{ cm}^2$			
2.05	2.05	3680	57.25
3.32	1.27	3740	58.16
4.60	1.28	3920	45.41
5.87	2.55	2620	40.73
9.69	2.55	2610	40.59
10.97	1.28	2880	44.79
12.24	1.27	2420	37.64
13.51	1.27	2270	35.30
14.79	1.28	2150	33.44
16.06	1.27	2220	34.52
18.61	2.55	1720	26.75
21.16	2.55	1820	28.30
23.70	2.54	1280	19.91
26.25	3.83	1180	18.35
31.35	3.82	1040	16.17
33.90	2.55	370	5.75
36.44	2.54	330	5.13
38.99	2.55	170	2.64
41.54	2.55	240	5.73
45.56	3.82	180	2.80
$\sum C_{N,i} \Delta x_i = 68867.20$			

Roll No. 8, Run No. 5,  $qt/\lambda = 15.65 \text{ cm}^2$

2.94	2.94	4080	54.62
4.22	1.28	5960	53.02
5.49	1.27	4060	54.35
6.13	0.64	5920	52.48
9.31	5.18	5840	51.41
10.58	1.27	5570	47.49
11.86	1.28	5350	44.85
13.67	1.27	5840	51.41
14.41	1.28	4800	54.89
15.68	1.27	5880	51.94

TABLE E-14 (Continued)

$x, \text{ cm}$	$\Delta x_i, \text{ cm}$	$C_{N,i}$	$S_{w,i} (\%)$
16.95	1.27	3890	52.08
19.50	2.55	3630	48.60
22.05	2.55	3440	46.05
24.60	2.55	2810	37.62
25.87	1.27	2360	31.60
27.14	1.27	2270	30.39
29.69	2.55	2160	28.92
30.97	1.28	1930	25.84
32.24	1.27	1690	22.63
34.79	2.55	1090	14.59
37.33	2.54	800	10.71
39.88	2.55	520	6.97
41.16	1.28	630	8.43
42.43	1.27	660	8.84
44.98	2.55	160	2.14
46.25	1.27	310	4.15
47.52	1.27	230	3.08
50.07	2.55	360	4.82

$$\sum C_{N,i} \Delta x_i = 116747.50$$

Roll No. 8, Run No. 5,  $\text{qt}/\#A = 13.11 \text{ cm}$

2.91	2.91	4910	59.23
4.20	1.29	4710	56.81
5.48	1.28	4400	53.07
8.04	2.56	4340	52.35
9.32	1.28	4800	57.90
10.60	1.28	3890	46.92
11.89	1.29	4320	52.11
13.17	1.28	3880	46.80
14.45	1.28	4050	48.85
15.73	1.28	4230	51.02
18.29	2.56	2900	34.98
20.86	2.57	3110	37.51
23.42	2.56	2280	27.50
25.98	2.56	1930	23.28
27.26	2.57	1440	17.37
31.11	2.57	930	11.22
32.39	1.28	720	8.68
34.95	2.56	660	7.96
37.51	2.56	300	3.62
40.08	2.57	200	2.41
42.64	2.56	180	2.17

TABLE F-14 (Continued)

213

$x, \text{ cm}$	$\Delta x_i, \text{ cm}$	$C_{N,i}$	$S_{w,i} (\%)$
45.20	2.56	390	4.70
46.48	1.28	380	4.38
47.77	1.29	470	5.07
50.33	2.56	230	2.77
$\sum C_{N,i} \Delta x_i = 108686.50$			
Roll No. 9, Run No. 5, qt/ $\phi\Lambda = 5.95 \text{ cm}$			
2.86	2.86	2840	30.55
4.06	1.30	2530	27.22
5.45	1.29	2490	26.79
6.75	1.30	2250	24.20
9.35	2.60	1860	20.01
10.64	1.29	1760	18.95
11.94	1.30	1750	18.82
13.24	1.30	1890	20.35
14.53	1.29	1430	15.76
15.83	1.30	1490	16.05
18.42	2.59	1060	11.40
21.02	2.60	970	10.43
23.61	2.59	910	9.79
26.21	2.60	580	6.24
27.50	2.59	540	5.81
31.39	2.59	990	10.65
33.99	2.60	720	7.75
36.58	2.59	570	6.13
39.18	2.60	590	6.55
41.77	3.89	570	5.98
46.96	3.89	420	4.82
49.55	2.59	280	3.01
52.15	2.60	70	0.75
$\sum C_{N,i} \Delta x_i = 55126.20$			
Roll No. 9, Run No. 6, qt/ $\phi\Lambda = 6.82 \text{ cm}$			
1.76	1.76	5780	58.44
5.04	1.28	3246	50.09
4.32	1.28	2380	56.80
5.61	1.29	2150	53.24
9.45	3.84	1640	25.36
10.73	1.28	1700	26.28
12.01	1.28	1530	23.96

TABLE F-14 (Continued)

214

$x$ , cm	$\Delta x_i$ , cm	$C_{N,i}$	$S_{w,i} (\%)$
13.29	1.28	1440	22.26
14.58	1.29	1460	22.37
15.86	1.28	1470	22.73
17.14	1.28	1280	19.79
19.70	2.56	1230	19.02
22.26	2.56	1010	15.62
24.83	2.57	780	12.06
26.11	1.28	750	11.60
27.59	1.28	750	11.60
29.95	2.56	80	1.24
31.23	1.28	0.0	0.0
32.52	1.29	90	1.39
35.08	2.56	60	-0.93
37.64	2.56	40	0.62
40.20	2.56	70	-1.08
41.49	1.29	30	0.46
$\sum C_{N,i} \Delta x_i = 44113.30$			
Roll No. 10, Run No. 7, qt/ $\#A = 7.71$ cm			
2.51	2.51	2880	71.67
3.73	1.22	2670	66.45
4.95	1.22	2460	61.22
6.18	1.23	1950	48.53
8.62	2.44	1780	44.30
9.85	1.23	1060	26.38
11.07	1.22	920	22.90
12.29	1.22	760	18.91
13.51	1.22	790	19.66
14.74	1.23	760	18.91
15.96	1.22	920	22.90
18.41	2.45	390	9.71
20.85	2.44	550	13.69
23.30	2.45	160	3.98
25.74	2.44	170	4.23
26.97	1.23	80	1.99
30.63	3.66	150	3.24
31.86	1.23	160	3.98
33.08	1.22	190	4.73
35.55	2.45	110	2.74
$\sum C_{N,i} \Delta x_i = 30980.10$			

TABLE F-14 (Continued)

215

$x, \text{ cm}$	$\Delta x_i, \text{ cm}$	$C_{N,i}$	$S_{w,i} (\%)$
Roll No. 11, Run No. 1, $\text{qt}/\phi A = 12.57 \text{ cm}$			
2.86	2.86	3945	64.01
4.16	1.30	3935	63.85
5.45	1.29	3445	55.90
6.75	1.30	2935	47.62
8.05	1.30	2540	41.21
9.35	1.30	2430	39.43
10.64	1.29	2485	40.32
11.94	1.30	2515	40.81
13.24	1.30	2120	34.40
14.53	1.29	2345	38.05
17.13	2.60	2410	39.10
19.72	2.59	2310	37.48
22.32	2.60	2205	55.78
24.91	2.59	1455	23.61
26.21	1.30	1350	21.90
30.10	3.89	1055	17.12
31.39	1.29	885	14.36
32.69	1.30	1055	17.12
35.28	2.59	1020	16.55
37.88	2.60	385	6.25
40.47	2.59	75	1.22
41.77	1.30	140	2.27
43.07	1.30	35	0.57
$C_{N,i} \Delta x_i = 77470.95$			
Roll No. 11, Run No. 2, $\text{qt}/\phi A = 9.45 \text{ cm}$			
1.11	1.11	4275	44.74
2.36	1.25	3900	40.82
3.62	1.26	3765	39.40
4.88	1.26	3515	36.79
6.14	1.26	3570	37.36
8.66	2.52	3510	34.64
9.92	1.26	3245	33.96
11.18	1.26	3150	32.97
12.44	1.26	3050	31.92
14.95	2.51	2755	28.83
17.47	2.52	2455	25.69
19.99	2.52	2615	27.37
22.51	2.52	2045	21.40
25.02	2.51	1895	19.83

TABLE E-14 (Continued)

216

$x$ , cm.	$\Delta x_i$ , cm.	$C_{N,i}$	$S_{w,i} (\%)$
26.28	1.26	1765	18.47
27.54	1.26	1750	18.32
30.06	2.52	1655	17.32
31.32	1.26	1560	16.33
32.58	1.26	1420	14.86
35.09	2.51	1070	11.20
37.61	2.52	540	5.65
40.13	2.52	200	2.09
41.39	1.26	50	0.52
$\sum C_{N,i} \Delta x_i = 90102.25$			
Roll No. 11, Run No. 3, qt/ $\phi A$ = 8.44 cm			
2.99	2.99	3820	51.04
5.51	2.52	3755	50.17
9.29	3.78	1885	25.19
10.55	1.26	1920	25.65
13.06	2.51	1485	19.84
15.58	2.52	1440	19.24
18.10	2.52	1605	21.44
20.62	2.52	1555	20.78
23.14	2.52	1350	18.04
25.65	2.51	1010	13.49
26.91	1.26	895	11.96
30.69	3.78	950	12.69
31.95	1.26	605	8.08
33.21	1.26	600	8.02
35.72	2.51	610	8.15
38.24	2.52	605	8.08
40.76	2.52	450	6.01
42.02	1.26	340	4.54
47.05	5.03	115	1.54
48.31	1.26	40	0.53
50.83	2.52	0.0	0.0
$\sum C_{N,i} \Delta x_i = 63169.30$			
Roll No. 13, Run No. 2, qt/ $\phi A$ = 8.47			
2.40	2.40	3360	63.91
5.68	1.28	3060	58.21
4.97	1.29	2860	54.40
6.25	1.28	2580	49.08

TABLE F-14 (Continued)

$x, \text{ cm}$	$\Delta x_i, \text{ cm}$	$C_{N,i}$	$S_{w,i} (\%)$
8.81	2.56	2020	38.42
10.09	1.28	1790	34.05
11.37	1.28	1570	29.86
13.94	2.57	1270	24.16
16.50	2.56	960	18.26
19.06	2.56	790	15.03
21.62	2.56	770	14.65
24.19	2.57	280	5.35
26.75	2.56	510	9.70
30.59	3.84	380	7.23
31.88	1.29	300	5.71
34.44	2.56	210	3.99
37.00	2.56	240	4.57
39.56	2.56	160	3.04
42.13	2.57	140	2.66
45.97	3.84	110	2.09
47.25	1.28	80	1.52
49.82	2.57	20	0.38
$\sum C_{N,i} \Delta x_i = 44528.70$			
Roll No. 13, Run No. 4, qt/ $\phi A = 8.47 \text{ cm}$			
2.40	2.40	3850	52.89
3.68	1.28	3320	45.61
4.97	1.29	3130	43.00
6.25	1.28	2710	37.23
8.81	2.56	2170	29.81
11.37	2.56	1710	23.49
13.94	2.57	1560	21.43
16.50	2.56	1400	19.23
19.06	2.56	1200	16.49
21.62	2.56	1000	13.74
24.19	2.57	900	12.56
26.75	2.56	920	12.64
30.59	3.84	870	11.95
31.88	1.29	760	10.44
34.44	2.56	700	9.62
37.00	2.56	610	8.38
39.56	2.56	510	7.01
42.13	2.57	440	6.05
45.97	3.84	350	4.81
47.25	1.28	370	5.08
49.82	2.57	350	4.81
$\sum C_{N,i} \Delta x_i = 61650.60$			

TABLE F-15  
WATER SATURATION DISTRIBUTION FROM  
FILM SCANNING - EFFECT OF VERTICAL  
BAR SIGNIFICANT

$x$ , cm	$\Delta x_i$ , cm	$C_{N,i}$	$S_{w,i} (\%)$	Corrected $C_{N,i}$	Corrected $S_{w,i} (\%)$
Roll No. 10, Run No. 1, qt/ $\phi A$ = 18.26 cm					
2.76	2.76	4460	61.93	5575	68.27
4.05	1.29	4830	67.06	6037	73.93
5.34	1.29	4780	66.37	5975	73.17
9.20	3.86	4490	62.34	5478	67.08
10.49	1.29	4450	61.79	5284	64.71
13.07	2.58	4570	63.45	5255	64.35
15.65	2.58	4250	59.01	4760	58.29
18.23	2.58	3880	53.87	4258	52.14
20.81	2.58	3990	55.40	4299	52.65
23.39	2.58	3480	48.32	3706	45.38
25.96	2.57	3240	44.99	3410	41.76
27.25	1.29	2600	36.10	2723	33.35
29.83	2.58	2090	29.02	2168	26.55
31.12	1.29	1890	26.24	1951	23.89
33.70	2.58	1810	25.13	1855	22.72
36.28	2.58	1290	17.91	1316	16.12
38.86	2.58	810	11.25	820	10.04
41.43	2.57	570	7.91	573	7.02
42.72	1.29	280	3.89	281	3.44
46.59	3.87	90	1.25	90	1.10
49.17	2.58	-30	-0.42	-30	-0.37
$\sum C_{N,i} \Delta x_i = 131512.90$		$\sum C_{N,i} \Delta x_i = 149110.54$			

Roll No. 10, Run No. 5, qt/ $\phi A$  = 19.38 cm

2.53	2.53	4830	64.71	6037	70.41
3.81	1.28	5090	68.19	6362	74.20
5.09	1.28	5340	71.54	6675	77.85
6.37	1.28	5410	72.48	6762	78.86
8.94	2.57	5140	68.86	6386	74.48
10.22	1.28	5070	67.92	6147	71.69
11.50	1.28	4950	66.31	5866	68.41
12.78	1.28	5290	70.87	6163	71.88
15.34	2.56	5190	69.53	5878	68.55
17.91	2.57	4920	65.91	5461	63.69

TABLE F-15 (Continued)

x, cm	$\Delta x_i$ , cm	$C_{N,i}$	$S_{w,i}$ (%)	Corrected $C_{N,i}$	Corrected $S_{w,i}$ (%)
20.47	2.56	4970	66.58	5417	63.18
23.03	2.56	4370	58.54	4698	54.79
25.60	2.57	3750	50.24	3975	46.36
26.88	1.28	3100	41.53	3270	38.14
30.72	3.84	2520	33.76	2621	30.57
32.00	1.28	1970	26.39	2039	23.78
33.29	1.29	1530	20.50	1580	18.43
35.85	2.56	610	8.17	625	7.29
38.41	2.56	160	2.14	163	1.90
40.97	2.56	90	-1.21	89	-1.04
$\sum C_{N,i} \Delta x_i = 144661.30$		$\sum C_{N,i} \Delta x_i = 166174.03$			

Roll No. 11, Run No. 4, qt/ $\phi A$  = 19.21 cm

3.27	3.27	4850	53.42	6062	59.70
4.56	1.29	4920	54.20	6150	60.57
5.85	1.29	4880	53.75	6100	60.08
8.43	2.58	4700	51.77	5769	56.82
9.72	1.29	4980	54.86	5964	58.74
11.01	1.29	4920	54.20	5769	56.82
12.30	1.29	4950	54.53	5717	56.30
13.59	1.29	4730	52.10	5392	53.10
16.17	2.58	4720	51.99	5275	51.95
18.74	2.57	4560	50.23	5016	49.40
21.32	2.58	4450	49.02	4806	47.33
23.90	2.58	4300	47.37	4612	45.42
26.48	2.58	4110	45.27	4357	42.90
30.55	3.87	3550	39.10	3719	36.63
31.64	1.29	3510	38.66	3659	36.04
43.21	2.57	3520	38.77	3643	35.88
36.79	2.58	3010	33.16	3093	30.46
39.37	2.58	2260	24.89	2311	22.76
41.95	2.58	1820	20.05	1847	18.10
45.82	3.87	930	10.24	937	9.23
47.11	1.29	630	6.94	633	6.23
49.68	2.57	300	3.30	300	2.95
52.26	2.58	250	2.75	250	2.46

 $\sum C_{N,i} \Delta x_i = 174394.10$  $\sum C_{N,i} \Delta x_i = 195057.05$ Roll No. 11, Run No. 7, qt/ $\phi A$  = 16.54 cm

3.56	3.56	5380	56.98	6725	64.04
4.84	1.28	5540	58.68	6897	65.68
6.12	1.28	5300	56.13	6413	61.07

TABLE F-15 (Continued)

$x$ , cm	$\Delta x_i$ , cm	$C_{N,i}$	$S_{w,i} (\%)$	Corrected $C_{N,i}$	Corrected $S_{w,i} (\%)$
8.68	2.56	5380	56.98	6200	59.04
9.96	1.28	5080	53.80	5778	55.02
11.24	1.28	4780	50.63	5389	51.52
13.81	2.57	4480	47.45	4950	47.14
16.37	2.56	4400	46.60	4796	45.67
18.93	2.56	4100	43.42	4418	42.07
21.50	2.57	3950	41.84	4217	40.16
24.06	2.56	3610	38.23	3818	36.36
26.62	2.56	3550	37.60	3727	35.49
27.90	1.28	2910	30.82	3048	29.03
30.47	2.57	2810	29.76	2922	27.83
31.75	1.28	2650	28.07	2749	26.18
34.31	2.56	2440	25.84	2519	23.99
36.87	2.56	2070	21.92	2122	20.21
39.44	2.57	1610	17.05	1646	15.67
42.00	2.56	1030	10.91	1048	9.98
43.28	1.28	410	4.34	416	3.96
45.84	2.56	520	5.51	526	5.01
47.12	1.28	370	3.92	374	3.56
49.69	2.57	0.0	0.0	0.0	0.00
$\sum C_{N,i} \Delta x_i = 156164.50$		$\sum C_{N,i} / \Delta x_i = 173687.31$			

Roll No. 12, Run No. 5, qt/ $\phi A = 24.35$  cm

3.17	3.17	3860	52.75	4825	57.57
4.45	1.28	4520	61.77	5650	67.41
5.73	1.28	4450	60.82	5562	66.36
8.30	2.57	4870	66.56	6087	72.62
9.58	1.28	4870	66.56	6087	72.62
10.86	1.28	4770	65.19	5962	71.15
13.42	2.56	4850	66.29	5929	70.74
15.99	2.57	4720	64.51	5617	67.02
18.55	2.56	4700	64.24	5452	65.05
21.11	2.56	4690	64.10	5347	63.79
23.67	2.56	4550	62.18	5085	60.67
26.24	2.57	4440	60.68	4873	58.14
27.52	1.28	4500	61.50	4894	58.39
30.08	2.56	3850	52.62	4129	49.26
31.36	1.28	3770	51.52	4006	47.79
33.93	2.57	3940	53.85	4157	49.36
36.49	2.56	3620	49.47	3756	44.81

TABLE F-15 (Continued)

$x, \text{ cm}$	$\Delta x_i, \text{ cm}$	$C_{N,i}$	$S_{w,i} (\%)$	Corrected $C_{N,i}$	Corrected $S_{w,i} (\%)$
39.05	2.56	2820	38.54	2890	34.48
41.61	2.56	1940	26.51	1964	23.43
42.90	1.29	1570	21.46	1582	18.87
45.46	2.56	1170	15.99	1170	13.96
46.74	1.28	710	9.70	710	8.47
49.30	2.56	0.0	0.00	0.0	0.00
$\sum C_{N,i} \Delta x_i = 178166.00$				$\sum C_{N,i} \Delta x_i = 204094.21$	
Roll No. 12, Run No. 6, qt/ftA = 30.47 cm					
3.43	3.43	4640	62.54	5800	67.29
4.71	1.28	4900	66.04	6125	71.06
5.99	1.28	4820	64.96	6025	69.90
8.55	2.56	4970	66.98	6212	72.07
9.83	1.28	5340	71.97	6675	77.44
12.40	2.57	5500	74.13	6875	79.76
14.96	2.56	5360	72.24	6673	77.41
17.52	2.56	5330	71.84	6476	75.13
20.09	2.57	5400	72.78	6426	74.55
22.65	2.56	5440	73.32	6351	73.68
25.21	2.56	5320	71.70	6105	70.82
26.49	1.28	5200	70.08	5915	68.62
27.77	1.28	5130	69.14	5784	67.10
30.34	2.57	5420	73.05	6030	69.95
31.62	1.28	4430	59.71	4895	56.79
32.90	1.28	4600	62.00	5048	58.56
35.46	2.56	4710	63.48	5099	59.15
38.03	2.57	4560	61.46	4879	56.60
40.59	2.56	4190	56.47	4431	51.40
41.87	1.28	3950	53.24	4147	48.11
43.15	1.28	3870	52.16	4054	47.03
45.71	2.56	2630	55.45	2722	51.58
47.00	1.29	2310	31.13	2379	27.60
49.56	2.56	900	12.13	920	10.67
$\sum C_{N,i} \Delta x_i = 226079.90$				$\sum C_{N,i} \Delta x_i = 262649.49$	
Roll No. 12, Run No. 7, qt/ftA = 20.97 cm					
3.04	3.04	3940	51.82	4925	57.15
4.52	1.28	4280	56.30	5350	62.09
5.61	1.29	4250	55.90	5312	61.65
9.45	3.84	4640	61.03	5800	67.31

TABLE F-15 (Continued)

$x, \text{ cm}$	$\Delta x_i, \text{ cm}$	$C_{N,i}$	$S_{w,i} (\%)$	Corrected $C_{N,i}$	Corrected $S_{w,i} (\%)$
10.73	1.28	4660	61.30	5755	66.79
13.29	2.56	4710	61.95	5640	65.45
15.86	2.57	4520	59.45	5243	60.84
18.42	2.56	4470	58.80	5051	58.62
20.98	2.56	4460	58.66	4962	57.58
23.55	2.56	4230	55.64	4600	53.58
26.11	2.56	4060	53.40	4344	50.41
27.39	1.28	4050	53.27	4293	49.82
31.23	3.84	3330	43.80	3447	40.00
33.80	2.57	3220	42.35	3292	38.20
36.36	2.56	2800	36.83	2821	32.74
38.92	2.56	2160	28.41	2160	25.07
41.49	2.57	1260	16.57	1260	14.62
42.77	1.28	700	9.21	700	8.12
45.33	2.56	540	7.10	540	6.27
46.61	1.28	380	5.00	380	4.41
49.17	2.56	0.0	0.00	0.0	0.00

$$\sum C_{N,i} \Delta x_i = 159425.30$$

$$\sum C_{N,i} \Delta x_i = 180700.03$$

## APPENDIX G

### ERROR ANALYSIS

In this Appendix the major sources of error will be pointed out and discussed briefly. Since the scope of the present study is not to correlate the experimental data, it is not intended to perform an analytical study of error propagation to achieve the variance and distribution of random error.

#### G.1 Pressure Drop Data

The error in the pressure drop data of the single phase flow is dependent on the transducer and flow rate measurements. The transducers and the pumps were calibrated in advance. To eliminate the possible error due to the head of fluid the transducers were always placed at a level below the lowest pressure tap so that an equal head was always applied on both sides of the transducer.

Some approximations are involved in measurement and calculation of the pressure drop and pressure gradient of the mixed zone for the displacement tests. There exists a small difference in specific gravity of the displacing and displaced fluids. For example in the case of water flood the difference in specific gravity was 0.04. Therefore, a change in fluid head is being created by advancing the front plane. This has been calculated and subtracted from the total pressure drop reading to obtain the pressure drop of the flooded zone reported in Table (F-7).

The pressure gradient of the mixed zone may be in error because of uncertainty in determining the exact length of the mixed zone. The length of the mixed zone is approximated as the length of the flooded zone,  $x_0$ .

The actual length of the mixed zone will be somewhat less than  $x_0$  if the plane of  $S_w = 1.0$  progress significantly past the inlet screen. Figures (V-21) to (V-37), however, show that the latter is not the case even for the moderate viscosity ratio; therefore, the error due to this problem cannot be significant.

The location of the first pressure tap introduces a different kind of error. The first pressure tap is located approximately two centimeters above the inlet screen; therefore, the first two centimeters of the flooded zone are being excluded from the pressure drop measurement. The error contribution of this segment is larger at the beginning of the displacement, and as the frontal plane proceeds its effect diminishes. To minimize this effect, the initial pressure history of the displacement is not being considered in calculating the pressure gradient of the flooded zone. In fact the pressure drop reading is taken from the time that the frontal plane has proceeded at least 10. cm. into the bed.

#### G.2 Frontal Plane Advance and Breakthrough Recovery

The data points in Figures (V-3) to (V-18) show some scattering. From the procedure described in Appendix F.2, it is clear that any measurement errors are small in comparison with the scatter. The scatter is attributable to the local non-homogeneity of the bed and also the random appearance of the fingers. For example a finger may be created due to the local non-homogeneity but does not necessarily grow and become prominent finger, or a prominent finger may stop growing and some other new finger may take over. This creates a statistical kind of scatter in instantaneous measurements of frontal advance rate.

Breakthrough recovery was determined by the slope of the curve fit of Figures (V-3) to (V-18) as well as from the breakthrough time measured by the stop watch. Close agreement was always obtained. Refer to Table (I-9).

### G. 3. Saturat<sup>o</sup>n Profile

It is useful to recall that saturation profiles presented in Figs. (V-21) to (V-37) were determined by scanning individual frames of the film. The procedure of constructing saturation profiles from the scanning data is given in Appendix (I-6). As described in section (IV-3), the measurement of diffused light along a scanning line was performed on a comparative basis with two frames of the movie film from each run; one before the displacement, when the bed was full of the oil, and the other at breakthrough. The concentration profile could be influenced by the steel bars appearing on the photographs and by uncertainty in matching position on the frames.

In section (IV-1.2), it was mentioned that there existed four steel bars on each side of the bed, three positioned laterally and one vertically along the bed. The bars appeared as bright lines on the photographs. These bright areas on the photographs gave minimum microdensitometer readings and so the lateral lines could be easily located by doing a rapid vertical scan and noting where minimum counts occurred. Position of the bar was then determined from reading of the position micrometer on the film carriage. After the positions of these lines were determined, the equivalent positions on the two frames were chosen.

Scanning was generally performed at 0.5 to 1 mm intervals. At the positions of the lateral bars the intervals were increased to approximately 5 mm so that any effect of the lateral bars could be eliminated.

Some error is introduced due to the fact that near to the bars the reference frame does not diffuse the same amount of light along different scanning lines. This situation arises because of the shadow and reflection of the steel bars. This error could be avoided if exact match of equivalent positions of the two frames were possible. An estimate based on an uncertainty of 0.5 mm in position showed that the error could be as large as 10% at positions very close to the bars. Actual error from this source is probably very much less than this.

Although the laterally positioned steel bars were excluded in scanning, the vertical bar could not be eliminated from the scanning. Since the bar always appears the same on both reference and frames after flooding, the instrument would always indicate a zero saturation at the position of the vertical bar. This effect is insignificant for several fingerings because the chance of hiding a finger under the bar in this case is small, and in fact, more or less random.

For moderate viscosity ratios, for which the bed is being swept more uniformly, some portion of the displacing fluid is always hidden under the bar. For a given scanning line the error in counts attributable to the vertical bar could be as large as 25% of the true counts, depending on the concentration beneath the bar. Note from Equation (F-5) that an increase of counts by 25% does not necessarily increase saturation by 25%, but always less. The most influence of the bar is at the beginning of the bed and the least at the end. That is at the position of  $S_w = 1$ , hundred percent of the influence exists while at the position of  $S_w = 0$  there is none. The existing value of  $S_w$  at each position gives the percentage of the total influence of the bar at that position. To avoid a trial-and-error procedure, the theoretical prediction

of  $S_w$  was chosen as the weight factor of this error.<sup>1</sup> Therefore,  $S_w$  was read off from the Figures (V-31) to (V-37) at each position and multiplied by the maximum influence of the bar (which was 25%) to obtain the error contribution of the bar at that position. The corrected values as well as the original data are presented in Table (F-15) of Appendix F. It is evident from Table (F-15) that 25% increase in the number of counts off-ray scanning changes the saturation data points approximately 1%. Therefore, in Figures (V-31) to (V-37), even the effect of vertical bars in the extreme limit does not change the shape of the experimental saturation profile significantly.

APPENDIX H  
EFFECTIVE VISCOSITY OF THE MIXED ZONE

Let us assume an element  $d\mathbf{x}$  of the mixed zone in figure H-1. Assuming that Darcy's law is valid, the pressure drop,  $\Delta p$ , of the element is given by

$$\Delta p = \frac{d\mathbf{p}}{dx} \cdot d\mathbf{x}$$

where  $d\mathbf{p}/dx$  is given by equation (H-3)

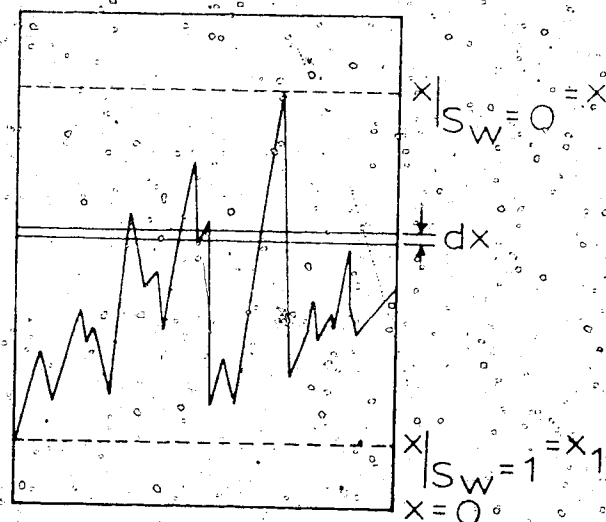


FIGURE H-1. SCHEMATIC REPRESENTATION OF THE MIXED ZONE.

Total pressure drop of the mixed zone is simply obtained by integrating Equation (H-1) between  $x_1$  and  $x_o$ ,

$$\Delta P = \int_{x_1}^{x_o} \left( \frac{dp}{dx} \right) dx \quad (H-2)$$

Defining an effective viscosity  $\mu_e$  for the mixed zone, Darcy's law can be written as,

$$\Delta P = \frac{q \mu_e}{KA} (x_o - x_1) \quad (H-3)$$

From Equations (H-1) to (H-3) therefore,

$$\mu_e = \frac{1}{x_o - x_1} \int_{x_1}^{x_o} \mu_a dx \quad (H-4)$$

The expressions of  $x_o$  and  $x_1$  are obtained from Equation (II-50) by substituting  $S_w = 0$  and unity respectively. The expression of  $x_1$  has already been given by Equation (II-54) and that of  $x_o$  is given below,

$$x_o = \frac{qt \ln M}{(M^2 1) \phi A} \quad (H-5)$$

Therefore,

$$x_o - x_1 = \frac{qt \ln M}{\phi A} \quad (H-6)$$

Equation (H-4) can be integrated either directly by substituting  $\mu_w$ ,  $x_0$ ,

Equation (H-34), and  $S_w$  from Equation (H-31) or, as a second approach, by transforming the variable  $x$  into  $S_w$ . In the second approach it is obtained from differentiating Equation (H-50). The advantage of this approach is that the procedure is being considered for polymer flood in which case no explicit relation for  $S_w$  in terms of  $x$  is not possible.

After straightforward algebraic manipulation, the final result for the Newtonian fluid is obtained as,

$$\frac{\mu_w}{\mu_0} = \frac{S_w + \frac{x_0}{x_1}}{1 - \frac{x_0}{x_1}}$$

which means that the effective viscosity of the mixed zone is constant, independent of  $x_0$  or  $x_1$ , and is simply equal to the arithmetic average of the displacing and displaced fluid.

Due to the complexity of  $S_w$  as a function of  $x$  shown by Equation (H-60), integration for the non-Newtonian fluid is not as simple as for the Newtonian. Equation (H-4) remains the same, in which  $x_0$  and  $x_1$  must be obtained from Equation (H-60) and  $\mu_w$  is substituted from Equation (H-62). Therefore,

$$x_0 = \frac{q t}{\phi A} \cdot \frac{M^{1/n} \ln M_p}{\ln(M_p^{1/n} - 1)} \quad (H-7)$$

$$x_1 = \frac{q t}{\phi A} \cdot \frac{\ln M_p}{M_p - 1} \quad (H-8)$$

Equation (II-66) is differentiated with respect to  $S_w$  to obtain  $dx$ ,

$$\frac{dx}{dS_w} = \frac{(qt \ln M_p) \left[ \left( n \mu_o - n \right) \frac{d\mu_a}{dS_w} + \left( \mu_o - n \mu_o - \mu_a \right) \frac{d\mu_o}{dS_w} \right]}{\left[ n \left( 1 - S_w \right) + S_w \right] \left( \mu_o - n \right) - 2 \left[ (1-n) \left( \mu_o - n \right) \right] \left( n \mu_a - n \mu_o + n \left( \mu_o - n \mu_o - \mu_a \right) \right)} \left( II-9 \right)$$

where,  $\mu$  is given by Equation (II-61) and,

$$\frac{d\mu_a}{dS_w} = \frac{-n \mu_a \ln M_p}{\left[ n \left( 1 - S_w \right) + S_w \right]^2} \quad (II-10)$$

$$\frac{d\mu_o}{dS_w} = \frac{(1-n) n \ln M_p}{\left[ n \left( 1 - S_w \right) + S_w \right]^2} \quad (II-11)$$

By substituting Equations (II-61, 62) and (II-7 to 11) into (II-4), on simplification one obtains,

$$\mu_c = \frac{k}{m} \left( I_1 + I_2 + I_3 \right) \quad (II-12)$$

where:

$$m = \frac{(M_p)^{1/n}}{n(M_p^{1/n} - 1)} - \left( \frac{1}{M_p - 1} \right) \quad (H-13)$$

and using  $\gamma = (n - nS_w + S_w)$

$$I_1 = \frac{\int_1^0 \frac{\left\{ -\left( n^2 m M_p \right) + (1-2n-n^2) (2nM_p) M_p^{(S_w-1)/Y} - (2nY)(1-n) - (2Y)(1-n)^2 (M_p^{(S_w-1)/Y}) \right\} M_p^{-2S_w/Y} dS_w}{(\gamma)^4 (1 - M_p^{-1/Y})^3}}{dS_w} \quad (H-14)$$

$$I_2 = u_0 \int_{1}^0 \left\{ (4n-1-n^2)(\ln M_p) M_p^{(-2S_w-1)/Y} + (n-1)^2 (\ln M_p)^2 M_p^{-(S_w+2)/Y} + [ (1-n)^2 + (1-n) M_p^{(S_w-1)/Y} ] M_p^{-(2S_w+1)/Y} \right\} dS_w$$


---


$$(H-15)$$

(H-16)

$$I_3 = u_0 \int_1^0 \left\{ - M_p^{-2(S_w+1)/Y} + 2Y(1-n) M_p^{-2(S_w+1)/Y} \right\} dS_w$$


---


$$(H-16)$$

As a check it is possible to show that at  $n = 1$  Equation (II-12) eventually produces Equation (II-33). It is clear that the integration of Equation (II-12) is extremely tedious if possible at all. Therefore an alternative method is proposed to approximate the viscosity of the mixed zone for the polymer solution.

The apparent viscosity of the polymer solution is estimated from the shear rate encountered in the bed. This estimated apparent viscosity is used in Equation (II-33) in place of  $\mu_w$  to approximate the effective viscosity of the mixed zone.

The wall shear rate for the packed bed based on the capillary tube model can be shown (40) to be equal to,

$$\gamma_w = \frac{3n+1}{4n} \frac{12 q}{A \sqrt{150 K \phi}} \quad (H-17)$$

Therefore, apparent viscosity based on wall shear rate,  $\eta_w$ , is equal to,

$$\eta_w = m (\gamma_w)^{n-1}$$

In Table (H-1) wall shear rate and the apparent viscosity,  $\eta_w$ , are reported for different flow rates and polymer solutions applied in this work. The effective viscosity and the predicted pressure gradient of the mixed zone are given in Table (F-8).

TABLE II-1

235

APPARENT VISCOSITY OF THE POLYMER  
SOLUTIONS BASED ON THE WALL  
SHEAR RATE

$\dot{\gamma}$ $\text{cm}^3/\text{sec}$	$\gamma_w$ $\text{sec}^{-1}$	$\eta_w = m \gamma_w^{n-1}$ poise
0.05% Separan AP-273, Large Beads		
1.5885	2.72	0.31
6.354	10.89	0.20
15.885	27.23	0.15
0.05% Separan AP-273, Small Beads		
1.5885	10.38	0.20
3.177	20.75	0.16
6.354	41.50	0.15
0.1% Separan AP-273, Large Beads		
6.354	11.45	0.50
15.885	28.64	0.34
0.1% Separan AP-273, Small Beads		
0.15885	1.13	1.99
0.6354	4.51	1.04
3.177	21.82	0.38
6.354	43.64	0.29
0.2% Separan AP-273, Large Beads		
0.3177	0.63	7.74
0.6354	1.27	5.26
1.5885	3.17	3.18
3.177	6.33	2.17
6.354	12.66	1.49
15.885	31.65	0.90

TABLE II-1 (Continued)

$q$ $\text{cm}^3/\text{sec}$	$\gamma_w$ $\text{sec}^{-1}$	$n_w = m \gamma_w^{n-1}$ poise
0.2% Separan AP-273, Small Beads		
3.177	24.12	1.04
0.2% Pusher 500, Small Beads		
0.15885	1.03	1.72
0.6354	4.13	1.11